SELF-IMMOLATIVE THIOCARBAMATES FOR STUDYING COS AND H_2S CHEMICAL BIOLOGY

by

ANDREA KATHARINE STEIGER

A DISSERTATION

Presented to the Department of Chemistry and Biochemistry
and the Graduate School of the University of Oregon
in partial fulfillment of the requirements
for the degree of
Doctor of Philosophy

December 2018

DISSERTATION APPROVAL PAGE

Student: Andrea Katharine Steiger

Title: Self-Immolative Thiocarbamates for Studying COS and H_2S Chemical Biology

This dissertation has been accepted and approved in partial fulfillment of the requirements for the Doctor of Philosophy degree in the Department of Chemistry and Biochemistry by:

Ramesh Jasti	Chairperson
Michael D. Pluth	Advisor
Darren W. Johnson	Core Member
Raghuveer Parthasarathy	Institutional Representative

and

Janet Woodruff-Borden	Vice Provost and Dean of the Graduate School

Original approval signatures are on file with the University of Oregon Graduate School.

Degree awarded December 2018

DISSERTATION ABSTRACT

Andrea Katharine Steiger

Doctor of Philosophy

Department of Chemistry and Biochemistry

December 2018

Title: Self-Immolative Thiocarbamates for Studying COS and H_2S Chemical Biology

In recent years, hydrogen sulfide (H_2S) has garnered interest as the third addition to the gasotransmitter family. Essential to human physiology, H_2S has roles in the cardiovascular, nervous, and respiratory systems and perturbations in physiological H_2S levels have been correlated to a variety of diseases. As a result, there has been significant interest in the development of H_2S-releasing compounds (H_2S donors) that can mimic slow, enzymatic production for research and therapeutic applications. While a large library of H_2S donors exists, several common drawbacks persist, such as: lack of spatial and temporal control, poorly understood mechanisms of release, uncontrolled kinetics, and low efficiency. These issues significantly limit the biological applications of many H_2S donors.

This dissertation describes recent work to provide biocompatible H_2S donors with controllable release kinetics using a robust, novel strategy for H_2S delivery that relies on rapid enzymatic hydrolysis of carbonyl sulfide (COS) to H_2S by the ubiquitous mammalian enzyme carbonic anhydrase (CA). Self-immolative thiocarbamates can be designed to release COS by a variety of stimuli, and in biological milieu this COS is rapidly converted to H_2S by CA. This strategy has enabled the development of the first analyte-replacement fluorescent probe for H_2S and has become a popular strategy for H_2S

delivery in a variety of applications. Additionally, the unexpected cytotoxicity profile of enzyme-activated COS/H_2S donors has piqued interest in COS chemical biology, and these donors are being used as tools for studying COS itself. This dissertation includes previously published and unpublished coauthored work.

CURRICULUM VITAE

NAME OF AUTHOR: Andrea Katharine Steiger

GRADUATE AND UNDERGRADUATE SCHOOLS ATTENDED:

University of Oregon, Eugene, OR
College of Wooster, Wooster, OH

DEGREES AWARDED:

Doctor of Philosophy, Chemistry, 2018, University of Oregon
Master of Science, Chemistry, 2016, University of Oregon
Bachelor of Arts, Chemistry, 2014, College of Wooster

PROFESSIONAL EXPERIENCE:

NSF Graduate Research Fellow, Department of Chemistry and Biochemistry, University of Oregon, Eugene, OR, 2016-2018

Graduate Teaching Fellow, Department of Chemistry and Biochemistry, University of Oregon, Eugene, OR, 2014-2016

Clare Boothe Luce Research Fellow, Department of Chemistry, College of Wooster, Wooster, OH, 2012-2014

GRANTS, AWARDS, AND HONORS:

NSF Graduate Research Fellowship 2016-2019

Honorable Mention, NSF Graduate Research Fellowship, 2015

Clare Boothe Luce Research Fellowship 2012-2014

PUBLICATIONS:

Y. Zhao, A. K. Steiger and M. D. Pluth, *Angew. Chem. Int. Ed., 2018*, DOI: 10.1002/anie.201806854.

V. Vivitsky, J. L. Mijkovic, T. Bostelaar, B. Adhikari, P. K. Yadav, A. K. Steiger, R. Torregrossa, M. D. Pluth, M. Whiteman, R. Banerjee, and M. R. Filipovic. *ACS Chem Biol,* 2018, DOI: 10.1021/acschembio.8b00463.

Y. Zhao,* A. K. Steiger* and M. D. Pluth, *Chem Commun*, 2018, **54**, 4951-4954.

A. K. Steiger, Y. Zhao, W. J. Choi, A. Crammond, M. R. Tillotson and M. D. Pluth, *Biochem. Pharmacol.*, 2018, **149**, 124-130.

A. K. Steiger, M. Marcatti, C. Szabo, B. Szczesny and M. D. Pluth, *ACS Chem Biol*, 2017, **12**, 2117-2123.

A. K. Steiger, Y. Zhao and M. D. Pluth, *Antioxid Redox Signal*, 2018, **28**, 1516-1532.

A. K. Steiger, Y. Yang, M. Royzen and M. D. Pluth, *Chem Commun*, 2016, **53**, 1378-1380.

A. K. Steiger, S. Pardue, C. G. Kevil and M. D. Pluth, *Journal of the American Chemical Society*, 2016, **138**, 7256-7259.

M. Pluth, T. Bailey, M. Hammers, M. Hartle, H. Henthorn and A. Steiger, *Synlett*, 2015, **26**, 2633-2643.

ACKNOWLEDGMENTS

I'd like to thank Professor Pluth for his guidance and the opportunities provided to me in his group. In addition, special thanks are due to Dr. Yu Zhao, who offered unparalleled mentorship to me throughout my graduate career. This work was supported in part by a NSF GRFP (DGE-1309047), the NIH (R01GM113030), and the NSF (CHE-1531189, CHE-1625529, CHE1427987).

For Mr. Mike McPheeters and the late Dr. Melissa M. Schultz

TABLE OF CONTENTS

Chapter Page

Chapter Page

LIST OF FIGURES

Figure Page

Figure Page

Figure Page

Figure Page

Figure Page

LIST OF TABLES

Table Page

LIST OF SCHEMES

Scheme Page

CHAPTER I

EMERGING ROLES OF CARBONYL SULFIDE (COS) IN CHEMICAL BIOLOGY: SULFIDE TRANSPORTER OR GASOTRANSMITTER?

This chapter includes previously published and coauthored material from Steiger, A.K.; Zhao, Y.; Pluth, M.D. "Emerging Roles of Carbonyl Sulfide (COS) in Chemical Biology: Sulfide Transporter or Gasotransmitter?" *Antioxid. Redox Signal.* **2018**, 28(16), 1516-1532.

1.1 Introduction

Small gaseous biomolecules, such as nitric oxide (NO), carbon monoxide (CO), and hydrogen sulfide (H_2S), have attracted significant attention due to their important physiological roles as signaling molecules.[1-10] Often referred to as gasotransmitters, these gases share several defining characteristics: they are membrane permeable, are generated endogenously by enzymes, and exert action on molecular targets at physiologically-relevant concentrations.[11, 12] We note that although commonly referred to as gaseous signaling molecules or gasotransmitters, these small gaseous molecules are actually solutes rather than gases when they act as signaling agents. In this dissertation, we use the terms gaseous signaling molecules and gasotransmitters to refer to the class of molecules rather than the physical state of the molecules in a biological environment. Highlighting the broad importance of these signaling molecules, gasotransmitter generation and/or metabolism has been implicated in diverse biological processes including vascular biology, immune functions, metabolism, and stress resistance/response.[2, 6, 13-19] In addition to the primary gasotransmitter criteria, recent and growing evidence supports a complex cross-talk and interconnectivity between NO, CO, and H_2S, suggesting that the interactions between these molecules play an important role in gasotransmitter function.[20-25] For example, H_2S inhibits CO production through regulation of heme oxygenase 1 (HO-1)[26, 27] and can either stimulate or inhibit different nitric oxide synthase (NOS) isoforms.[15-19] Similarly, both NO and CO inhibit H_2S production from heme-containing cystathionine β-synthase (CBS).[28, 29] Complementing regulatory interactions

through enzymatic synthesis, NO and H_2S also react through different redox pathways to generate reactive sulfur, nitrogen, and oxygen species (RSONS), including thionitrous acid (HSNO), perthionitrite ($SSNO^-$), and nitroxyl (HNO), which further intertwine these gasotransmitters.[22-24, 30, 31]

Despite the significant research on the chemical biology of NO, CO, and H_2S, investigations into other potential gasotransmitters, such as SO_2, NH_3, or COS, remain significantly underdeveloped (Figure 1.1).[11, 32] Both sulfur dioxide (SO_2) and ammonia (NH_3) are produced enzymatically in mammalian cells and are interconnected with established gasotransmitters, giving credence to the suggestion that they may play significant roles in biology. For example, SO_2 can be generated from H_2S by NADPH oxidase or from thiosulfate ($S_2O_3^{2-}$) by thiosulfate sulfurtransferase.[33, 34] Alternatively, cysteine oxidation by cysteine dioxygenase (CDO) generates cysteine sulfonate, and subsequent transamination by aspartate aminotransferase (AAT) generates β-sulfinylpyruvate, which spontaneously decomposes to extrude pyruvate and SO_2.[35, 36] Although still in its infancy, investigations into the possible biological actions of SO_2 have demonstrated roles as a vasorelaxant and also in providing protection against myocardial ischemia-reperfusion injury.[34] Additionally, NH_3 is formed in many pathways, including deamination of amino acids, nucleic acids, nucleotides, and nucleosides, as a byproduct of transsulfuration enzymes, including H_2S-producing CSE and CBS, and from urea recycling.[11] Once formed, NH_3 may not only provide a viable form of nitrogen for DNA and RNA synthesis but also may contribute to acid-base buffering capacity. Additionally, NH_3 has been demonstrated to increase inducible nitric oxide synthase (iNOS) expression in cultured astrocytes [37] and also to increase iNOS and neuronal nitric oxide synthase (nNOS) expression in animal models of hyperammonenemia.[38]

Unlike SO_2 or NH_3, pathways for enzymatic COS synthesis in mammals have yet to be identified, although COS has been detected in various biological tissues and in exhaled breath, supporting the presence of pathways for endogenous generation (*vide infra*).[39-41] Furthermore, COS shares an interconnection with H_2S generation through the action of different metalloenzymes, including carbonic anhydrase (CA) activity, which rapidly converts COS to H_2S.[42-44] Although historical investigations on terrestrial COS

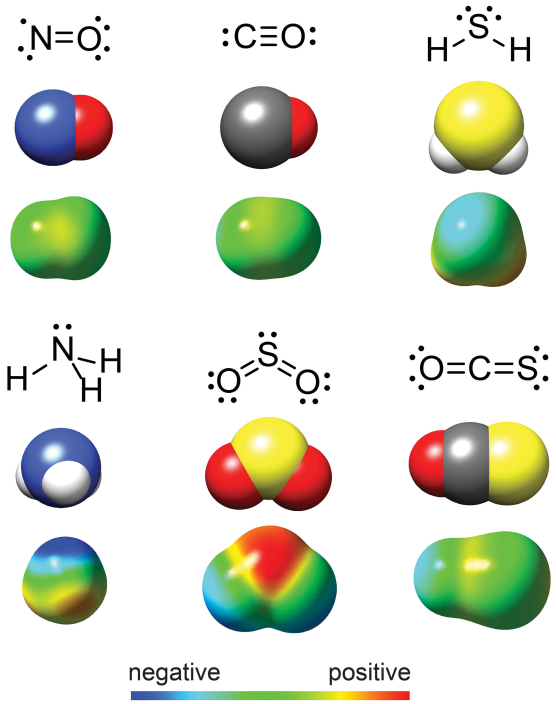

Figure 1.1 Structures, space filling models, and electrostatic potential maps of NO, CO, H_2S, NH_3, SO_2, and COS.

have focused on its atmospheric presence and importance in the global sulfur cycle, contemporary chemical investigations have focused primarily on COS-mediated peptide-bond formation under prebiotic conditions, many of which suggest important roles of COS in origin of life chemical ligation.[45, 46] When taken together with the potential role of COS in thermophilic origin of life theories, COS detection in tissues, as well as its cell permeability and moderate water solubility, suggest that COS may play a much more significant role in mammalian chemical biology than initially appreciated. Building on these factors, this review focuses on current knowledge on biological COS formation and consumption, growing evidence that COS may play roles in sulfide transport and disease pathology, emerging chemical tools for investigating COS in biological contexts, and the potential role of COS as a new member of the gasotransmitter family.

1.2 Basic Properties

Carbonyl sulfide (COS, CAS 463-58-1; also referred to carbon oxysulfide, carbon monoxide monosulfide, carbon oxide sulfide, OCS) is a colorless and odorless gas in its pure form.[47] Initially misidentified as a mixture of carbon dioxide (CO_2) and H_2S due to

its rotten egg smell in an impure state, COS was first characterized by Than in 1867 by the reaction of CO with elemental sulfur vapor in a glowing porcelain tube (eq. 1).[48] Although removal of CO impurities was not practical from the initial preparations, experimental modification allowed for generation and purification of COS by acid-mediated hydrolysis of thiocyanate salts (eq. 2).[48] This reaction can be used to prepare COS in the laboratory, but the produced gas requires significant purification due to common contamination by gaseous impurities.[49] Commercial sources of high purity COS (often >97.5%) often contain significant levels of H_2S as the main impurity. Although only moderately soluble in water, COS is stable in acidic solution but undergoes base-mediated hydrolysis to generate H_2S and CO_2.[47] As a moderately lipophilic gas (log $P_{oct}(COS) = 0.79$ by comparison to log $P_{oct}(NO) = 0.70$),[50] the dipole moment of COS is more similar to that of NO, CO, and H_2S rather than the significantly more polar SO_2 and NH_3. These properties suggest a sufficient lipid solubility to enable cell membrane permeability and also penetration to the central nervous system. Basic properties of COS, as well as those of H_2S, NO, CO, SO_2, and NH_3 are provided in Table 1.1.

$$CO + S \rightarrow COS \qquad \text{(eq 1)}$$

$$KSCN + 2\ H_2SO_4 + H_2O \rightarrow COS + KHSO_4 + NH_4HSO_4 \qquad \text{(eq 2)}$$

Table 1.1 Basic physical properties of COS and other biologically-relevant gaseous molecules receiving attention as confirmed or potential gasotransmitters.

Physical property	**COS**	**H_2S**	**NO**	**CO**	**SO_2**	**NH_3**
Molecular weight (g/mol)	60.08	34.08	30.01	28.01	64.06	17.03
Density (g/mL)	1.028	1.36	1.34	1.14	2.63	0.769
Melting point (°C)	-138.8	-82	-164	-205.0	-72	-77.8
Boiling point (°C)	-50.2	-60	-152	-191.5	-10	-33.3
Dipole moment (D)	0.65	0.97	0	0.12	1.62	1.42
Solubility (H_2O, mol/L, 25 °C)	2.0×10^{-2}	1.1×10^{-1}	1.9×10^{-3}	9.9×10^{-4}	1.7	31

1.2.1 Toxicity and Safety

Much like H_2S, NO, and CO, COS is a flammable gas that is toxic in high concentrations. COS is a skin, eye, nose, throat, and lung irritant, matching many of the topical toxicity characteristics of H_2S. These similarities are likely due to the hydrolysis of COS to form H_2S upon contact with different mucosal membranes, which typically contain CA thus facilitating H_2S generation (*vide infra*). Similarly, in toxicological investigations of COS, treatment of rats with the CA inhibitor acetazolamide (AAA) reduces measured blood levels of H_2S, and also the toxicity of COS, suggesting that at least some of the observed COS toxicity is due to CA-mediated metabolism to H_2S.[42, 51] Although specific hazardous concentrations of COS are not specified by the US Environmental Protection Agency (EPA), different reports have documented irritation in the upper respiratory tract at concentrations above 20 mg/L.[52] Low to moderate concentrations are accepted to elicit lachrymatory effects, photophobia, nausea, increased salivation, headache, mental confusion, as well as other characteristics.[52] Higher COS concentrations can result in decreased vision, tachycardia, and collapse, and continuous exposure to COS concentrations of 0.1% (v/v) can result in death within two hours due to respiratory paralysis. A limited number of animal studies have investigated acute or chronic COS toxicity, but toxicological investigations of 50 ppm levels of COS in rabbits for up to 7 weeks did not impact the myocardial ultrastructure significantly.[53] Similarly, toxicological investigations in rats revealed LC_{50} of over 2000 mg/m^3 with further investigations classifying COS as a non-carcinogenic, low-toxicity fumigant.[54]

1.2.2 Natural Sources

COS is the most prevalent sulfur-containing gas in Earth's atmosphere and is produced by both biological and chemical pathways (Figure 1.2).[52, 55] Primary abiotic COS emissions occur from volcanos, hot springs, and oceans, with biotic sources stemming from soils, trees, marshes, plant roots, manure, microorganisms, and biomass burning (see section 3 for more detailed information).[56] Up to one half of terrestrial COS is generated from secondary production in the global sulfur cycle through oxidation of atmospheric dimethyl sulfide (Me_2S) and carbon disulfide (CS_2).[56] Anthropogenic sources of COS, which include aluminum production, coal and automobile fuel burning,

and industrial desulfurization, contribute minimally to global COS production, but more recent estimates indicate that industry and manufacturing may produce more COS than has been previously reported.[57] Measurement of atmospheric COS levels from Antarctic ice cores have shown that COS levels have risen over the last 350 years, which has been attributed to human sources of industrialization.[58] Once produced, COS is more stable in the atmosphere than the common sulfur-containing gases Me_2S, H_2S, and CS_2, which results in a prolonged atmospheric lifetime of about four years.[59] As a result, COS is generally transported from the troposphere to the stratosphere, where it undergoes photodissociation and oxidation to SO_2 and sulfate particles, therefore influencing stratospheric ozone concentrations.[52, 60] The long atmospheric lifetime, as well as its formation from CS_2 in the atmosphere, make COS the primary sulfur gas in Earth's atmosphere, with measured concentrations of 0.5 ppb.[56]

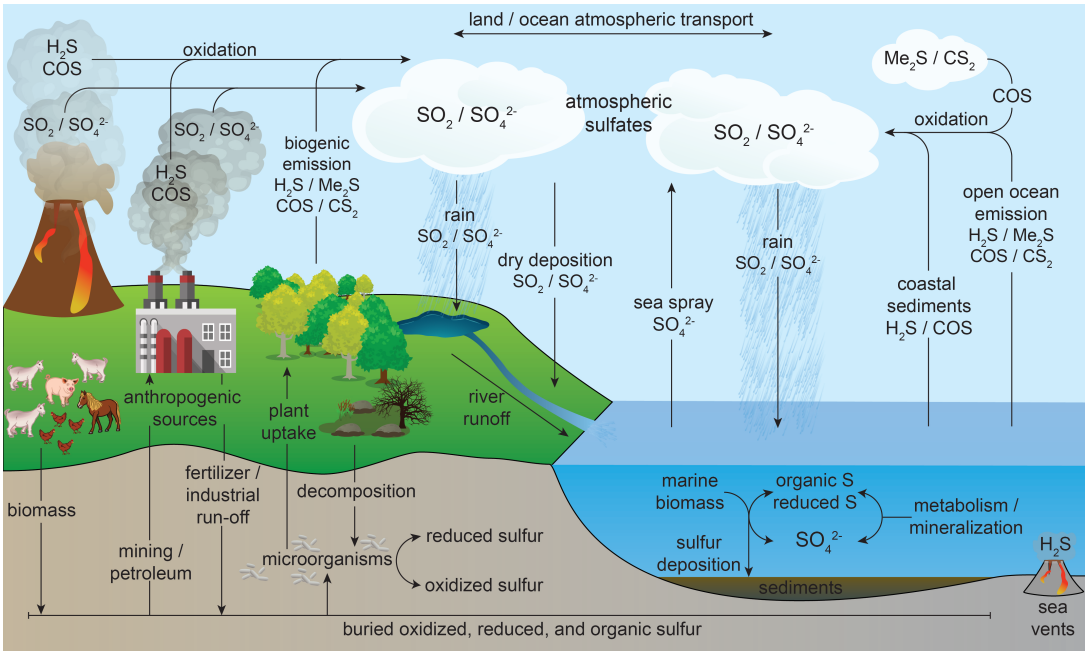

Figure 1.2 Simplified overview highlighting the roles of COS in the global sulfur cycle. Primary COS emission sources include volcanoes and hot springs, biomass, and open ocean emission. Approximately one half of atmospheric COS is generated from the oxidation of Me_2S and CS_2 in the global sulfur cycle. Primary anthropogenic sources include aluminum production, coal and automobile fuel burning, and industrial desulfurization. Once produced, COS has a longer atmospheric lifetime than Me_2S, H_2S, or CS_2 and is typically transported to the stratosphere, where it undergoes photodissociation and oxidation to SO_2 and sulfate particles. COS uptake also occurs in plants, soils, marine algae, and microbes, which often convert COS to CO_2.

Although oxidation of COS to sulfate occurs in the atmosphere by hydroxyl radical, the major sink of atmospheric COS is uptake by many plants, soils, marine algae, and microbes, which often convert COS to CO_2. This conversion is typically mediated by the ubiquitous enzyme CA as well as other COS-metabolism enzymes (*vide infra*). In addition to COS metabolism by CA, some plants are able to convert COS to CS_2, as demonstrated by increased CS_2 release after COS absorption by moist soils.[61] These observations suggest a link between CS_2 and COS not only in the atmosphere, but also in soils and vegetation.

1.3 Biological Roles of COS

Growing evidence supports the importance of reactive sulfur species in biology, but surprisingly little attention has focused on the most-prevalent sulfur-containing gas in Earth's atmosphere: COS. Reported investigations into the biological roles of COS remain sporadic and our understanding of the potential roles physiological and pharmacological roles of COS remain underdeveloped. Despite these limited reports, enzymatic COS production and consumption is well documented, and COS generation in cell culture and in exhaled breath in human subjects suggests a broader role for this important gas in diverse biological processes.

1.3.1 Enzymatic Consumption of COS

Carbonic anhydrases (CAs) are a family of ubiquitous metalloenzymes that catalyzes the reversible hydration of CO_2 to bicarbonate (HCO_3^-).[62, 63] CAs are comprised of five classes found primarily in vertebrates (α-CAs), higher plants and some prokaryotes (β-CAs), archaebacteria (γ-CAs), and diatoms (δ-CAs and ξ-CAs). Although not its natural substrate, CA is also able to readily hydrolyze COS to H_2S, providing a broad enzymatic platform for redox-neutral conversion of COS to H_2S. The catalytic efficiency (k_{cat}/K_M) of CA-mediated COS conversion to H_2S is less efficient than the canonical CO_2 metabolism (~8 x 10^7 M^{-1} s^{-1}),[64] but still boasts a high catalytic efficiency of 2.2 x 10^4 $M^{-1}s^{-1}$ for bovine CA-II (Table 1.2).[65] Drawing parallels to CA, other enzymes are also able to catalyze the hydrolysis of COS even though it is not their natural substrate. For example CS_2 hydrolase, nitrogenase, CO dehydrogenase, and ribulose-1,5-

bisphosphate carboxylase oxygenase (RuBisCO), have all been reported to hydrolyze COS.[66-69] Of these enzymes, CS_2 hydrolase, initially isolated from acidophilic and thermophilic archaea extremophiles[66] exhibits the greatest catalytic efficiency of enzymatic COS hydrolysis (Table 1.2). Because the distribution of this enzyme is limited to extreme and sulfur-rich environments, such as sulfotaras, it is unlikely that CS_2 hydrolase contributes significantly to global COS consumption. The only known example of an enzyme for which COS is the natural substrate is carbonyl sulfide hydrolase (COSase), which was recently identified, purified from *T thioparus* strain THI115, and characterized.[70, 71] COSase shares both a high sequence homology and shares a similar Zn(II) active site with the β-CAs and are structurally similar to enzymes in clade D of the β-CA phylogenetic tree.[70] Importantly, COSase has a higher efficiency than widely-distributed enzymes able to catalyze COS hydrolysis, suggesting that it may play an important role in the global consumption of atmospheric COS. Although less efficient than COSase, other metalloenzymes, such as CO dehydrogenase,[68] RuBisCO,[69] and nitrogenase [67] have been shown to metabolize COS in plants and bacteria with varied levels of catalytic efficiency (Table 1.2).

Table 1.2 COS degrading enzymes and associated enzyme kinetic parameters. Modified from reference 70.[70]

Enzyme	**Organism**	**k_{cat} (s^{-1})**	**K_m (μM)**	**k_{cat}/K_M (M^{-1} s^{-1})**	**Ref.**
CS_2 hydrolase	*Acidianus* sp. Strain A1-3	1800	22	8.2×10^7	66
COSase	*T thioparus* strain THI115	58	60	9.6×10^5	70
CO dehydrogenase	*Rhodospirillum rubrum* ATCC11170^T	0.52	2.2	2.4×10^5	68
CA	*Bos taurus*	41	1.9×10^3	2.2×10^4	65
RuBisCO	*Spinacia oleracea*	3.8	1.8×10^3	2.2×10^3	69
RuBisCO	*Rhodospirillum rubrum*	6.3	5.6×10^3	1.1×10^3	69
Nitrogenase	*Azotobacter vinelandii*	0.16	3.1×10^3	5.2×10^1	67

1.3.2 Biological Production of COS

Thiocyanate (SCN^-) is a common organic anion found in plants, mammals, and natural environments. In plants, SCN^- is formed from the hydrolysis of glucosinolates, often found in Cruciferae (Brassicaceae) by glucosidases.[72] In mammals, SCN^- is commonly found in saliva, blood, and milk, and derives from ingestion of glucosinolates, often derived from broccoli, cauliflower, and other cruciferous vegetables, as well as from cyanide (CN^-) detoxification by the ubiquitous enzyme rhodanese.[73] Although mammalian thiocyanate degradation primarily occurs through peroxidation by myeloperoxidase and lactoperoxidase,[74] at a microbial level, a number of chemoorganotrophic bacteria are able to degrade SCN^- as a source of nitrogen and sulfur. Furthermore, chemolithoautotrophic sulfur bacteria, such as *Thiobacillus thioparus*, have been identified that utilize SCN^- as their primary energy source.[75] More specifically, the enzyme thiocyanate hydrolase (SCNase), which catalyzes the hydrolysis of SCN^- to COS and NH_3 (eq. 3), was initially isolated and identified in *T. thioparus* strain THI115.[76] SCNase consists of three subunits (α (19 kDa), β (23 kDa), and γ (32 kDa)), which share a high sequence homology to bacterial nitrile hydratases, and maintains an unusual distorted square pyramidal low-spin Co(III) active site.[77] Thiocyanate hydrolase has also been identified as the primary enzyme for initiating SCN^- hydrolysis in the sulfur-oxidizing bacterium *Thiohalophilus thiocyanoxidans*.[78]

$$SCN^- + 2\ H_2O \rightarrow COS + NH_3 + OH^- \qquad \text{(eq 3)}$$

In addition to SCNase, COS can also be formed from archaeal CS_2 hydrolase, which converts CS_2 to H_2S and CO_2, but proceeds through intermediate generation of COS.[66] CS_2 hydrolase, isolated from *Acidianus* A1-3, which is a hyperthermophilic Archaea that lives in volcanic solfataras, has a structure that is similar to typical β-CAs, but does not hydrolyze CO_2. Instead, this enzyme has evolved a highly hydrophobic tunnel that serves as a filter by blocking the entrance of CO_2 into the active site, which is otherwise identical to that of CA.[79] Similarly, in mammalian systems, CS_2 can be metabolized to COS by the mixed-function oxidase enzyme system. Liver damage, as well as a measureable decrease in the concentration of cytochrome P450, is observed

when rats are treated with CS_2.[80-82] This damage has been attributed to the binding of reactive sulfur species that are released during the hydrolysis of CS_2 to COS. Once released, the COS is further metabolized to H_2S, most likely by hepatic CA. Alternatively, COS can function as a suicide substrate for cytochrome P450, generating CO_2 but also reactive sulfur species that react with and inhibit the P450.[81]

1.3.3 Abiotic COS generation

In addition to enzymatic COS generation, abiotic COS production of has also been demonstrated. Because much of the COS in the atmosphere derives from open waters, a number of studies have investigated possible mechanisms of COS formation, such as the reaction of carbonyl groups of dissolved organic compounds with thiyl radicals.[83] Interestingly, and possibly of more direct biological relevance, is the direct reaction of polysulfides with CO to generate COS.[84] Inorganic polysulfides play an important role in the global sulfur cycle and such polysulfides, as well as their organic counterparts, are now understood to be of increasing importance in the biological action of H_2S.[85-89] By using inorganic polysulfides and CO, both of which are abundant in aquatic systems, mechanistic investigations revealed that the rate of COS generation had a first-order dependence in both CO and the molar sum of polysulfide species in solution.[84] Although further investigations are needed to determine whether the reaction kinetics, pH, and temperature dependence make such mechanisms of COS formation viable under physiological conditions, these observations highlighted the interconnected role of COS with CO and polysulfides.

1.3.4 COS Detection in Mammalian Systems

Although the precise mechanisms of COS biosynthesis in eukaryotes remain unknown, two primary pathways for COS genesis have been postulated in investigations of COS in the body: metabolism (or impaired metabolism) of sulfur containing precursors, and direct generation by cohabitating bacteria. COS has also been detected as a metabolite of different sulfur-containing drugs, supporting that abnormal metabolism of sulfur-containing compounds may, in part, contribute to COS generation. One simple example of such is disulfiram (tetraethylthiuram disulfide), which functions as an

acetaldehyde dehydrogenase inhibitor and is commonly used for treatment of chronic alcoholism.[50] Reduction of the dithiocarbamate disulfide in disulfuram, followed by partial hydrolysis to form diethylthiocarbamate, may provide a path for COS extrusion, although it is also possible that initial CS_2 release generates COS as a metabolic byproduct. Additionally, metabolism of the commonly-used dithiocarbamate pesticides has also been demonstrated to release COS. Although such systems provide convenient examples of COS in biological contexts, the high concentrations of such sulfur-containing molecules significantly simplifies COS detection. By contrast, detection of endogenous COS remains significantly more challenging. These challenges arise primarily from the likely low levels of COS as well as the efficient metabolism of COS by CA to form H_2S, which has so far necessitated detection of COS from only gaseous biological samples or from the headspace of samples, where COS can be isolated outside of a CA-rich environment. Despite these challenges, observation of COS in mammalian cell culture, *ex vivo* tissues, and exhaled breath has provided compelling evidence for the importance of COS in biology and implications for COS involvement in various pathologies.

One strategy for COS detection is to monitor the gas content of the headspace over cell culture or *ex vivo* tissues. One benefit of this approach is that analysis of the headspace is readily accessible through standard GC-MS techniques or by various spectroscopic techniques.[90] In one such example, headspace analysis of porcine coronary artery (PCA) and cardiac muscle tissue *in vitro* demonstrated COS formation by GC-MS analysis.[41] In addition, COS was found to induce arterial dilation. Moreover, stimulation of PCA with acetylcholine and calcium ionophore A23187 resulted in increased COS levels, suggesting that muscarinic acetylcholine receptors (mAChRs), which have already been shown to be involved in production of CO, NO, and H_2S leading to vasorelaxation,[91-96] may also be involved in COS genesis. Although a simple example, these experiments may suggest a promising starting point for future COS investigations.

In addition to detection of COS in the headspace of tissue culture experiments, COS has also been detected in exhaled breath, providing evidence for the role of COS as a potential gaseous biomarker for various disease states. For example, investigations into the presence of sulfur gases in patients with cystic fibrosis (CF) revealed measurable

differences between COS levels in inhaled and exhaled breath.[39] As a whole, CF patients had a reduced uptake of atmospheric COS by comparison with healthy patients. Furthermore, CF patients with reduced pulmonary function exhibited greater COS levels in exhaled breath than normal patients, with a strong inverse correlation between COS concentration and all four indices of pulmonary function in CF patients, with no correlation observed in normal patients. Prior research has also demonstrated an inverse correlation between pulmonary function and respiratory bacterial load,[97-99] which when taken together, provide support for the hypothesis that cohabitating bacteria may play an important role in biological COS generation. Consistent with this hypothesis, recent studies have reported that CA distribution and activity may be altered in CF patients,[100-102] suggesting a lower potential for COS metabolism. One hypothesis, which is consistent with the experimental data, is that impairment of CA function/expression in CF patients may reduce COS metabolism in the lungs which, when coupled with increased bacterial load and COS production in the respiratory tract, may result in higher COS levels observed in exhaled gas. On the basis of these observations, these studies suggest that exhaled COS may provide a potential non-invasive biomarker for bacterial colonization of the respiratory tract of CF patients.

Furthering the potential role of COS as a biomarker for lung pathologies in exhaled breath, COS has also been investigated as a potential marker of acute rejection (AR) after organ transplant. AR after lung allograft is a major risk factor for bronchiolitis obliterans (BO), which is one of the primary causes of death in lung transplant patients. Early detection and diagnosis of AR typically requires routine biopsies, which are invasive and associated with pulmonary complications. In a study investigating the efficacy of non-invasive breath testing for AR monitoring, comparisons between healthy, non-rejection patients and AR patients did not provide significant differences in exhaled ethane, isoprene, acetone, or H_2S, all compounds that are potential organ transplant related biomarkers. Only exhaled COS levels were demonstrated to provide a biomarker for AR, with elevated COS levels observed for AR patients by contrast to non-rejection patients. Furthermore, individual patient tracking documented examples of COS levels increasing with worsening AR and decreasing with AR resolution. Although the direct COS origin was not identified, the authors hypothesized that abnormal metabolism of

sulfur-containing compounds in AR patients may be responsible for the observed increase in exhaled COS.

In addition to direct lung pathologies, COS levels in exhaled breath have also been characterized in various stages of liver disease.[40] When compared to patients with normal liver function, patients with hepatocellular injury (grouped to include: alcoholic cirrhosis, autoimmune cirrhosis, cryptogenic cirrhosis, fulminant hepatitis, hepatitis B, hepatitis C, 1-antitrypsin deficiency, and steatohepatitis) exhibited elevated COS levels in exhaled breath. Additionally, COS, but not CS_2 or Me_2S, was found to correlate with the severity of disease, resulting in increasing COS levels in early, mid, and end stage liver disease, potentially providing a diagnostic tool for early detection. By contrast, patients with bile duct injury diseases (grouped to include: cystic fibrosis, primary biliary cirrhosis, sclerosing cholangitis, and biliary obstruction) exhibited reduced COS levels in exhaled breath. These human studies are consistent with previous observations in isolated rat hepatocytes and liver microsomes, which have been observed to generate COS, possibly from CS_2 metabolism or metabolism of other sulfur-containing compounds.[51] These data are also consistent with previous experiments where COS has been observed in exhaled breath of rats exposed to CS_2, suggesting that the observed COS may be due to metabolism of CS_2 or, by analogy, the incomplete metabolism of other sulfur-containing compounds.[80]

The above examples provide key demonstrations of COS generation from metabolic abnormalities or bacterial colonization associated with disease, but also provide compelling evidence for the necessity of further exploration into potential metabolic pathways of COS in biology. Although mammalian COS production from natural sources remains poorly understood, one possible route for COS synthesis is SCN^- hydrolysis by SCNase, although the presence of this enzyme has yet to be reported in mammals. Given that COS has been detected in biological samples, particularly in non-diseased tissues, elucidation of possible enzymatic pathways for COS production remains an important area of investigation. Importantly, these studies additionally suggest a key role of bacterial colonization in COS generation in mammalian systems. In the cases of exhaled breath analysis, a distinct interplay between the host, mammalian tissues, and

bacterial colonization not only suggests a complex landscape in COS generation, but also may provide access to a convenient method of detection for a variety of disease states.

1.4 COS Chemistry

The most simple reactions of COS, including hydrolysis, oxidation, reduction, and dissociation, have been known for many years and are the main subject of a thorough COS review published in 1957.[47] Since then, COS chemistry has expanded to address environmental concerns associated with COS contaminants in industrial settings, and catalysts for the low temperature rapid hydrolysis of COS have been developed. Although the most basic chemical reactions are well researched, more complex and biologically-relevant COS-related reactions remain less understood, even though contemporary investigations suggest important biological roles for COS stemming from initial thermophilic origin of life chemistry.

1.4.1 Simple Reactions of COS

Shortly after the initial synthesis of COS, early reactivity studies demonstrated that COS reacts with primary amines (**1**), such as excess aniline to generate diphenylurea and H_2S.[48] In such reactions, COS initially reacts with the amine to generate a stable, often isolable monothiocarbamate (**2**), which subsequently extrudes HS^- to furnish an electrophilic isocyanate (**3**). In the presence of excess amine, the isocyanate intermediate is trapped by the amine to generate the urea product (**4**) (Figure 1.3). By tuning the reaction conditions, the generated isocyanate can also react with other nucleophiles, such as thiols, to furnish thiocarbamate esters (**5**). Although challenging to control the reaction conditions and stoichiometries on laboratory scale syntheses, these reactions are commonly used industrially in the manufacture ureas and thiocarbamates for use as herbicides and pesticides. Because COS is also known to a be a sulfur contaminant in natural gas and hydrocarbon streams, the chemistry detailed above can be utilized for COS removal through the addition of primary amines during the purification process.[103]

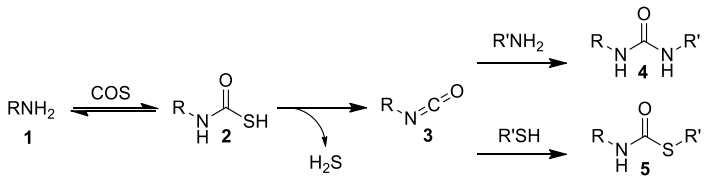

Figure 1.3 Amines react reversibly with COS to generate thiocarbamates, which can release H_2S to afford electrophilic isocyanates. These isocyanates can be trapped in synthetically-useful reactions to generate ureas and thiocarbamate esters.

1.4.2 Implications in Origins of Life and Prebiotic Bond Formation

In addition to the role of COS in laboratory scale and industrial syntheses, contemporary investigations have focused on the potential role of COS in nascent bond-forming reactions under prebiotic conditions. Perhaps unsurprisingly, the volcanic and geothermal generation of COS, as well as its bond forming potential with simple nucleophiles, appears consistent with the thermophilic origin of life requirements. Much of this work stems from studies by Hirschmann and co-workers in 1971 focused on peptide formation from 2,5-thiazolidinediones, in which a footnote comments that traces of dipeptides were formed from phenylalanine thiocarbamate– a known reaction product of amines with COS.[104]

Over 30 years later, more detailed investigations into origin of life peptide synthesis were performed by mimicking volcanic or hydrothermal environments. Using prebiotic building blocks such as CO, nickel and iron sulfides ((Ni,Fe)S), and a reducing atmosphere of H_2S or CH_3SH at elevated temperatures (Figure 1.4a), amino acids (**6**) combined successfully to form dipeptides (**7**). Amino acid chirality was lost, however, likely due to the presence of metal sulfides that may promote racemization of the stereocenter of the anhydride intermediate under the harsh conditions investigated. Trace amounts of COS were detected during the course of the dipeptide-forming reactions, which was consistent with a proposed mechanistic explanation that involved COS as a key intermediate required to generate the thioanhydride (**9**) prior to dipeptide (**10**) formation (Figure 1.4b). Supporting the necessity of COS in these reactions, dipeptides were still formed if CO and H_2S were replaced with COS, although removal of (Ni,Fe)S abolished dipeptide formation. Highlighting the feasibility of metal-mediated formation of COS, a recent report demonstrated the ability of Mo(II) complexes to function as pre-

catalysts for the photocatalytic generation of COS from CO and S_8 under relatively mild conditions.[105]

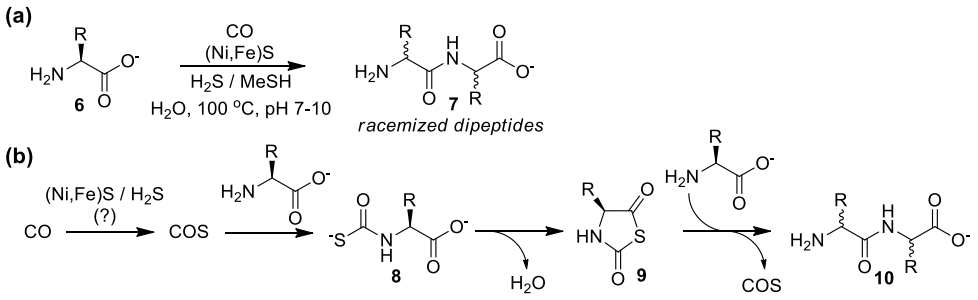

Figure 1.4 (a) Hydrothermal generation of dipeptides in the presence of (Ni,Fe)S, H_2S/MeSH, and CO. (b) The proposed mechanism for this conversion generates COS as a key intermediate.

Furthering investigations into the role of COS in primordial amino acid chemistry, an elegant study by Ghadiri and co-workers demonstrated that COS can facilitate the direct formation of small peptides from amino acids in water under mild conditions in the absence of metal sulfides (Figure 1.5).[46] Remarkably, even the simplest conditions, such as addition of excess COS gas to an aqueous buffered solution of phenylalanine resulted in 7% dipeptide formation after 2 days at 25 ºC. Further investigations revealed quantitative formation of thiocarbamate (**8**) upon addition of COS to a pH 8.9 buffered solution. Importantly, this intermediate showed good hydrolytic stability, and studies using analytically pure phenylalanine thiocarbamate showed it to be a competent intermediate in the peptide bond formation. Such reactions are proposed to occur through formation of a cyclic *N*-carboxyanhydride (Leuchs' anhydride, **11**), which functions as a versatile platform for subsequent reactions with different nucleophiles. Formation of this anhydride, however, requires extrusion of HS^- from the thiocarbamate intermediate, which is hindered both by the stability of the thiocarbamate intermediate as well as by the poor leaving group ability of hydrosulfide anion. In further optimization of peptide bond formation, significant rate enhancements were observed in the presence of metal ions, oxidizing agents, and electrophilic alkylating agents, suggesting that such species (or Lewis acids in general) may facilitate decomposition of the monothiocarbamate intermediate and subsequent H_2S release.

In addition to simple peptide forming reactions, the activation of amino acids by COS has been demonstrated to be a more general pathway to biologically-relevant peptide functionalization. For example, under mild aqueous conditions, COS facilitates the formation of aminoacyl phosphates (**13**) from amino acids and inorganic phosphate. Under identical conditions, no aminoacyl phosphates are observed in the absence of COS. Similarly, when inorganic phosphate is replaced with adenylic acid (5'-AMP), several amino acids produced aminoacyl adenylates (**15**), which are important for protein biosynthesis. Furthermore, in the presence of Ca(II) and an amino acid, COS was also found to facilitate pyrophosphate (**14**) formation through intermediate generation of an aminoacyl-phosphate anhydride. Combined with the above evidence that COS mediates peptide formation, this work suggests that both prebiotic peptide synthesis and

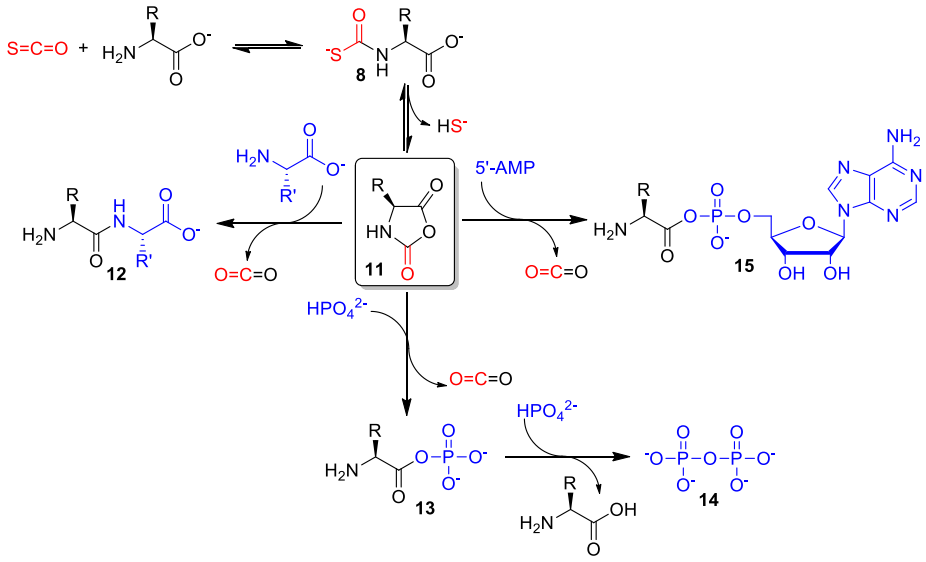

Figure 1.5 Prebiotic chemistry mediated directly by COS including formation of peptides, aminoacyl phosphates, and inorganic phosphates. Each pathway proceeds through COS-mediated formation of thiocarbamate **8**, followed by sulfide extrusion to generate electrophilic intermediate **11** (Leuchs' anhydride), which functions as a versatile platform for subsequent reactions with different biologically-relevant nucleophiles.

phosphoryl transfer reactions might have relied on a common, COS-activated precursor.[106]

Although the atmospheric levels of COS are unlikely to generate suitable concentrations of the required thiocarbamate intermediates to facilitate efficient peptide

coupling under global prebiotic conditions, the higher temperatures and COS levels near geothermal locales of COS generation could likely facilitate access to the reaction manifolds associated with these important prebiotic bond forming reactions. More importantly, these studies set the stage for establishing the potential role of COS in biologically-relevant reactions and intermediate generation, paving the way for future applications of COS chemistry.

1.5 Emerging Tools for COS Investigations

Both chemical and biological tools are needed to expand our understanding of the potential roles of COS in biology. Because direct knockout, overexpression, and blockage of the enzymes associated with production of the currently identified gasotransmitters have proven essential in studying the chemical biology of these gases, the definitive identification of COS-producing enzymes or pathways will be equally important. Prior to such information, downregulation of biological COS will remain a significant challenge. In the interim, one potential strategy to increase COS bioavailability is to shunt pathways associated with COS metabolism. For example, because of the wide distribution of CA and its high activity toward COS hydrolysis, the use of CA inhibitors and/or enzymatic knockout could potentially be used to increase COS accumulation. Inhibition of CA by small molecules is a well-researched field,[107-112] and a variety of methods are available for strong inhibition of a variety of CA isoforms. Unfortunately, such inhibition studies would also alter the normal CO_2 / HCO_3^- equilibrium, and thus normal buffering capacities and cellular pH levels, likely leading to complicating effects. Additionally, even small changes in pH would also alter the distribution of H_2S and HS^-, likely leading to confounding results.

Prior to insights gleaned from such investigations, the development of small molecule chemical tools for COS research may offer an attractive platform for expanding our understanding of COS in biology. Chemical tools for detection and delivery of the canonical gasotransmitters NO, CO, and H_2S have been invaluable for investigating the multifaceted roles of these important biological molecules,[113-130] suggesting that similar constructs may find utility for COS investigations. Reaction-based fluorescent probe development for COS is likely to remain a significant challenge based on the inherent

reactivity of COS. Because COS is a weaker electrophile than CO_2, strategies to intercept COS by nucleophilic trapping are likely to be plagued by unwanted side reactivity leading to significant selectivity challenges. By contrast to reaction-based detection motifs, small molecules that release COS may offer a more attractive first line of tools for investigating COS in different biological contexts.

1.5.1 General Strategies to Develop COS Donors.

Because of the structural similarities between COS and CO_2, many decarboxylation reactions can be engineered to release COS rather than CO_2 by simple replacement of an oxygen atom with a sulfur in the parent scaffold. This basic design concept enables structurally-diverse COS donors that provide access to both triggered- / active-release donors, such as those that respond to specific biological or biorthogonal stimuli, as well as slow- / passive-release donors, such as those activated by hydrolysis or reaction with ubiquitous cellular enzymes and nucleophiles. Additionally, easily-accessible control compounds are available through synthesis of analogous carbamate compounds, which release CO_2 rather than COS. Access to such control compounds are instrumental in differentiating the biological effects of the donor scaffolds themselves from the released COS. Recognizing the potential powerful utility of engineered COS release, our lab was the first to harness such motifs to develop COS-releasing small molecules.[131] Since this initial report, we have been delighted that other researchers are using related strategies to broaden the palette of COS-releasing motifs available for future biological investigations.

The key breakthrough in our initial design was recognizing that self-immolative benzyl carbamates (Figure 1.6a),[132, 133] often used as delivery platforms for prodrugs, fluorophores, and other small-molecules,[134-137] could be modified to release COS rather than CO_2 by exchanging the canonical carbamate linker with a thiocarbamate (Figure 1.6b). In a proof-of-concept demonstration of this approach, we established the utility of on-demand COS-extrusion as a strategy to access both analyte replacement fluorescent probes and triggered COS/H_2S donors (See Chapter II).[131] The early motivation of this work was to address a major challenge in reaction-based probes for small molecule analytes, especially RSONS. Activation of these reporter scaffolds results in analyte

consumption, thus perturbing homeostasis. Exploitation of the self-immolative decomposition of thiocarbamates to release COS enabled the generation of the first examples of analyte replacement fluorescent probes, which react with (and consume) H_2S to produce a turn-on fluorescent response, concomitant with the release one equivalent of caged H_2S in the form of COS, thus providing progress toward analyte homeostasis in reaction-based detection systems (Figure 1.6c). By using an H_2S-reactive azide trigger, which is reduced to an amine upon reduction by H_2S, we established that the subsequent self-immolative cascade reaction extrudes COS, which is quickly hydrolyzed to H_2S by CA. Importantly, this donor motif was found to be stable in whole mouse blood prior to trigger activation, thus highlighting the biological stability of these platforms. Control experiments on thiocarbamate motifs lacking a latent fluorophore demonstrated that triggered reductive cleavage by *tris*(2-carboxyethyl)phosphine (TCEP) in mouse blood resulted in COS donation with nearly 50% efficiency and conversion to H_2S by CA. Additionally, addition of the CA inhibitor AAA abrogated H_2S production *in vitro*, confirming that H_2S release is a result of CA-mediated COS hydrolysis. Although this initial report provided an important contribution toward H_2S detection technology, the broader impact is providing a viable and highly tunable COS donating strategy for accessing chemical tools for expanding our understanding of the chemical biology of COS.

1.5.2 Triggered/Active Release of COS

Furthering the strategies outlined above, simple changes to the general self-immolative thiocarbamate scaffold can provide access to new donor motifs with more specific functions. Notably, incorporation of protecting groups that selectively respond to specific stimuli and result in on-demand COS release may provide access to highly targeted COS donors with utility in investigating the chemical biology of COS, as well as for site-selective COS/H_2S donation. Such triggerable donors can be expected to be useful in therapeutic applications where COS delivery is targeted to a specific location as well as for studying COS delivery with a high level of temporal control.

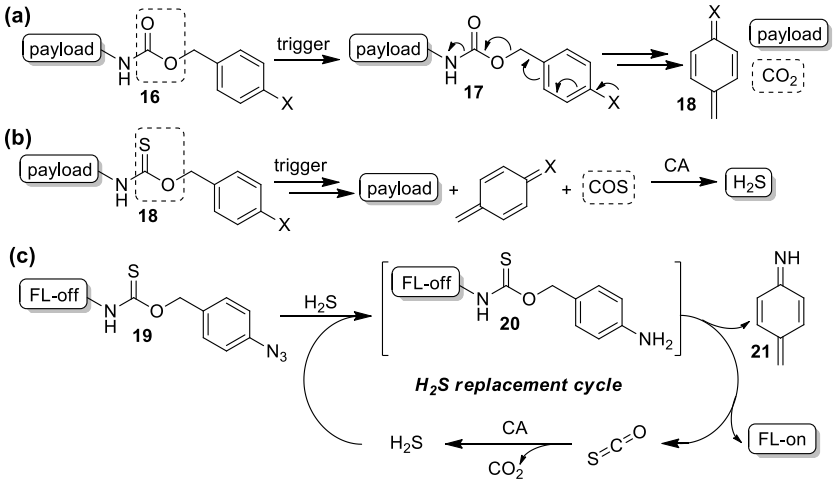

Figure 1.6 (a) Established strategy of using protected benzylcarbamates to deliver a payload after trigger activation. (b) Translation of this delivery technique by using protected benzylthiocarbamates enables access to COS releasing motifs. (c) Initial application of caged COS release to develop analyte replacement fluorescent probes for H_2S based on azide reduction.

ROS Triggered COS Donors. A powerful application of such responsive donors is the judicious choice of triggering analytes associated with contexts in which H_2S can exert beneficial action. For example, because H_2S has been demonstrated to provide protection against increased oxidative stress, a system in which COS release is triggered by reactive oxygen species (ROS) should not only provide access to actively-triggered COS donors, but also provide a platform with high pharmacological potential. Using an ROS-cleavable aryl boronate as the protecting group,[138, 139] we developed a class of COS donors that respond to increased ROS levels (Figure 1.7a).[140] Highlighting the responsive nature of this design platform, COS is released from PeroxyTCM-1 in a dose-dependent manner upon addition of H_2O_2 as well as other ROS and is quickly converted to H_2S by CA.

Supporting *in vitro* investigations, stimulation of endogenous ROS production in Raw. 264.7 cells by addition of phorbol 12-myristate 13-acetate (PMA) resulted in COS/H_2S release from PeroxyTCM-1, as evidenced by an increase in fluorescence when imaged with the H_2S-responsive probe HSN2.[141] Providing early insights into the potential of such donors to impart cellular protections under conditions of increased oxidative stress, PeroxyTCM-1 exhibited a dose-dependent increase in cell viability in HeLa cells treated with exogenous H_2O_2, which is consistent with ROS protection.

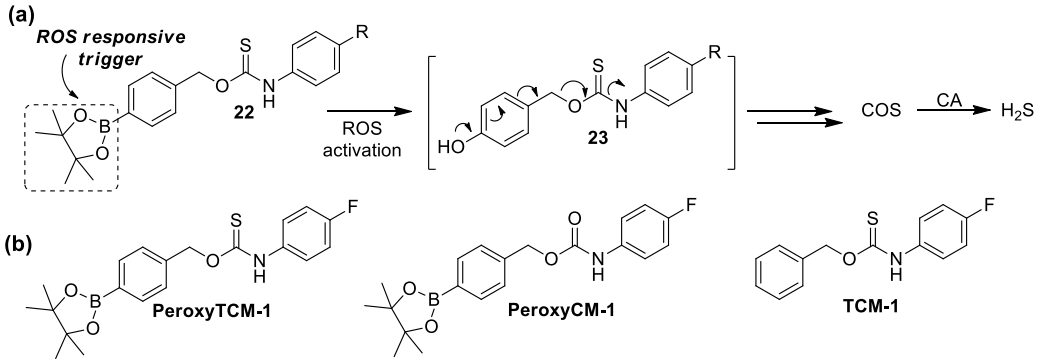

Figure 1.7 (a) Strategy for using ROS-responsive aryl boronates to access ROS-triggered COS/H_2S donors. (b) Structure of ROS-triggered COS donor PeroxyTCM-1 and control compounds PeroxyCM-1, which releases CO_2, and TCM-1, which lacks the ROS-activated trigger.

Importantly, the use of carbamate control compound PeroxyCM-1 or triggerless TCM-1 (Figure 1.7b) did not recapitulate the cytoprotective effects, suggesting that the observed cytoprotection was indeed due to the COS/H_2S release rather than from the organic scaffold or reaction byproducts. In addition, *in vitro* investigations also demonstrated that H_2O_2 can react directly with COS to generate H_2S, thus decreasing the need for CA and also highlighting the importance of COS as a potential ROS scavenger.

Bio-orthogonal COS Release (See Chapter III). COS donors triggered through bio-orthogonal methods have also been reported. One advantage of this approach is that the donor constructs are stable until exposure to a benign external stimulus and release COS without the need for a detrimental cellular trigger. Additionally, bio-orthogonal methods allow for the potential of high spatial and temporal resolution, as evidenced by the utility of such strategies for targeted drug delivery.[142, 143] For example, incorporation of a COS-releasing thiocarbamate into the cyclooctene reaction partner of the inverse-electron demand Diels-Alder (IEDDA) click reaction between cyclooctenes and tetrazines[144-146] enabled access to "click-and-release" COS donors (Figure 1.8).[147] The initial cyclooctene-tetrazine click reaction generates a thiocarbamate-functionalized dihydropyridazine (**26**), which after spontaneous tautomerization, deprotonation, and rearomatization releases the cyclooctylpyridazine product (**29**), benzylamine, and COS. Direct COS release was confirmed by GC-MS, and H_2S production was observed after incubation with CA. Although preliminary biological compatibility was demonstrated in

whole blood and plasma, further biological investigations and applications are needed to establish the fidelity of this platform in more complex contexts and to improve on the efficiency and rate of COS release.

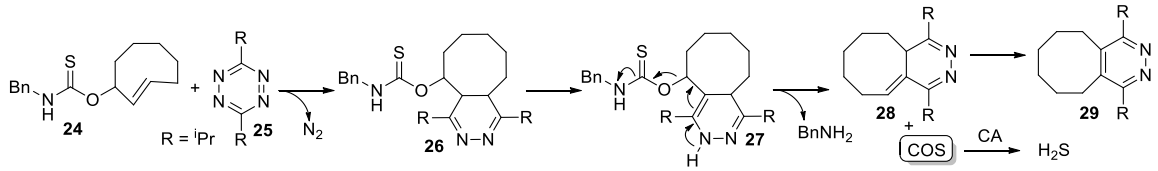

Figure 1.8 Bio-orthogonal COS donors based on the IEDDA click reaction.

1.5.3 Continuous/Passive Release of COS

A complementary approach to access caged COS donors is to develop continuous release COS donors, which are activated by ubiquitous cellular nucleophiles or enzymes. Such donors would result in continuous, rather than triggered, COS release, thus increasing basal COS levels in an otherwise normal physiological environment. Similar to well-known hydrolytically-activated donors for NO and H_2S,[148, 149] these compounds are likely to contribute to an important class of tools for investigating COS chemical biology.

Nucleophile activation. Matson and co-workers recently investigated *N*-thiocarboxyanhydrides (NTAs, Figure 1.9a) as COS-releasing molecules.[150] These electrophiles release COS upon reaction with nucleophiles, and are analogous to the thiocarboxyanhydrides proposed by Hirschmann in studies of peptide couplings (**9**, Figure 1.4).[104] In these scaffolds, COS release likely occurs through initial formation of an thiocarbamate intermediate (**30**) akin to those observed by Ghadiri and co-workers in COS-mediated peptide forming reactions (Figure 1.9b).[46] After preparing small molecule (NTA1) and polymeric (polyNTA1) derivatives (Figure 1.9a), GC-MS experiments confirmed that the NTA derivatives release COS in the presence of mild biological nucleophiles, such as glycine. As further evidence of COS formation, the addition of CA resulted in H_2S formation, which was confirmed using an H_2S-responsive electrode. Because alkylthiocarbamates similar to **30** have been used previously as efficacious CA inhibitors,[151] fine tuning of the structure of NTA derivatives and the resultant thiocarbamate intermediates may enable further tuning of rates of COS hydrolysis to H_2S.

Cell culture investigations demonstrated the ability of NTA1, but not polyNTA1, to promote cell proliferation in brain-derived endothelial cells at levels akin to that observed by treatment with NaSH. As a whole, these continuous release NTA platforms provide a simple scaffold for further modifications based on the simplicity of the COS-releasing core and offer the benefit of innocuous peptide byproducts after COS release.

Ubiquitous enzyme activation. Complementing COS donors that function by reaction with bioavailable nucleophiles, Chakrapani and co-workers recently reported thiocarbamate (**32**) and thiocarbonate (**33**) containing COS-donor motifs responsive to ubiquitous cellular esterases.[152] Leveraging the design strategies outlined in sections 5.1-2, installation of an ester functional group, which is cleaved by intracellular esterases,[153] generates a phenolic intermediate (**34**) that initiates the subsequent self-immolative collapse to extrude COS (Figure 1.9c). Esterase-mediated release of COS and subsequent conversion to H_2S by CA was confirmed *in vitro* using both the methylene blue (MB) assay and also an H_2S-responsive electrode. COS/H_2S release was also confirmed in MCF-7 cells using the H_2S-responsive probe NBD-fluorescein.[154] One difference of these platforms from those outlined in sections 5.1-2 is the use of an *S*-alkylthiocarbamate rather than an *O*-alkylthiocarbamate, as well as investigation into COS/H_2S release from thiocarbonates in addition to thiocarbamates. Preliminary mechanistic investigations suggest that the choice of thiocarbamate versus thiocarbonate may impact the rate limiting step of COS extrusion, thus providing a pathway for further control and tuning of reaction kinetics and release profiles.

1.5.4 Outstanding Questions

Although the recent introduction of a variety of COS donor compounds provides simple ways to introduce exogenous COS into biological samples, the direct CA-mediated metabolism of COS to H_2S represents a significant challenge in differentiating the biological actions of COS from those associated with H_2S. Additionally, because COS metabolism by CA generates CO_2/HCO_3^- in addition to H_2S, it is important to consider the total amount of COS metabolized in a system to ensure buffering capacities are not exceeded by these otherwise innocuous products. Answers to such questions will

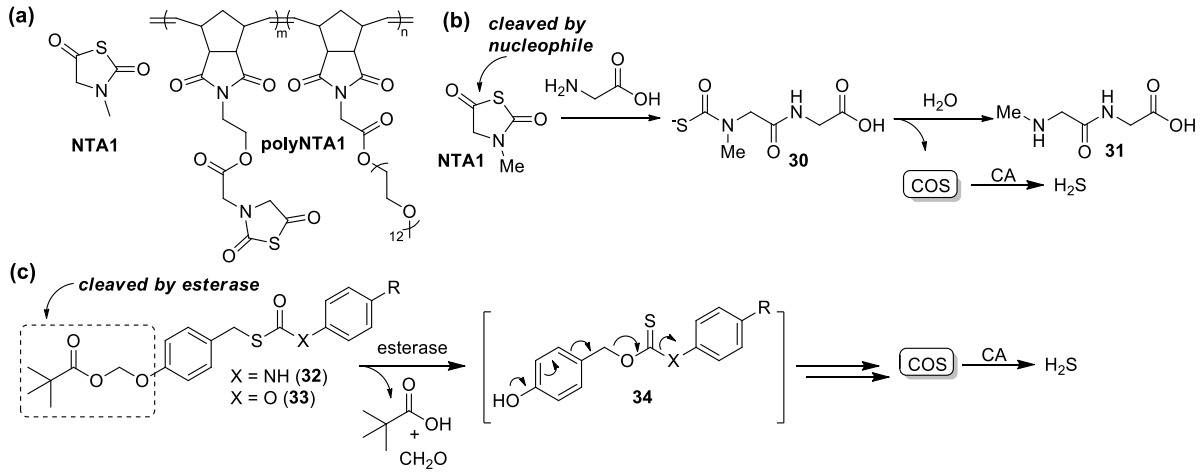

Figure 1.9 Continuous-release COS donors including (a) *N*-thiocarboxyanhydride (NTA) COS-releasing molecules NTA1 and polyNTA1. (b) Proposed mechanism of COS release from NTA-based donors. (c) Esterase-cleaved COS donors and associated mechanism of COS release.

likely require thoughtful and careful applications of available H_2S and COS donors used in concert to investigate specific biomolecular questions. Whether available COS donors function merely as clever sources of biological H_2S, or whether the released COS imparts different outcomes in biological contexts remains to be determined. If realized, COS-releasing molecules that provide outcomes distinct from those attributed to available H_2S donors will likely play a significant role in assessing the and advancing not only the role of COS as a potential gasotransmitter, but also its role in potential therapeutic applications associated with human health.

1.6 Conclusions

Key challenges remain in further elucidating the chemical biology of COS, but our current, albeit limited, understanding of the biological production and consumption of COS suggests that it may play diverse roles. Could COS be poised to be the next on the list of established gasotransmitters? This distinction will first require identification of enzymatic COS production in higher organisms and evidence that COS and H_2S function independently. It is also possible that COS functions primarily as a source of 'caged' H_2S that is liberated by CA metabolism. Such a pathway is intriguing because it would provide a source of reduced sulfur that is not ionizable through acid-base equilibria at physiological pH, and that is less susceptible to ambient or enzymatic oxidation through

direct action of oxidases or sulfur:quinone oxidoreductase (SQR),[155] thus bypassing interaction with the sulfane-sulfur pool.[156] Additionally, the neutral state of COS could enable distribution to locales that would otherwise be challenging for H_2S/HS^- alone. Finally, there is compelling evidence that COS stems from bacterial generation, especially in certain disease pathologies. In these cases, COS could provide a transport mechanism from pathogen to host. Even if eukaryotic COS synthesis is not a major source of endogenous COS, a thorough understanding of the role that COS plays in these diseases will likely be beneficial in early detection and treatment. When viewed more broadly, the absence of well-established metabolic pathways for COS formation in eukaryotic systems paired with the presence of COS-producing pathways from simple and abundant sulfur sources by a variety of bacteria may paint a broader, yet fundamentally underexplored picture of the COS functions in sulfur biology and transport.

In this dissertation, I report novel chemical tools for studying COS and H_2S chemical biology through the development of self-immolative thiocarbamates that can be triggered to release COS by a variety of stimuli. In Chapter II, I describe the first report of this strategy, initially established to address a significant problem in reaction-based detection of H_2S: consumption of the analyte. In Chapters III and IV, I expand the library of thiocarbamate-based, COS-releasing scaffolds and report two novel H_2S donation strategies: bioorthogonally-activated and cysteine-selective. In Chapters V and VI, I adapt this COS-releasing motif to develop H_2S donors that are activated by ubiquitous enzymes, and in the process reveal unexplored physiological properties of COS itself. Finally, in Chapter VII, I survey a wide-range of scaffolds that could be used as COS-releasing core motifs for cytotoxicity and CA inhibition and suggest ideal structures for researchers developing COS donors. Chapters II through VII contain both unpublished and previously published, coauthored material as is specified at the start of each chapter.

CHAPTER II

SELF-IMMOLATIVE THIOCARBAMATES PROVIDE ACCESS TO TRIGGERED H_2S DONORS AND ANALYTE REPLACEMENT FLUORESCENT PROBES

This chapter includes previously published and coauthored material from Steiger, A.K.; Pardue, S.; Kevil, C.G.; Pluth, M.D. "Self-Immolative Thiocarbamates Provide Access to Triggered H_2S Donors and Analyte Replacement Fluorescent Probes" *J. Am. Chem. Soc.* **2016**, 138, 7256-7259.

2.1 Introduction

The advent of chemical tools to probe and manipulate biochemical processes has revolutionized how biological processes are investigated.[157-159] Spawning from initial investigations into fluorescent proteins,[160, 161] small molecule fluorescent reporters now comprise a key pillar of investigative chemical biology with a remarkable diversity of fluorescent tagging and measurement technologies.[162, 163] Recent years have witnessed a significant expansion of sensor development to include chemical tools for imaging different transition metal, alkali, and alkali earth ions.[164-166] Many of these sensors provide real-time, quantitative measurements of ion fluxes due to the reversible interaction of the sensor with the analyte, thus providing methods for imaging the dynamic process of metal ion trafficking associated with signaling events ranging from Ca^{2+} sparks during muscle contraction[167] to Zn^{2+} fluxes during mammalian egg fertilization.[168] Complementing such investigative tools are small molecule donors that release caged analytes at controllable rates.[124, 169-171] Such platforms provide powerful methods to control levels of specific analytes, which often include pro-drugs, metal ions, or small reactive sulfur, oxygen, and nitrogen species (RSONS), in different biological contexts.

In the last two decades, RSONS have emerged as important bioinorganic molecules involved in myriad biological processes, many of which have been elucidated by utilizing chemical tools for small molecule detection and delivery. RSONS are

involved in the complex cellular redox landscape and are often involved in oxidative stress responses, immune responses and signaling pathways, as well as other emerging roles.[172] For example, NO, HNO, and $ONOO^-$ play important roles ranging from smooth muscle relaxation to immune response[173] and are largely intertwined with reactive oxygen species, such as O_2^- and H_2O_2, which are critical in oxidative stress responses and have been implicated in various aging mechanisms.[174] Similarly, reactive sulfur species, such as H_2S, hydropolysulfides ($HS_{n>1}^-$), and persulfides (RSSH) have recently garnered interest as important signaling molecules with roles in long term potentiation and cardiovascular health.[2] By contrast to their metal ion counterparts, RSONS are often fleeting nature and often react irreversibly with cellular targets. This heightened reactivity has provided chemists with significant challenges in developing constructs that can release these molecules under controlled conditions, but have also provided different strategies to devise chemical tools for their detection by engineering reactive groups onto sensing platforms that react selectively albeit irreversibly with the analyte of interest.[175]

Although small molecule donors and reaction-based probes have provided significant insights into the roles of RSONS in biology, key needs remain. For example, engineering donors with precise but modifiable triggers to enable analyte release in response to specific stimuli and developing reaction-based probes that do not irreversibly consume the analyte would enable new insights into RSONS biology. Motivated by these needs, as well as our interest H_2S chemistry, we report here a new caged H_2S releasing strategy and provide proof-of-concept applications in both small-molecule donor and reaction-based probe design. By leveraging triggerable self-immolative thiocarbamates, we demonstrate access to easily-modifiable H_2S donors that can be triggered by external stimuli (Figure 2.1a), and address common issues of analyte consumption in reaction-based fluorescent probes (Figure 2.1b) by developing analyte-replacement reaction-based platforms (Figure 2.1c).

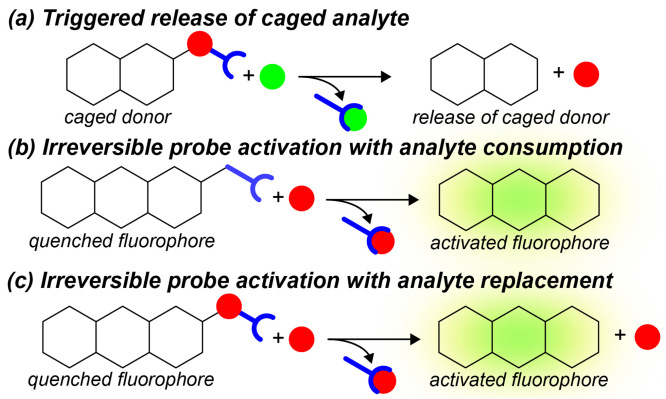

Figure 2.1 (a) Caged donors triggered by different stimuli. (b) Reaction-based probes typically consume the target analyte. (c) Analyte-replacement reaction-based probes enabled by incorporation of caged analytes into reaction-based motifs.

2.2 Results and Discussion

Development of analyte-replacement sensing platforms requires two important components: a versatile H_2S donation motif that releases H_2S in response to a specific triggering event and a method to couple this caged donor to a reaction-based sensing platform with an optical output. As a proof-of-concept design toward this objective, we chose to use H_2S-mediated azide reduction for our sensing platform, which has emerged as the most common method for H_2S detection and exhibits high selectivity for H_2S over other RSONs (Figure 2.2a).[176] Although a number of H_2S-donating motifs have been reported and have found utility as important research tools,[122-124] none of these fit the design requirement of our approach. To develop an H_2S donating motif compatible with our design requirements, we reasoned that common strategies in drug and fluorophore release, namely the self-immolative cascade decomposition of *para*-functionalized benzyl carbamates (Figure 2.2b),[132, 133, 177] could be modified to enable triggered H_2S release. Because self-immolative carbamates release an amine-containing payload and extrude CO_2 as a byproduct, we reasoned that replacing the carbonyl oxygen with a sulfur atom to generate a thiocarbamate would result in carbonyl sulfide (COS) rather than CO_2 release (Figure 2.2c). In a biological environment, COS is quickly hydrolyzed to H_2S and CO_2 by carbonic anhydrase (CA), which is a ubiquitous enzyme present in plant and mammalian cells.[42, 110] The second byproduct of the thiocarbamate self-immolation is a reactive quinone methide, which rapidly rearomatizes upon reaction with available nucleophiles, such as water or nucleophilic amino acids such as cysteine.[178, 179] On the basis of the

requirements outlined above, we expected that a quenched fluorophore could be functionalized with a *p*-azidobenzylthiocarbamate to enable H_2S-mediated azide reduction to form the transient aryl amine intermediate, which would subsequently undergo the self-immolative cascade reaction to extrude COS/H_2S and liberate the fluorophore to access an analyte-replacement sensing motif (Figure 2.2d).

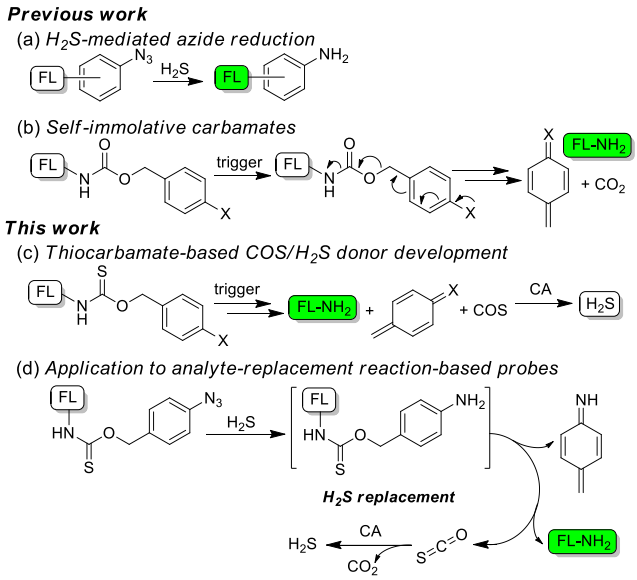

Figure 2.2 Established strategies for (a) H_2S-mediated azide reduction and (b) self-immolative carbamates to deliver an amine-bound fluorophore. Incorporation of self-immolative thiocarbamates enables access to (c) triggered H_2S donors, and (d) analyte replacement probes.

To confirm that the COS could serve as a potential source of H_2S donation, we first established that independently prepared COS could be efficiently hydrolyzed to H_2S by CA. Upon addition of COS gas to deoxygenated aqueous buffer (PBS, 1 mM CTAB, pH 7.4) containing CA from bovine erythrocytes, we observed rapid H_2S production using an H_2S-responsive electrode. In the absence of CA, negligible current was observed from COS alone, which is consistent with slow and pH-dependent, nonenzymatic hydrolysis in water (Figure A4).[180] We also observed a dose-dependent reduction in H_2S production upon addition of the CA inhibitor acetazolamide (AAA),[108] which confirmed the enzymatic hydrolysis of COS by CA (Figure 2.3).

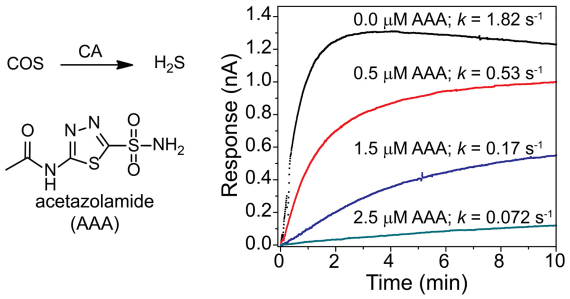

Figure 2.3 Conversion of COS to H_2S by carbonic anhydrase (CA) with varying concentrations of CA inhibitor acetazolamide (AAA) in PBS buffer, pH 7.4.

We next prepared model thiocarbamates to confirm that the proposed decomposition cascade to release COS occurs efficiently and to demonstrate the biological compatibility of this donor motif. We incorporated an azide in the *para* position of the benzylthiocarbamate to function as the H_2S-responsive trigger for self-immolation and COS release. To facilitate NMR identification of the products, we first prepared azidobenzylthiocarbamate **1** with a *p*-fluoroaniline payload, and the corresponding carbamate **2** as a control compound (Figure 2.4a-c). Although **2** should undergo the same self-immolative decomposition upon azide reduction, it releases CO_2 rather than COS, and thus should not donate H_2S upon reaction with CA. To monitor the reactivity of the model compounds under controlled reaction conditions, we used *tris*(2-carboxyethyl)phosphine (TCEP), an azide-reducing agent, to trigger self-immolation, due to its near-instantaneous reduction of azides. In each case, ^{1}H, $^{13}C\{^{1}H\}$, and ^{19}F NMR spectroscopy was used to monitor the reaction after reduction of the model complexes by TCEP. Consistent with our design hypothesis, we observed the disappearance of the benzylic peak, loss of the thiocarbonyl carbon peak, and formation of new resonances upon self-immolation by NMR spectroscopy (Figure A1-A3). All such changes were observed within 5 minutes of TCEP addition, confirming the rapid self-immolation of the scaffold upon reduction, and were consistent with COS release from the thiocarbamate scaffold upon azide reduction.

Having confirmed that CA rapidly catalyzes COS hydrolysis, we next investigated the H_2S-donating ability of model compounds **1** and **2** under identical conditions. Monitoring thiocarbamate **1** in buffer containing CA did not result in H_2S formation, confirming that the thiocarbamates do not react directly with CA and that aryl

azides are stable in the presence of CA (Figure A5). Upon injection of TCEP, however, rapid release of H_2S was observed, indicating that azide reduction to an amine is essential to trigger self-immolation and COS release. Additionally, repeating the experiment with added AAA significantly reduced the rate of H_2S production, confirming that uninhibited CA is required for significant H_2S production from the triggered thiocarbamate scaffold (Figure 2.4d). Finally, the analogous carbamate (**2**) was investigated under identical conditions, and as expected no H_2S was produced upon addition of TCEP, confirming that the sulfur-containing thiocarbamate is required for H_2S formation. In total, these experiments demonstrate the validity of using thiocarbamates as a triggerable source of H_2S release in aqueous solution, which we expect will prove fruitful for researchers interested in the pharmacological and physiological roles of sulfide donating molecules.[122, 123]

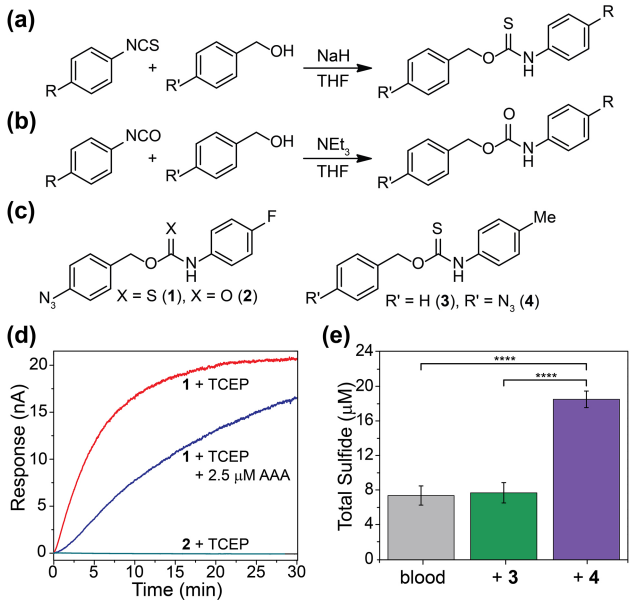

Figure 2.4 (a,b) Synthesis of model thiocarbamates and carbamates. (c) Model compounds. (d) H_2S release from **1** after reduction by TCEP in the presence of CA, under identical conditions with the addition of AAA (2.5 µM,), and from carbamate **2**. (e) Quantification of total sulfide in whole mouse blood after treatment 25 µM **3** and **4** after 30 min of incubation time in the presence of excess TCEP.

Expanding on our cuvette-based studies, we also investigated H_2S release from model thiocarbamates in whole mouse blood to expand on the efficacy of H_2S release from thiocarbamates in biologically-relevant contexts. Although murine systems provide

a convenient model, mice have among the lowest CA levels in mammals, with murine blood only containing about 15% of the CA present in human blood,[181] and thus represent a challenging target for sulfide release mediated by CA. To quantify total sulfide levels, we used the monobromobimane (mBB) method which allows for the analytical measurement of different sulfide pools and is compatible with many types of biological samples.[182] Measurement of the total sulfide, which includes free sulfide as well as bound sulfane-sulfur, revealed background levels of 8 μM, which are higher than total sulfide levels commonly observed and reported in plasma, but are consistent with the high sulfane-sulfur content in red blood cells.[183, 182] We prepared thiocarbamate 3, which lacks the azide trigger, to confirm that the thiocarbamate group was stable in whole blood and did not release COS without activation of the trigger group, and compared results obtained with this model compound with azide-functionalized **4**. Total sulfide levels were measured for each compound, as well as the control, after 30 minutes of incubation with excess TCEP (Figure 2.4e). Consistent with our expected results, only samples containing donor 4 with the azide trigger increased total sulfide levels in blood ($p \leq 0.0001$). These results establish the stability of the thiocarbamate in biological milieu and confirm that endogenous CA in murine blood, even though significantly lower than in most other biological environments,[181] is sufficient to hydrolyze the COS released from thiocarbamates after the self-immolation cascade is triggered, highlighting the efficacy of this H_2S-releasing strategy in biological environments.

Having confirmed the viability of triggered H_2S release with the model compounds, we next applied this design to incorporate a fluorophore to access an H_2S-responsive fluorescent probe that releases H_2S upon H_2S detection. Our primary goal was to demonstrate that the thiocarbamate group could be appended to common fluorophore motifs and efficiently quench the fluorescence. We chose to use the methylrhodol (MeRho)[184] fluorophore due to its high quantum yield and single fluorogenic amine, which could be readily converted into the desired thiocarbamate. Since the azide-functionalized scaffold would be triggered by H_2S to release both MeRho and COS, this would function as a fluorescent H_2S probe that would replenish sulfide through the release of COS. To access the desired scaffold, we treated MeRho with thiocarbonyldiimidazole (TCDI) and NEt_3 in DMF to afford methylrhodol isothiocyanate

(MeRho-NCS) in 60% yield. Subsequent treatment with 4-azidobenzyl alcohol and NaH afforded the methylrhodol thiocarbamate azide (MeRho-TCA) in 35% yield (Figure 2.5a). We note that one benefit of this simple synthetic route is that almost any fluorophore containing a fluorogenic nitrogen can be functionalized with the benzylazide thiocarbamate group, thus providing access to a diverse library of fluorophores.

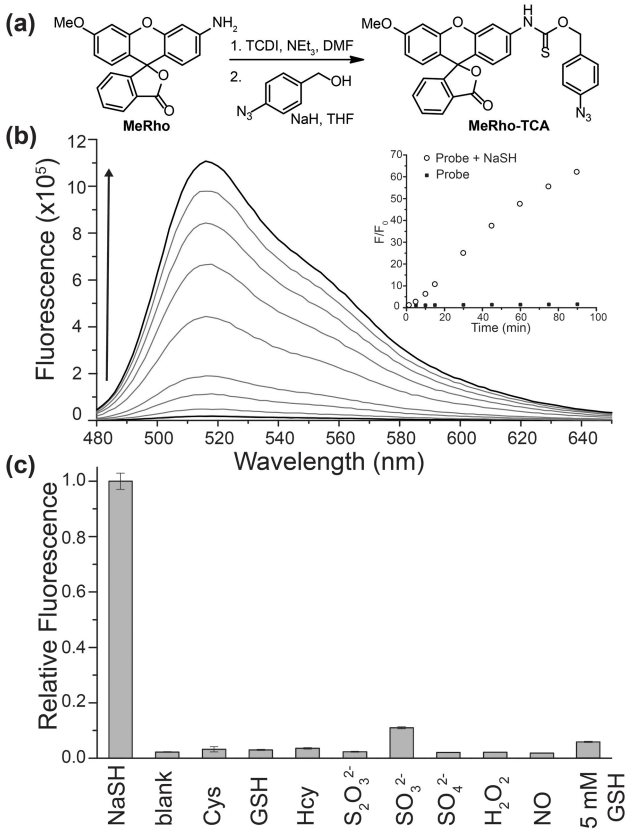

Figure 2.5 (a) Synthesis of MeRho-TCA. (b) Fluorescence response of MeRho-TCA to H_2S. Inset shows integrated fluorescence over time by comparison to MeRho-TCA in the absence of NaSH. (c) Selectivity of MeRho-TCA for H_2S over other RSONs. Conditions: 5 μM probe, 250 μM RSONs unless noted otherwise, in PBS buffer, 1 mM CTAB, pH 7.4, 37 °C. λ_{ex} = 476 nm, λ_{em} = 480-650 nm.

With a sulfide-replenishing H_2S probe in hand, we investigated the fluorescence response upon addition of sulfide. Treatment of MeRho-TCA with 50 equiv. of NaSH in aqueous buffer (PBS, 1 mM CTAB, pH 7.4) resulted in a 65-fold fluorescence turn-on over 90 minutes (Figure 2.5b). Additionally, we confirmed that the MeRho-TCA scaffold was selective for HS^- over other RSONs, by measuring the fluorescence response to Cys,

GSH, Hcy, $S_2O_3^{2-}$, SO_3^{2-}, SO_4^{2-}, H_2O_2, and NO (Figure 2.5c). As expected, the MeRho-TCA scaffold exhibited excellent selectivity for sulfide over other RSONs, demonstrating that the thiocarbamate linker group did not erode the selectivity of the azide trigger, and also establishing that the MeRho-TCA scaffold can function as a viable H_2S reporter. Because MeRho-TCA releases H_2S upon reaction with H_2S, we note that one consequence of this analyte replacement approach is that the resultant fluorescence response is not directly proportional to the initial H_2S concentration. Additionally, in isolated systems, two equiv. of HS^- are required for complete azide reduction, suggesting that the first-generation analyte-replacement scaffolds only replace one half of the consumed sulfide.[185] It is also possible, however, that in biological media one equiv. of a thiol may play a role in H_2S-mediated azide reduction, which remains a question for future investigations. In the present system, preliminary mechanistic investigations indicate that H_2S-mediated azide reduction is the rate-limiting step of the self-immolative process, and that the subsequent release of COS and hydrolysis by CA to form H_2S is rapid. Taken together, these data highlight the potential of this strategy to access analyte-replacement, reaction-based fluorescent scaffolds.

2.3 Conclusions

In summary, we have outlined and demonstrated a new strategy for triggered H_2S release based on self-immolative thiocarbamates. Importantly, this strategy provides solutions to key challenges associated with both H_2S delivery and detection. Thiocarbamate-based H_2S donors provide a new, versatile, and readily modifiable platform for developing new H_2S donor motifs that can be triggered by endogenous or biorthogonal triggers. Similarly, this same H_2S donation strategy can be coupled to fluorescent probe development to access reaction-based fluorescence reporters that replace the analyte that has been consumed by the detection event. In a broader context, we expect that the self-immolative thiocarbamate donors will find significant utility as a potential platform for academic and potentially therapeutic H_2S donors. The following Chapters will show numerous examples of self-immolative thiocarbamates as triggerable COS/H_2S donors activated by a variety of stimuli. In Chapter III, we report the first

example of a bio-orthogonal H_2S donor using a self-immolative thiocarbamate to release COS upon activation.

2.4 Experimental Details

2.4.1 Materials and Methods

Reagents were purchased from Sigma-Aldrich or Tokyo Chemical Industry (TCI) and used as received. *p*-Azidobenzylalcohol,[186] *O*-(4-azidobenzyl)-*N*-tolylthiocarbamate,[187] methylrhodol,[184] and COS gas[49] were synthesized as previously reported. Spectroscopic grade, inhibitor-free THF was deoxygenated by sparging with argon followed by passage through a Pure Process Technologies solvent purification system to remove water and then stored over 4Å molecular sieves in an inert atmosphere glove box. Deuterated solvents were purchased from Cambridge Isotope Laboratories and used as received. Silica gel (SiliaFlash F60, Silicycle, 230-400 mesh) was used for column chromatography. Preparatory chromatography was performed on Silicycle SiliaPlates (1 mm thickness). ^{1}H, $^{13}C\{^{1}H\}$, and ^{19}F NMR spectra were recorded on a Bruker 600 MHz instrument. Chemical shifts are reported in ppm relative to residual protic solvent resonances. H_2S electrode data were acquired with a World Precision Instruments (WPI) ISO-H2S-2 sensor connected to a TBR4100 Free Radical Analyzer. Fluorescence spectra were obtained on a Quanta Master 40 spectrofluorometer (Photon Technology International) equipped with a Quantum Northwest TLC-50 temperature controller at 37.0 ± 0.05 °C. UV-visible spectra were acquired on a Cary 100 spectrometer equipped with a Quantum Northwest TLC-42 dual cuvette temperature controller at 37.00 ± 0.05 °C. All air-free manipulations were performed under an inert atmosphere using standard Schlenk techniques or an Innovative Atmospheres N_2-filled glove box.

Spectroscopic Materials and Methods. Phosphate buffered saline (PBS) tablets (1X, CalBioChem) and cetyl trimethylammonium bromide (CTAB) were used to make buffered solutions (PBS, 140 mM NaCl, 3 mM KCl, 10 mM phosphate, 1 mM CTAB, pH 7.4) in Millipore water. Buffer solutions were sparged with N_2 to remove dissolved oxygen and stored in an N_2-filled glovebox. Anhydrous sodium hydrosulfide (NaSH) was purchased from Strem Chemicals and handled under nitrogen. Aqueous stock solutions of

NaSH were prepared in buffer in an N_2-filled glovebox immediately prior to use. Stock solutions of MeRho-TCA were prepared in an N_2-filled glovebox in DMSO and stored at -25 °C until immediately before use. Septum-sealed cuvettes from Starna Scientific were used to obtain spectroscopic measurements under anaerobic conditions.

H_2S Electrode Materials and Methods. Phosphate buffered saline (PBS) tablets (1X, CalBioChem) and cetyl trimethylammonium bromide (CTAB) were used to make buffered solutions (PBS, 140 mM NaCl, 3 mM KCl, 10 mM phosphate, 1 mM CTAB, pH 7.4) in Millipore water. Buffer solutions were sparged with N_2 to remove dissolved oxygen and stored in an N_2-filled glovebox. Carbonic anhydrase (CA) from bovine erythrocytes (≥3,500 W/A units/mg) was obtained from Sigma Aldrich and a 1% CA stock solution was prepared in deoxygenated buffer (50 mM PIPES, 100 mM KCl, pH 7.4) in a glovebox, and the absorbance at 280 nm (1 cm path length cuvette) at 37 °C was measured to be 3.825. The concentration of the stock solution was calculated to be 67 μM using $\varepsilon_{280}^{1\%} = 19$ for CA.[188] The stock solution was stored under nitrogen at 4 °C and warmed to room temperature immediately before use. Stock solutions of *tris*(2-carboxyethyl)phosphine (TCEP) and acetazolamide (AAA) were prepared under N_2 with degassed buffer (PBS, pH 7.4) immediately prior to use. Thiocarbamate and carbamate stock solutions were prepared in an N_2-filled glovebox in DMSO and stored at -25 °C until immediately before use.

General Procedure for H_2S Electrode Experiments. Scintillation vials containing 20.00 mL of phosphate buffer (140 mM NaCl, 3 mM KCl, 10 mM phosphate, 1 mM CTAB, pH 7.4) were prepared in an N_2-filled glovebox. A split-top septum cap was placed on the vial after probe insertion and the headspace was sparged with N_2. The WPI electrode was then inserted into the vial and the measured current was allowed to equilibrate before starting the experiment. With moderate stirring, the CA stock solution (50 μL, 67 μM) was injected, followed by subsequent injections of acetazolamide (10-50 μL of a 10 mM stock solution in PBS buffer), COS gas (10 μL, 0.345 μmol), TCA stock solution (10 mM in DMSO), or TCEP stock solution (10 mM in PBS buffer).

General Procedure for Fluorescence Measurements. In an N_2-filled glovebox, a septum-sealed cuvette was charged with 3.00 mL of buffer (140 mM NaCl, 3 mM KCl, 10 mM phosphate, 1 mM CTAB, pH 7.4). The cuvette was removed from the glovebox and MeRho-TCA (60 μL of a 1 mM stock solution) was injected into the vial, after which a background spectrum was recorded. The desired analytes were then introduced, and the fluorescence spectrum was measured at designated time points.

General Procedure for Measurement of Total Sulfide in Mouse Blood. Mice were maintained at the association for assessment and accreditation of laboratory animal care international-accredited Louisiana State University Health Science Center - Shreveport animal resource facility and maintained in accordance with the National Research Council's guide for care and use of laboratory animals. All animal studies were approved by the institutional animal care and use committee (protocol P-12-011) and conformed to the guide for the care and use of laboratory animals published by the National Institutes of Health. Mice were anesthetized by IP injection with 150 mg/kg ketamine and 10 mg/ kg xylazine. Mouse whole blood was collected from the retroorbital capillary plexus from three C57BL/6J male mice and diluted 1:50 in PBS (phosphate buffered saline pH 7.4) or red blood cell lysing buffer (Sigma, St Louis). Samples were treated with either **3** or **4** at a final concentration of 25 μM. A separate set of blood samples were left untreated and used for baseline sulfide measurements. Once mixed with either compound **3** or **4**, half of each sample was treated with 10 mM TCEP (tris(2-carboxyethyl)phosphine hydrochloride) for 30 minutes while the other half remained untreated. Sulfide bioavailability was subsequently measured in all samples using the MBB method as previously reported.[182, 189, 190]

2.4.2 Syntheses

General procedure for the preparation of thiocarbamates. Sodium hydride (60% in oil, 1.25 mmol) was added to a solution of the isothiocyanate (1 mmol) and the benzyl alcohol (1 mmol) in anhydrous THF (6-12 mL). The reaction mixture was stirred at room temperature under nitrogen for 18 hours. After the solvent was removed under reduced pressure, CH_2Cl_2 was added, and the resulting solution was washed with water and brine.

The organic layer was dried over sodium sulfate and filtered. The solvent was removed by rotary evaporation and the crude product was purified using either column chromatography (hexanes:EtOAc gradient) or silica gel preparatory thin layer chromatography (3:2 hexanes:EtOAc).

O-(4-Azidobenzyl)-N-(4-fluorophenyl)thiocarbamate ***(1).*** Purification via preparatory TLC (3:2 hexanes/EtOAc) yielded the product as a pure white solid (107.9 mg, 35% yield). ^{1}H NMR (600 MHz, DMSO-d_6) δ (ppm): 7.23-7.50 (m, 4H), 7.06-7.13 (m, 4H), 7.44-7.48 (br s, 2H). Two rotomers were observable by ^{13}C{^{1}H} and ^{19}F NMR: ^{13}C{^{1}H} NMR (150 MHz, DMSO) δ (ppm): 189.4 (187.9 minor), 161.3 (159.7 minor), 140.6 (d, *J*=15.4 Hz), 135.4 (134.3 minor), 133.7 (133.0 minor), 126.8 (125.5 minor), 120.1 (130.9 minor), 116.5 (m), 71.0 (72.7 minor). ^{19}F NMR (470 MHz, DMSO-d_6) δ (ppm): -115.9 (-116.4 minor). FTIR (ATR, cm^{-1}): 3199, 3039, 2109, 1607, 1543, 1503, 1404, 1339, 1280, 1220, 1168, 1014, 857, 787, 658.

O-(4-Azidobenzyl)-N-(4-fluorophenyl)carbamate ***(2).*** *p*-Azidobenzyl alcohol (57.5 mg, 0.386 mmol) and NEt_3 (54 mL, 0.39 mmol) were combined in dry THF (2 mL), and 4-fluorophenylisocyanate (44 mL, 0.39 mmol) was added dropwise. The reaction mixture was stirred under nitrogen at room temperature and shielded from light for 24 hours. The solvent was evaporated under reduced pressure, and the crude product was purified by preparatory TLC (2:1 hexanes/EtOAc) to yield the pure product as a white solid (61.8 mg, 56%). ^{1}H NMR (600 MHz, DMSO-d_6) δ (ppm): 9.79 (s, 1H), 7.48-7.44 (m, 4H), 7.10-7.15 (m, 4H), 5.12 (s, 2H). ^{13}C{^{1}H} NMR (150 MHz, DMSO-d_6) δ (ppm): 158.4, 156.9, 153.4, 139.2, 135.4, 133.5, 130.0, 119.2, 115.4 (d, *J*= 22.2 Hz), 65.2. ^{19}F NMR (470 MHz, DMSO-d_6) δ (ppm): -120.82. HRMS (*m/z*): $[M + Na]^+$ calcd for $[C_{14}H_{11}FN_4O_2Na]^+$ 309.0764, found 309.0601.

*O-(4-Benzyl)-N-tolylthiocarbamate (**3**).* Purification via column chromatography (hexanes/EtOAc gradient) yielded the product as a pure white solid (173.7 mg, 68%). ^{1}H NMR (600 MHz, DMSO-d_6) δ (ppm): 11.11 (s, 1H), 7.57-7.44 (m, 2H), 7.43-7.32 (m, 4H), 7.23-7.06 (m, 3H), 5.49-5.58 (br s, 2H), 2.26 (s, 3H). ^{13}C{^{1}H} NMR (150 MHz,

DMSO-d_6) δ (ppm): 187.4, 186.8, 136.0, 135.6, 135.1, 134.4, 134.0, 129.2, 128.8, 128.4, 128.3, 128.2, 128, 122.9, 121.2, 72.0, 70.3, 20.4. HRMS (*m/z*): $[M + H]^+$ calcd for $[C_{15}H_{16}NOS]^+$ 258.0953, found 258.0948.

Methylrhodol-isothiocyanate ***(MeRho-NCS).*** Methylrhodol (200 mg, 0.577 mmol) and NEt_3 (480 µL, 3.46 mmol) were combined in dry DMF (2 mL) in oven-dried glassware. Thiocarbonyldiimidazole (TCDI, 211 mg, 1.16 mmol) was dissolved in dry DMF (6 mL) and added dropwise to the solution. The reaction mixture was stirred under nitrogen at room temperature for 24 hours then quenched with water. The organic layer was extracted with EtOAc, washed three times with aqueous LiCl (5%, 20 mL), dried over $MgSO_4$, and the solvent was evaporated under reduced pressure. The crude product was purified using preparatory TLC on an oven-dried prep plate using dry hexanes:EtOAc (1:1) and isolated as a white solid (134 mg, 60%). ^{1}H NMR (600 MHz, $CDCl_3$) δ (ppm): 8.03 (d, *J*=7.5 Hz, 1H), 7.68 (t, *J*=7.4 Hz, 1H), 7.63 (t, *J*=7.5 Hz, 1H), 7.15-7.12 (m, 2H), 6.89 (dd, J_1= 8.5, J_2=2.1 Hz, 1H), 6.80-6.76 (m, 2H), 6.70 (d, *J*=8.8 Hz, 1H), 6.64 (dd, J_1= 8.9, J_2=2.5 Hz, 1H), 3.84 (s, 3H). ^{13}C{^{1}H} NMR (150 MHz, $CDCl_3$) δ (ppm): 169.3, 161.7, 153.0, 152.1, 151.9, 137.8, 135.4, 133.4, 130.2, 129.5, 129.2, 126.5, 125.4, 123.9, 121.4, 118.5, 114.2, 112.4, 110.8, 101.1, 82.2, 55.8. FTIR (ATR, cm^{-1}): 2922, 2852, 2017, 1761, 1607, 1563, 1495, 1416, 1324, 1247, 1099, 1079, 941. HRMS (*m/z*): $[M + H]^+$ calcd for $[C_{22}H_{13}NO_4SH]^+$ 388.0644, found 388.0471.

O-(4-Azidobenzyl)-N-methylrhodolthiocarbamate ***(MeRho-TCA).*** In oven-dried glassware, MeRho-NCS (134 mg, 0.346 mmol) was dissolved in dry THF (5 mL). p-Azidobenzylalcohol (150 mg, 1.00 mmol) was dissolved in dry THF (5 mL) and added to the solution of MeRho-NCS. Sodium hydride (60% in mineral oil, 18 mg, 0.45 mmol) was added and the reaction mixture was stirred at room temperature under nitrogen and protected from light for 24 hours. The solvent was evaporated under reduced pressure and the crude product was dissolved in EtOAc. The organic layer was washed with water and brine and dried over sodium sulfate. The product was purified by preparatory TLC (5% MeOH in DCM) while protected from light, to yield the pure product as a pale yellow solid (65 mg, 35%). ^{1}H NMR (600 MHz, $CDCl_3$) δ (ppm): 8.26 (br s, 1H), 8.02 (d, J=7.6

Hz, 1H), 7.67 (td, J_1=7.5, J_2=1.3 Hz, 1H), 7.62 (td, J_1=7.5, J_2=1.0 Hz, 1H), 7.43 (d, J=8.4 Hz, 2H), 7.14 (d, J=7.5 Hz, 1H), 7.05 (d, J=8.4 Hz, 2H), 6.78 (d, J=2.5 Hz, 1H), 6.73 (d, J=8.2 Hz, 1H), 6.69 (d, J=8.8 Hz, 1H), 6.62 (dd, J_1=8.8, J_2=2.5 Hz, 1H), 5.59 (br s, 2H), 3.84 (s, 3H). $^{13}C\{^1H\}$ NMR (150 MHz, $CDCl_3$) δ (ppm): 206.9, 169.3, 161.5, 152.9, 152.3, 151.7, 140.6, 135.1, 130.3, 129.9, 129.0, 128.8, 126.6, 125.1, 123.9, 119.3, 116.9, 115.9, 112.0, 110.9, 109.2, 100.9, 82.5, 55.6, 53.5, 30.9, 29.7, 29.3. HRMS (m/z): $[M + H]^+$ calcd for $[C_{29}H_{20}N_4O_5SH]^+$ 537.1233, found 537.0827.

CHAPTER III

BIO-ORTHOGONAL "CLICK-AND-RELEASE" DONATION OF CAGED CARBONYL SULFIDE (COS) AND HYDROGEN SULFIDE (H_2S)

This chapter includes previously published and coauthored material from Steiger, A.K; Yang, Y.; Royzen, M.; Pluth, M.D. "Bio-orthogonal "Click-and-Release" Donation of Caged Carbonyl Sulfide (COS) and Hydrogen Sulfide (H_2S)." *Chem. Commun.* **2017**, 53, 1378-1380.

3.1 Introduction

With the recent addition of hydrogen sulfide (H_2S) to the list of biologically-relevant gasotransmitters,[2] significant efforts have focused on developing H_2S donors as powerful research, and potentially therapeutic, tools.[122, 124] Available synthetic slow-release donors have already made major impacts in H_2S research, and several small molecule H_2S donors have already entered clinical trials.[123] Despite this promise, providing temporal control over H_2S release remains a major challenge, and there is significant interest in developing synthetic H_2S donors that are activated by well-defined triggering mechanisms that enable on-demand H_2S release.

Aligned with this need, we recently pioneered the use of carbonyl sulfide (COS)-releasing molecules as a strategy to access responsive H_2S donors. We demonstrated that self-immolative thiocarbamates can be triggered to decompose and release COS, which is rapidly converted to H_2S by the ubiquitous enzyme carbonic anhydrase (CA).[131] Analogous to the broad applications of self-immolative carbamates as delivery platforms for prodrugs, fluorophores, and other biologically-relevant payloads, thiocarbamates provide a highly tunable platform on which the triggering mechanism can be engineered to initiate self-immolation and COS release by specific analytes of interest. Since our initial report on caged COS/H_2S release, passive H_2S donation from small molecule and polymeric *N*-thiocarboxyanhydrides[150] as well as responsive ROS-triggered donors that provide protection against cellular oxidative stress have been reported.[140] Missing from current COS/H_2S donor technologies are platforms activated by bio-orthogonal triggers to

allow precise temporal control for H_2S release. Motivated by this need, we report here the first example of bio-orthogonal activation of COS/H_2S release through adaptation of the well-developed inverse-electron demand Diels-Alder (IEDDA) click reaction to release COS/H_2S (Scheme 3.1).

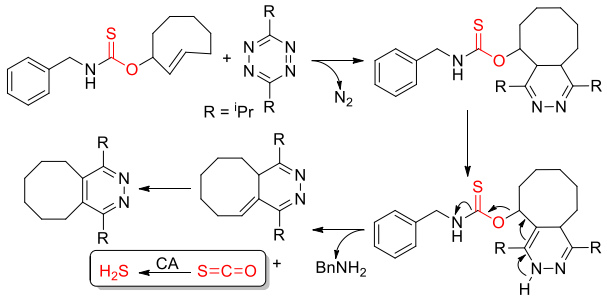

Scheme 3.1 IEDDA reaction of thiocarbamate-functionalized TCO **1** with tetrazine to generate COS/H_2S.

3.2 Results and Discussion

The IEDDA reaction between a *trans*-cyclooctene (TCO) and a tetrazine is a proven platform for bio-orthogonal click reactions in living systems.[144-146] In addition to providing an important biocompatible bond-forming tool, the IEDDA reaction has also been adapted for targeted drug release by using functionalized benzylic carbamates, which can be triggered to undergo self-immolative decomposition following the click reaction and subsequently release the attached drug, as well as CO_2 as a byproduct.[142, 191, 192] We envisioned that a similar strategy could be leveraged to develop a fully bio-orthogonal COS/H_2S releasing platform by using a benzylic thiocarbamate-functionalized TCO (Scheme 3.1). The initial IEDDA click reaction would generate the thiocarbamate-functionalized dihydropyridazine, which after tautomerization, deprotonation, and rearomatization can extrude COS, $BnNH_2$, and the cyclooctylpyridazine product. To test this hypothesis, we prepared TCO **1** by treating (E)-cyclooct-2-enol with benzyl isothiocyanate in the presence of NaH.[142] In parallel, we prepared the analogous carbamate-functionalized TCO **2**, which undergoes the same IEDDA reaction but releases CO_2 rather than COS (Scheme 3.2). Both TCO **1** and **2** are isolated as the axial isomer, which is estimated to be significantly more reactive than the analogous equatorial isomer.[193] Importantly, this design strategy provides simple synthetic access to both the thiocarbamate donor and key carbamate control compounds. Additionally, click-and-

release CO donors were recently reported utilizing an intramolecular Diels-Alder reaction, thus supporting the validity of our approach for accessing biorthogonal gasotransmitter release.[194]

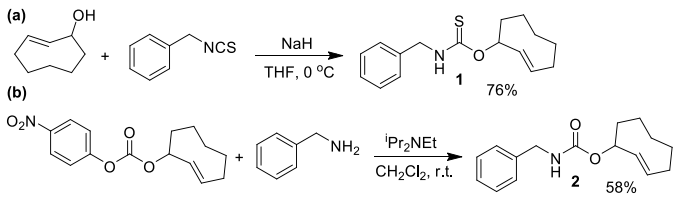

Scheme 3.2 Synthesis of thiocarbamate-functionalized COS/H_2S donor TCO **1** and the associated carbamate-functionalized control compound TCO **2**.

To confirm that the IEDDA reaction would initiate self-immolative decomposition of the thiocarbamate moiety, we monitored the reaction of **1** and 2 equiv. of bis-isopropyl-1,2,4,5-tetrazine in wet methanol-d_4 by ^{1}H NMR spectroscopy (Figure 3.1a). Within 5 minutes of tetrazine addition, we observed disappearance of the alkene peaks (5.3-5.7 ppm), indicative of cycloaddition. New resonances corresponding to $BnNH_2$ were subsequently observed at 4.25 ppm, while **1** continues to decompose over 24 hours. Due to the complexity of this reaction and the different potential intermediates that could be formed en-route to COS extrusion, we also monitored product formation by mass spectrometry. Consistent with our design hypothesis we observed the re-aromatized IEDDA product ($M+H^+$ 247.239), $BnNH_2$ ($M+H^+$ 108.091), and COS ($M+H^+$ 61.044) (Figure 3.1b,c) using direct analysis in real time mass spectrometry (DART-MS). Taken together, these data indicate that addition of the tetrazine to **1** results in the expected click reaction and initiates self-immolation of the thiocarbamate moiety, thus producing COS.

Having confirmed the fidelity of the IEDDA reaction, we next investigated click-and-release H_2S-donation from this system in aqueous buffer at physiological pH (PBS, pH 7.4) using an H_2S-selective electrode (Figure 3.2). Non-enzymatic background

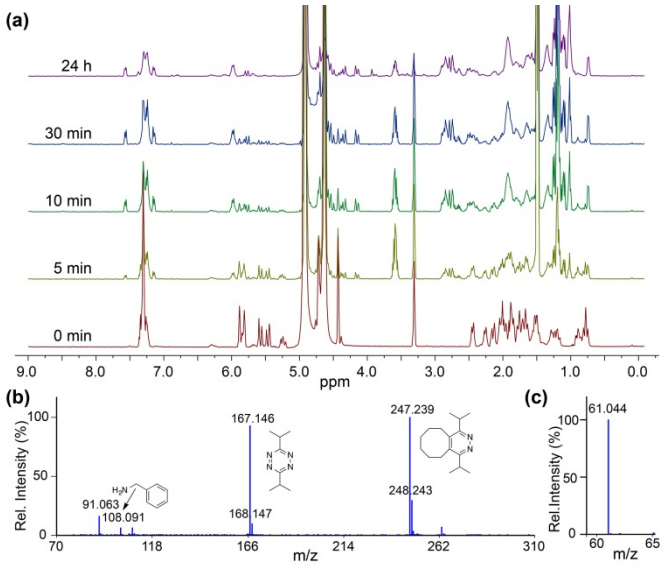

Figure 3.1 (a) ^{1}H NMR spectra of the reaction of **1** and tetrazine. (b) ESI-MS of reaction products, confirming self-immolation. (c) MS confirmation of COS formation.

hydrolysis of COS to H_2S is very slow at physiological pH, but is rapid in the presence of carbonic anhydrase (CA). Using biologically-relevant CA concentrations (25 μg/mL) we first monitored TCO **1** alone and confirmed that H_2S is not released spontaneously in the presence of CA. As anticipated, the bis-isopropyl-1,2,4,5-tetrazine alone also failed to produce an H_2S response. We next monitored H_2S release from TCO **1** (50 μM) with varying concentrations of tetrazine (5 – 25 equiv.) and observed increased H_2S production in the presence of excess tetrazine. Using a calibration curve, we measured 12 μM H_2S release from 50 μM TCO **1** with 25 equiv. of tetrazine, resulting in an H_2S release efficiency of approximately 25%. As additional confirmation of the importance of CA for H_2S formation, we performed identical reactions in the presence of acetazolamide (AAA, 2.5 μM), a known CA inhibitor. Furthermore, use of the control compound TCO **2** in the presence of excess tetrazine failed to generate COS/H_2S. Together, these data confirm that the IEDDA click reaction is necessary to generate COS, and that uninhibited CA is required for efficient conversion of this released COS to H_2S at physiological pH.

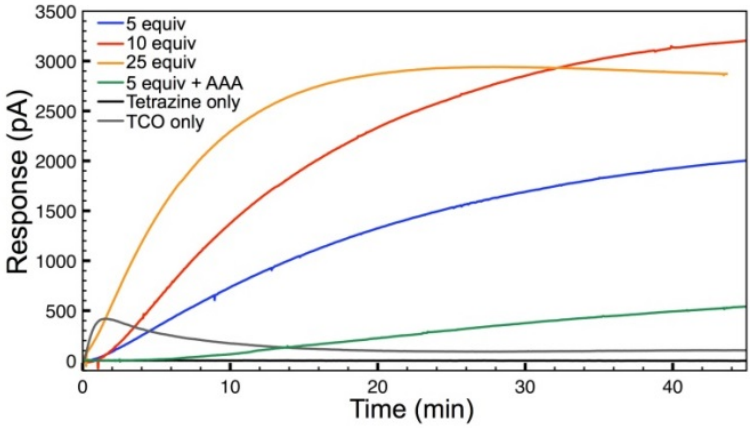

Figure 3.2 H_2S release profiles from TCO **1** (50 μM) with 5-25 equiv of tetrazine in the presence of CA (25 μg/mL) in buffer (PBS, pH 7.4).

To demonstrate the basic biological compatibility of the reaction, we also investigated H_2S release from TCO **1** (50 μM) with the tetrazine (500 μM) in complex media (Figure 3.3). For these experiments, we chose to use whole sheep and bovine blood due to the presence of CA. Using sheep blood and plasma, diluted 1:1 in PBS (pH 7.4) with no additional CA added, a similar H_2S release profile was observed using an H_2S-selective electrode. Additionally, H_2S production was also observed in diluted whole bovine blood, although the process was slower. These experiments confirm that bio-orthogonal click-and-release strategy has significant potential within a biological environment and endogenous CA levels are sufficient to allow for H_2S donation from the released COS. Additionally, we confirmed the cellular compatibility of TCO **1** using the CCK-8 cell viability assay, which indicated that concentrations up to 100 μM of TCO **1** are not cytotoxic in N2A neuroblastoma cells (Figure B1).

In an effort to expand this strategy to a cellular environment, we attempted to obtain cell images using a variety of fluorescent probes for H_2S, including HSN2, WSP-5, and SF7-AM.[141, 195, 196] Unfortunately, we found that the click-and-release reaction was not compatible with these current fluorescent detection strategies for H_2S. This observation was confirmed in cuvette-based fluorimetry studies as well, in which no fluorescent turn-on was observed after several hours despite the production of H_2S, as confirmed by H_2S-electrode experiments. Although unexpected, this outcome may be due to slower and/or less-efficient COS/H_2S release from this first-generation IEDDA platform than from previously reported COS/H_2S donors. In a closed system, it is also

possible that the tetrazine may also scavenge the generated H_2S, as evidenced by a recent report demonstrating that H_2S can partially reduce dialkoxy tetrazines to the dihydrotetrazine.[197] Therefore, future investigations into the differential reactivity of H_2S with substituted tetrazines appears warranted, both to increase the biocompatibility in this system and also to increase the initial efficiency of the IEDDA click reaction.[198] For example, demonstrated recent report highlighted that the efficiency of the IEDDA reaction can be improved through strategic choice of the tetrazine. These, as well as other modifications to the thiocarbamate scaffold are expected to provide much more efficient H_2S release from future click and release scaffolds.

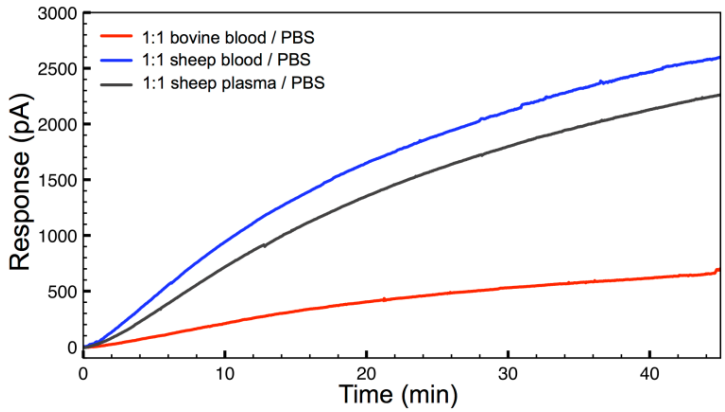

Figure 3.3 H_2S release profiles from TCO **1** (50 μM) with 10 equiv of tetrazine in whole bovine blood (red), whole sheep blood (blue), and sheep plasma (grey), diluted 1:1 with buffer (PBS, pH 7.4).

3.3 Conclusions

In summary, we have reported the first example of COS/H_2S donors activated by a bio-orthogonal trigger, which provides a significant step toward developing controllable H_2S donors with high temporal resolution. Given the novelty of this bio-orthogonal reaction in the field of sulfide donation, as well as the significant impact that similar click strategies have provided to adjacent fields in chemical biology, we anticipate that future optimization of this system will result in fast and highly targeted method for H_2S donation. In Chapter IV, we design a more generalized scaffold for COS/H_2S delivery using a self-immolative thiocarbamate activated by cysteine, a ubiquitous biothiol.

3.4 Experimental Details

3.4.1 Materials and Methods

All organic chemicals were purchased from Krackeler Scientific and used without further purification. Chromatographic purifications were conducted using SiliaSphere™ spherical silica gel 5μm, 60 Å silica gel (Silicycle). Thin layer chromatography (TLC) was performed on SiliaPlate™ silica gel TLC plates (250 μm thickness) purchased from Silicycle. ^{1}H and $^{13}C\{^{1}H\}$ NMR spectra were acquired a Bruker NMR instrument at 400 MHz (^{1}H) and 100 (^{13}C) MHz. Mass spectra were acquired using a DART-SVP ion source (IonSense, Saugus, MA, USA) coupled to a JEOL AccuTOF time-of-flight mass spectrometer (JEOL USA, Peabody, MA, USA) in positive ion mode. The DART ion source parameters were: grid voltage, 250 V; gas heater temperature, 350 °C. The mass spectrometer settings were: ring lens voltage, 5 V; orifice 1 voltage, 20 V; orifice 2 voltage, 5 V; peak voltage 600 V. Spectra were obtained at 1 scan per second. The helium flow rate for the DART source was 2.0 L s^{-1}.

H_2S Electrode Materials and Methods. Phosphate buffered saline (PBS) tablets (1X, CalBioChem) were used to make buffered solutions (PBS, 140 mM NaCl, 3 mM KCl, 10 mM phosphate, pH 7.4) in Millipore water. Buffer solutions were sparged with N_2 to remove dissolved oxygen and stored in an N_2-filled glovebox. Whole bovine blood, whole sheep blood, and sheep serum were obtained from Carolina Biological Supply Company, stored at 4 °C, and warmed to room temperature immediately before use. Carbonic anhydrase (CA) from bovine erythrocytes (≥3,500 W/A units/mg) was obtained from Sigma Aldrich and a 1% CA stock solution was prepared in deoxygenated buffer (PBS, 140 mM NaCl, 3 mM KCl, 10 mM phosphate, pH 7.4) in a glovebox, and stored under nitrogen at 4 °C and warmed to room temperature immediately before use. Stock solutions of TCO **1** (10 mM) and tetrazine **2** (100 mM) were prepared in the dark in an N_2-filled glovebox in DMSO and stored, shielded from light, at -25 °C. Stock solutions were thawed at room temperature immediately before use.

General Procedure for H_2S Electrode Experiments. Scintillation vials containing 20.00 mL of degassed phosphate buffer (PBS, 140 mM NaCl, 3 mM KCl, 10 mM phosphate,

pH 7.4) were prepared in an N_2-filled glovebox. A split-top septum cap was placed on the vial after probe insertion and the headspace was sparged with Ar. For electrode experiments in complex media, whole blood or serum (2.50 mL) was pipetted into a 10 mL vial with phosphate buffer (PBS, 140 mM NaCl, 3 mM KCl, 10 mM phosphate, pH 7.4) and stirred prior to the start of the experiment. The WPI electrode was then inserted into the vial and the measured voltage was allowed to equilibrate before starting the experiment, and the vial was wrapped in foil to shield the reaction from light. With moderate stirring, CA stock solution (50 µL, 2.5 µg/mL) was injected when applicable, followed by subsequent injections of acetazolamide (10 µL, 2.5 µM, 10 mM stock solution in PBS buffer), TCO stock (10 mM in DMSO), or tetrazine stock solutions (100 mM in DMSO).

3.4.2 Syntheses

(E)-Cyclooct-2-enyl benzylcarbamate ***(1).*** A solution of (*E*)-cyclooct-2-enyl 4-nitrophenyl carbonate (500 mg, 1.7 mmol) in CH_2Cl_2 (5 mL) was added to a solution containing benzylamine (370 µL, 3.4 mmol) and *N*,*N*-diisopropylethylamine (880 µL, 5.1 mmol) in CH_2Cl_2 (5 mL). The reaction mixture was stirred at room temperature under a nitrogen atmosphere for 18 h. The reaction mixture was diluted with CH_2Cl_2 (50 mL) and washed with water (20 mL). The organic layer was dried over Na_2SO_4 and concentrated. The title product was purified by flash chromatography using a 9:1 mixture of hexanes:ethyl acetate to provide the product as a white powder (260 mg, 58%). ^{1}H NMR ($CDCl_3$, 400 MHz) δ: 7.36-7.26 (m, 5H), 5.83 (t, *J* = 12.3 *Hz*, 1H), 5.54 (d, *J* = 17.8 *Hz*, 1H), 5.37 (s, 1H), 5.16 (bs, 1H), 4.38 (d, *J* = 5.5 *Hz*, 2H), 2.47 (d, *J* = 10.9 *Hz*, 1H), 2.09-1.82 (m, 5H), 1.72-1.45 (m, 3H), 1.11-1.03 (m, 1H), 0.84-0.76 (m, 1H), which matches the previously-reported ^{1}H NMR spectrum: Versteegen, R. M.; Rossin, R.; ten Hoeve, W.; Janssen, H. M.; Robillard, M. S. *Angew. Chem. Int. Ed.* **2013**, *52*, 14112-14116.

O-(E)-Cyclooct-2-enyl N-benzylcarbamothioate ***(2).*** A solution of (*E*)-cyclooct-2-enol (120 mg, 0.95 mmol) in 1 mL THF was added dropwise to a suspension of NaH (45 mg, 1.13 mmol, 60% in mineral oil) in 1 mL THF. The resulting suspension was stirred at 0 ºC for 1 h under a nitrogen atmosphere. A solution of benzyl isothiocyanate (150 mg, 1.0

mmol) in 1 mL THF was added dropwise, and the mixture was stirred for an additional hour at 0 ºC. The reaction was quenched by addition of saturated aqueous $NaHCO_3$ (2 mL). The aqueous layer was extracted with ethyl acetate (3 x 10 mL), and the combined organic phases were dried with $MgSO_4$. The title product was isolated as a white powder by flash chromatography using a 3:1 solution of hexanes:ether as a mobile phase (199 mg, 76%). *Note*: Slow rotation around the thiocarbamate group results in the observation of rotational isomers on the NMR timescale, which results in a doubling of peaks in the NMR spectrum. This phenomenon has been observed previously in for thiocarbmates. ^{1}H NMR ($CDCl_3$, 400 MHz) δ: 7.58 (br s, 1H), 7.34-7.28 (m, 10H), 6.68 (br s, 1H), 5.92 (d, *J* = 10.9 *Hz*, 2H), 5.83-5.78 (m, 1H), 5.60-5.43 (m, 3H), 4.76 (d, *J* = 5.5 *Hz*, 2H), 4.47 (d, *J* = 6.8 *Hz*, 2H), 2.47 (d, *J* = 5.5 *Hz*, 1H), 2.37 (d, *J* = 9.6 *Hz*, 1H), 2.20-2.06 (m, 2H), 2.05-1.32 (m, 13H), 1.11-1.09 (m, 1H), 0.87-0.77 (m, 3H). $^{13}C\{^1H\}$ NMR ($CDCl_3$, 100 MHz) δ: 189.45, 188.63, 136.88, 136.74, 132.61, 132.18, 130.92, 130.19, 128.61, 128.58, 127.86, 127.68, 127.52, 127.20, 80.81, 79.17, 49.05, 47.02, 40.38, 40.37, 35.84, 35.83, 35.79, 35.67, 28.90, 28.80, 24.34, 24.20. HRMS (ESI) *m/z*: calcd. for $C_{16}H_{22}NOS$ $[M+H]^+$ 276.1422; found 276.1444

Bis-isopropyl-1,2,4,5-tetrazine. Isobutyronitrile (691 mg, 10 mmol) and zinc triflate (182 mg, 0.5 mmol) were combined with anhydrous hydrazine (1.6 mL) and stirred at 60 ºC for 24 h under nitrogen atmosphere. The reaction mixture was diluted with DMF (2 mL). An aqueous solution of $NaNO_2$ (3.5 g in 50 mL) was slowly added. Inside a thoroughly ventilated fume hood, an aqueous 2M solution of HCl was added slowly until reaching pH~3. (Caution! The last step generates highly toxic fumes, containing reactive nitrogen species.) The product was extracted with CH_2Cl_2 (3x100 mL), dried with Na_2SO_4 and concentrated. The title product was obtained by chromatography using 1% Et_2O in pentane (1.2 g, 72%). ^{1}H NMR ($CDCl_3$, 400 MHz) δ: 3.62 (sep, *J* = 6.8 *Hz*, 2H), 1.51 (d, *J* = 6.9 *Hz*, 12H). $^{13}C\{^1H\}$ NMR ($CDCl_3$, 100 MHz) δ: 173.69, 34.14, 21.22. HRMS (DART) *m/z*: calcd. for $C_8H_{15}N_4$ $[M+1]^+$ 167.1297; found 167.1306

CHAPTER IV

CYSTEINE-ACTIVATED HYDROGEN SULFIDE (H_2S) DELIVERY THROUGH CAGED CARBONYL SULFIDE (COS) DONOR MOTIFS

This chapter includes previously published and coauthored material from Zhao, Y.; Steiger, A.K; Pluth, M.D. "Cysteine-Activated Hydrogen Sulfide (H_2S) Delivery through Caged Carbonyl Sulfide (COS) Donor Motifs" *Chem. Commun.* **2018**, 54, 4951-4954.

4.1 Introduction

Hydrogen sulfide (H_2S) has joined the gasotransmitter family since its first recognition as an endogenous neuromodulator in 1996.[199] Four main enzymes, including cystathionine β-synthase (CBS) and cystathionine γ-lyase (CSE), are responsible for endogenous H_2S production, converting cysteine (Cys) and homocysteine (Hcy) to H_2S.[2, 200, 201] Significant efforts have been contributed to develop H_2S releasing agents (H_2S donors) because the regulation of H_2S levels has been found to mediate a wide variety of physiological processes, including anti-inflammation, oxidative stress reduction, and vasorelaxation.[124, 129, 202-204] Although sulfide salts, such as sodium hydrosulfide (NaHS) and sodium sulfide (Na_2S), have been widely used in the field, they are far from ideal donors because they release H_2S spontaneously, resulting in a concentrated bolus of sulfide that oxidizes rapidly and does not mimic well-regulated endogenous H_2S production. The use of these inorganic sulfide sources has even led to contradictory results,[124] demonstrating the need for improved sources of H_2S. These limitations suggest that controllable H_2S donors, which are stable, only release H_2S upon activation by certain stimuli, and have slower and controllable kinetics of sulfide release, are key research tools for H_2S investigations.

Aligned with this need, our group recently reported the use of caged-carbonyl sulfide (COS) molecules as new H_2S donors.[131, 205] Unlike other known H_2S donors, which directly release H_2S as the activation product, COS-based donors are activated to release COS, which is quickly converted to H_2S by the ubiquitous enzyme carbonic anhydrase (CA). We have demonstrated that caged-thiocarbamates and thiocarbonates

can serve as promising COS donors and can be activated to release COS through a self-immolative cascade reaction.[206] One important advantage of this strategy is that COS-releasing scaffolds can be designed to deliver H_2S under well-defined conditions. For example, H_2S delivery from these caged-COS donors can be modulated by judicious trigger selection, and the rate of release can be manipulated through modification of the donor structure.[206] Following our initial report, we, as well as others, have expended this strategy to include donors activated by different triggers, such as reactive oxygen species (ROS),[140, 206] esterases,[152, 207] nucleophiles,[150] click chemistry,[147] and light[208, 209] (Figure 4.1).

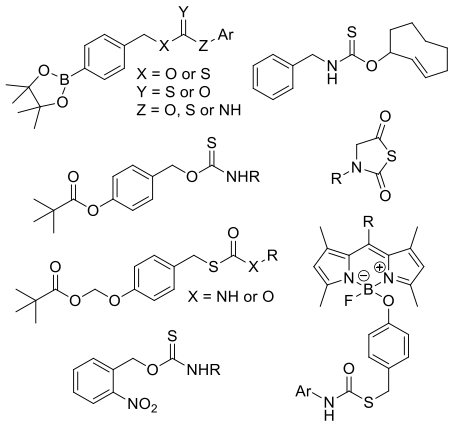

Figure 4.1 Examples of currently available COS-based H_2S donors that are activated by different triggering stimuli.

Cellular nucleophiles play crucial roles in biological systems. Among these, thiol species, such as Cys and reduced glutathione (GSH), attract the most attention due to their cellular abundance and potent reactivity. Cys and GSH have been widely used to trigger biologically active molecules and prodrugs to release caged compounds, including sulfur dioxide (SO_2),[210, 211] nitroxyl (HNO),[212] and anti-cancer drugs.[213] Importantly, thiol activation strategies have been adopted in H_2S donor development and several thiol labile H_2S donors exhibit promising protections in animal models with some of them currently in clinical trials.[124, 202, 204] Motivated by these findings, we report here the first example of a Cys-activated COS/H_2S donor through functionalization of a thiocarbamate with a Cys-reactive acrylate moiety. We envision that such thiocarbamate compounds will expand the current COS-based H_2S donor family and serve as promising research tools for H_2S studies.

The reactions of Cys with acrylates in the preparation of substituted 1,4-thiazepines have been known for decades.[214, 215] The initial attack by Cys on the acrylate generates a thioether, which then undergoes an intramolecular cyclization to yield 1,4-thiazepines. This cyclization strategy has been leveraged by Strongin,[216] as well as others,[217-220] to design a series of acrylate-based fluorescent probes for Cys detection. Similarly, the Berreau group has recently used a similar approach to develop a class of Cys-responsive CO donors.[221] Building from these approaches, we adopt the Cys-acrylate reaction as a triggering mechanism to access new COS/H_2S donors in which an aryl acrylate-functionalized thiocarbamate is activated through a Cys-mediated addition/cyclization sequence. The resultant phenolic intermediate then undergoes a 1,6-elimination to release COS, which is quickly converted to H_2S by CA (Scheme 4.1).

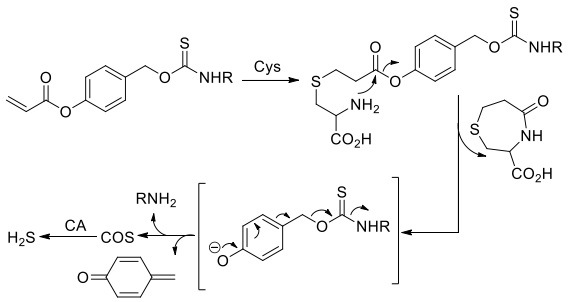

Scheme 4.1 General design of Cys-triggered COS/H_2S release from caged-thiocarbamate donors.

4.2 Results and Discussion

To test our hypothesis that acrylate-functionalized thiocarbamates could serve as Cys-triggered COS/H_2S donors, we prepared *O*-alkyl cysteine-sensitive thiocarbamate (**OA-CysTCM-1**) with an aryl acrylate trigger and an aniline payload by reacting 4-(hydroxymethyl)phenyl acrylate and phenyl isothiocyanate. Upon activation, **OA-CysTCM-1** releases COS, which is quickly hydrolyzed to H_2S by CA. In addition to **OA-CysTCM-1**, we also prepared the corresponding carbamate (**OA-CysCM-1**) and triggerless thiocarbamate (**OA-TCM-1**)[222] control compounds. **OA-CysCM-1**, obtained from the reaction between 4-(hydroxymethyl)phenyl acrylate and phenyl isocyanate, is expected to undergo the same Cys activation but would release CO_2 instead of COS. **OA-TCM-1**, on the other hand, maintains the thiocarbamate scaffold but lacks the acrylate

trigger, and thus is not expected to react with Cys or decompose to otherwise release COS (Scheme 4.2).

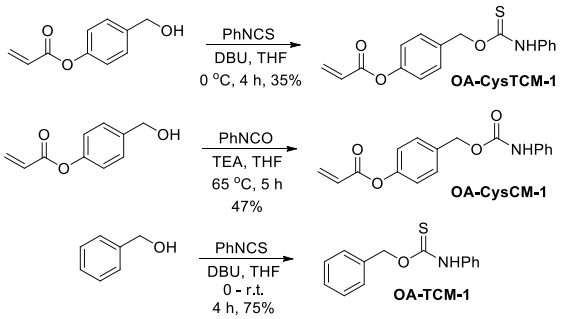

Scheme 4.2 Synthesis of **OA-CysTCM-1**, **OA-CysCM-1**, and **OA-TCM-1**.

To evaluate Cys-activated H_2S release from the donor motif, we used the methylene blue (MB) assay to monitor H_2S release from **OA-CysTCM-1** (50 μM) in the presence of Cys (0 – 500 μM) in PBS buffer (pH 7.4, 10 mM) containing cellularly-relevant concentrations of CA (25 μg/mL). The MB assay was chosen to measure H_2S production since it has been widely used to detect H_2S from previously developed Cys-activated H_2S donors. In the absence of Cys, **OA-CysTCM-1** was stable in aqueous buffer and did not release COS/H_2S spontaneously. By contrast, the addition of Cys led to a dose-dependent COS/H_2S release from **OA-CysTCM-1** (Figure 4.2). These results demonstrate that **OA-CysTCM-1** can be activated by Cys and the resultant COS is quickly converted to H_2S in the presence of CA.

To further demonstrate that the observed H_2S release is due to Cys activation via the proposed mechanism, we pretreated Cys with *N*-ethylmaleimide (NEM), a Cys scavenger, for 20 min, followed by the addition of **OA-CysTCM-1**. When compared to the regular activation conditions (Figure 4.3, bar 1), NEM pretreatment significantly diminished H_2S release from **OA-CysTCM-1**, confirming that Cys was required for donor activation (Figure 4.3, bar 2). No H_2S release was observed in the absence of CA, and, similarly, pretreatment of CA with acetazolamide (AAA), a CA inhibitor, also failed to provide H_2S, confirming that H_2S release from **OA-CysTCM-1** proceeds through a COS-dependent pathway (Figure 4.3, bars 3 and 4).

In addition to Cys, other biologically relevant nucleophiles, such as GSH, oxidized glutathione (GSSG), Hcy, *N*-acetylcysteine (NAC), serine (Ser), and lysine

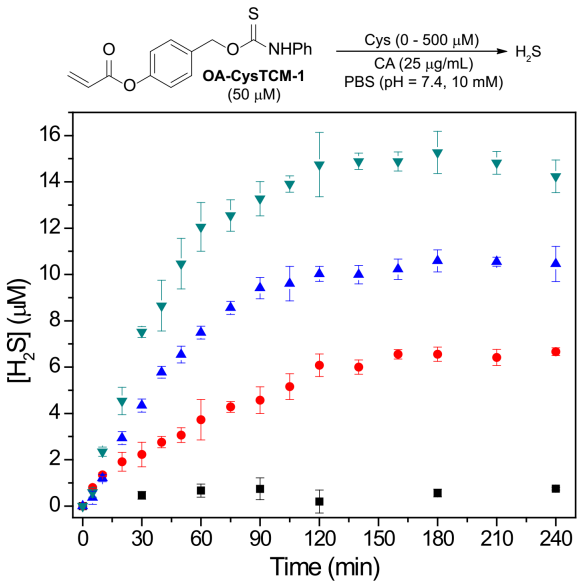

Figure 4.2 COS/H_2S Release from **OA-CysTCM-1** (50 μM) in the presence of 0 μM (black), 50 μM (red), 250 μM (blue), and 500 μM (green) Cys. The experiments were performed in triplicate and results are expressed as mean ± SD (n = 3).

(Lys), were evaluated towards donor activation. As expected, none of these species triggered **OA-CysTCM-1**, and no COS/H_2S release was observed due to the lack of the addition/cyclization activation sequence (Figure 4.3, bars 5-10). We also evaluated Cys-triggered COS/H_2S release from **OA-CysTCM-1** in the presence of GSH. In these experiments, **OA-CysTCM-1** (50 μM) was co-incubated with Cys (500 μM) and GSH (0 – 1000 μM) and COS/H_2S release was monitored by MB assay (Figure C2). A decrease of H_2S release was observed as GSH concentration increased, indicating a potential GSH-induced donor consumption. Although the effects of GSH were not significant in aqueous buffer, it should be taken into consideration when applying donors in biological systems. Since the acrylate trigger may be prone to esterase-catalyzed hydrolysis, we also incubated **OA-CysTCM-1** with porcine liver esterase (PLE) to determine whether common esterases could generate COS/H_2S release. Although we did observe H_2S release, it was significantly less efficient than Cys activation (Figure 4.3, bar 11). As expected, treatment of control compounds **OA-CysCM-1** and **OA-TCM-1** with Cys in the presence of CA failed to generate H_2S, demonstrating that both the aryl-acrylate trigger and the caged COS-containing thiocarbamate scaffold are crucial for COS release from this scaffold (Figure 4.3, bars 12 and 13). Taken together, these selectivity studies

demonstrate that **OA-CysTCM-1** is highly sensitive towards Cys activation to release COS/H_2S and inert to activation by other biomolecules, such as GSH, GSSG, Hcy, NAC, Ser, and Lys.

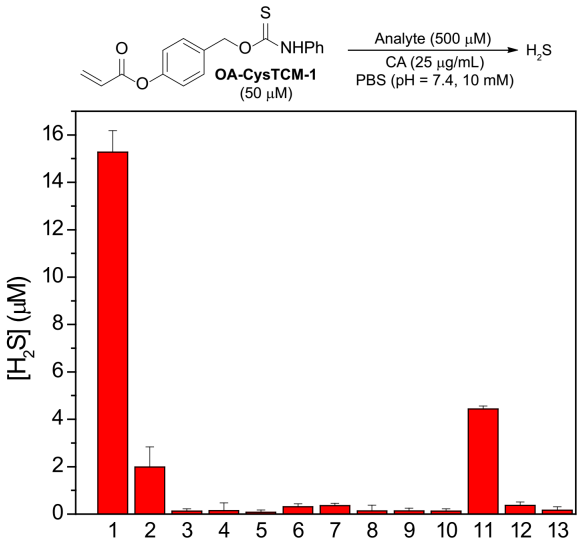

Figure 4.3 COS/H_2S Release from **OA-CysTCM-1** (50 μM) in the presence of cellular nucleophiles (500 μM): (1) Cys, (2) Cys + NEM (10 mM), (3) Cys - CA, (4) Cys + AAA (10 μM), (5) Hcy, (6) NAC, (7) GSH (5.0 mM), (8) Ser, (9) Lys, (10) GSSG, and (11) PLE (1 U/mL). Cys (500 μM) effects on **OA-CysCM-1** (12), and **OA-TCM-1** (13) toward COS/H_2S release. H_2S concentration was measured after 3-h incubation. The experiments were performed in triplicate and the results were expressed as mean ± SD (n = 3).

We next sought to confirm that **OA-CysTCM-1** would release COS/H_2S upon reaction with Cys in a cellular environment. We incubated bEnd.3 cells with **OA-CysTCM-1** in the presence of Cys and visualized H_2S-release using SF7-AM, a cell-trappable H_2S-responsive fluorescent probe.[196] In the absence of **OA-CysTCM-1**, negligible SF7-AM fluorescence was observed, suggesting a minimum amount of endogenous H_2S present in bEnd.3 cells. By contrast, addition of **OA-CysTCM-1** resulted in a significant increase in SF7-AM fluorescence, confirming that **OA-CysTCM-1** can be activated by Cys to release H_2S in a cellular environment (Figure 4.4). These results demonstrate that **OA-CysTCM-1** is a potent COS/H_2S donor and Cys-triggered H_2S delivery can be visualized in complex biological systems, indicating applications of **OA-CysTCM-1** as a potential H_2S-related therapeutic or research tool.

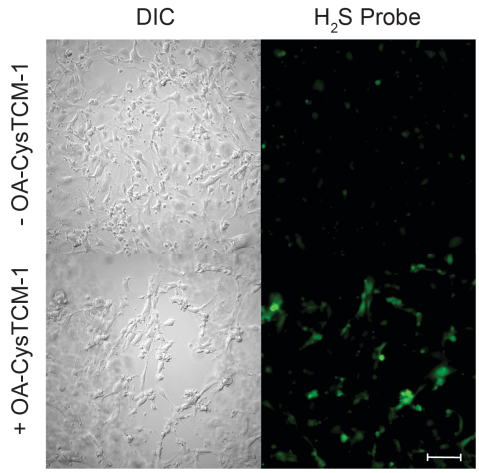

Figure 4.4 H_2S Release from **OA-CysTCM-1** in bEnd.3 cells. Top: DIC (left) and GFP (right) channels with cysteine (250 μM) and SF7-AM (5 μM). Bottom: DIC (left) and GFP (right) channels with cysteine (250 μM), **OA-CysTCM-1** (100 μM), and SF7-AM (5 μM). Scale bar represents 100 μM.

4.3 Conclusions

In summary, we prepared and evaluated **OA-CysTCM-1** as a Cys-triggered COS/H_2S donor. Our studies demonstrate that **OA-CysTCM-1** is stable in aqueous media and does not release COS/H_2S until being activated by Cys. Importantly, H_2S delivery from **OA-CysTCM-1** is observed in a cellular environment, indicating **OA-CysTCM-1** can be used as a new efficacious Cys labile COS/H_2S donor in complex biological systems. Taken together, our investigations demonstrate that H_2S delivery from **OA-CysTCM-1** can be controlled and regulated through a COS-dependent pathway, making **OA-CysTCM-1** a new member of COS-based H_2S donor family with potential applications in the study of both H_2S and COS chemical biology, especially when used in combination with available Cys-activated H_2S donors. Activation of the donors developed in this chapter still results in consumption of biological thiols, however, and Chapter V addresses this limitation through the design of a COS/H_2S donor activated by a ubiquitous intracellular enzyme.

4.4 Experimental Details

4.4.1 Materials and Methods

Reagents were purchased from Sigma-Aldrich, Tokyo Chemical Industry (TCI), Fisher Scientific, or VWR and used directly as received. SF7-Am was synthesized as

previously reported.[196] Silica gel (SiliaFlash F60, Silicycle, 230−400 mesh) was used for column chromatography. Deuterated solvents were purchased from Cambridge Isotope Laboratories (Tewksbury, Massachusetts, USA). ^{1}H and $^{13}C\{^{1}H\}$. NMR spectra were recorded on Varian 300 MHz, Bruker 500 MHz or Bruker 600 MHz NMR instruments at the indicated frequencies. Chemical shifts are reported in ppm relative to residual protic solvent resonances. Methylene blue (MB) absorbances were measured using an Agilent Cary 100 UV-Vis spectrometer. b.End3 cells were purchased from ATCC (Manassas, Virginia, USA). Cell imaging experiments were performed on a Leica DMi8 fluorescence microscope, equipped with an Andor Zyla 4.2+ sCMOS detector.

H_2S Release from OA-CysTCM-1 in PBS. An OA-CysTCM-1 stock solution (0.100 mL, 10.0 mM in DMSO) was added to 20.0 mL of PBS (pH 7.40, 10.0 mM) containing CA (25.0 μg/mL) in a 25-mL scintillation vial. A Cys stock solution (0.100 M in H_2O) was then added to generate the desired Cys working concentrations as shown in Figure 3. Next, 0.300 mL aliquots of the reaction mixture were transferred to UV cuvettes containing 0.300 mL of MB cocktail (0.0600 mL zinc acetate (1.00% w/v), 0.120 mL $FeCl_3$ (30.0 mM in 1.20 M HCl), and 0.120 mL *N,N*-dimethyl-*p*-phenylene diamine (20.0 mM in 7.20 M HCl) at different time points. The absorbance at 670 nm was then measured after 1 hour and was converted to H_2S concentration by using the H_2S calibration curve as shown in Figure C1.

Selectivity Evaluation of H_2S Release from OA-CysTCM-1 (Figure 3). All experiments were completed in 2.00 mL of PBS containing CA (25.0 μg/mL). After 3 hours of incubation at room temperature, 0.300 mL of the reaction aliquot was transferred to a UV cuvette containing 0.300 mL of the MB cocktail. The absorbance at 670 nm was then measured after 1 hour by the MB assay.

Bar 1: Added Cys (10.0 μL, 0.100 M in H_2O), followed by the addition of **OA-CysTCM-1** (10.0 μL, 10.0 mM in DMSO).
Bar 2: Added Cys (10.0 μL, 0.100 M in H_2O), followed by the addition of NEM (2.50 mg). After 20 min, **OA-CysTCM-1** (10.0 μL, 10.0 mM in DMSO) was added.

Bar 3: Added Cys (10.0 μL, 0.100 M in H_2O), followed by the addition of **OA-CysTCM-1** (10.0 μL, 10.0 mM in DMSO).
Bar 4: Added Cys (10.0 μL, 0.100 M in H_2O), followed by the addition of AAA (2.00 μL, 10.0 mM in DMSO). After 20 min, **OA-CysTCM-1** (10.0 μL, 10.0 mM in DMSO) was added.
Bar 5: Added Hcy (10.0 μL, 0.100 M in H_2O), followed by the addition of **OA-CysTCM-1** (10.0 μL, 10.0 mM in DMSO).
Bar 6: Added NAC (10.0 μL, 0.100 M in H_2O), followed by the addition of **OA-CysTCM-1** (10.0 μL, 10.0 mM in DMSO).
Bar 7: Added GSH (10.0 μL, 0.100 M in H_2O), followed by the addition of **OA-CysTCM-1** (10.0 μL, 10.0 mM in DMSO).
Bar 8: Added Ser (10.0 μL, 0.100 M in H_2O), followed by the addition of **OA-CysTCM-1** (10.0 μL, 10.0 mM in DMSO).
Bar 9: Added Lys (10.0 μL, 0.100 M in H_2O), followed by the addition of **OA-CysTCM-1** (10.0 μL, 10.0 mM in DMSO).
Bar 10: Added GSSG (10.0 μL, 0.100 M in H_2O), followed by the addition of **OA-CysTCM-1** (10.0 μL, 10.0 mM in DMSO).
Bar 11: Added PLE (20.0 μL, 1.00 U/μL), followed by the addition of **OA-CysTCM-1** (0.100 mL, 10.0 mM in DMSO).
Bar 12: Added Cys (10.0 μL, 0.100 M in H_2O), followed by the addition of **OA-CysCM-1** (10.0 μL, 10.0 mM in DMSO).
Bar 13: Added Cys (10.0 μL, 0.100 M in H_2O), followed by the addition of **OA-TCM-1** (10.0 μL, 10.0 mM in DMSO).

*Cellular Imaging of H_2S Release from **OA-CysTCM-1***. b.End 3 cells were plated in poly-D-lysine coated plates (MatTek) containing 2 mL of DMEM and incubated at 37 °C under 5% CO_2 for 24 h. The confluent cells were washed with PBS and then incubated with SF7-AM (5.00 μM) for 30 min. The cells were then washed with PBS and incubated with either **OA-CysTCM-1** (100 μM) and cysteine (250 μM) or cysteine (250 μM) alone for 30 min. Prior to imaging, cells were washed with PBS and bathed in 2 mL of PBS. Cell imaging was performed on a Leica DMi8 fluorescent microscope using DIC for

brightfield and a standard GFP filter cube for fluorescence imaging and 100 ms and 50 ms exposure times, respectively. The scale bar represents 100 μm.

4.4.2 Syntheses

S1. The benzyl alcohol compound **S1** was prepared using a known procedure.[223] Briefly, K_2CO_3 (207 mg, 1.50 mmol) was dissolved in acetone/H_2O (25.0 mL, v/v 4:1), followed by the addition of acryloyl chloride (90.5 mg, 1.00 mmol) at 0 ^oC. To this reaction mixture, a solution of 4-hydroxybenzyl alcohol (124 mg, 1.00 mmol) was added dropwise and the reaction solution was stirred at 0 °C for 4 h. Brine was then added, and the reaction mixture was extracted with DCM (3 x 25.0 mL). The organic layers were collected, dried over $MgSO_4$, and concentrated under vacuum. The product **S1** was isolated as a clear oil (42.0%) after purification by column chromatography. ^1H NMR (500 MHz, $CDCl_3$) δ (ppm): 7.43 (d, J = 5.0 Hz, 2H), 7.16 (d, J = 5.0 Hz, 2H), 6.64 (d, J = 15.0 Hz, 1H), 6.36 (m, 1H), 6.05 (d, J = 10.0 Hz, 1H), 4.73 (s, 2H), 1.75 (br, 1H). $^{13}C\{^1H\}$ NMR (125 MHz, $CDCl_3$) δ (ppm): 164.6, 150.0, 138.5, 132.7, 128.1, 127.9, 121.6, 64.8.

OA-CysTCM-1. **S1** (178 mg, 1.00 mmol) and phenyl isothiocyanate (135 mg, 1.00 mmol) were dissolved in THF (15.0 mL) and cooled to 0 ^oC. DBU (152 mg, 1.00 mmol) was then added, and the reaction solution was stirred at 0 °C for 4 h. The reaction mixture was then quenched by adding brine, and the aqueous solution was extracted with DCM (3 x 25.0 mL). The organic layers were collected, dried over $MgSO_4$, and concentrated under vacuum. **OA-CysTCM-1** was isolated as white solid (35.4%) after purification by column chromatography. Two sets of NMR resonances showed up due to slow rotation around the thiocarbamate functional group at room temperature. ^1H NMR (500 MHz, DMSO-d_6) δ (ppm): 11.24 (s, 1H), 7.68 (br, 1H), 7.52 (br, 2H), 7.34 (br, 3H), 7.22 (br, 3H), 6.54 (d, J = 15.0 Hz, 1H), 6.42 (dd, J = 15.0, 5.0 Hz, 1H), 6.17 (d, J = 10.0 Hz, 1H), 5.55 (d, J = 50.0 Hz, 2H). $^{13}C\{^1H\}$ NMR (150 MHz, DMSO-d_6) δ (ppm): 187.8, 187.4, 164.6, 150.5, 134.2, 130.3, 129.9, 129.3, 128.9, 128.1, 125.6, 123.3, 122.3, 72.0, 70.3. IR (cm^{-1}): 3228, 3039, 2919, 1734, 1592, 1547, 1494, 1446, 1402, 1335, 1293, 1146, 1018, 968. HRMS m/z $[M + Na]^+$ calcd. for $[C_{17}H_{15}NNaO_3S]^+$ 336.0670; found 336.0673.

OA-CysCM-1. **S1** (178 mg, 1.00 mmol) and phenyl isocyanate (119 mg, 1.00 mmol) were dissolved in THF (15.0 mL) and cooled to 0 ^{o}C. TEA (101 mg, 1.00 mmol) was then added, and the reaction solution was heated to 65 °C and stirred for 5 h. The reaction mixture was then quenched by adding brine and the aqueous solution was extracted with DCM (3 x 25.0 mL). The organic layers were collected, dried over $MgSO_4$, and concentrated under vacuum. **OA-CysCM-1** was isolated as white solid (47.0%) after purification by column chromatography. ^{1}H NMR (300 MHz, $CDCl_3$) δ (ppm): 7.43 (t, *J* = 9.0 Hz, 4H), 7.32 (t, *J* = 9.0 Hz, 2H), 7.15 (d, *J* = 9.0 Hz, , 2H), 7.09 (t, *J* = 9.0 Hz, 1H), 6.91 (br, 1H), 6.64 (dd, *J* = 15.0, 3.0 Hz, 1H), 6.35 (dd, *J* = 18.0, 9.0 Hz, 1H), 6.04 (dd, *J* = 12.0, 3.0 Hz, 1H), 5.20 (s, 2H). ^{13}C{^{1}H} NMR (125 MHz, $CDCl_3$) δ (ppm): 164.6, 153.4, 150.5, 137.8, 133.8, 132.8, 129.6, 129.1, 127.8, 123.5, 121.7, 118.8, 66.3. IR (cm^{-1}): 3367, 3064, 1735, 1709, 1634, 1598, 1532, 1502, 1447, 1407, 1318, 1298, 1234, 1198, 1167, 1071, 982, 901, 819. HRMS m/z $[M + Na]^+$ calcd. for $[C_{17}H_{15}NNaO_4]^+$ 320.0899; found 320.0897.

CHAPTER V

INHIBITION OF MITOCHONDRIAL BIOENERGETICS BY ESTERASE-TRIGGERED COS/H_2S DONORS

This chapter includes previously published and coauthored material from Steiger, A.K.; Marcatti, M.; Szabo, C.; Szczesny, B.; Pluth, M.D. "Inhibition of Mitochondrial Bioenergetics by Esterase-Triggered COS/H_2S Donors" *ACS Chem. Biol.* **2017**, 12(8), 2117-2123.

5.1 Introduction

Hydrogen sulfide (H_2S) is an endogenously-produced signaling molecule that plays critical roles in mammalian biology. Physiological sulfide levels are tightly regulated, and enzymatic production derives primarily from cysteine and homocysteine metabolism by cystathionine-β-synthase (CBS), cystathionine-γ-lyase (CSE), and 3-mercaptopyruvate transferase (3-MST).[2] Continually broadening in scope, H_2S plays important roles in cardioprotection,[224] inflammation,[225] vasodilation,[226] as well as other processes. Because of this diversity, there is significant interest in developing both research and therapeutic strategies for regulating sulfide levels in different biological contexts.[129] At the biological level, inhibition, knockout, and/or overexpression of H_2S-producing enzymes can be used to modulate endogenous H_2S levels. Alternatively, chemical approaches using exogenous H_2S donation often provide a more convenient and broader approach. For example, inorganic sulfide salts, such as NaSH and Na_2S provide a convenient source of sulfide, however, the large and instantaneous bolus of sulfide released from such salts is often rapidly oxidized and fails to mimic the continuous H_2S release associated with enzymatic synthesis, thus limiting the utility of these exogenous H_2S sources.[227] Because of these limitations, developing small molecules that undergo specific reactions to release H_2S in a controlled manner to more closely mimic well-regulated enzymatic production remains an important goal.[122, 124] Aligned with these needs, naturally-occurring polysulfides such as diallyl trisulfide (DATS), which releases sulfide upon reaction with thiols,[89, 228] hydrolysis-based H_2S donors such as GYY4137 and ADT-OH,[229, 230] which slowly produce H_2S in water, and a palette of thiol-activated donors, have all been developed.[124, 170] Although such donors have been used in

applications ranging from probe development to *in vivo* studies, key challenges include low H_2S donation efficiencies from hydrolysis-based donors and thiol consumption and redox perturbation from polysulfides and thiol-activated donors.

As a step toward addressing these challenges, our group recently developed a new H_2S donation strategy based on the intermediate release of carbonyl sulfide (COS), which is rapidly hydrolyzed to H_2S by the ubiquitous enzyme carbonic anhydrase (CA).[131] By leveraging well-established work on the triggered decomposition of benzylic carbamates commonly used in pro-drug and fluorophore release strategies,[132, 231, 232] we demonstrated that self-immolative thiocarbamates can be readily engineered to respond to different stimuli and release COS/H_2S. Specifically, cleavage of an analyte-specific protecting group unmasks a phenol, which then undergoes a self-immolative decomposition to release COS. Importantly, this strategy enables significant control over H_2S donation depending on the trigger and provides access to important carbamate control compounds, which release CO_2/H_2O rather than COS/H_2S. Furthermore, although COS hydrolysis by CA is rapid, some evidence suggests that COS may have unique roles in chemical biology, as evidenced by COS detection in the headspace above ex vivo porcine coronary arteries and by increased COS levels in exhaled breath from patients with cystic fibrosis, organ rejection, or liver disease.[39-41, 233] Therefore, although self-immolative thiocarbamates have recently been shown to be useful as responsive H_2S donors, they may also provide a platform for future studies of COS chemical biology. Following our initial report of caged COS/H_2S release, we have expanded this approach to include COS/H_2S donors activated by reactive oxygen species (ROS)[140] and to access bio-orthogonal "click-and-release"[131] donors based on *trans*-cyclooctene / tetrazine click chemistry. Related COS-based donors based on nucleophilic addition to small molecule and polymeric cyclic N-thiocarboxyanhydrides resulting in the release of COS have also emerged recently.[150] Although the nucleophile-based donors provide slow H_2S release akin to enzymatic synthesis, the required consumption of cellular nucleophiles, such as thiols, to release COS/H_2S is similar to other thiol-activated donors.

To address these limitations, we viewed that installation of an ester as the triggering group to thiocarbamate-based platforms would provide access to slow-release COS/H_2S donors upon ester cleavage by intracellular esterases that do not require

consumption of cellular nucleophiles for activation (Scheme 5.1). The strategy of using intracellular esterases to cleave esterified moieties on small molecules is a well-established method used extensively to impart cellular trappability, improve membrane permeability, and in the activation of caged pro-drugs and other biological payloads.[153, 234-236] Additionally, activation by intracellular esterases eliminates the consumption of cellular nucleophiles for activation. Consistent with this design strategy, the Wang group recently reported esterase-triggered H_2S donors utilizing a trimethyl lock unmasking of caged thioacids and demonstrated their anti-inflammatory effects.[171] Similarly, during the preparation of this manuscript an esterase-activated *S*-alkyl thiocarbamate COS/H_2S donor was reported, but detailed biological applications were not investigated.[152] Here, we report the design, evaluation, and application of esterase-activated COS/H_2S donors and provide further insights into the influence of COS donors on cellular bioenergetics.

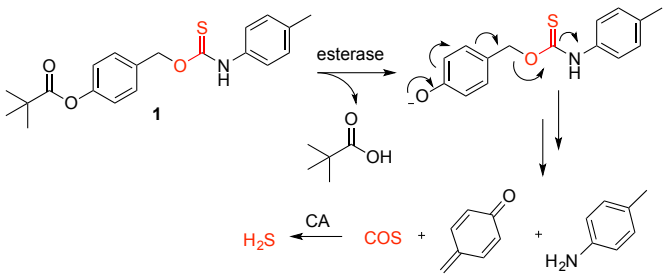

Scheme 5.1 Design of esterase-triggered self-immolative COS/H_2S donors and proposed COS/H_2S release mechanism.

5.2 Results and Discussion

Triggered COS/H_2S donors benefit from a high degree of modularity and facile introduction of different triggering functionalities. To access an esterase-functionalized thiocarbamate, we first prepared 4-pivaloyl benzyl alcohol in one step,[237] which was then treated with *p*-tolylisothiocyanate in the presence of DBU to afford donor **1** in moderate yield (Scheme 5.2). The analogous carbamate control **2** was prepared in good yield by treating 4-pivaloyl benzyl alcohol with *p*-tolylisocyanate and DBU. Carbamate **2** provides an important control compound that undergoes the same self-immolative decomposition as **1**, but releases CO_2 instead of COS, thus enabling separation of the action of COS/H_2S from that of the organic byproducts formed after donor activation.

Additionally, we also prepared triggerless thiocarbamate **3** as a control compound to test the thiocarbamate stability toward esterases.

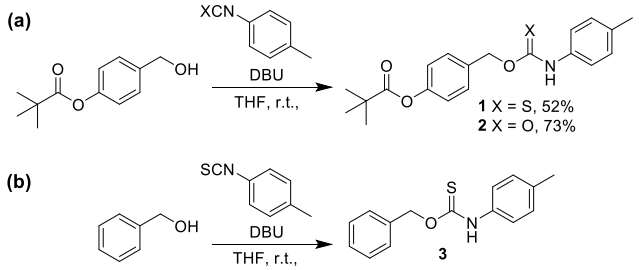

Scheme 5.2 (a) Synthesis of H_2S donor **1**, CO_2-releasing analogue **2**, and triggerless thiocarbamate **3**.

The mechanism of the cascade decomposition of similar benzyl carbamates has established previously to release CO_2, the amine payload, and a quinone methide intermediate.[132, 135, 231, 232] The final fate of the electrophilic quinone methide is dependent on which nucleophiles are present in the system, and is often scavenged by water to form 4-hydroxy benzylalcohol, or can be scavenged by biological nucleophiles to afford thiol or amine-derived conjugates.[238, 239] To confirm similar reactivity in the present system, we first demonstrated that the addition of porcine liver esterase (PLE) initiated a self-immolative decomposition reaction as anticipated. After stirring **1** (14 mM) with PLE (28 U/mL) in PBS (pH 7.4) with 10% DMSO for 48 hours, the organic layer was extracted and analyzed by NMR spectroscopy and mass spectrometry (Figure 1). Loss of the benzylic and thiocarbamate N-H protons at ~5.5 ppm and 11.1 ppm, respectively, in the ^{1}H NMR spectrum of the reaction mixture confirmed self-immolation (Figure 3.1a). As further evidence of the triggered cascade decomposition, the broad NMR resonances characteristic of O-alkyl thiocarbamates, which is due to the slow rotation around the thiocarbamte moiety on the NMR time scale, sharpen significantly upon ester cleavage with PLE. Additionally, the ^{13}C{^{1}H} NMR spectrum after treatment with PLE (Figure 3.1b), clearly showed the loss of the C=S and benzylic carbon resonances at 185 and 70 ppm, respectively. Both the ^{1}H and ^{13}C{^{1}H} NMR spectra also show the formation of new aromatic species corresponding to several products, which were further characterized using mass spectrometry. Because the generated *p*-quinone methide is electrophilic, we expect that it would be scavenged by biological nucleophiles, such as

thiols, amines, or water, under physiological conditions. The mass spectrum acquired of the reaction mixture after treatment with PLE clearly showed formation of *p*-toluidine (m/z: 107.0) and the product corresponding to *p*-toluidine trapping of the *o*-quinone methide intermediate (m/z: 214.1) as expected (Figure D1). Taken together, the NMR spectroscopy and mass spectrometry studies confirm self-immolation of the scaffold as described in Scheme 5.1.

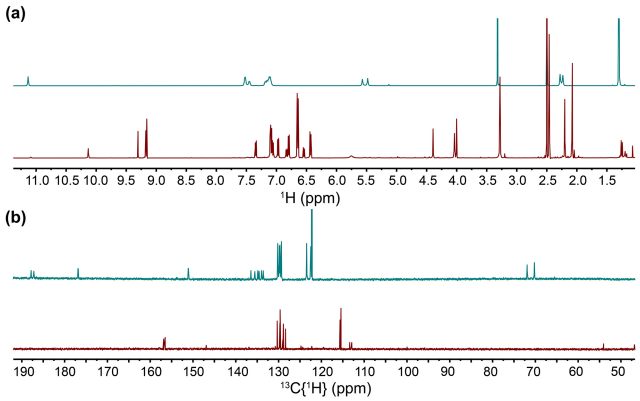

Figure 5.1 (a) ^{1}H NMR spectrum of **1** before (top) and after (bottom) treatment with PLE. (b) $^{13}C\{^{1}H\}$ NMR spectrum of **1** before (top) and after (bottom) stirring with PLE. (c) Mass spectrum of the products resulting from the decomposition of **1** upon reaction with PLE.

With esterase-triggered donors in hand, we first confirmed that **1** was stable in aqueous solution in the absence of esterase. We next verified that addition of **1** to pH 7.4 PBS buffer containing physiologically relevant levels of CA (25 µg/mL) did not result in H_2S generation when monitored using an H_2S-selective electrode, confirming that the esterase does not cleave thiocarbamates directly (Figure 5.2a). Further control experiments using the parent benzyl thiocarbamate **3**, which lacks the ester trigger, confirmed that the benzyl thiocarbamate moiety is not cleaved directly by PLE. Having confirmed the stability of the donor platform prior to activation, we next treated **1** with 1 U/mL PLE in the presence of CA and observed immediate H_2S release (Figure 5.2a). As expected, increasing the PLE concentration to 20 U/mL under otherwise identical conditions resulted in significantly faster H_2S release. Additionally, treatment of **1** with acetazolamide (AAA), a known CA inhibitor, significantly reduced the rate of H_2S production, confirming that CA is necessary for COS conversion to H_2S under the

reaction conditions. Supplementing the H_2S electrode measurements, we also confirmed H_2S release from **1** using an H_2S-responsive fluorescent probe (Figure 5.2b). Consistent with the electrode data, incubation of 50 µM **1** with 5 µM MeRho-Az[184] in the presence of CA and 1 U/mL PLE resulted in a fluorescence turn-on consistent with H_2S release. We also attempted to obtain fluorescent live cell images by incubating **1** in BEAS 2B cells with MeRho-Az, but the high cytotoxicity of **1** and limited permeability of MeRho^{Az} in BEAS 2B cells limited our ability to obtain high quality images. Taken together, these data demonstrate that the thiocarbamate donors are stable until activated by esterases and release H_2S in a COS-dependent manner.

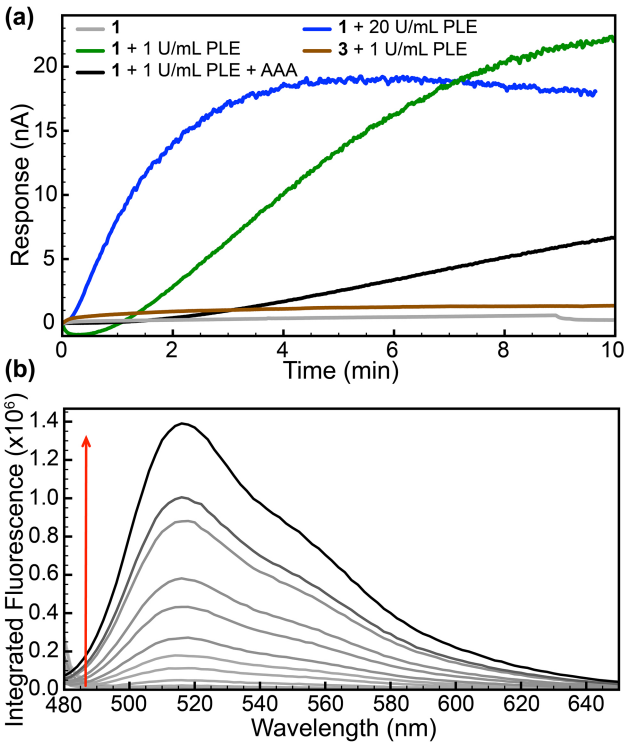

Figure 5.2 (a) H_2S release from **1** in PBS (pH 7.4) in the presence of CA (25 µg/mL) with 1 U/mL (green trace) or 20 U/mL (blue trace) PLE. Addition of CA inhibitor AAA (2.5 µM) significantly reduces H_2S release (black trace). No H_2S release was observed from **1** in the absence of esterase (grey trace) or from thiocarbamate **3** lacking an ester trigger (brown trace). (b) Detection of H_2S released from **1** with the H_2S-responsive probe MeRho-Az. Conditions: 50 µM 1, 5 µM MeRho-Az, 25 µg/mL CA, 1 unit/mL PLE, 3 mL PBS (pH 7.4). 37 °C, λ_{ex}= 476 nm, λ_{em}= 480-650 nm.

We next investigated the cytotoxicity of **1**-**3** on BEAS 2B cells by measuring the reduction of a tetrazolium compound (MTT) to formazan by metabolically active cells,

and by measuring the release of lactate dehydrogenase (LDH) due to permeability of the plasma membrane, which is a sign of necrotic cell death. BEAS 2B human lung epithelial cells exhibit low expression of all three canonical H_2S-producing enzymes, CBS, CSE, and 3-MST.[240] To provide suitable comparisons with commonly-used synthetic donors, we first obtained comparable cytotoxicity data for known H_2S donors GYY4137 and mitochondrially-targeted AP39 (Figure 5.3a,b).[241] When compared to the DMSO vehicle, GYY4137 showed no significant cytotoxicity up to 30 μM using either the MTT or LDH assay. Similarly, AP39 showed minimal cytotoxicity at 30 μM and none at lower concentrations, indicating that neither of these H_2S donors are significantly cytotoxic. By contrast, 10 μM of **1** resulted a significant decrease cell viability and increase in LDH levels, which was not observed for control compounds **2** or **3** (Figure 5.3c,d). The lack of cytotoxicity of control compound **2** suggests that the mechanism of cytotoxicity does not result from the formation of the electrophilic *p*-quinone methide intermediate[242] because this species is formed upon activation of both donor **1** and control compound **2**. Similarly, compound **3** does not reduce cell viability, confirming that the observed cytotoxicity of **1** relies on triggering by cellular esterases and is not a result of the thiocarbamate scaffold itself. Importantly, the esterase-triggered COS/H_2S donor **1** provides a significantly different toxicological profile from other commonly-used H_2S donors.

To investigate the underpinnings of the increased cytotoxicity of **1**, and because H_2S is a well-known inhibitor of mitochondrial cytochrome c oxidase,[243] we analyzed the mitochondrial respiration of BEAS 2B cells treated with **1**-**3** using an Extracellular Flux Analyzer.[244] As expected, incubation of BEAS 2B cells with increasing concentrations of **1** for 24 hours negatively affected all major bioenergetics parameters, namely oxygen consumption linked with basal respiration, maximal respiration, and ATP synthesis (Figure 5.4a-f). These reductions are consistent with known inhibitory effects of H_2S on cellular bioenergetics, primarily through inhibition of mitochondrial cytochrome c oxidase (Complex IV). By contrast, control compound **2** did not negatively impact the measured bioenergetics parameters, but rather resulted in increases in basal respiration and ATP synthesis. Compound **3** had no effect on basal respiration or ATP synthesis, and only slightly decreased maximal respiration at 10 μM. To better compare these results with known H_2S donors, we also analyzed the mitochondrial respiration of BEAS 2B

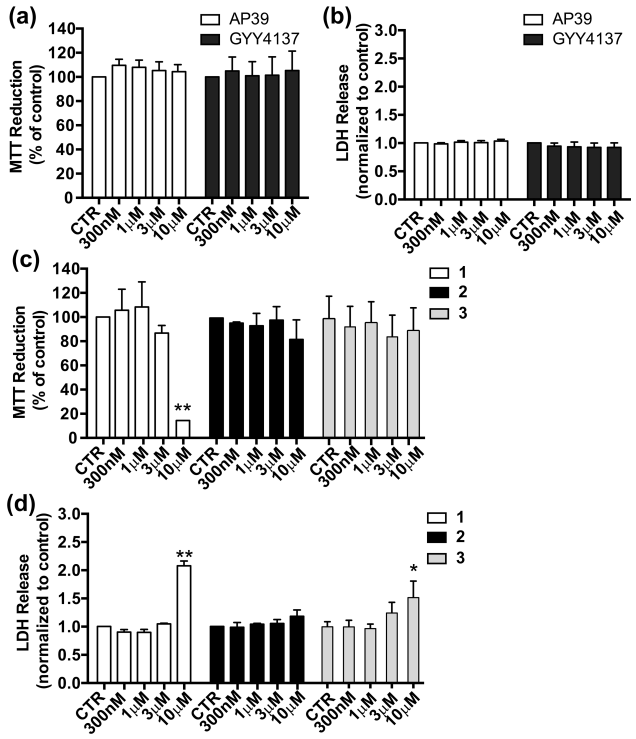

Figure 5.3 Cell viability studies of AP39, GYY4137, and **1**-**3** in BEAS 2B using the (a,c) MTT and (b,d) LDH cell viability assays.

cells incubated with AP39 and GYY4137 under the same conditions (Figure 5.4g-i). We failed to observe significant inhibition of cellular bioenergetics at the observed concentrations, raising the possibility that the inhibitory effects of **1** may not be from H_2S release alone, but could also be due to direct COS inhibition of cytochrome c oxidase,[245, 246] which has been reported previously but received less scrutiny than direct H_2S inhibition. Our previous investigations with ROS-activated[140] and "click-and-release"[131] COS/H_2S donors did not reveal donor cytotoxicity below 100 μM, suggesting that the observed cytotoxicity from **1** may be amplified by specific localization of the esterase-activated **1** or efficient release H_2S in local environments associated with the mitochondrial respiratory chain.

5.3 Conclusions

In conclusion, we have designed an easy-to-access, esterase-triggered COS/H_2S donor and shown that it is rapidly activated by esterases to generate H_2S *in vitro* using isolated PLE. Using toxicity assays and bioenergetics measurements, we demonstrated

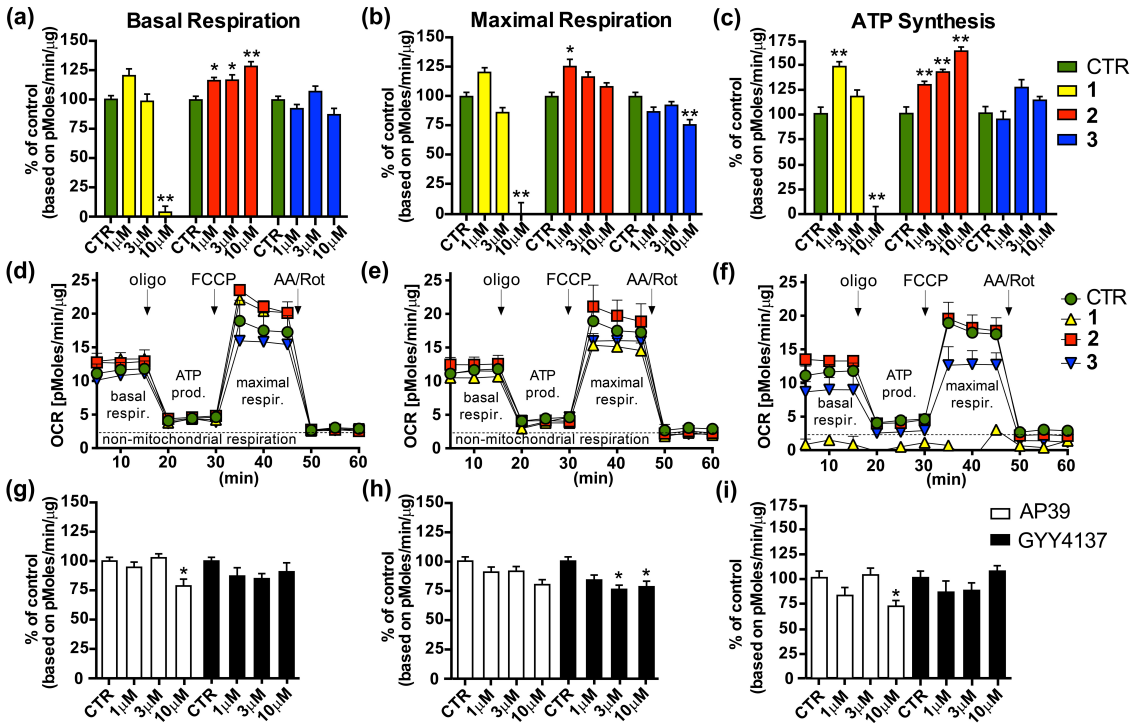

Figure 5.4 Cellular bioenergetics analysis including (a) basal respiration, (b) maximal respiration, and (c) ATP synthesis in BEAS 2B cells upon addition of 1-10 μM of **1-3** as well as full bioenergetics data at (d) 1 μM, (e) 3 μM, and (f) 10 μM. For comparison, data was additionally collected for (g) basal respiration, (h) maximal respiration, and (i) ATP synthesis of BEAS 2B cells incubated with AP39 and GYY4137. Abbreviations: oligo: oligomycin, FCCP: carbonyl cyanide 4-(trifluoromethoxy)phenylhydrazone, AA/Rot: antimycin A and rotenone. Values represent the means ± SEMs from three independent biological experiments each with five replicates. The values that are significantly different by Student's t test are indicated by asterisks as follows: **, $P < 0.01$; *, $P < 0.05$.

that the increased cytotoxicity of **1** is due inhibition of mitochondrial respiration, whereas carbamate control compound **2** and triggerless thiocarbamate **3** failed to negatively perturb normal bioenergetics. Using AP39 and GYY4137, we confirmed that the disruption of cellular bioenergetics observed from **1** is significantly different than is seen with other H_2S donors, potentially suggesting that either the amount of produced H_2S, specific localization of the esterase-triggered scaffold, or direct inhibition of mitochondrial respiration by COS itself is responsible for the observed cytotoxicity. As a whole, the esterase-cleaved donor reported here provides a slow-release method of COS/H_2S release in cellular environments. Further work investigating the relationship

between the kinetics of COS release and the cytotoxicity of esterase-activated donors is reported in Chapter VI.

CHAPTER VI

TUNABLE ESTERASE-TRIGGERED SELF-IMMOLATIVE THIOCARBAMATES PROVIDE INSIGHTS INTO COS CYTOTOXICITY

This chapter includes unpublished, coauthored material written by myself and C.M Levinn with editorial assistance by M.D. Pluth. The experimental work was performed by either myself or C.M Levinn.

6.1 Introduction

Hydrogen sulfide (H_2S), the most recent addition to the gasotransmitter family,[199] plays important physiological roles in the cardiovascular,[247] respiratory, as well as other organ systems.[2] Significant interest in both research and therapeutic strategies for H_2S delivery has led to the development of a library of synthetic small molecules that release H_2S (H_2S donors) by using different strategies.[122, 129, 248-250] In one recently-developed approach, our group, as well as others, has reported H_2S donors based on the triggerable, self-immolative decomposition of thiocarbamates to release carbonyl sulfide (COS), which is rapidly hydrolyzed to H_2S by the ubiquitous mammalian enzyme carbonic anhydrase (CA).[131] This COS-dependent H_2S-releasing strategy is highly tunable and allows for triggering of H_2S release by a variety of stimuli, including ROS,[140, 208] nucleophiles,[150] cysteine,[251] and light.[208, 209, 252]

In addition to functioning as a precursor for CA-mediated H_2S release, COS is the most prevalent sulfur-containing gas in Earth's atmosphere, and plays important roles in the global sulfur cycle. Despite this significance, few studies have investigated the physiological properties of COS directly.[205] Currently, there are no known mechanisms of eukaryotic COS biosynthesis, although it has been shown that acetylcholine stimulation of porcine coronary artery (PCA) leads to an observed increase in COS, indicating that muscarinic acetylcholine receptors (mAChRs) could play a role in regulating COS synthesis.[41] Additionally, it has been detected in the headspace of porcine coronary artery and cardiac muscle,[41] suggesting potential endogenous production. COS has also been recognized COS as an exhaled breath biomarker for a variety of diseases,

including cystic fibrosis[39] and liver disease and rejection,[40, 233] which suggests a possible role in disease physiology. The consumption of COS by CA is well established and COS toxicity closely resembles that of H_2S, which is likely due to CA-mediated hydrolysis within mucous membranes upon exposure. The rapid conversion of COS to H_2S, with an associated rate constant of $2.2x10^4$ $M^{-1}s^{-1}$ (for bovine carbonic anhydrase II), makes COS a convenient source of sulfide, but also makes disentangling the chemical biology of COS from H_2S more challenging.[65]

We recently reported an esterase-triggered COS-mediated H_2S donor,[207] wherein ester cleavage reveals an intermediate phenol that undergoes a 1,4-self-immolation cascade to release COS, followed by rapid hydrolysis to H_2S. Contrary to previous reports of similar donors, however, these compounds exhibit significant cytotoxicity and fully inhibited major mitochondrial bioenergetic pathways in bronchial epithelium BEAS2B cells. Similar cytotoxicity profiles were not observed for other H_2S donors, including NaSH, GYY4137, or AP39, at similar concentrations. Furthermore, analogous CO_2-releasing carbamate control compound were non-cytotoxic, confirming that the observed cytotoxicity or bioenergetics impacts were not due to organic byproducts of donor activation. Taken together, these results led to the hypothesis that the observed effects could be due to a buildup of COS. Supporting this hypothesis, the rate of small ester cleavage by mammalian esterases is likely faster (around $5.1x10^4$ – $5.8x10^5$ $M^{-1}s^{-1}$) than the rate of CA-mediated COS hydrolysis to H_2S,[65, 253] which would result in a buildup of intracellular COS. Here we extend this hypothesis by preparing a library of esterase-cleaved COS-releasing donors in which the steric bulk of the ester and the electronic properties of the aniline payload are modified, and demonstrate that the differential cytotoxicity of these donors maps to the COS release rates, thus furthering the hypothesis that COS may exert different biological effects than H_2S alone (Figure 6.1).

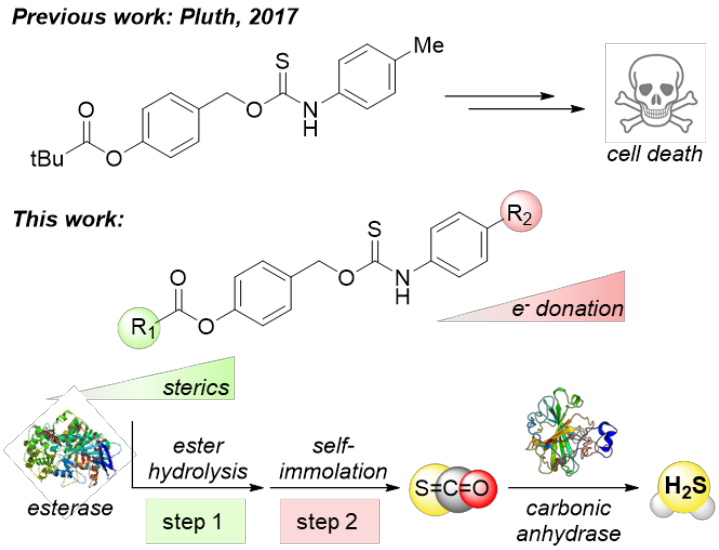

Figure 6.1 Esterase-triggered thiocarbamate-based H_2S donors exhibit increased cytotoxicity, potentially due to the buildup of intracellular COS.

6.2 Results and Discussion

To further investigate whether the cytotoxicity of these esterase-activated COS/H_2S donor could be related to COS directly, we chose to probe the relationship between COS release rates and the corresponding cytotoxicity. We hypothesized that if COS buildup was responsible for the observed cytotoxicity, then esters cleaved more quickly should result in increased cell death, whereas esters cleaved more slowly should have a diminished effect. In the esterase-activated donors, the rate of COS release depends not only on the rate of ester cleavage ("triggering"), but also on the rate of self-immolative decomposition. There have been a number of reports demonstrating that rate of esterase activity varies directly with the steric bulk of the ester being cleaved,[254, 255] providing a rational strategy for manipulating the rate of triggering by intracellular esterases. Similarly, recent work has demonstrated that the electronics of the amine payload can affect the rate of thiocarbamate self-immolation.[152, 206] To probe the relationship between rate of ester cleavage, self-immolative decomposition, and cytotoxicity, a suite of esterase-activated COS donors with varying ester sizes and payloads were prepared to shed some light on the assumed innocence of COS.

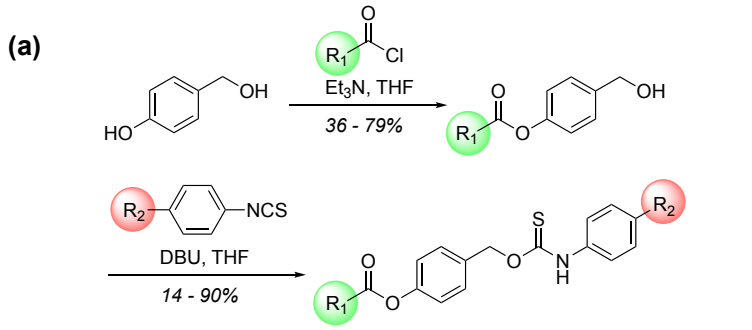

	R_1	X	yield
TCM1	Me	S	14%
TCM2	Cp	S	39%
TCM3	iPr	S	31%
TCM4	MeCp	S	61%
TCM5	tBu	S	64%
TCM6	Ph	S	22%
TCM7	Cy	S	29%
TCM8	1-Ad	S	26%
TCM9	2-Nap	S	76%
CM1	Me	O	36%
CM2	Cp	O	57%
CM3	iPr	O	52%
CM4	MeCp	O	90%
CM5	tBu	O	83%
CM6	Ph	O	79%
CM7	Cy	O	79%
CM8	1-Ad	O	53%
CM9	2-Nap	O	71%

	R_2	X	yield
TCM10	Ph	S	45%
TCM5	Me	S	64%
TCM11	H	S	55%
TCM12	F	S	58%
TCM13	CF_3	S	51%
TCM14	NO_2	S	47%
CM10	Ph	O	56%
CM5	Me	O	83%
CM11	H	O	78%
CM12	F	O	75%
CM13	CF_3	O	90%
CM14	NO_2	O	80%

Figure 6.2 (a) Synthetic scheme for the development of a library of esterase-activated thiocarbamate COS/H_2S donors (**TCM1-14**) and (b) table showing all compounds used in this study (**TCM1-14** and **CM1-14**) with yields.

To probe the effects of steric bulk on the rate of COS release and cytotoxicity of esterase-triggered COS donors, we prepared a library of thiocarbamates functionalized with different esters. To prepare the donors, we first treated 4-hydroxy benzyl alcohol with different alkyl and aryl carbonyl chlorides to afford the corresponding esters. Reaction with *p*-tolyl isothiocyanate furnished the desired thiocarbamates (**TCM1** to **TCM9**) in 14-90% yield (Figure 6.2a). In parallel, we also prepared the carbamate control compounds, which release CO_2 rather than COS, by treatment of the carbonyl chloride intermediates with *p*-tolyl isocyanate (Figure 6.2b). To investigate the role of electronic modulation of the aniline payload on the rate of self-immolation and cytotoxicity of these compounds, a similar synthetic sequence was followed to access

esterase-triggered COS donors with electron-rich and electron-deficient amine payloads, (**TCM10** to **TCM14**).

With the library of esterase-activated COS/H_2S donors in hand, we next measured the H_2S release from these compounds in the presence of CA and porcine liver esterase (PLE). Direct detection of H_2S using a sulfide-selective electrode is simple and fast, but analogous methods for rapid COS detection directly in solution. For this reason, we added excess CA to these experiments to ensure no buildup of COS and used the detection of H_2S as an indirect measurement of COS release. We treated compounds **TCM1** – **TCM9** (Figure 6.2b, left) and **TCM10** – **TCM14** (Figure 6.2b, right) with 5 U/mL PLE in the presence of CA (25 μg/mL) in PBS buffer (pH 7.4) and observed H_2S release from each of compounds using a H_2S-sensitive electrode. This data confirms that physiologically relevant amounts of CA and PLE are sufficient to result in H_2S release from each of these donors. Consistent with our expectation that steric changes to the esters would results in different cleavage rates, we observed significantly different H_2S release rates and efficiencies from the donor compounds containing a variety of different ester groups (Figure 3a). For example, donors with bulkier esters (cyclohexyl (**TCM7**), adamantyl (**TCM8**), or naphthyl (**TCM9**), yellow, orange, and light blue, respectively) generated H_2S more slowly than those with smaller esters (methyl (**TCM1***),* t-butyl (**TCM5**), or methyl cyclopropyl (**TCM4**), dark green, grey, and magenta, respectively). This qualitatively confirms that donors containing larger ester groups produce COS/H_2S more slowly, consistent with slower hydrolysis by PLE.

H_2S release kinetics were also compared for a library of *t*-butyl ester functionalized donors containing a variety of electronically modulated amine payloads. We hoped to systematically decrease the rate of COS release through the introduction of electron-donating groups, although acidification of the N-H proton of the thiocarbamate has been reported to decrease the rate of COS release from similar donors functionalized with electron-withdrawing groups as well.[206] Consistent with this hypothesis, the introduction of either strongly electron-withdrawing (NO_2 (**TCM14**), CF_3 (**TCM13**), pink and purple, respectively) or electron-donating (Ph (**TCM10**), black) groups decreased the rate and efficiency of the donors, indicating that both electron-withdrawing and electron-donating groups slow down the rate of self-immolation following esterase hydrolysis.

The donors containing weakly electronically modified amine payloads **TCM5, TCM11, and TCM12)** appear to have very similar initial rates (Figure 6.3b).

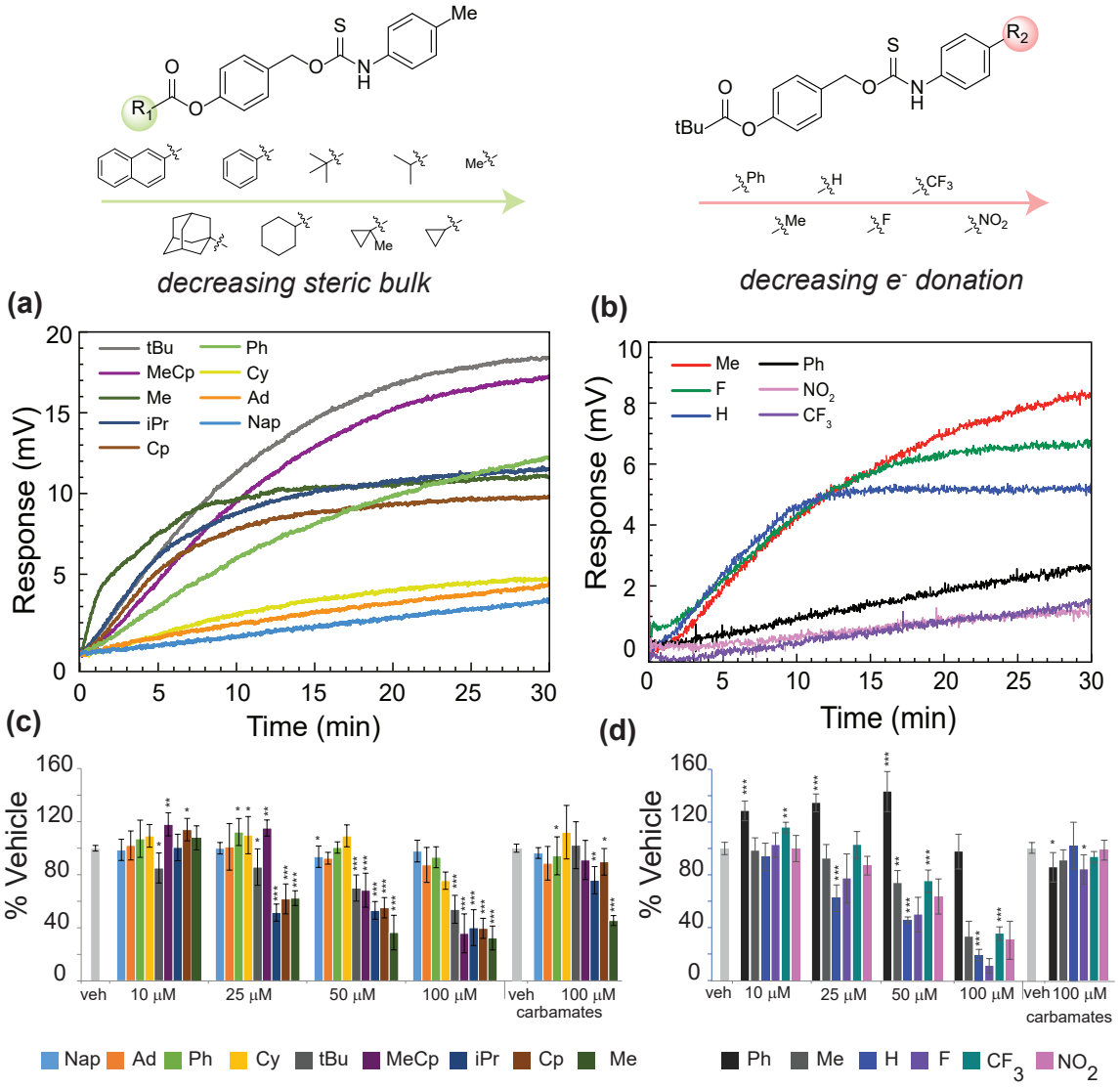

Figure 6.3 H_2S release curves for compounds (a) TCM1 – TCM9 and (b) TCM5, TCM 10-TCM14) in the presence of PLE (5 U/mL) and CA (25 µg/mL) at pH 7.4. (b and c) Cytotoxicity of compounds in HeLa cells. Data for donors (TCM1 – TCM14) is shown for 10 – 100 µM and compared to the cytotoxicity of the carbamate control compounds (CM1 – CM14) at 100 µM. (b) Cytotoxicity data for donors containing varying ester groups (TCM1 – TCM9), with steric bulk of the ester group decreasing from left to right. (c) Cytotoxicity data for donors containing varying amine payloads (TCM5, TCM10 – TCM14), with electronic donating-ability of the payload decreasing from left to right. Results are expressed as mean ± SD (n=6). The values that are significantly different by Student's t test are indicated by asterisks as follows: ***, $p < 0.001$ **, $p < 0.01$; *, $p < 0.05$.

We next sought to determine whether the observed differences in COS/H_2S release rates translated to differences in cytotoxicities of compounds **TCM1 – TCM14**. To probe these effects, we incubated HeLa cells with the COS donor compounds at 10, 25, 50, and 100 μM for 90 minutes and measured the resultant cell viability against the vehicle using the formazan dye-based CCK-8 cytotoxicity assay. We found that the cytotoxicity of the donors increased as the size of the ester decreased (Figure 6.3c), with the smallest ester (Me, **TCM1**) resulting in about 70% cell death at 100 μM. No significant cell death was observed, however, when cells were incubated with 100 μM of **TCM9**, which requires hydrolysis of a much larger naphthyl ester and has a much slower rate of COS/H_2S release. To confirm that the observed cytotoxicity was not due to the organic byproducts of the donor constructs after activation, we also investigated the cytotoxicity of the corresponding carbamate control compounds (**CM1** – **CM14**) using the same conditions. Overall, we found significantly less cytotoxicity of all of the carbamates up to 100 μM. No significant trend was observed in the cytotoxicity of the donors as the electronics of the payload were changed. While many of these donors (**TCM5, TCM11** – **TCM14**) were cytotoxic, even as low as 25 μM, we did not find any correlation between cytotoxicity and the electronics of the amine payload (Figure 6.3d). Since the mechanism of decomposition of these donors may change due to acidification of the N-H proton, the cytotoxicity likely does not correspond to the rate of COS production.

This work provides evidence that cellular accumulation of COS is cytotoxic. Importantly, the cytotoxicity observed from many of these COS donors was completely eliminated when HeLa cells were incubated with the analogous, CO_2-releasing carbamates, which control for all other byproducts, suggesting that COS directly for the observed effects. Cell death is dose-dependent for all of the cytotoxic COS-releasing compounds, and in general, the most cytotoxic donors were also found the have the most rapid kinetics of H_2S release in the presence of CA. Overall, the hypothesis that the inclusion of a larger ester on these donors would decrease the rate of hydrolysis and prevent the build-up of COS was found to hold true. We were not able to systematically decrease the rate of COS release through electronic modulation of the amine payloads, but did find that both strongly electron-withdrawing and electron-donating groups diminished COS/H_2S release, consistent with two previously suggested effects: that

electron-donating groups decrease the rate of self-immolation, and electron-withdrawing groups can result in a change in the mechanism of H_2S release due to acidification of the N-H proton on the thiocarbamate.[206] Due to a potential change in mechanism supported by a decrease in H_2S production from donors containing electron-withdrawing payloads, it is impossible to correlate the cytotoxicity of these particular donors with their rate of COS/H_2S release.

In addition to providing new insights into the differential impacts of COS and H_2S, this work also increases the tools available for increasing basal H_2S concentrations without the need for external triggering mechanisms or consumption of cellular nucleophiles. To confirm that these donors release COS/H_2S in a cellular environment, we incubated 100 μM Cy-TCM (**TCM7**) with SF7-AM in HeLa cells and observed an increase in fluorescence corresponding to H_2S donation from the scaffold (Figure 6.4). This confirms the basic cellular viability of this compound as an H_2S donor. Although the faster donors are too cytotoxic for use, the slower donors form library of enzyme-activated COS/H_2S donors viable for use *in vivo*.

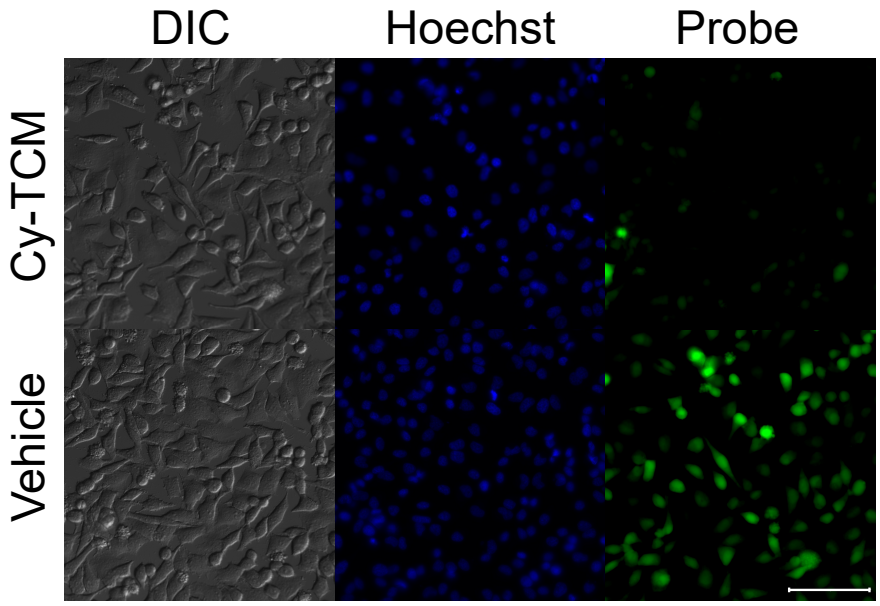

Figure 6.4 Live-cell imaging of H_2S release from TCM7in HeLa cells. HeLa cells were treated with SF7-AM (5 μM) and Hoescht (5 μg/mL) for 30 min, washed, and incubated with FBS-free DMEM containing TCM7 (100 μM, top) or DMSO (0.5%, bottom) for one hour. Cells were then washed and imaged in PBS. Scale bar represents 100 μM.

6.3 Conclusions

In conclusion, this work supports the hypothesis that rapid accumulation of COS likely results in cytotoxicity.[207] Conclusively disentangling the effects of COS delivery from the physiological effects of H_2S will require a systematic study of COS, the various CA isoforms, and the potential for subcellular localization of COS delivery from various donors. The work reported here suggests the likely role of COS in the cytotoxicity of many of these compounds, and provides is an important piece of early evidence that COS delivery may produce a cellular response that is different than that observed from H_2S alone. In Chapter VII, a variety of potential COS donor scaffolds are investigated for their cytotoxicity and CA inhibition properties to inform researchers on the best donor scaffolds for studying COS and H_2S chemical biology.

6.4 Experimental Details

6.4.1 Materials and Methods

Reagents were purchased from Sigma-Aldrich or Tokyo Chemical Industry (TCI) and used as received. SF7-AM was synthesized as previously reported.[196] Spectroscopic grade, inhibitor-free THF was deoxygenated by sparging with argon followed by passage through a Pure Process Technologies solvent purification system to remove water. Deuterated solvents were purchased from Cambridge Isotope Laboratories and used as received. Silica gel (SiliaFlash F60, Silicycle, 230-400 mesh) was used for column chromatography. ^{1}H, $^{13}C\{^{1}H\}$, and ^{19}F NMR spectra were recorded on a Bruker 500 or 600 MHz instrument (as indicated). Chemical shifts are reported in ppm relative to residual protic solvent resonances. Mass spectrometric measurements were performed on a Xevo Waters ESI LC/MS instrument or by the University of Illinois, Urbana Champaign MS facility. H_2S electrode data were acquired with a Unisense H_2S Microsensor Sulf-100 connected to a Unisense Microsensor Multimeter. All air-free manipulations were performed under an inert atmosphere using standard Schlenk techniques or an Innovative Atmospheres N_2-filled glove box. HeLa cells were purchased from ATCC (Manassas, Virginia, USA). Cell imaging experiments were performed on a Leica DMi8 fluorescence microscope, equipped with an Andor Zyla 4.2+ sCMOS detector.

H_2S Electrode Experiments. Scintillation vials containing 20.00 mL of phosphate buffer (140 mM NaCl, 3 mM KCl, 10 mM phosphate, pH 7.4) were prepared in an N_2-filled glovebox. The Unisense electrode was inserted into the vial and the vial was capped with a split-top septum to minimize oxidation. The current was allowed to equilibrate prior to starting the experiment. With moderate stirring, the CA stock solution (50 μL) was injected, followed by subsequent injections of TCA stock solution (50 μL) and PLE stock solution (100 μL). H_2S release was monitored until leveling off.

CCK-8 Cell Viability Experiments. HeLa cells were cultured in Dulbecco's modified Eagle's medium (DMEM) supplemented with 10% fetal bovine serum (FBS) and 1% penicillin/streptomycin at 37 °C under 5% CO_2. 96-well plates were seeded with 15,000 cells/well overnight then washed, incubated in FBS-free DMEM containing vehicle (0.5% DMSO), TCA (10-100 μM), or carbamate (10-100 μM) for 90 minutes. Cells were then washed with PBS and CCK-8 solution (1:10 in FBS-free DMEM) was added to each well, and cells were incubated for 1-2 hours at 37 °C under 5% CO_2. The absorbance at 450 nm was measured using a microplate reader and the cell viability was measured and normalized to the vehicle group. Results are expressed as mean ± SD (n=6). *P* values were calculated using a Student's T-test in Excel compared to DMSO alone.

Cell Imaging. HeLa cells were cultured in Dulbecco's modified Eagle's medium (DMEM) supplemented with 10% fetal bovine serum (FBS) and 1% penicillin/streptomycin at 37 °C under 5% CO_2. Imaging dishes were seeded with HeLa cells overnight and then washed and incubated with SF7-AM (5 μM) and Hoechst 33342 (5 μg/mL) in FBS-free DMEM for 30 min. Cells were then washed with PBS and incubated with either Cy-TCM (100 μM) or vehicle (DMSO, 0.5%) in FBS-free DMEM for 60 minutes prior to being washed with PBS and imaged.

6.4.2 Syntheses

General procedure for the synthesis of phenol esters. 4-Hydroxy benzyl alcohol (1.0 equiv.) was dissolved in anhydrous THF (0.1 M solution), under and atmosphere of N_2. The solution was cooled to 0 °C, followed by addition of Et_3N. The reaction mixture was let stir for 5 minutes, after which the carbonyl chloride was added dropwise over 20 minutes. The resultant mixture was stirred at 0 °C until the completion of the reaction

indicated by TLC. The reaction was quenched by adding brine (30 mL), and the aqueous solution was extracted with ethyl acetate (3 x 20 mL). The organic layers were combined, dried over anhydrous $MgSO_4$, and concentrated under reduced pressure. The crude product was purified by silica column chromatography. Full spectroscopic data for each compound is reported in Appendix E. The preparation of MeCp-OH is also reported in the Appendix E..

General procedure for preparation of thiocarbamates. The functionalized benzyl alcohol (1.0 equiv.) was dissolved in anhydrous THF (0.2 M solution) under an atmosphere of N_2. Aryl isothiocyanate (1.1 equiv.) was added, followed by DBU (1.25 equiv.) at 0 °C. The resultant mixture was warmed to rt and stirred monitored by TLC. The reaction was quenched upon observation of by-product formation by TLC by addition of brine (20 mL), and extracted with EtOAc (3 x 20 mL). The combined organic layers were dried over anhydrous $MgSO_4$ or Na_2SO_4, concentrated under reduced pressure, and purified by silica column chromatography. Full spectroscopic data for each compound is reported in Appendix E.

General procedure for preparation of carbamate controls. Functionalized benzyl alcohol (1.0 equiv.) was dissolved in anhydrous THF (0.1 M solution) under an atmosphere of N_2. Aryl isocyanate (0.90 equiv.) was added, followed by DBU (1.25 equiv.) at 0 °C. The resultant mixture was warmed to rt and stirred monitored by TLC. The reaction was quenched upon observation of by-product formation by TLC by addition of brine (20 mL), and extracted with EtOAc (3 x 20 mL). The combined organic layers were dried over anhydrous $MgSO_4$, concentrated under reduced pressure, and purified by silica column chromatography. Full spectroscopic data for each compound is reported in Appendix E.

CHAPTER VII

INVESTIGATIONS INTO THE CARBONIC ANHYDRASE INHIBITION OF COS-RELEASING DONOR CORE MOTIFS

This chapter includes previously published and coauthored material from Steiger, A.K; Zhao, Y.; Choi, W.J.; Tillotson, M.R.; Crammond, A.; Pluth, M.D. "Investigations into the Carbonic Anhydrase Inhibition of COS-Releasing Donor Core Motifs" *Biochem. Pharmacol.* **2017**, 149, 124-130.

7.1 Introduction

Hydrogen sulfide (H_2S), now well established as an important gaseous signaling molecule, has been implicated in a wide variety of physiological processes since its initial recognition in 1996.[12, 199, 256] H_2S is produced endogenously and maintained at low (mid-nanomolar) concentrations, and the administration of exogenous sulfide has been shown to provide a therapeutic benefit in various applications, including reduction of myocardial infarct size, vasodilation, and decrease in inflammation.[2, 9] For example, GYY4137 and AP39, which undergo slow hydrolysis to release H_2S, have been shown to exhibit anti-inflammatory activity.[229, 257] Additionally, appending H_2S donor scaffolds to non-steroidal anti-inflammatory drugs (NSAIDs) has been used to generate a number of H_2S-NSAID hybrids including ATB-346 and NBS-1120, which are based on naproxen and aspirin derivatives, respectively (Figure 7.1). Aligned with these positive impacts, new H_2S donation strategies are emerging rapidly, and a number of H_2S-releasing compounds are currently in clinical trials.[123, 204] Recent goals in improving upon H_2S-based therapeutics have included triggerable donation in response to specific (and variable) stimuli, controllable rates of H_2S release, and the ability to append the H_2S-releasing moiety to a variety of scaffolds to potentially access H_2S-drug hybrids.

Building from these needs, our lab recently introduced a new strategy for H_2S donation by using self-immolative carbonyl sulfide (COS)-releasing motifs (Figure 7.2a), which leverages the rapid hydrolysis of COS to H_2S by carbonic anhydrase (CA), a ubiquitous mammalian zinc metalloenzyme that normally catalyzes the hydrolysis of CO_2

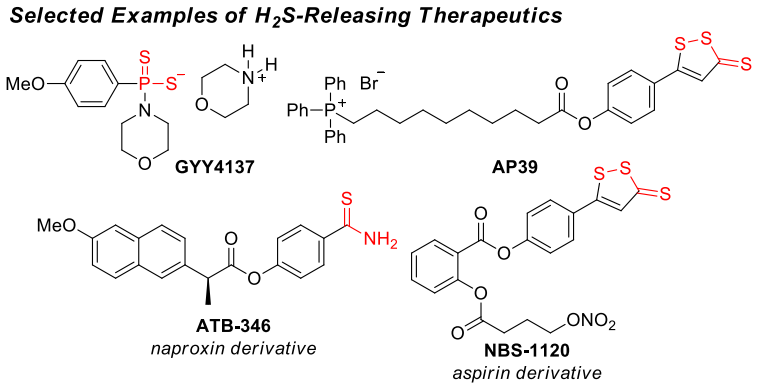

Figure 7.1 Selected examples of H_2S-releasing therapeutics currently in various stages of clinical development.

under near diffusion-limited rates to regulate blood pH levels and tissue CO_2 transport.[258, 259] Since our initial report,[131] a number of related COS-donating scaffolds have been reported for H_2S release.[140, 147, 150, 152, 207-209] Complementing slow-release COS donors,[150] a common strategy has been to engineer the triggered self-immolative COS release, which can be activated by different stimuli, including ROS,[140] esterase,[152, 207] light,[208, 209] and bio-orthogonal triggers[147] (selected triggered examples are shown in Figure 7.2b). In addition to providing functional H_2S donor platforms, the availability of such COS donors may allow for the investigation of COS chemical biology, which has been largely under-studied.[205] Because CA is required for the efficient conversion of COS to H_2S in all of the above scaffolds, it is imperative to not only understand the mechanism of CA activity in COS hydrolysis, but to also to determine whether any of the COS-donating motifs are functional CA inhibitors. Significant prior research has focused on identifying CA inhibitors for therapeutic uses, such as treatment of glaucoma, epilepsy, and mountain sickness, and is the topic of numerous recent reviews.[108, 111, 259] Because the structural scope of active CA inhibitors is broad and includes many sulfur-containing molecules, including dithiocarbamates and trithiocarbonates,[260, 261] and we wanted to determine whether the sulfur-containing cores of possible COS-releasing scaffolds (Figure 7.2c) exhibit CA inhibition. If a COS-releasing motif functions as a viable CA inhibitor, donor scaffolds built from such motifs are unlikely to find widespread utility as functional H_2S donors. Because efficient H_2S release from COS donors relies on CA activity, such investigations are important in understanding the scope of potential COS-

releasing structural motifs.

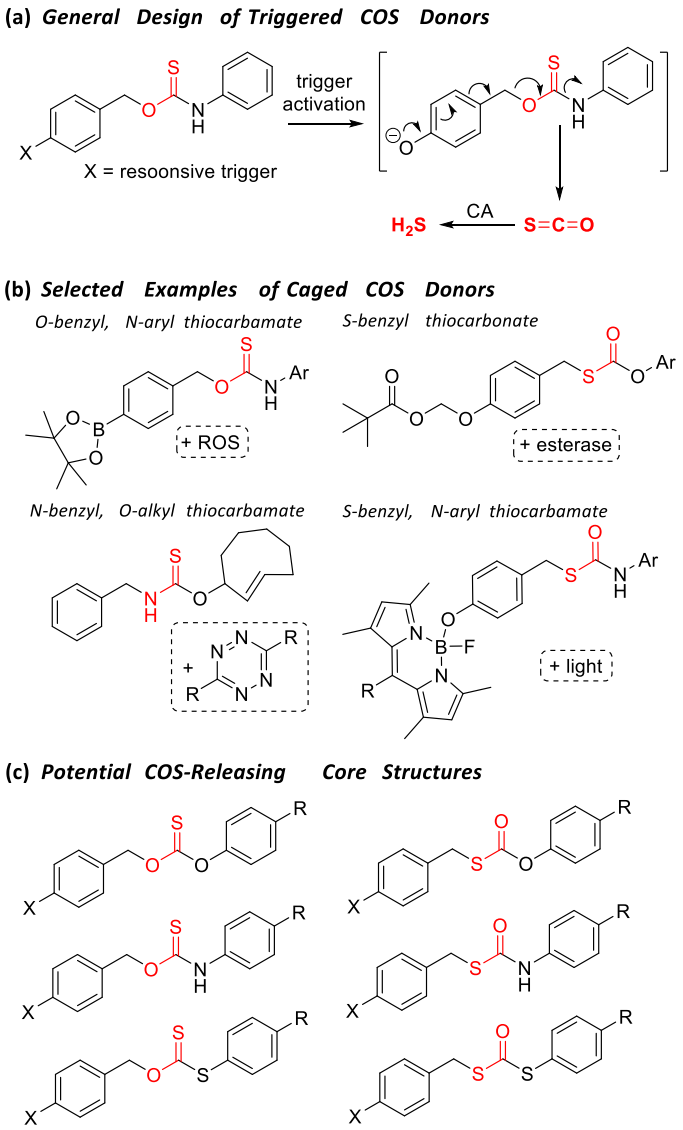

Figure 7.2 (a) General strategy for H_2S generation from COS-releasing molecules. A caged thiocarbamate is shown as an example system. (b) Selected examples of triggered COS donors with different core structural motifs. (c) Potential thiocarbonate, thiocarbamate, and dithiocarbonate motifs that could function as COS/H_2S donors.

7.2 Results

7.2.1 Synthesis of Model Compounds

The 15 model compounds used in our investigations were prepared using two general procedures. In synthetic procedure A (Figure 7.3a), one equivalent of an alcohol, thiol, or amine was combined with one equivalent of phenyl isothiocyanate or phenyl

isocyanate and base and was stirred until completion of the reaction. Following an extraction and purification by column chromatography, compounds **1**, **2**, **6**, **9**, and **14-15** were isolated in 20-88% yield. In synthetic procedure B (Figure 7.3b), one equivalent of the alcohol, thiol, or amine starting material was combined with one equivalent of phenyl chloroformate and base. When the reaction was complete, the product was washed, extracted, and purified by column chromatography. Compounds **3-5**, **7-8**, and **10-13** were isolated in 32-82% yield.

Our initial report of caged COS release utilized an *O*-alkyl thiocarbamate scaffold, but *S*-alkyl thiocarbamates and thiocarbonates have also been reported.[152, 209] Depending on the placement of the COS moiety in the caged core, there different constitutional isomers that can release COS, which motivated our selection of model compounds **1-5** (Figure 7.3c). Similarly, the availability of caged CO_2 compounds, which generate CO_2/H_2O rather than COS/H_2S, prompted our investigation of control compounds **6-8** (Figure 7.3d). Additionally, the recent interest in CS_2 donor development prompted our inclusion of dithiocarbamates **9-10** (Figure 7.3e).[262] Finally, we included isomers **11-15** as control compounds, which have similar functional motifs but lack the caged COS core (Figure 7.3f). For each of these model compounds, our goal was to determine whether the core structures exerted cytotoxicity or cell proliferative effects and also to measure the CA inhibition profiles for each compound to better guide future COS donor development.

7.2.2 Cytotoxicity Evaluation

Prior to measuring CA inhibition profiles, we first measured the cytotoxicity of each compound in A549 human lung adenocarcinoma cells using the CCK-8 cell proliferation assay. We chose concentrations ranging from 10 – 100 μM for each compound, which corresponds to the general concentration ranges typically used in biological experiments that use H_2S-donating compounds. Incubation of A549 with 10, 25, 50, or 100 μM of each compound did not result in significant cytotoxicity or proliferation, suggesting that the inherent core structures from each model compound do not significantly impact cell viability (Figure 7.4).

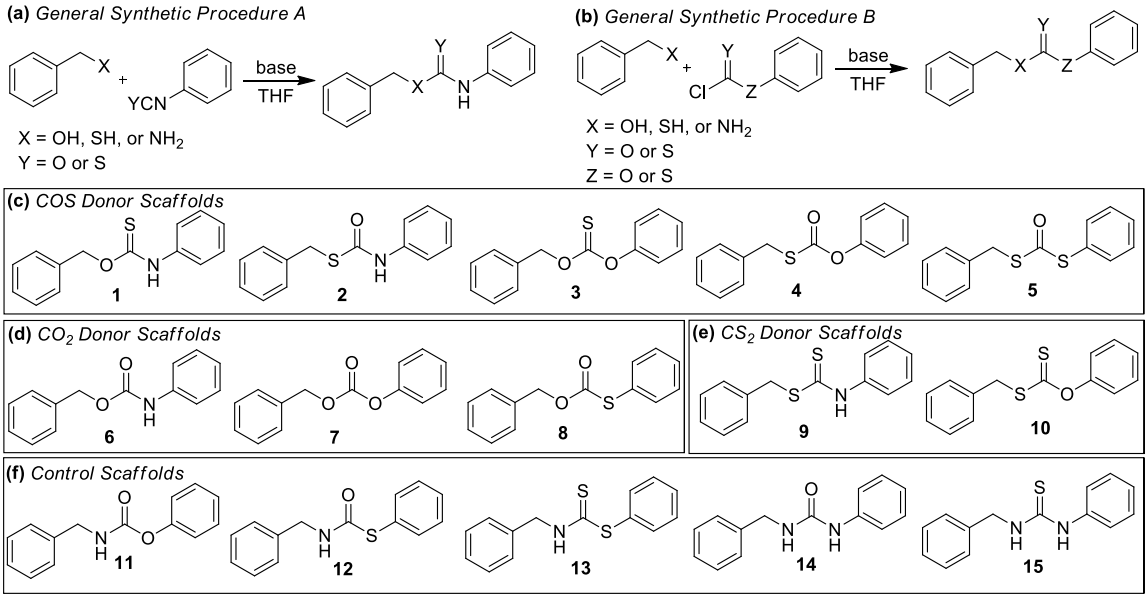

Figure 7.3 (a), (b) General synthetic procedures to prepare model compounds. Structures of the model compounds prepared and investigated in this study include (c) COS donor scaffolds (**1**-**5**), (d) CO_2 donor scaffolds (**6**-**8**), (e) CS_2 donor scaffolds (**9**-**10**), and (f) control scaffolds (**11**-**15**).

7.2.3 Determination of CA Inhibitors

To investigate the potential CA inhibition properties of each of the selected scaffolds, we used CA-mediated *p*-nitrophenyl acetate (pNPA) hydrolysis as a model system for measuring CA activity / inhibition. The CA-mediated hydrolysis of pNPA is slower than the near diffusion-limited hydrolysis of CO_2, and the *p*-nitrophenol (pNP) product has a characteristic absorbance at 405 nM, thus providing a simple method to measure CA activities by UV-vis spectroscopy (Figure 7.5a)[263]. For each compound, we measured the rate of pNPA hydrolysis to pNP and compared these observed rates to those of CA alone, as well as the rate in the presence of the common CA inhibitor acetazolamide (AAA). In each case, the rate of production of pNP was then fit directly to a first-order exponential equation. Of the 15 compounds tested, 11 failed to produce significant changes in the rate of pNPA hydrolysis, suggesting that these compounds do not exhibit significant CA inhibition at concentrations typically used in H_2S donor experiments. Four compounds, however, were found to inhibit CA activity: **2, 9, 12,** and **13**. Of these compounds, **2** and **9** were moderate inhibitors and decreased the rate of

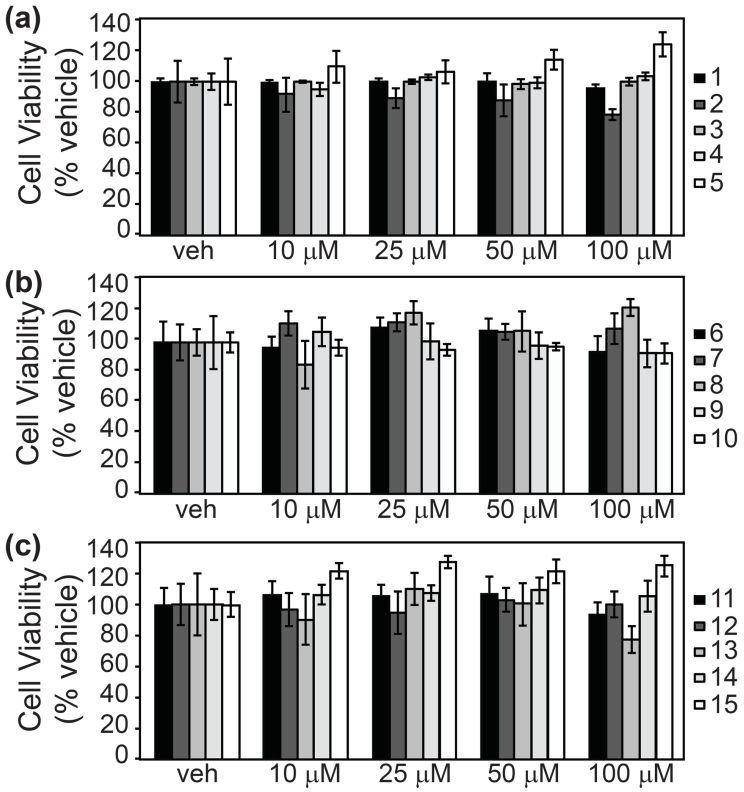

Figure 7.4 CCK-8 cytotoxicity assay of compounds 1-15. The cytotoxicity of each compound was investigated in A549 cells at 10, 25, 50 and 100 μM using the CCK-8 cell counting assay and compared to the DMSO vehicle. (a) caged COS scaffolds (**1-5**), (b) caged CO_2 (**6-8**) and CS_2 (**9-10**) scaffolds, and (c) control scaffolds (**11-15**).

pNPA hydrolysis by about 50%. By comparison, compounds **12** and **13** were much more effective CA inhibitors and decreased the rate of hydrolysis to approximately that seen in the presence of AAA, which is recognized as a strong CA inhibitor (Figure 7.5b-f).

7.2.4 Inhibition studies with potential decomposition products

In addition to the 15 compounds examined above, we also investigated the CA inhibition properties of thiophenol and benzyl thiol because these thiols could potential be generated as hydrolysis and/or decomposition products of **2**, **9**, **12**, and **13**. (*vide infra*). We found both thiophenol and benzyl thiol to inhibit CA (Figure 7.5e). The rate of hydrolysis in the presence of thiophenol alone was found to be similar to that of **12** and **13**, both of which, if deprotonated, would decompose to thiophenol. Similarly, the rate of pNPA hydrolysis observed in the presence of benzyl thiol is similar to that of **2** and **9**, which would decompose to benzyl thiol.

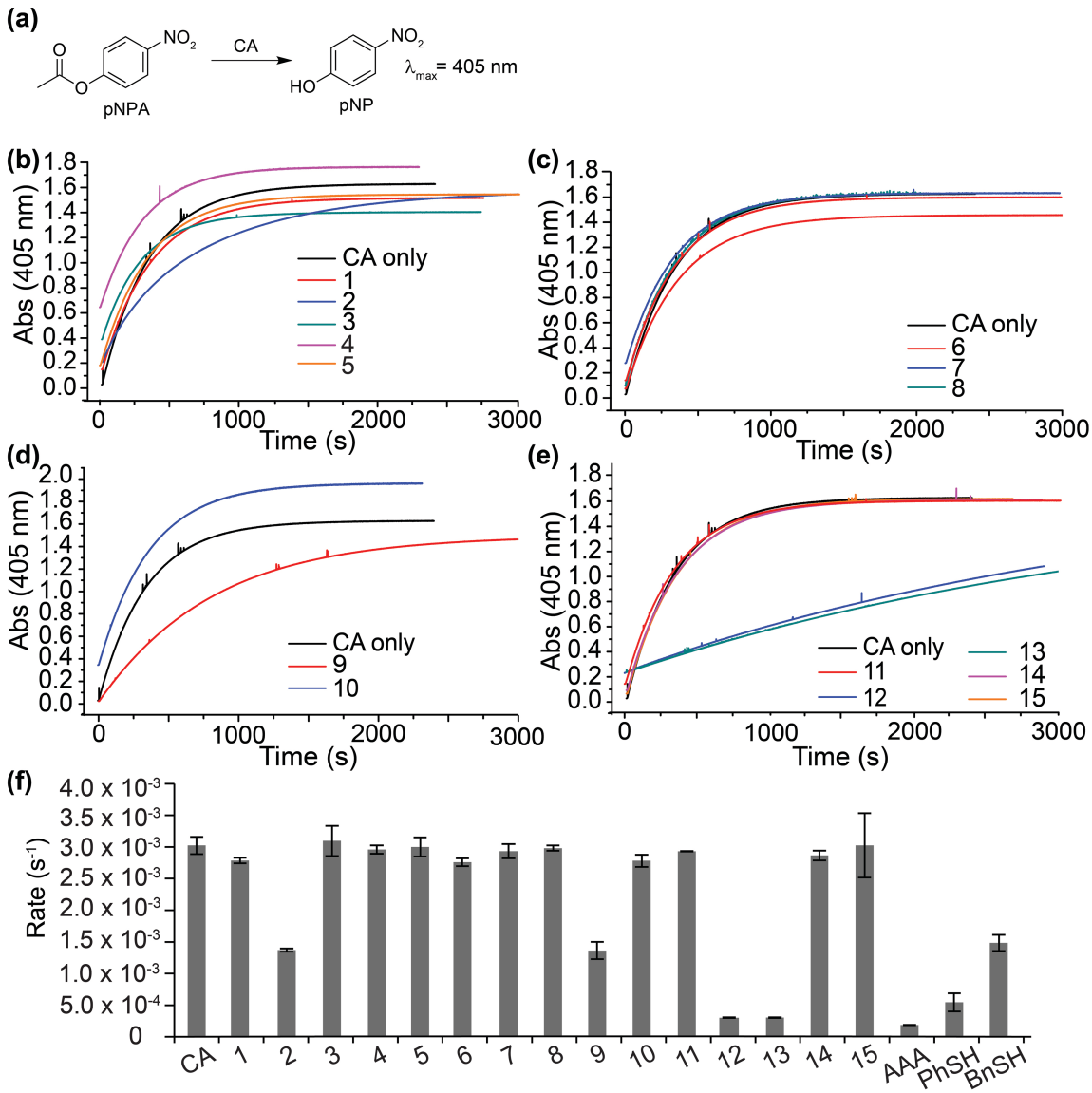

Figure 7.5 (a) CA-mediated hydrolysis of pNPA to form pNP. pNPA assay of (b) caged COS scaffolds, (c) caged CO_2 scaffolds, (d) caged CS_2 scaffolds, and (e) control scaffolds. (f) Absorbance data was fit to a first order exponential to determine rate of hydrolysis in the presence of each compound and compared to AAA, PhSH, and BnSH.

7.3 Discussion

The recent introduction and adoption of triggered COS-releasing compounds for H_2S donation highlights the potential of this strategy to access a broad class of H_2S donors with potential therapeutic properties. In addition to providing functional COS/H_2S donor platforms, the use analogous CO_2/H_2O-releasing compounds provide key control compounds that undergo the same self-immolative chemistry to generate the same

organic byproducts as the canonical donors, but which do not release COS/H_2S. For all such scaffolds, a key component of the COS/H_2S donor strategy is the requirement of CA-mediated COS hydrolysis to H_2S. Because of this requirement, the donor motifs should not interfere with CA activity. With these considerations in mind, we wanted to measure cytotoxicity profiles and CA inhibition data for these potential COS-releasing moieties to help determine the most promising scaffolds for caged COS release.

We identified a library of 15 compounds that include known and potential caged COS scaffolds, caged CO_2 and CS_2 motifs, and related control compounds as described in the Results section. Although each of these compounds represents a scaffold that could be used in a donor or control compound, they do not contain triggering moieties to allow for decomposition, meaning that they should not release COS spontaneously. By investigating the cytotoxicity and CA inhibition profile of each core motif, we hoped to identify the core structures with high CA compatibility for future COS/H_2S donor design.

As outlined in the Results section, none of the prepared model compounds were found to be cytotoxic in A549 cells at concentrations below 100 μM, suggesting that the core motifs are not inherently cytotoxic at concentration ranges typically used in H_2S donation studies. Of the 15 compounds investigated, however, we did identify four compounds that inhibit CA activity: **2**, **9**, **12**, and **13** (Figure 7.6a). At first, the only similarity between these compounds appeared to be the presence of a sulfur atom adjacent to the thiocarbonyl moiety. We also noticed, however, a unifying characteristic of these compounds is that deprotonation of the amide NH could lead to decomposition to form a thiol-containing byproduct (benzyl thiol for **2** and **9** or thiophenol for **12** and **13**, Figure 7.6b). We hypothesized that these thiol byproducts may be responsible for the observed inhibitory properties, rather than the carbamate scaffolds themselves. Further supporting this hypothesis, we measured the inhibitory effects of benzyl thiol and thiophenol. Benzyl thiol exhibited similar CA inhibitory profiles to **2** and **9**, and thiophenol inhibited CA similarly to **12** and **13**. Aside from the shown CA inhibition properties, this additionally suggests the instability of these scaffolds at even moderately basic conditions, making them less reliable as COS donor constructs or as suitable controls.

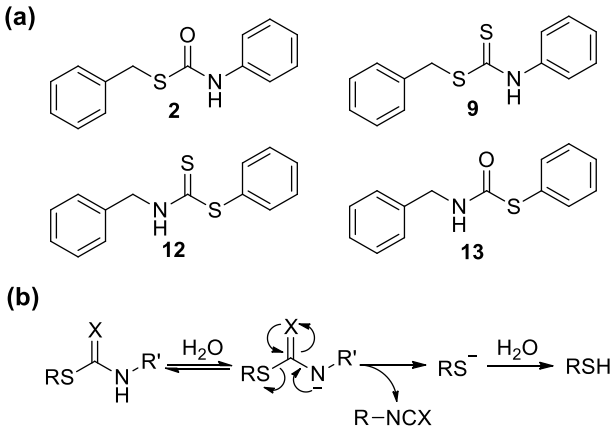

Figure 7.6 (a) Structures of compounds identified as CA inhibitors. (b) Mechanism for production of thiophenol or benzyl thiol following deprotonation of **2**, **9**, **12**, or **13**.

7.4 Conclusions

In combination with recent work investigating stability and rate of COS/H_2S release from different COS-releasing scaffolds,[206] the present work provides an important resource for selecting the best scaffolds for COS donation in the design of H_2S therapeutics. Four scaffolds (**1**, **3**, **4**, and **5**) were identified that have either been reported to release COS or are likely to release COS through self-immolation that do not inhibit CA. These motifs are likely ideal starting points in the design of new COS/H_2S donor motifs. Although this work provides the first insights into the potential CA inhibition properties of COS/H_2S donor scaffolds, any structural modifications could impact the extent of inhibition, which will likely require future constructs to be tested for CA inhibition directly. Additionally, the identification of thiocarbamate **2** as a CA inhibitor should not completely eliminate this *S*-alkyl thiocarbamate motif from consideration as a COS/H_2S donor core, because further functionalization of the core structure may impact or reduce the CA inhibition profiles. Indeed, similar scaffolds have been shown to be successful COS donors in recent reports.[152, 209] Future work is required to determine the precise consequences of using a COS donor that inhibits CA as an H_2S donor, but the efficiency, rate of decomposition, and rate of H_2S production may all be affected. Through the rational selection of COS donor cores that provide efficacious COS/H_2S release rates, suitable stability in the presence of biological milieu, and minimal CA inhibition, we expect the field of COS/H_2S donors will continue to expand rapidly and provide access to new motifs with pharmacologically-relevant activities. Chapter VIII

will summarize the progress made in the development of self-immolative scaffolds for COS/H_2S delivery reported in this dissertation.

7.4 Experimental Details

7.4.1 Materials and Methods

Synthetic Materials. Reagents were purchased from Sigma-Aldrich, Alfa-Aesar, or Tokyo Chemical Industry (TCI) and used as received. Compounds **1-15** were synthesized as previously reported. Spectroscopic grade, inhibitor-free THF and DCM were deoxygenated by sparging with argon followed by passage through a Pure Process Technologies solvent purification system to remove water. Deuterated solvents were purchased from Cambridge Isotope Laboratories and used as received. Silica gel (SiliaFlash F60, Silicycle, 230-400 mesh) was used for column chromatography. ^{1}H, and $^{13}C\{^{1}H\}$ NMR spectra were recorded on a Bruker 500 MHz instrument. Chemical shifts are reported in ppm relative to residual protic solvent resonances.

Spectroscopic Materials. Tris-HCl buffer was prepared from Tris hydrochloride (Sigma, 50 mM) and deionized water obtained from a Synergy UV Millipore Water System and adjusted to pH 8.5 with a SevenMulti pH Probe (Mettler Toledo). UV-visible spectra were acquired on a Cary 60 UV-vis spectrometer equipped with a Quantum Northwest TC 1 temperature controller.

Cell Culture Materials. A549 cells obtained from ATCC were grown in a 5% CO_2 incubator at 37 °C in Dulbecco's Modified Eagle Medium (Gibco, high glucose, phenol red) with 5% FBS (VWR) and 1% penicillin streptomycin (Gibco). Cells were passaged (up to p 25) every 1-3 days upon reaching 85-90% confluency. Absorbance measurements were acquired using a Tecan Safire2 microplate reader.

Cytotoxicity Assays. Stock solutions of the compounds (20 mM, 10 mM, 5 mM, 2 mM) were prepared in DMSO via serial dilution and used to make 100 μM, 50 μM, 25 μM, and 10 μM solutions of each compound in DMEM (no phenol red, no FBS). 96-Well plates were seeded with ~20,000 cells/well overnight prior to cytotoxicity experiments.

Cells were washed with PBS (Gibco) and incubated with the desired compound or with vehicle (0.5% DMSO) for one hour prior to being washed with PBS and incubated with CCK-8 solution (10% in DMEM). After 1 hour, the absorbance at 450 nm was measured on a plate reader, and the cell survival was calculated as a percent of the control and normalized to the vehicle group. The results are expressed as mean ± SD (n = 6).

Determination of CA Inhibition. Stock solutions of each compound (20 mM in DMSO), acetazolamide (20 mM in DMSO), *p*-nitrophenylacetate *(*pNPA, 15 mM in ethanol), and CA (7.5 mg/mL in Tris buffer) were prepared and stored at 2-4 °C until immediately prior to use. pNPA (20 µL) was injected into the Tris HCl buffer (3 mL) immediately followed by the desired compound of interest (7.5 µL) with stirring at 37.00 ± 0.05 °C. Data collection began immediately prior to injection of CA (20 µL) and continued until the production of pNP was complete, as determined by a plateau in absorbance at 405 nm. Absorption data was fit to a first-order exponential equation in Origin 8 to obtain pseudo first-order rate data, which are reported in units of s^{-1}. All trials were completed in triplicate and rates are reported as mean ± SD (n = 3).

7.4.2 Syntheses

General synthetic procedure A. The alcohol, thiol, or amine starting material (1.0 equiv.) was combined with phenyl isothiocyanate or phenyl isocyanate (1.0 equiv.) in anhydrous THF (15 mL) at 0 °C, followed by the addition of base (1.2 equiv.). The resultant mixture was stirred at 0 °C for 20 min, after which the ice bath was removed, and the reaction mixture was stirred at r.t. until the completion of the reaction as indicated by TLC. The reaction was quenched by adding brine (30 mL), and the aqueous solution was extracted with ethyl acetate (3 × 15 mL). The organic layers were combined, dried over $MgSO_4$, and evaporated under vacuum. The crude products from each reaction were purified by column chromatography.

Compound **1** was prepared from benzyl alcohol and phenyl isothiocyanate in the presence of NaH. (yield: 75%). The characterization data match the reported data.[140] Compound **2** was prepared from benzyl mercaptan and phenyl isocyanate in the presence of NaH. (yield: 38%). The characterization data match the reported data.[264] Compound **6**

was prepared from benzyl alcohol and phenyl isocyanate in the presence of TEA (yield: 20%) The characterization data match the reported data.[265] Compound **9** was prepared from benzyl mercaptan and phenyl isothiocyanate in the presence of NaH. (yield: 75%). The characterization data match the reported data.[266] Compound **14** was prepared from benzyl amine and phenyl isocyanate in the presence of TEA. (yield: 88%). The characterization data match the reported data.[267] Compound **15** was prepared from benzyl amine and phenyl isothiocyanate in the presence of TEA. (yield: 64%). The characterization data match the reported data.[268]

General synthetic procedure B. The alcohol, thiol, or amine starting material (1.0 equiv.) was combined with the phenyl chloroformate reagent (1.0 equiv.) in anhydrous DCM (15 mL) at 0 °C, followed by the addition of base (1.0 equiv.). The resultant solution was stirred at 0 °C for 20 min, after which the ice bath was removed, and the reaction mixture was stirred at r.t. until the completion of the reaction as indicated by TLC. The reaction was quenched by adding brine (30 mL), and the aqueous solution was extracted with ethyl acetate (3 × 15 mL). The organic layers were combined, dried over $MgSO_4$, and evaporated under vacuum. The crude products from each reaction were purified by column chromatography.

Compound **3** was prepared from benzyl alcohol and phenyl chlorothionoformate in the presence of pyridine. (yield: 57%). ^{1}H NMR (500 MHz, $CDCl_3$) δ (ppm): 7.55 (m, 7H), 7.33 (t, J = 10.0 Hz, 1H), 7.16 (d, J = 10.0 Hz, 2H), 5.60 (s, 2H). $^{13}C\{^1H\}$ NMR (125 MHz, $CDCl_3$) δ (ppm): 195.0, 153.5, 134.2, 129.6, 128.8, 128.7, 128.6, 126.6, 122.0, 75.6. Compound **4** was prepared from benzyl mercaptan and phenyl chloroformate in the presence of TEA. (yield: 73%). The characterization data match the reported data.[269] Compound **5** was prepared from benzyl mercaptan and phenyl thiochloroformate in the presence of TEA (yield: 71%). ^{1}H NMR (500 MHz, DMSO-d_6) δ (ppm): 7.53 (m, 5H), 7.32 (m, 4H), 7.27 (m, 1H), 4.25 (s, 2H). $^{13}C\{^1H\}$ NMR (125 MHz, DMSO-d_6) δ (ppm): 188.6, 137.3, 135.8, 131.1, 130.2, 129.4, 129.1, 127.9, 126.5, 34.9. Compound **7** was prepared from benzyl alcohol and phenyl chloroformate in the presence of TEA. (yield: 62%). The characterization data match the reported data.[270] Compound **8** was prepared from benzyl alcohol and phenyl thiochloroformate in the presence of NaH.

(yield: 32%). ^{1}H NMR (500 MHz, CDCl3) δ (ppm): 7.57 (m, 2H), 7.44 (m, 3H), 7.39 (m, 5H), 5.29 (s, 2H). ^{13}C{^{1}H} NMR (125 MHz, CDCl3) δ (ppm): 167.9,135.0, 134.9, 129.6, 129.2, 128.6, 128.5, 127.7, 69.4. Compound **10** was prepared from benzyl mercaptan and phenyl chlorothionoformate in the presence of pyridine. (yield: 43%). The characterization data match the reported data.[271] Compound **11** was prepared from benzyl amine and phenyl chloroformate in the presence of TEA. (yield: 82%). The characterization data match the reported data.[272] Compound **12** was prepared from benzyl amine and phenyl thiochloroformate in the presence of pyridine. (yield: 57%). ^{1}H NMR (500 MHz, DMSO-d_6) δ (ppm): 8.85 (s, 1H), 7.46 (m, 2H), 7.41 (s, 3H), 7.35 (t, J = 5.0 Hz, 2H), 7.26 (d, J = 10.0 Hz, 3H), 4.32 (s, 2H). ^{13}C{^{1}H} NMR (125 MHz, DMSO-d_6) δ (ppm): 164.6, 139.3, 135.4, 129.4, 129.3, 129.1, 128.8, 127.8, 127.5, 44.7. Compound **13** was prepared from benzyl amine and phenyl chlorodithioformate in the presence of TEA. (yield: 49%). ^{1}H NMR (500 MHz, $CDCl_3$) δ (ppm): 7.61 (m, 2H), 7.50 (m, 3H), 7.32 (m, 3H), 7.17 (d, J = 10.0 Hz, 2H), 6.86 (br, 1H), 4.86 (d, J = 5.0 Hz, 2H). ^{13}C{^{1}H} NMR (125 MHz, $CDCl_3$) δ (ppm): 195.3, 135.8, 135.6, 131.2, 130.4, 128.9, 128.6, 128.0, 127.5, 50.2.

CHAPTER VIII

CONCLUDING REMARKS

The significant interest in H_2S as the newest gasotransmitter has motivated chemists and chemical biologists to develop a suite of chemical tools to study physiological H_2S. These tools are can be broadly classified into two main categories: scaffolds to detect H_2S (H_2S probes) and small molecules that release H_2S (H_2S donors). Significant progress has been made in the design of H_2S probes that are sensitive and selective for H_2S as well as in the development of H_2S donors that are well-controlled and contain a variety of functional groups. Several key challenges remain, however, including irreversible consumption of sulfide during detection in living systems and the use of donors that are poorly representative of enzymatic production of H_2S. The work reported in this dissertation addresses many of the concerns and limitations that are commonly encountered in the development of chemical tools for H_2S. An analyte-replacement fluorescent probe for H_2S was reported that can simultaneously detect H_2S and release an equivalent of sulfide in the form of COS to help maintain homeostasis. This was the first report of the triggerable release of COS from self-immolative thiocarbamates and the use of COS as a source of sulfide through rapid hydrolysis to H_2S in the presence of the ubiquitous mammalian enzyme, CA. Today, self-immolative thiocarbamates are a robust and highly tunable strategy for H_2S delivery. The donors reported herein represent only a portion of the COS/H_2S donors reported to date, but show that this strategy can be modified with ease to produce donors relevant for certain research and therapeutic applications. Additionally, the cytotoxicity of some of the enzyme-activated donors reported in this dissertation has piqued interest in COS chemical biology. While COS biology has been largely ignored in the past, the recent introduction of COS delivery agents may allow for more detailed investigations into this field. Significant work remains to be done to elucidate the physiological effects of COS from those of H_2S. The rapid enzymatic consumption of COS and subsequent hydrolysis to H_2S in mammalian tissues complicates simple experiments that may be done to observe the effects of COS. CA inhibition or knockdown experiments may provide some

insight into COS biology, however, since CA is responsible for regulation of intracellular pH, numerous other variable are likely to influence the results of such investigations. Since many CA isoforms exist, and the isoforms that rapidly hydrolyze COS are so far unidentified, there are potentially more complex, isoform-specific experiments that can be imagined. Finally, since there are currently only very limited methods to detect COS in biological milieu (i.e. headspace gas chromatography above tissue samples), the development of additional chemical tools, especially selective probes for COS, may be necessary to reach an in-depth understanding of COS in physiology. The work in this dissertation will hopefully serve as a springboard into a flourishing new field of COS chemical biology.

APPENDIX A
CHAPTER II SUPPLEMENTARY INFORMATION

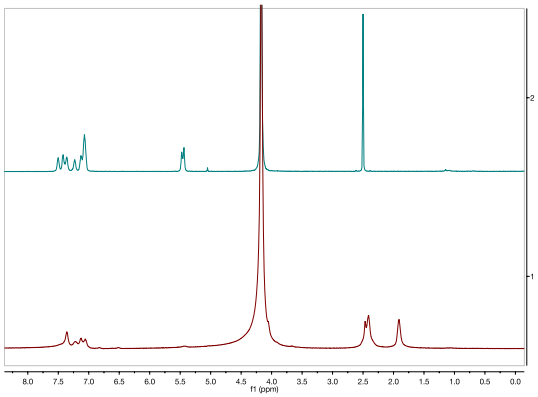

Figure A1. ^{1}H NMR spectra of **1** before (top) and after (bottom) TCEP addition.

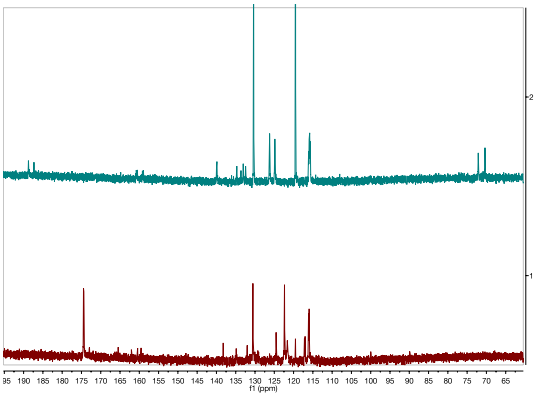

Figure A2. ^{13}C{^{1}H} NMR spectra of **1** before (top) and after (bottom) TCEP addition.

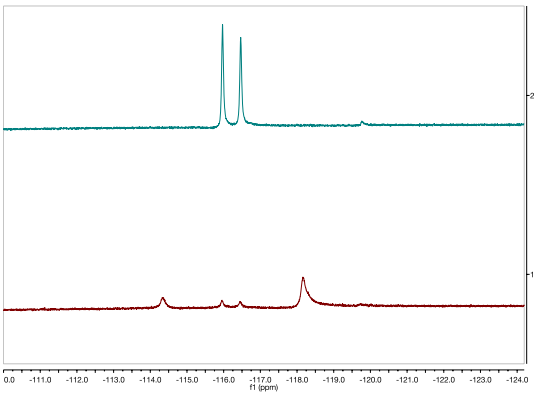

Figure A3. ^{19}F NMR spectra of **1** before (top) and after (bottom) TCEP addition. The presence of multiple signals is a result of multiple decomposition products that form following self-immolation due to the nucleophilicity of the resulting aniline species and the electrophilicity of the azaquinone methide byproduct.

Sulfide Electrode Experiments

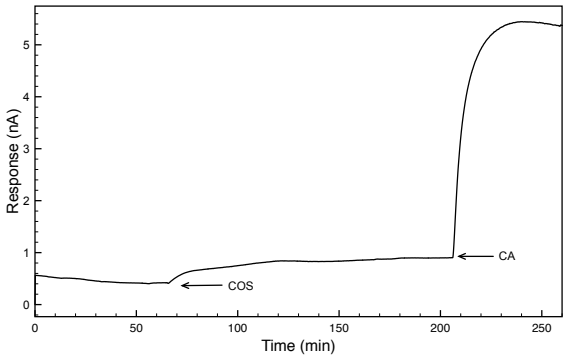

Figure A4. Addition of COS to PBS buffer results in minimial H_2S formation until the addition of carbonic anhydrase (CA).

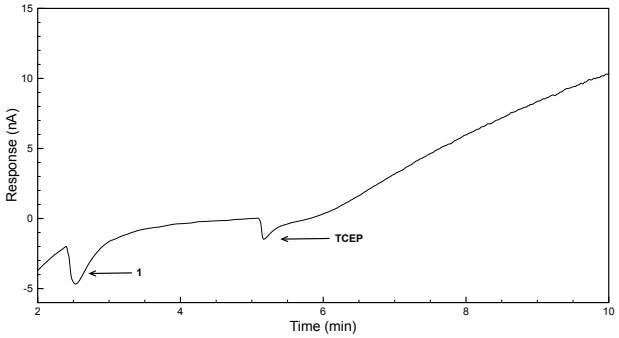

Figure A5. No H_2S is formed from **1** in PBS buffer until TCEP is added.

NMR Spectra

^{1}H (600 MHz, DMSO-d_6), $^{13}C\{^{1}H\}$ (150 MHz, DMSO-d_6), and ^{19}F NMR (564 MHz, DMSO-d_6) NMR Spectra of **1**

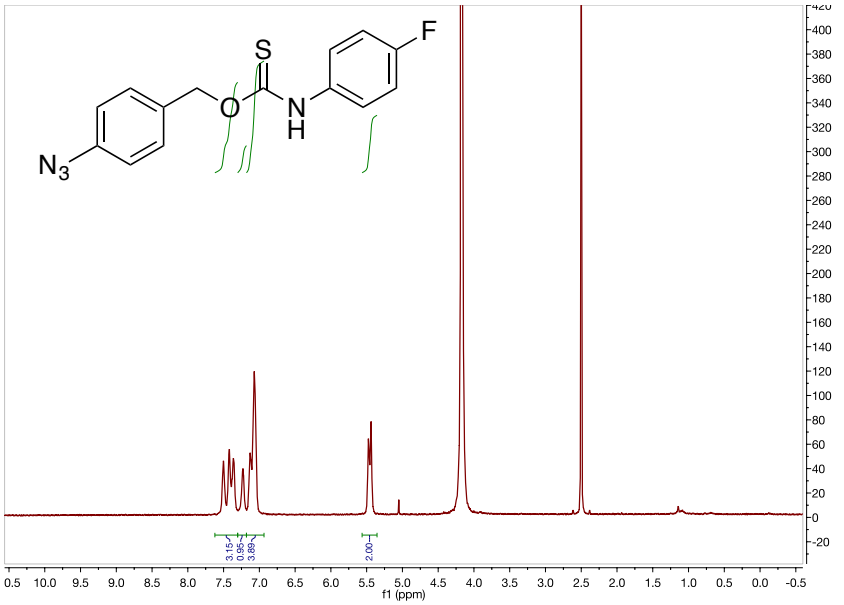

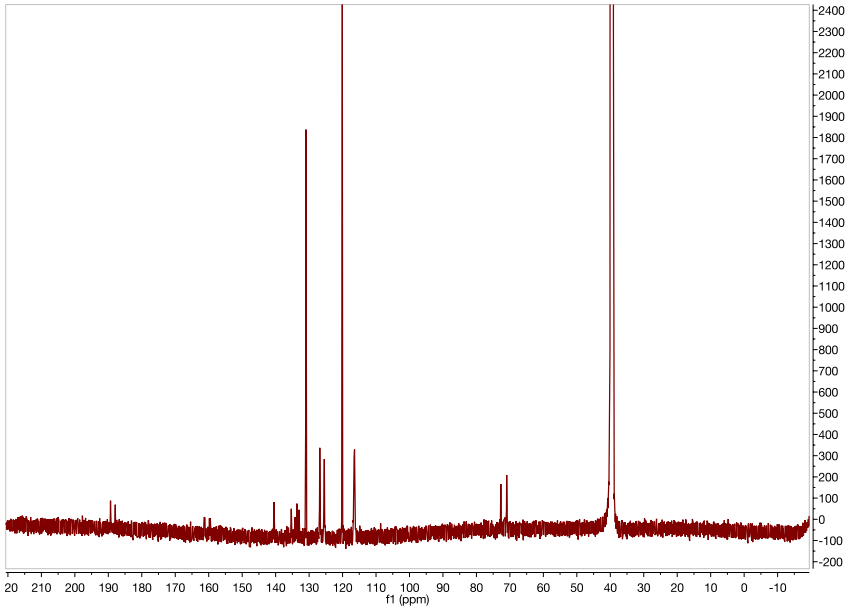
2400
2300
2200
2100
2000
1900
1800
1700
1600
1500
1400
1300
1200
1100
1000
900
800
700
600
500
400
300
200
100
0
-100
-200
20 210 200 190 180 170 160 150 140 130 120 110 100 90 80 70 60 50 40 30 20 10 0 -10
f1 (ppm)

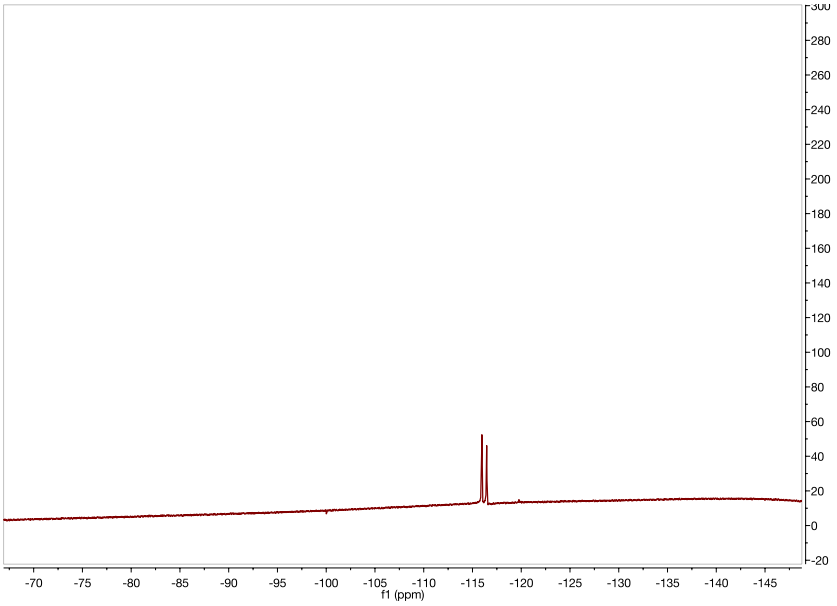
300
280
260
240
220
200
180
160
140
120
100
80
60
40
20
0
-20
-70 -75 -80 -85 -90 -95 -100 -105 -110 -115 -120 -125 -130 -135 -140 -145
f1 (ppm)

^{1}H (600 MHz, DMSO-d_6) and ^{13}C{^{1}H} (150 MHz, DMSO-d_6) NMR Spectra of **3**

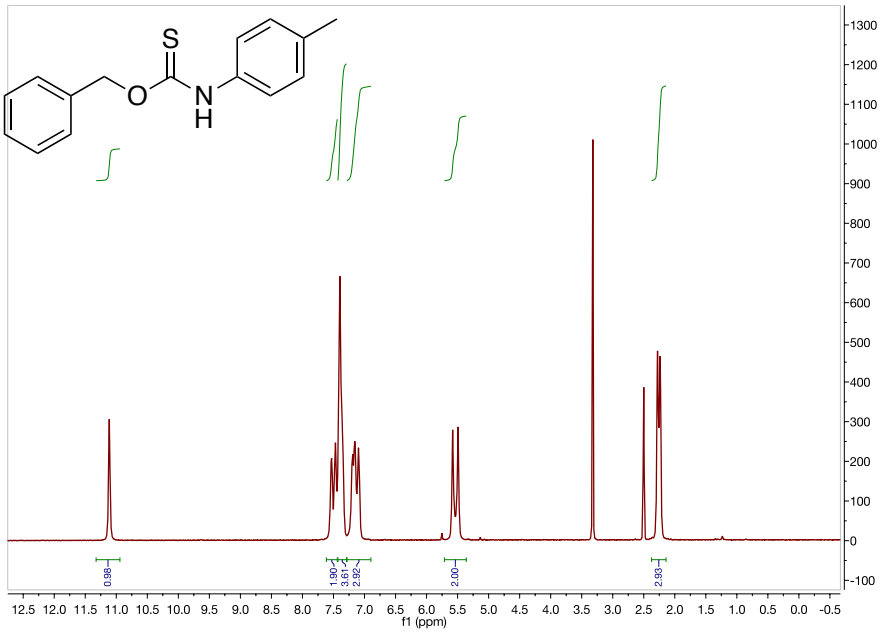

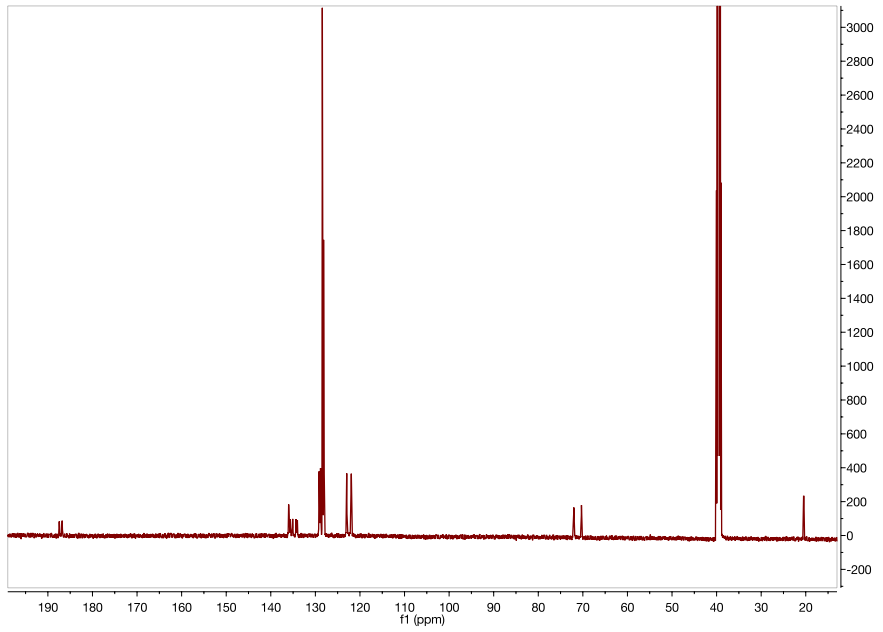

^{1}H (600 MHz, DMSO-d_6), ^{13}C{^{1}H} (150 MHz, DMSO-d_6), and ^{19}F NMR (564 MHz, DMSO-d_6) NMR Spectra of **4**

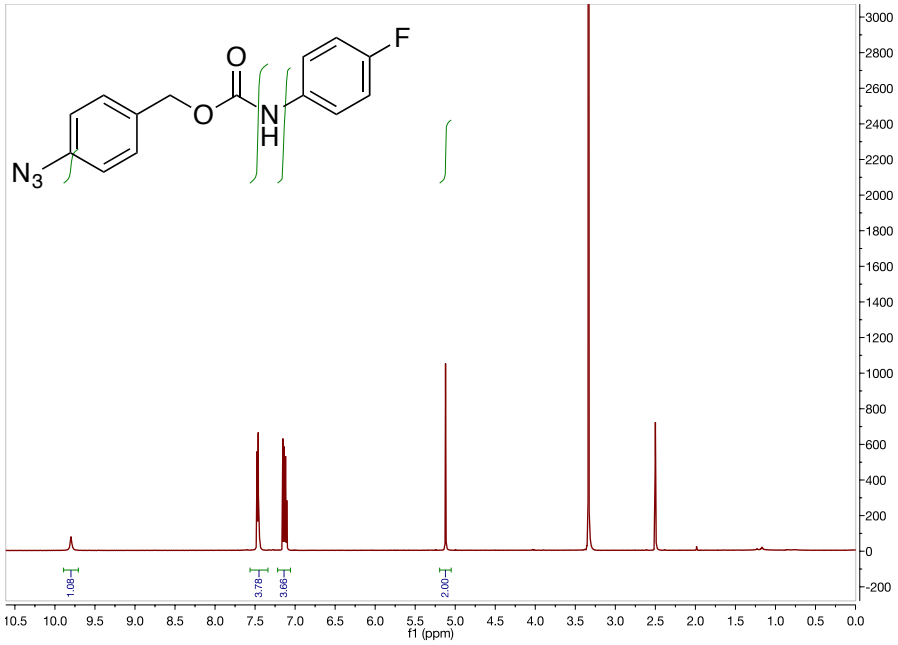

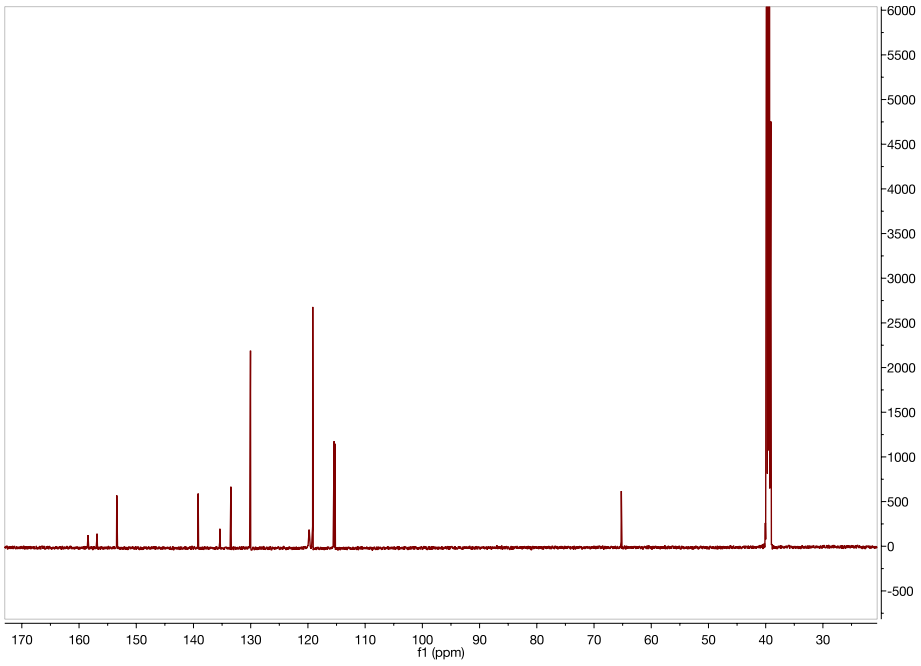

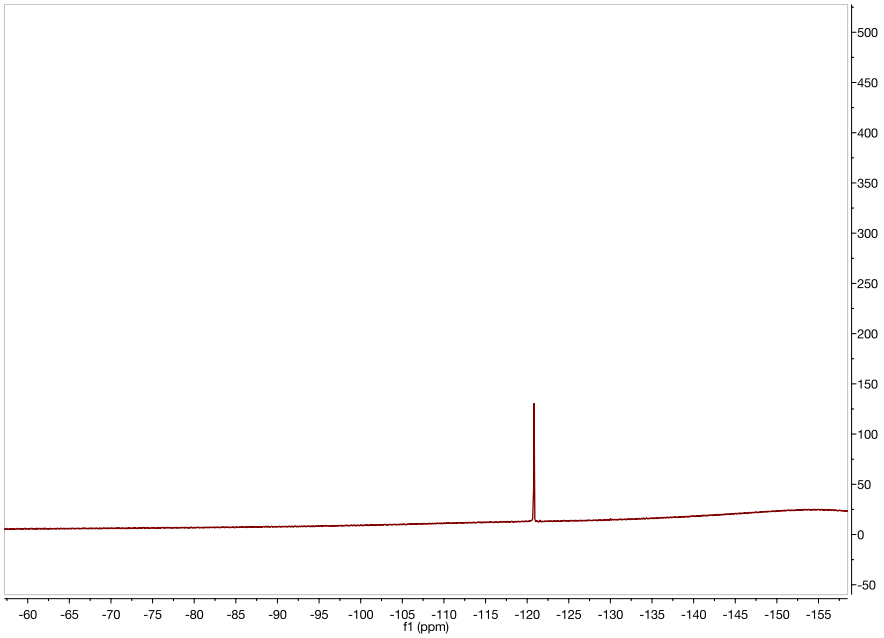

^{1}H (600 MHz, $CDCl_3$) and $^{13}C\{^{1}H\}$ (150 MHz, $CDCl_3$) NMR Spectra of **MeRho-NCS**

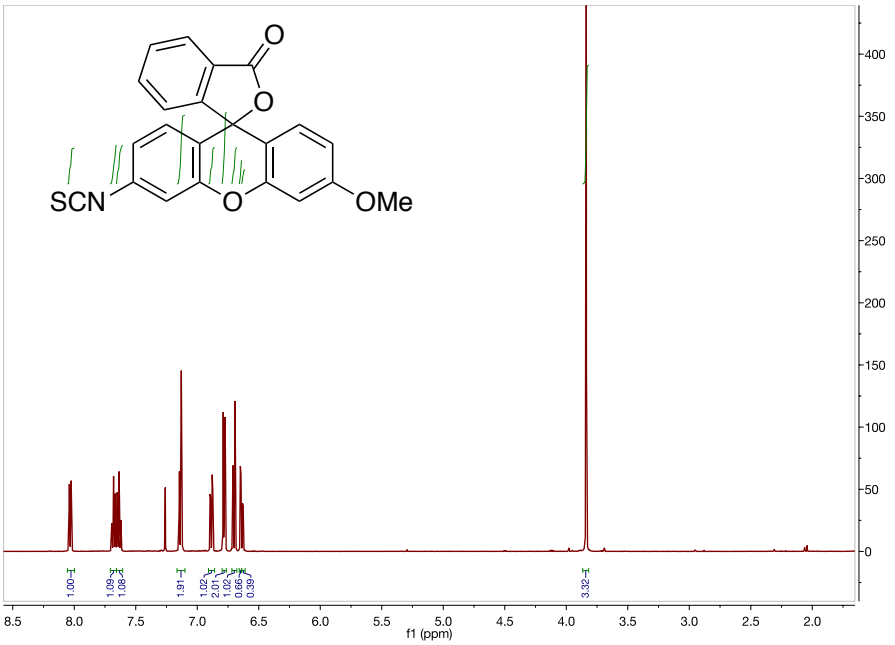

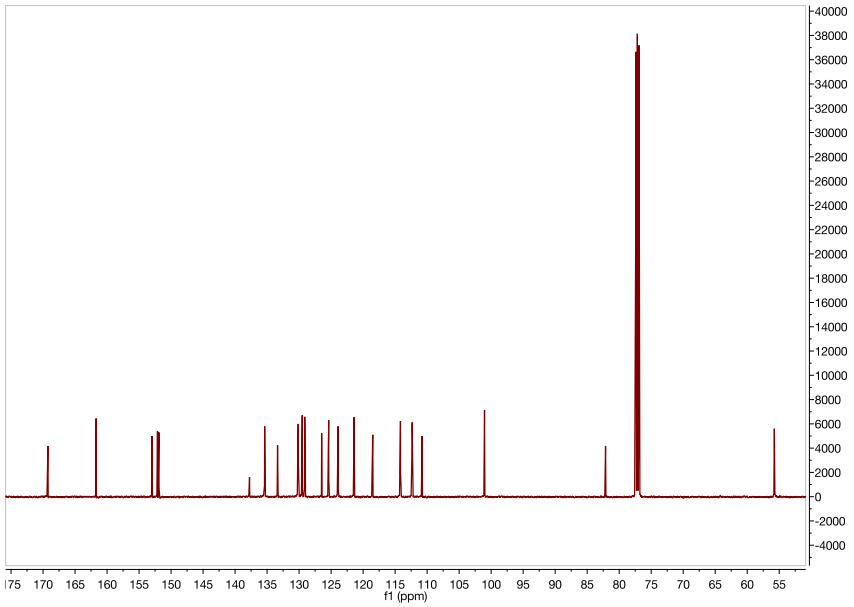

^{1}H (600 MHz, $CDCl_3$) and $^{13}C\{^{1}H\}$ (150 MHz, $CDCl_3$) NMR Spectra of **MeRho-TCA**

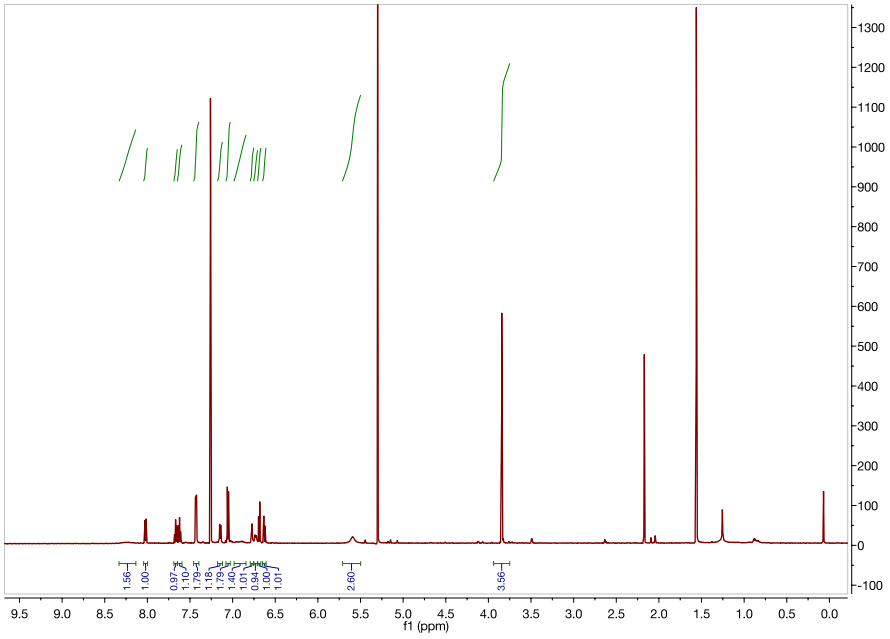

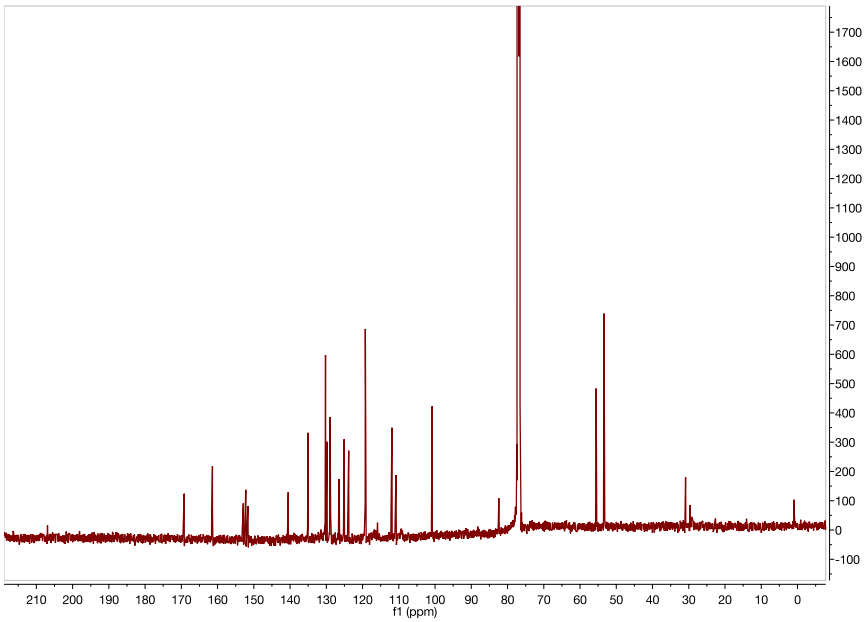
1700
1600
1500
1400
1300
1200
1100
1000
900
800
700
600
500
400
300
200
100
0
-100
210 200 190 180 170 160 150 140 130 120 110 100 90 80 70 60 50 40 30 20 10 0
f1 (ppm)

APPENDIX B

CHAPTER III SUPPLEMENTARY INFORMATION

Cytotoxicity of TCO 1

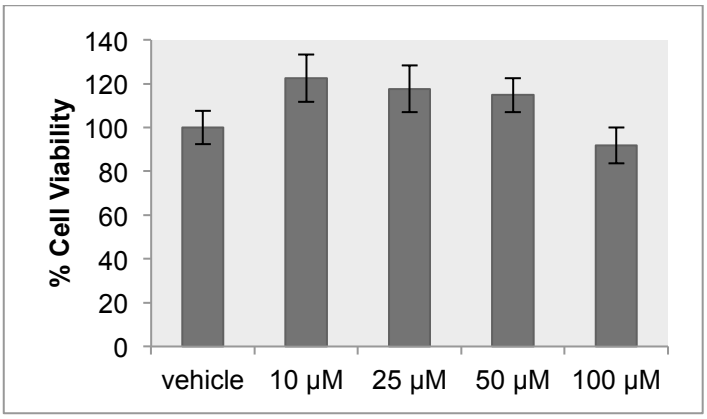

Figure B1. N2A cells were cultured in high glucose Dulbecco's modified Eagle's medium (DMEM) supplemented with 10% fetal bovine serum (FBS) and 1% penicillin/streptomycin at 37 °C under 5% CO_2. Once confluent, cells were incubated in FBS-free DMEM containing vehicle (0.5% DMSO) or TCO **1** (10 – 100 μM) for 3 hours in a 96-well plate. CCK-8 solution (10% in FBS-free DMEM) was added to each well, and cells were incubated for 3 hours at 37 °C. The absorbance at 450 nm was measured by using a microplate reader. The cell viability was measured and normalized to the vehicle group. Results are expressed as mean ± SEM (n = 6).

NMR Spectra

^{1}H (400 MHz, $CDCl_3$) NMR Spectra of **1.**

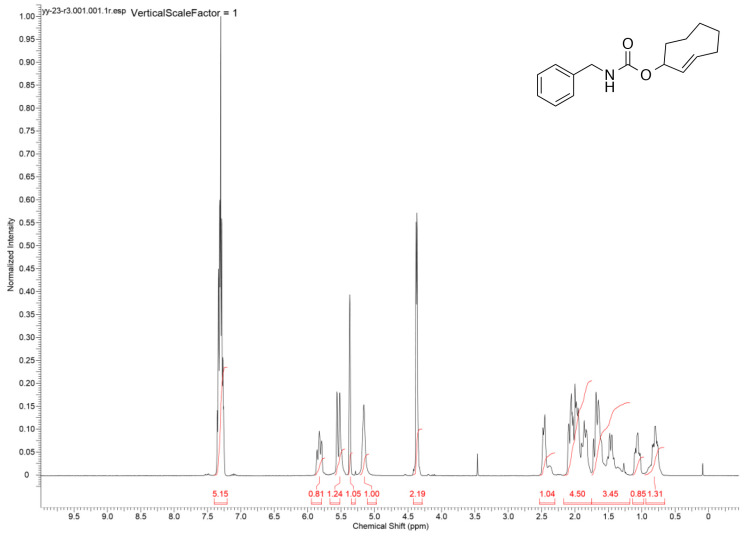

^{1}H (400 MHz, $CDCl_3$) and $^{13}C\{^{1}H\}$ (100 MHz, $CDCl_3$) NMR Spectra of **2**.

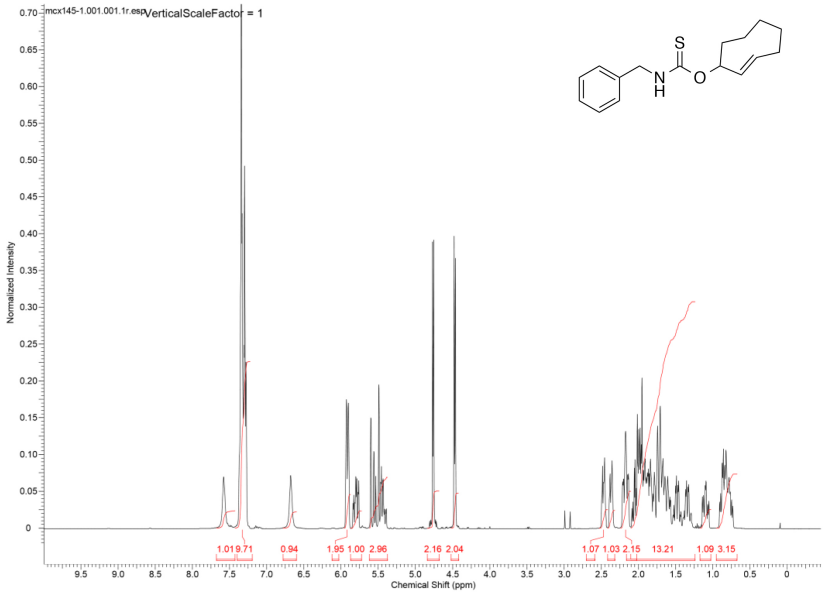

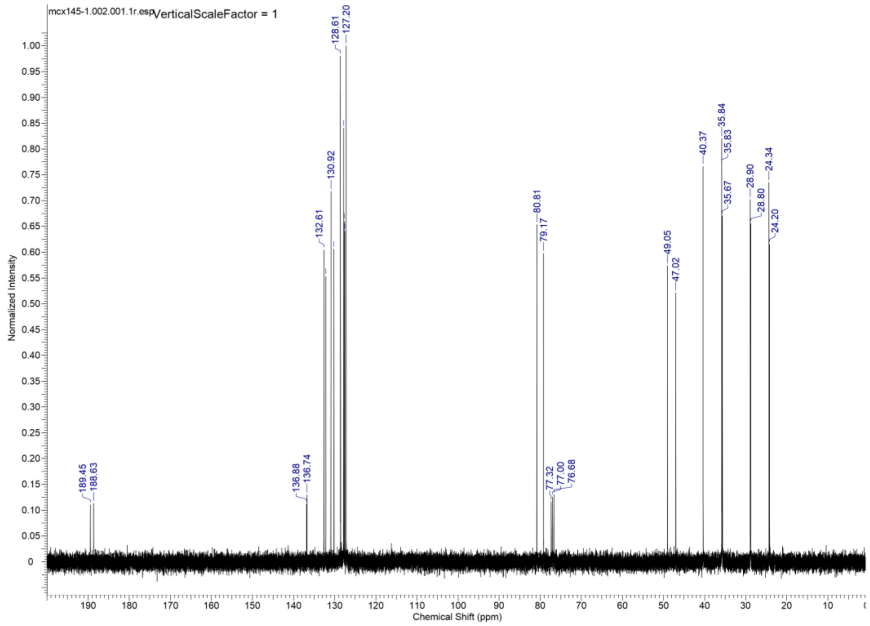

^{1}H (400 MHz, $CDCl_3$) and $^{13}C\{^{1}H\}$ (100 MHz, $CDCl_3$) NMR Spectra of Bis-isopropyl-1,2,4,5-tetrazine.

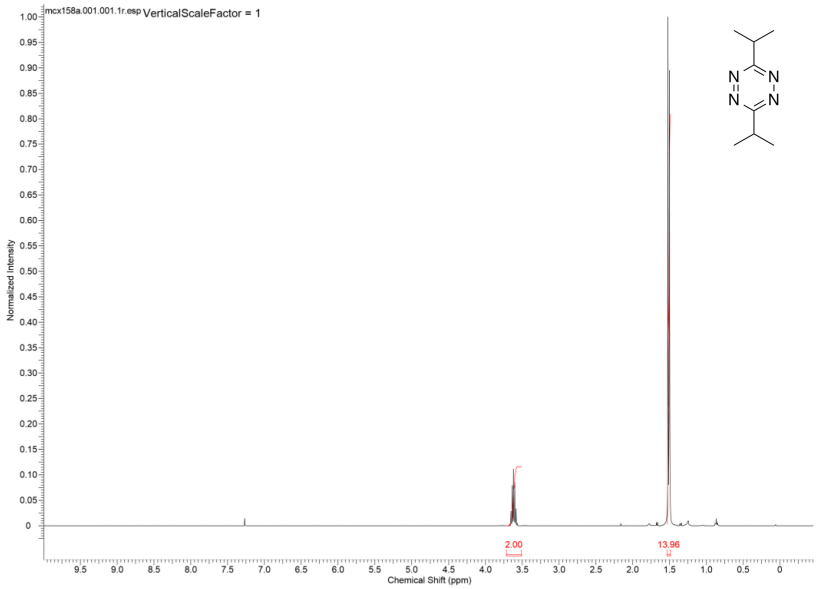

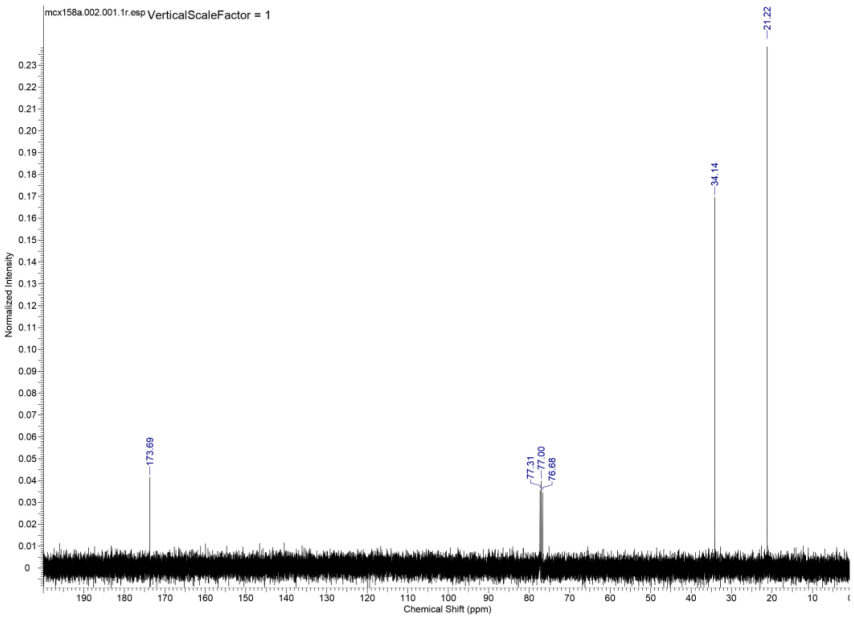
mcx158a.002.001.1r.esp VerticalScaleFactor = 1
Normalized Intensity
Chemical Shift (ppm)
173.69
77.31
77.00
76.68
34.14
21.22

APPENDIX C

CHAPTER IV SUPPLEMENTARY INFORMATION

H_2S Calibration Curve

UV cuvettes (1.50 mL capacity) were charged with 0.500 mL of the MB cocktail (*vide infra*) and 0.500 mL of PBS buffer (pH 7.40, 10.0 mM). The resultant solution was mixed thoroughly, followed by the addition of an NaSH stock solution (1.00 mM) to make the final H_2S concentrations of 1.00, 3.00, 5.00, 10.0, 15.0, and 20.0 μM. The MB solution was allowed to react with H_2S for 1 hour before measuring the absorbance at 670 nm.

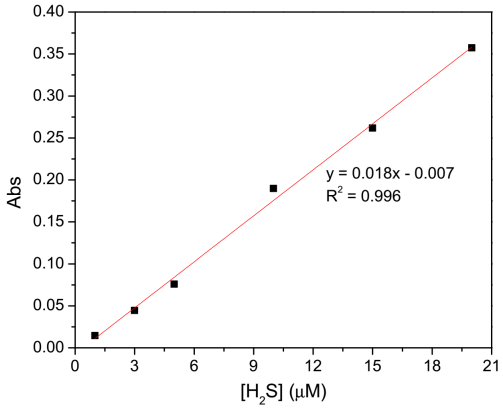

Figure C1. H_2S calibration curve for the MB assay.

Cys-Triggered H_2S Release from OA-CysTCM-1 in the Presence of GSH

An **OA-CysTCM-1** stock solution (0.100 mL, 10.0 mM in DMSO) was added to 20.0 mL of PBS (pH 7.40, 10.0 mM) containing CA (25.0 μg/mL) in a 25-mL scintillation vial. A Cys stock solution (100 μL, 100 mM in H_2O) and a GSH stock solution (50.0 μL, 100 μL, or 200 μL, 100 mM in H_2O) were then added so that the working Cys and GSH concentration ratios are 2:1, 1:1, and 1:2, respectively. Next, 0.300 mL aliquots of the reaction mixture were transferred to UV cuvettes containing 0.300 mL of MB cocktail (0.0600 mL zinc acetate (1.00% w/v), 0.120 mL $FeCl_3$ (30.0 mM in 1.20 M HCl), and 0.120 mL *N,N*-dimethyl-*p*-phenylene diamine (20.0 mM in 7.20 M HCl)) at different time points. The absorbance at 670 nm was then measured after 1

hour and was converted to H_2S concentration by using the H_2S calibration curve as shown in Figure C1.

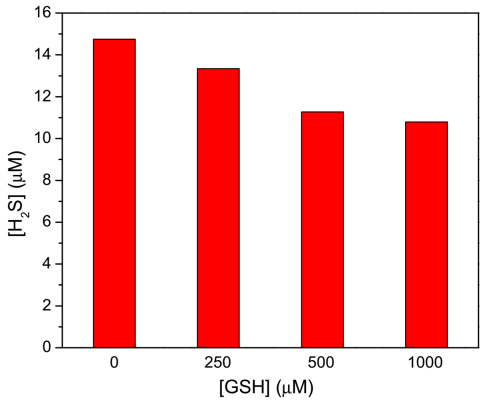

Figure C2. GSH Effects on Cys-triggered COS/H_2S release from **OA-CysTCM-1** (50 μM). The Cys concentration was 500 μM in all experiments, and H_2S concentrations were measured after 2-h incubation.

Fluorescence Imaging of H_2S Release from OA-CysTCM-1

A stock solution of SF7-AM (1.50 μL, 20.0 mM in DMSO) was added to a vial containing PBS (pH 7.40, 3.00 mL), cysteine (250 μM), and carbonic anhydrase (25.0 μg/mL). Fluorescence measurements (λ_{ex} = 488 nm, λ_{em} = 498-700 nm) were taken either immediately upon addition of SF7-AM or after addition of **OA-CysCM-1** (15.0 μL, 20.0 mM in DMSO) or **OA-CysTCM-1** (15.0 μL, 20.0 mM in DMSO) and taken periodically throughout the course of 120 minutes.

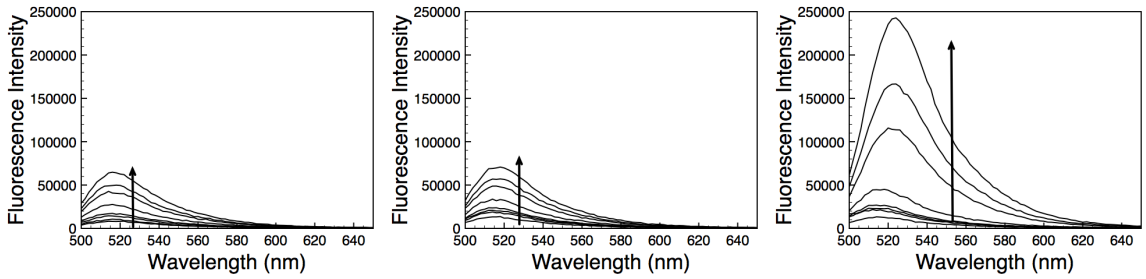

Figure C3: Fluorescence response of SF7-AM (5.00 μM) with cysteine (250 μM) and carbonic anhydrase (25.0 μg/mL) (left); upon addition of **OA-CysCM-1** (50.0 μM, middle); and upon addition of **OA-CysTCM-1** (50.0 μM, right) over the course of 120 minutes. λ_{ex} = 488 nm.

NMR Spectra

^{1}H (500 MHz, $CDCl_3$) and $^{13}C\{^{1}H\}$ (125 MHz, $CDCl_3$) NMR Spectra of **S1**.

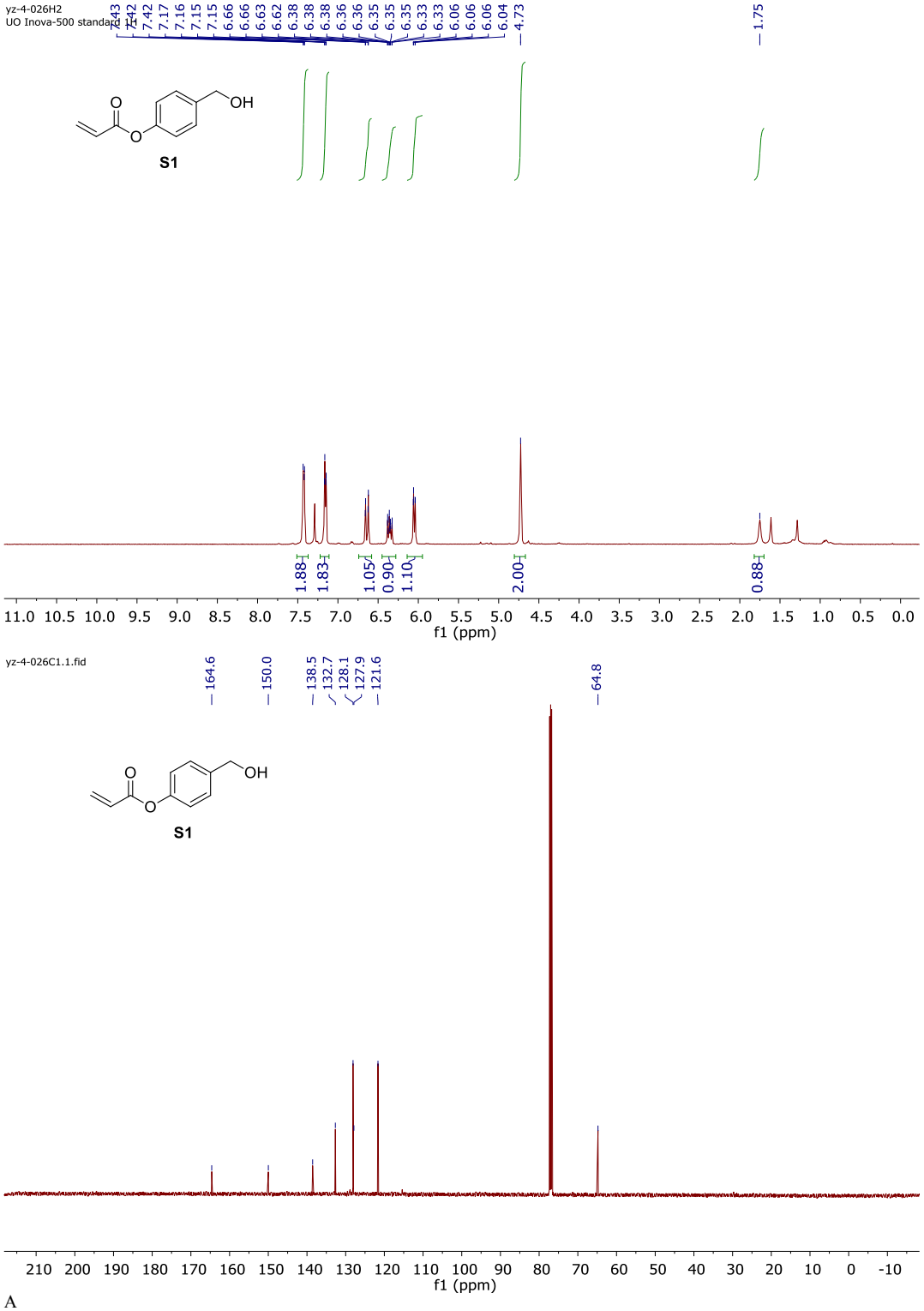

A

^{1}H (500 MHz, DMSO-d_6) and ^{13}C{^{1}H} (150 MHz, DMSO-d_6) NMR Spectra of **OA-CysTCM-1**. Two sets of NMR resonances showed up in ^{13}C NMR spectrum due to slow rotation around the thiocarbamate functional group at room temperature

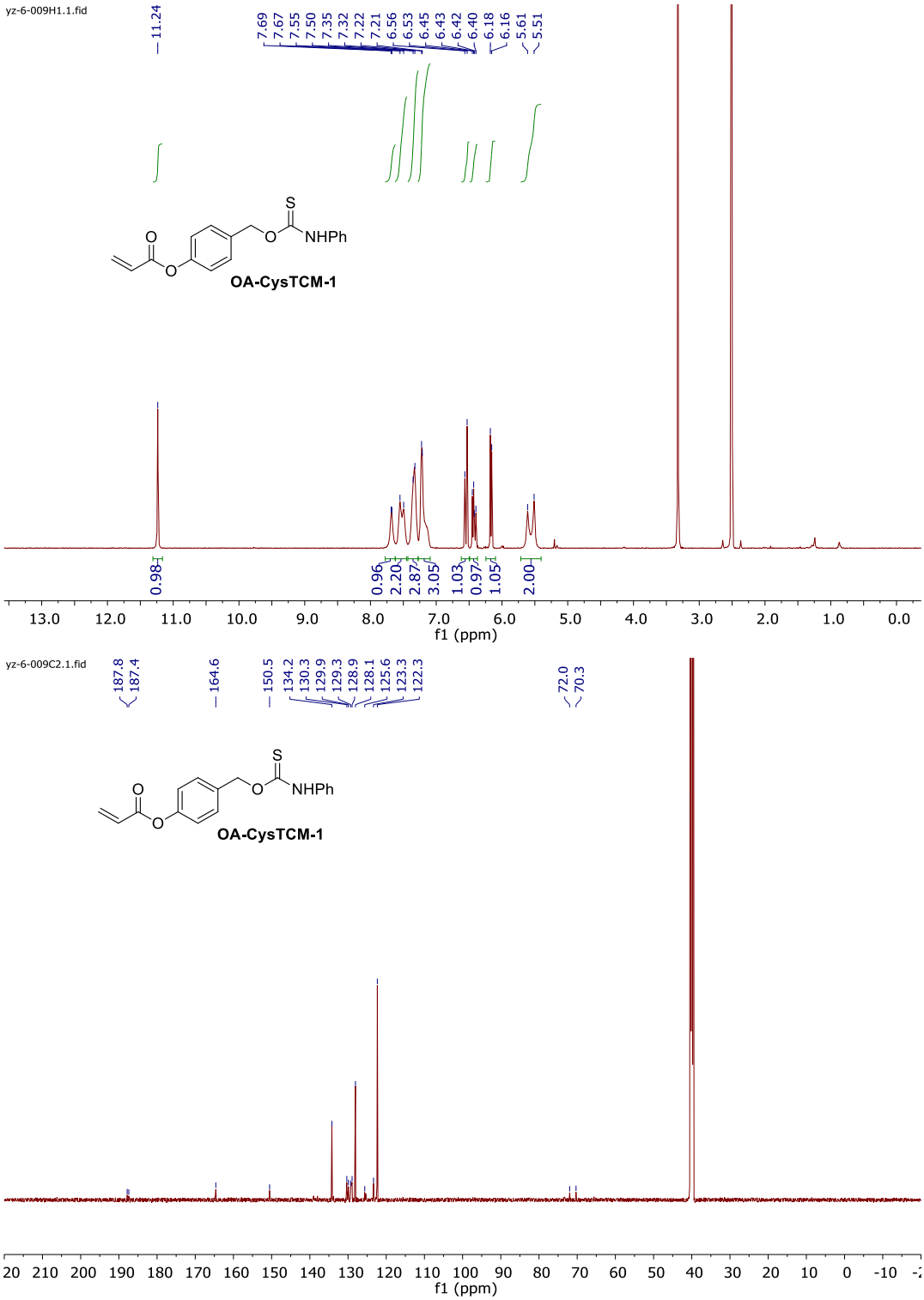

^{1}H (500 MHz, $CDCl_3$) and $^{13}C\{^{1}H\}$ (125 MHz, $CDCl_3$) NMR Spectra of **OA-CysCM-1**.

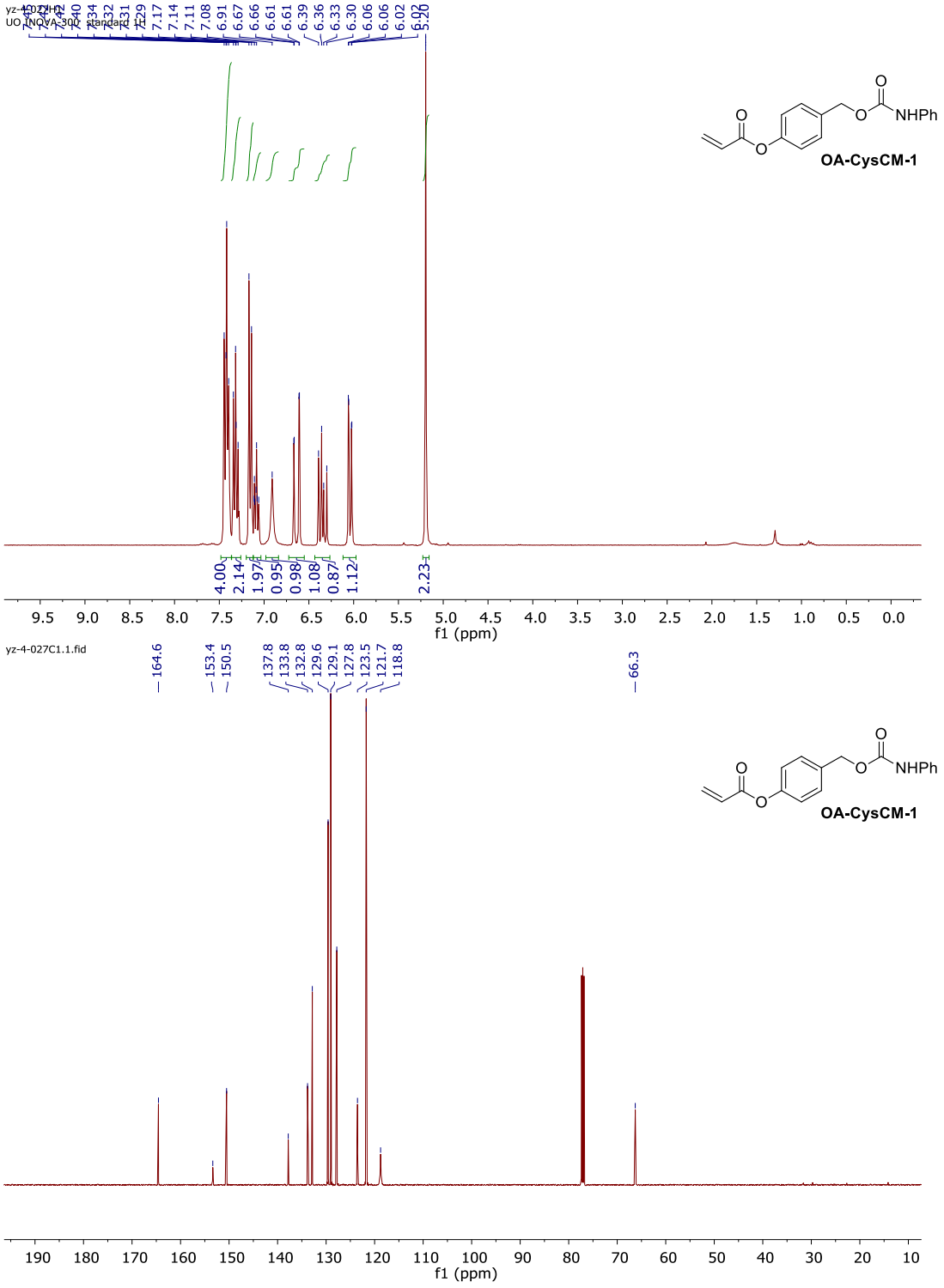

APPENDIX D
CHAPTER V SUPPLEMENTARY INFORMATION

Mass Spectrometry Data

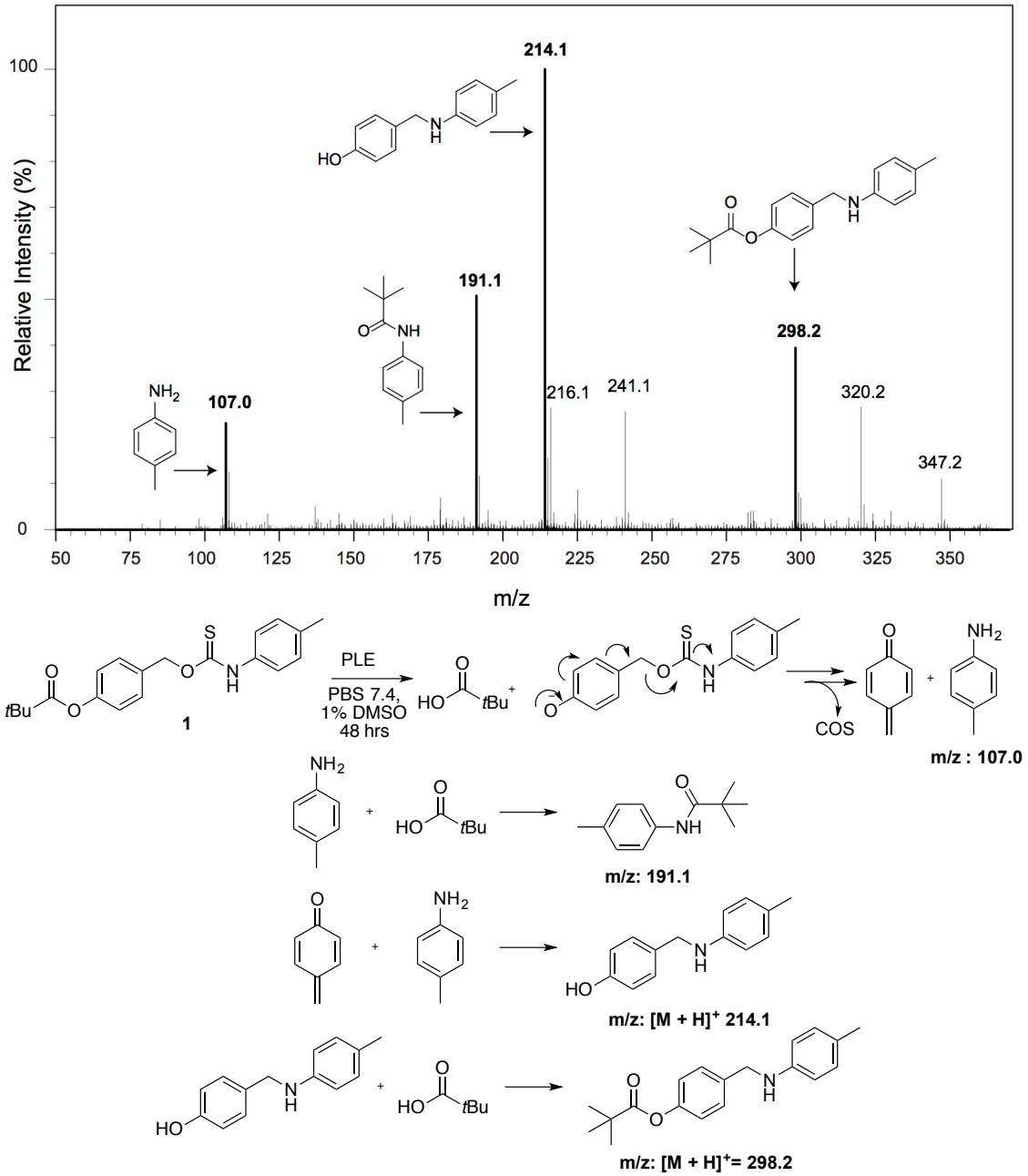

Figure D1. Mass spectrum of the reaction byproducts formed after stirring **1** with PLE in PBS buffer (pH 7.4, 1% DMSO) for 48 hours. Structures of potential byproducts have been labeled with their respective masses and reaction schemes detailing formation of these byproducts are shown.

Cytotoxicity of Na_2S

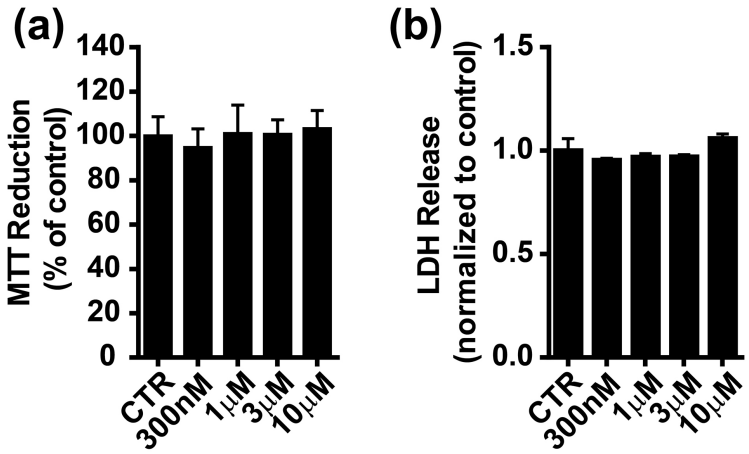

Figure D2. Cell viability studies of Na_2S in BEAS 2B cells using the (a) MTT and (b) LDH cell viability assays.

Cytotoxicity of 1 and 2 in HeLa cells

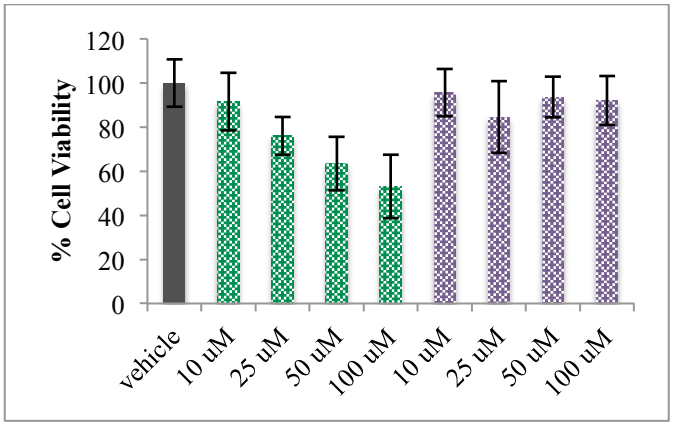

Figure D3. Cytotoxicity assay of donor **1** and control compound **2** in HeLa cells using the CCK-8 assay. HeLa cells were cultured in a 96-well plate overnight in Dulbecco's modified Eagle's medium (DMEM) supplemented with 10% fetal bovine serum (FBS) and 1% penicillin/streptomycin at 37 °C under 5% CO_2 and washed with PBS pH 7.4 prior to incubation in FBS-free DMEM containing vehicle (0.5% DMSO, black bar), **1** (green bars, 10-100 μM), or **2** (purple bars, 10-100 μM) for 1 hour. CCK-8 solution (10% in FBS-free DMEM) was added to each well, and cells were incubated for 3 hours at 37 °C. The absorbance at 450 nm was measured using a microplate reader. The cell viability was measured and normalized to the vehicle group. Results are expressed as mean ± SD (n=6).

NMR Spectra

^{1}H (600 MHz, DMSO-d_6) and $^{13}C\{^{1}H\}$ (150 MHz, DMSO-d_6) NMR Spectra of **1**

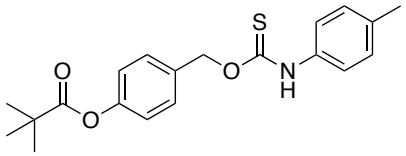

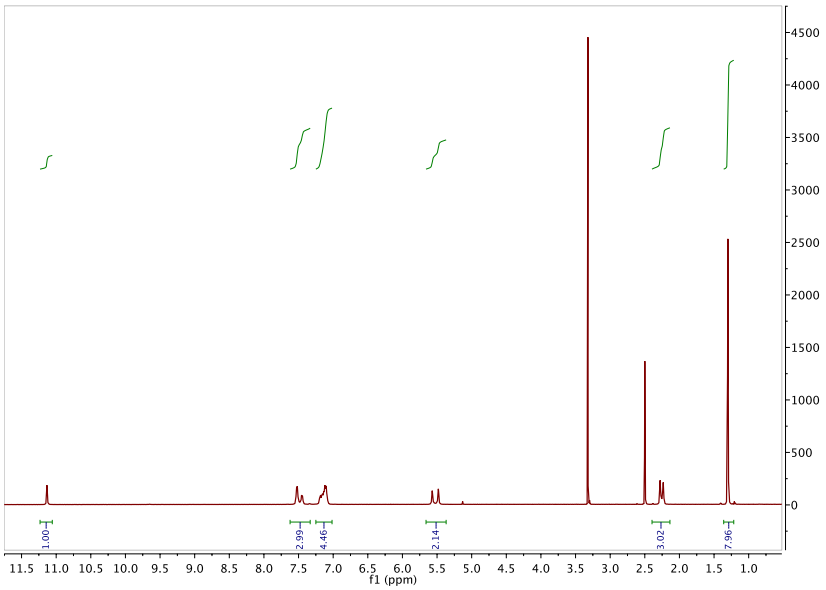

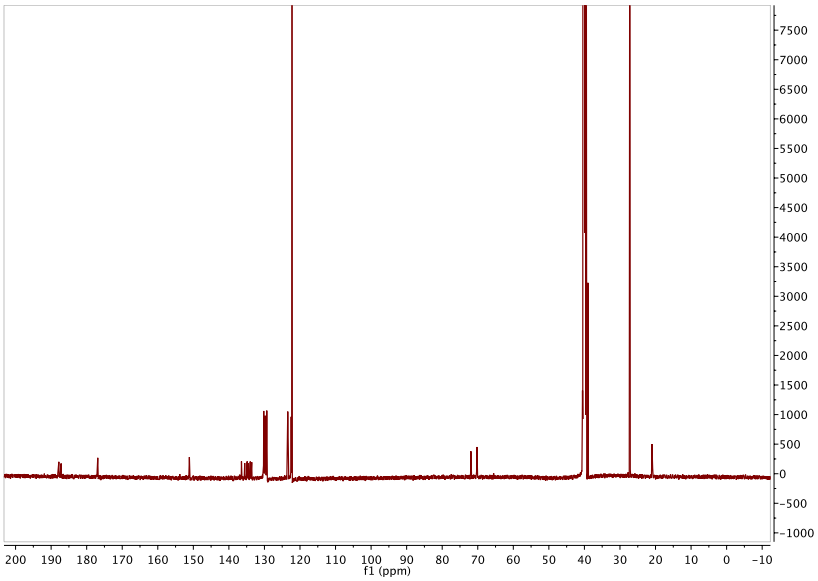

^{1}H (600 MHz, DMSO-d_6) and ^{13}C{^{1}H} (150 MHz, DMSO-d_6) NMR Spectra of **2**

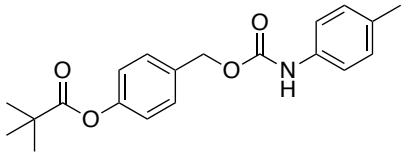

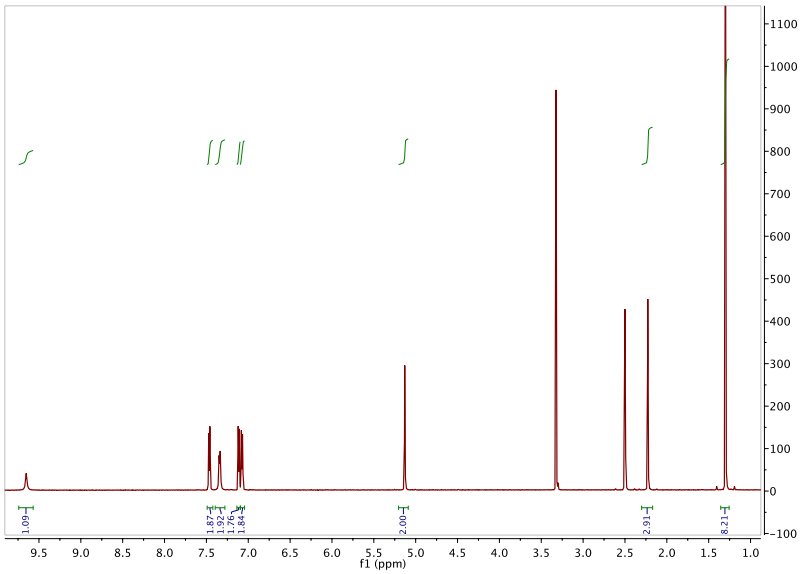

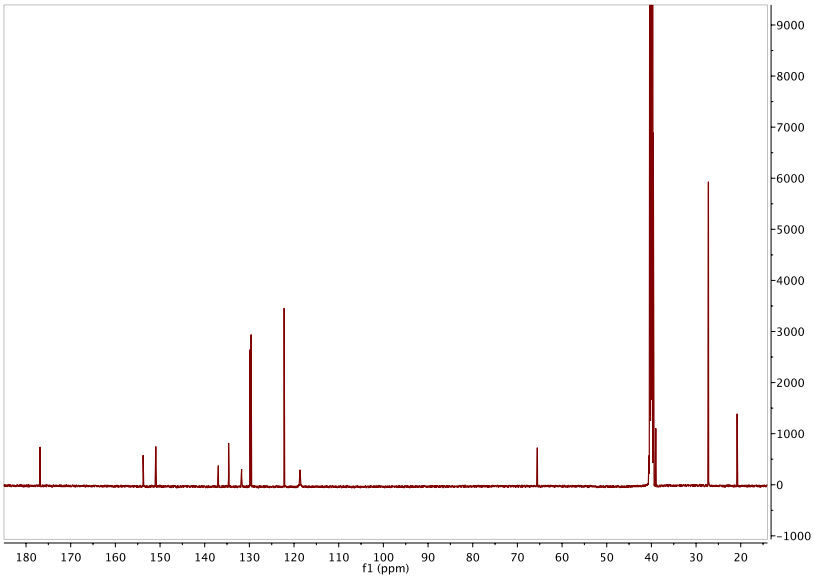

APPENDIX E

CHAPTER VI SUPPLEMENTARY INFORMATION

Synthesis / Spectral Details of Prepared Compounds

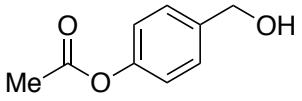

Me-OH was prepared with 4-hydroxybenzyl alcohol and acetyl chloride according to the general synthetic procedure described above. (324 mg, 48% yield). Spectral data is in agreement with those reported in the literature.[273]

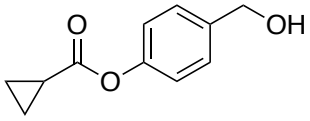

Cp-OH was prepared with 4-hydroxybenzyl alcohol and cyclopropanecarbonyl chloride according to the general synthetic procedure described above. (506 mg, 65% yield). Spectral data is in agreement with those reported in the literature.[274]

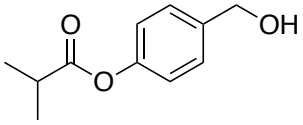

iPr-OH was prepared with 4-hydroxybenzyl alcohol and isobutyryl chloride according to the general synthetic procedure described above. (423 mg, 54% yield). Spectral data is in agreement with those reported in the literature.[275]

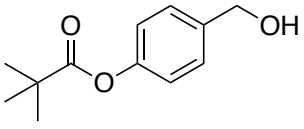

tBu-OH was prepared with 4-hydroxybenzyl alcohol and pivaloyl chloride according to the general synthetic procedure described above. (329 mg, 39% yield). Spectral data is in agreement with those reported in the literature.[237]

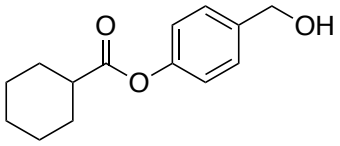

Cy-OH was prepared with 4-hydroxybenzyl alcohol and cyclohexanecarbonyl chloride according to the general synthetic procedure described above. (388 mg, 41% yield). Spectral data is in agreement with those reported in the literature.[275]

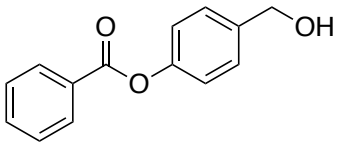

Ph-OH was prepared with 4-hydroxybenzyl alcohol and benzoyl chloride according to the general synthetic procedure described above. (726 mg, 79% yield). Spectral data is in agreement with those reported in the literature.[276]

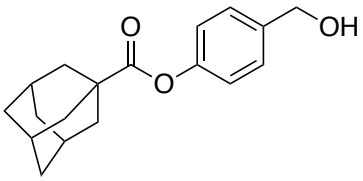

Ad-OH was prepared with 4-hydroxybenzyl alcohol and 1-adamantanecarbonyl chloride according to the general synthetic procedure described above. (416 mg, 36% yield). ^{1}H NMR (500 MHz, $CDCl_3$) δ (ppm): 7.37 (d, *J*=8.22 Hz, 2H), 7.05 (d, *J*=8.22 Hz, 2H), 4.69 (d, *J*=1.65 Hz, 2H), 2.86 (bs, 1H), 2.11 (m, 3H), 2.08 (d, *J*=3.17 Hz, 6H), 1.79 (d, *J*=3.51 Hz, 6H). ^{13}C{^{1}H} NMR (125 MHz, $CDCl_3$) δ (ppm): 176.30, 150.52, 138.15, 128.01, 121.67, 64.78, 41.03, 38.76, 34.46, 27.92. IR (cm^{-1}) 3515.75, 2903.27, 2853.32, 1718.00, 1504.69, 1452.47, 1222.53, 1189.10, 1160.28, 1040.92. HRMS m/z $[M + H]^+$ calcd. For $[C_{18}H_{15}O_3]^+$ 279.1021; found 279.1030.

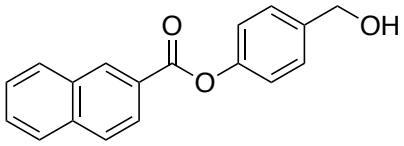

Nap-OH was prepared with 4-hydroxybenzyl alcohol and 2-naphthoyl chloride according to the general synthetic procedure described above. (660 mg, 59% yield). ^{1}H NMR (500 MHz, $CDCl_3$) δ (ppm): 8.83 (s, 1H), 8.23 (dd, *J*=8.6, 1.7 Hz, 1H), 8.04 (d, *J*=8.1 Hz, 1H), 7.99 (d, *J*=8.6 Hz, 1H), 7.96 (d, *J*=8.1 Hz, 1H), 7.67 (ddd, *J*=8.1, 6.8, 1.3 Hz, 1H), 7.62 (ddd, *J*=8.1, 6.8, 1.3 Hz, 1H), 7.50 (d, *J*=8.6 Hz, 2H), 7.30 (d, *J*=8.6 Hz,

2H), 4.78 (s, 2H), 1.66 (bs, 1H). $^{13}C\{^{1}H\}$ NMR (125 MHz, $CDCl_3$) δ (ppm): 165.42, 150.48, 138.57, 135.85, 132.51, 131.97, 129.50, 128.67, 128.42, 128.19, 127.86, 126.87, 126.69, 125.46, 121.91, 64.88. IR (cm^{-1}) 3319.86, 3058.22, 2867.44, 2360.09, 2341.52, 1734.43, 1631.12, 1596.86, 1508.04, 1463.36, 1418.26, 1387.99, 1352.95, 1280.24, 1225.79, 1194.70, 1164.29, 1080.76, 1013.92. HRMS m/z $[M + H]^+$ calcd. For $[C_{18}H_{23}O_3]^+$ 287.1647; found 287.1647.

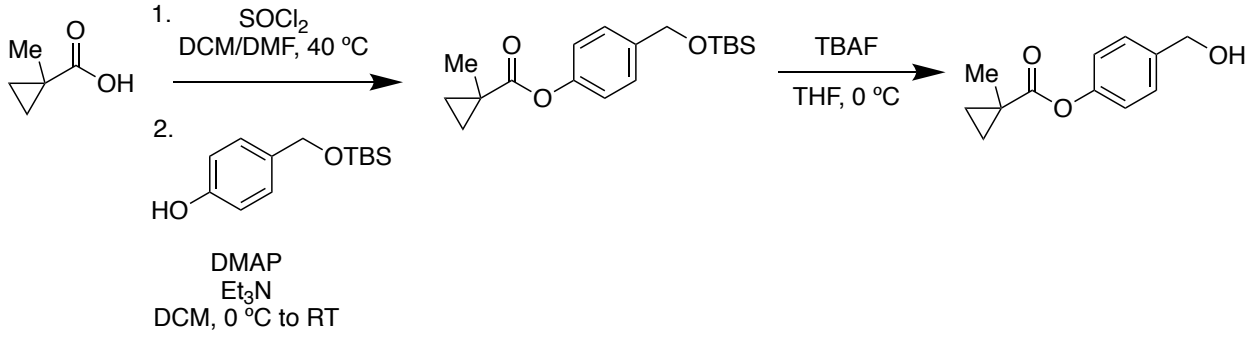

MCp-OH was prepared from the corresponding carboxylic acid. MCp-COOH (1.50 g, 1.0 equiv.) was dissolved in anhydrous dichloromethane (3.0 mL, 5.0 M solution), followed by addition of anhydrous DMF (60 µL, 0.05 equiv.). The reaction mixture was heated to reflux, and $SOCl_2$ (1.20 mL, 1.1 equiv.) was added dropwise under reflux. The reaction mixture was stirred under reflux for two hours, then concentrated under reduced pressure. The crude reaction mixture was re-dissolved in a minimum of dichloromethane and added dropwise to a stirring solution of 4-(TBS-hydroxymethyl)phenol (2.0 g, 0.56 equiv.), triethylamine (3.51 mL, 1.68 equiv.), and DMAP (500 mg, 0.28 equiv.) in dichloromethane (60 mL, 0.25 M solution). Upon completion (as determined by TLC) the reaction was quenched with 20 mL of brine, and extracted with methylene chloride (3 x 20 mL). The combined organic layers were dried over anhydrous magnesium sulfate, and purified by silica column chromatography to yield 1.03 g (21% yield over two steps). MCp-OTBS (1.03 g, 1.0 equiv.) was dissolved in anhydrous THF (32 mL, 0.1 M solution) under an atmosphere of nitrogen, and cooled to 0 °C. TBAF (3.20 mL 1.0 M in THF, 1.0 equiv.) was added dropwise. The reaction was let stir for 30 minutes, quenched with brine (10 mL), and extracted with ethyl acetate (3 x 20 mL). The combined organic layers were dried over anhydrous $MgSO_4$, concentrated under reduced pressure, and purified by silica column chromatography to yield MCp-OH as a white solid (365 mg, 55% yield). ^{1}H NMR (500 MHz, $CDCl_3$) δ (ppm): 7.37 (d, *J*=8.40 Hz, 2H), 7.06 (d, *J*-=8.40 Hz, 2H), 4.67 (s, 2H), 1.90 (bs, 1H), 1.44 (m, 5H), 0.86 (m, 2H). $^{13}C\{^{1}H\}$ NMR (125 MHz, $CDCl_3$) δ (ppm): 174.73, 150.38, 138.25, 127.97, 121.65, 64.73, 19.45, 18.81, 17.47. IR (cm^{-1}) 3356.76, 2969.77, 1736.30, 1652.94, 1606.43, 1507.08, 1465.16, 1419.78, 1388.80, 1324.07, 1163.95, 1120.74, 1013.39. HRMS m/z $[M + H]^+$ calcd. For $[C_{12}H_{15}O_3]^+$ 207.1021; found 207.1019.

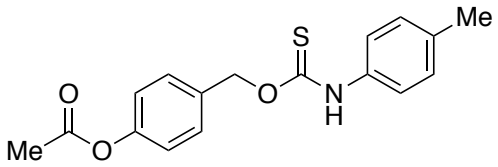

TCM1 was prepared with *p*-tolyl isothiocyanate and Me-OH according to the general synthetic procedure described above. (25 mg, 14% yield). ^{1}H NMR (500 MHz, DMSO-d_6, 60 °C) δ (ppm): 10.99 (s, 1H), 7.69-6.93 (m, 8H), 5.55 (s, 2H), 2.28 (bs, 6H). Broadness is observed in the ^{1}H NMR spectrum due to rotation around the C-N bond of the thiocarbamate. ^{13}C{^{1}H} NMR (125 MHz, DMSO-d_6, 25 °C) δ (ppm) 187.81, 187.20, 169.67, 150.82, 136.45, 135.55, 134.86, 134.57, 134.01, 133.63, 130.23, 129.78, 129.69, 129.35, 123.41, 122.47, 122.38, 71.89, 70.26, 60.23, 21.32, 21.24, 21.00, 20.90, 14.57. Splitting of peaks is observed in the ^{13}C{^{1}H} NMR spectrum due to slow rotation around the C-N bond of the thiocarbamate, yielding rotamers. IR (cm^{-1}) 3195.71, 3170.76, 3100.82, 3030.76, 2950.80, 1753.55, 1593.68, 1540.73, 1507.65, 1455.32, 1405.65, 1365.85, 1342.19, 1218.90, 1206.36, 1186.16, 1173.45, 1162.22. HRMS m/z [M + H]$^{+}$ calcd. For $[C_{17}H_{18}NO_3S]^{+}$ 316.1007; found 316.1016.

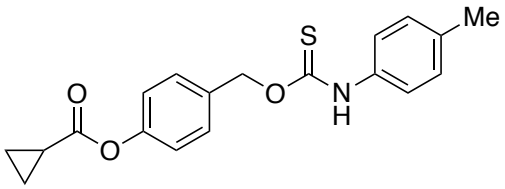

TCM2 was prepared with *p*-tolyl isothiocyanate and Cp-OH according to the general synthetic procedure described above. (65 mg, 39% yield). ^{1}H NMR (500 MHz, DMSO-d_6, 60 °C) δ (ppm): 10.97 (s, 1H), 7.65-6.97 (m, 8H), 5.55 (s, 2H), 2.28 (s, 3H), 1.89 (m, 1H), 1.05 (m, 4H). Broadness is observed in the ^{1}H NMR spectrum due to rotation around the C-N bond of the thiocarbamate. ^{13}C{^{1}H} NMR (125 MHz, DMSO-d_6, 25 °C) δ (ppm): 187.81, 187.19, 173.35, 150.77, 136.46, 135.55, 134.86, 134.57, 134.02, 133.64, 130.20, 129.78, 129.69, 129.35, 123.42, 122.47, 122.33, 71.88, 70.24, 21.00, 20.90, 13.06, 9.52. Splitting of peaks is observed in the ^{13}C{^{1}H} NMR spectrum due to slow rotation around the C-N bond of the thiocarbamate, yielding rotamers. IR (cm^{-1}) 3231.59, 3173.53, 3099.77, 3029.41, 2921.09, 1854.61, 1741.51, 1594.89, 1544.77, 1509.09, 1461.52, 1422.56, 1400.67, 1384.26, 1338.06, 1313.36, 1288.42, 1213.37, 1163.87, 1142.12. HRMS m/z [M + H]$^{+}$ calcd. For $[C_{19}H_{20}NO_3S]^{+}$ 342.1164; found 342.1174.

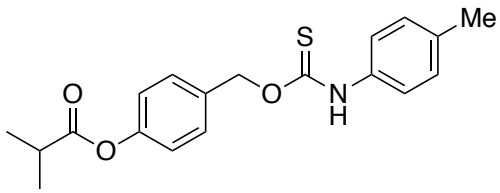

TCM3 was prepared with *p*-tolyl isothiocyanate and iPr-OH according to the general synthetic procedure described above. (52 mg, 31% yield). ^{1}H NMR (500 MHz, DMSO-d_6, 60 °C) δ (ppm): 10.97 (1H, s), 7.67 – 6.94 (bm, 8H), 5.56 (s, 2H), 2.83 (sept, *J*=7.84, 1H), 1.25 (d, *J*=7.84, 6H). Broadness is observed in the ^{1}H NMR spectrum due to rotation around the C-N bond of the thiocarbamate. ^{13}C{^{1}H} NMR (125 MHz, DMSO-d_6, 25 °C) δ (ppm): 187.83, 187.21, 175.48, 150.91, 136.47, 135.56, 134.84, 134.57, 134.00, 133.61, 130.23, 130.21, 129.80, 129.67, 129.34, 123.42, 122.47, 122.27, 71.91, 70.25, 33.78, 30.83, 20.98, 19.13. Splitting of peaks is observed in the ^{13}C{^{1}H} NMR spectrum due to slow rotation around the C-N bond of the thiocarbamate, yielding rotamers. IR (cm^{-1}) 3214.13, 3108.42, 3040.44, 2969.4, 2922.05, 1751.35, 1594.68, 1540.86, 1507.24, 1402.57, 1340.66, 1316.76, 1288.55, 1228.48, 1189.68. HRMS m/z $[M + H]^+$ calcd. For $[C_{19}H_{21}NO_3S]^+$ 344.1320; found 344.1308.

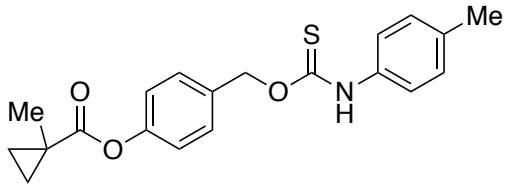

TCM4 was prepared with p-tolyl isothiocyanate and MCp-OH according to the general synthetic procedure described above. (100 mg, 61% yield). ^{1}H NMR (500 MHz, DMSO-d_6, 60 °C) δ (ppm): 10.99 (s, 1H), 7.66-6.99 (m, 8H), 5.54 (s, 2H), 2.28 (s, 3H), 1.38 (s, 3H), 1.34 (q, *J*=3.84, 2H), 0.92 (q, *J*=3.84, 2H). Broadness is observed in the ^{1}H NMR spectrum due to rotation around the C-N bond of the thiocarbamate. ^{13}C{^{1}H} NMR (125 MHz, DMSO-d_6, 25 °C) δ (ppm): 187.82, 187.18, 174.36, 150.97, 136.46, 135.55, 134.85, 134.56, 133.93, 133.53, 130.13, 129.77, 129.68, 129.34, 123.43, 122.46, 122.34, 71.92, 70.24, 21.00, 20.89, 19.43, 18.90, 17.31. Splitting of peaks is observed in the ^{13}C{^{1}H} NMR spectrum due to slow rotation around the C-N bond of the thiocarbamate, yielding rotamers. IR (cm^{-1}) 3208.15, 3172.09, 3102.38, 3034.45, 2969.61, 2924.52, 2868.84, 1739.32, 1592.23, 1541.25, 1508.68, 1449.58, 1421.32, 1398.13, 1334.24, 1315.04, 1287.58, 1211.63, 1189.86, 1166.87, 1123.90, 1013.25. HRMS m/z $[M + H]^+$ calcd. For $[C_{20}H_{22}NO_3S]^+$ 356.1320; found 356.1311.

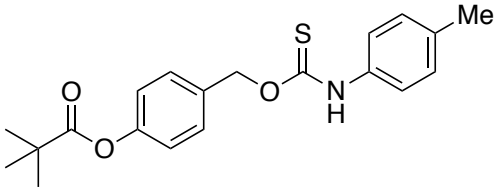

TCM5 was prepared with p-tolyl isothiocyanate and tBu-OH according to the general synthetic procedure described above. (109.4 mg, 64% yield). Spectral data is in agreement with those reported in the literature.[207]

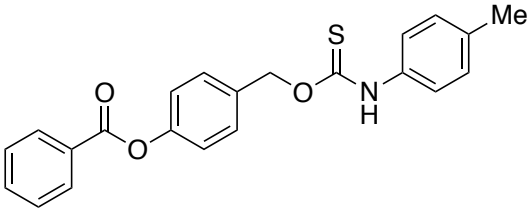

TCM6 was prepared with p-tolyl isothiocyanate and Ph-OH according to the general synthetic procedure described above. (34 mg, 22% yield). ^{1}H NMR (500 MHz, DMSO-d_6, 60 °C) δ (ppm): 11.00 (s, 1H), 8.15 (m, 2H), 7.75 (m, 1H), 7.64 (m, 2H), 7.58-7.11 (m, 8H), 5.59 (s, 2H), 2.28 (s, 3H). Broadness is observed in the ^{1}H NMR spectrum due to rotation around the C-N bond of the thiocarbamate. ^{13}C NMR (125 MHz, DMSO-d_6, 25 °C) δ (ppm): 187.84, 187.21, 165.06, 150.94, 136.47, 135.57, 134.87, 134.58, 134.31, 133.96, 133.91, 130.27, 129.90, 129.85, 129.72, 129.70, 129.62, 129.47, 129.36, 129.31, 123.44, 122.56, 122.50, 71.92, 70.25, 21.01, 20.91. Splitting of peaks is observed in the ^{13}C{^{1}H} NMR spectrum due to slow rotation around the C-N bond of the thiocarbamate, yielding rotamers. IR (cm^{-1}) 3200.22, 3156.21, 3092.37, 3028.96, 2969.84, 2925.83, 1728.56, 1591.53, 1538.83, 1508.72, 1449.12, 1398.19, 1365.23, 1338.94, 1312.68, 1263.16, 1249.22, 1225.59, 1209.75, 1188.14, 1174.53, 1079.50, 1056.59. HRMS m/z $[M + H]^+$ calcd. For $[C_{22}H_{22}NO_3S]^+$ 378.1164; found 378.1165.

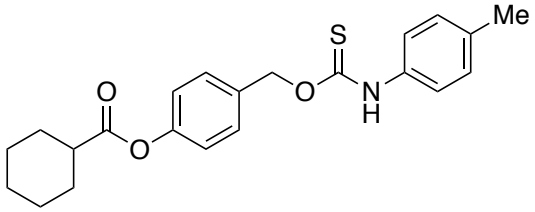

TCM7 was prepared with p-tolyl isothiocyanate and Cy-OH according to the general synthetic procedure described above. (46 mg, 29% yield). ^{1}H NMR (500 MHz, DMSO-d_6, 60 °C) δ (ppm): 10.97 (s, 1H), 7.62 – 7.14 (m, 8H), 5.55 (s, 2H), 2.61 (m, 1H), 2.28 (s, 3H), 2.00 (d, *J*=12.2, 2H), 1.75 (m, 2H), 1.64 (2, *J*=13.1, 1H), 1.52 (m, 2H), 1.36 (m, 2H), 1.29 (m, 1H). Broadness is observed in the ^{1}H NMR spectrum due to rotation around the C-N bond of the thiocarbamate. ^{13}C{^{1}H} NMR (125 MHz, DMSO-d_6, 25 °C) δ (ppm): 187.82, 187.20, 174.30, 150.91, 136.46, 135.56, 134.85, 134.57, 133.97, 133.58, 130.22, 129.81, 129.68, 129.61, 129.34, 123.42, 122.47, 122.32, 71.91, 70.25, 42.51, 28.93, 25.74, 25.18, 21.00, 20.90. Splitting of peaks is observed in the ^{13}C{^{1}H} NMR spectrum due to slow rotation around the C-N bond of the thiocarbamate, yielding rotamers. IR (cm^{-1}) 3203.91, 3176.67, 3030.10, 2930.06, 2854.13, 1752.75, 1527.52, 1511.28, 1386.41, 1311.79, 1208.06, 1178.02, 1165.88, 1147.76, 1114.41, 1017.32. HRMS m/z $[M + H]^+$ calcd. For $[C_{22}H_{26}NO_3S]^+$ 384.1633; found 384.1629.

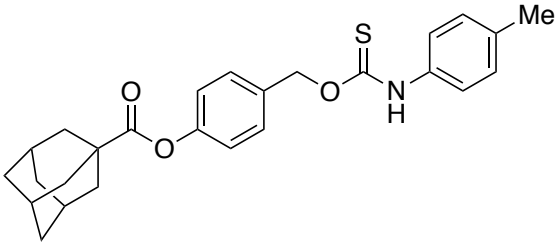

TCM8 was prepared with p-tolyl isothiocyanate and Ad-OH according to the general synthetic procedure described above. (40 mg, 26% yield). ^{1}H NMR (500 MHz, DMSO-d_6, 60 °C) δ (ppm): 10.98 (s, 1H), 7.57 – 7.05 (m, 8H), 5.55 (s, 2H), 2.28 (s, 3H), 2.06 (bs, 3H), 2.01 (bs, 6H), 1.75 (bs, 6H). Broadness is observed in the ^{1}H NMR spectrum due to rotation around the C-N bond of the thiocarbamate. ^{13}C{^{1}H} NMR (125 MHz, DMSO-d_6, 25 °C) δ (ppm): 187.83,187.19, 175.84, 151.07, 136.47, 135.55, 134.86, 134.57, 133.95, 133.54, 130.21, 129.84, 129.68, 129.35, 123.43, 122.47, 122.29, 71.93, 70.25, 60.23, 40.85, 40.53, 38.68, 36.31, 34.85, 30.25, 27.73, 27.62, 21.24, 21.15, 21.00, 20.90, 14.57. Splitting of peaks is observed in the ^{13}C{^{1}H} NMR spectrum due to slow rotation around the C-N bond of the thiocarbamate, yielding rotamers. IR (cm^{-1}) 3223.67, 3181.01, 3109.75, 3039.47, 2917.77, 2904.34, 2848.45, 1743.95, 1595.09, 1535.42, 1508.71, 1450.52, 1422.61, 1396.44, 1333.48, 1316.48, 1305.39, 1270.40, 1224.40, 1178.41, 1165.19, 1043.19. HRMS m/z [M + H]$^{+}$ calcd. For $[C_{26}H_{30}NO_3S]^{+}$ 436.1946; found 436.1943.

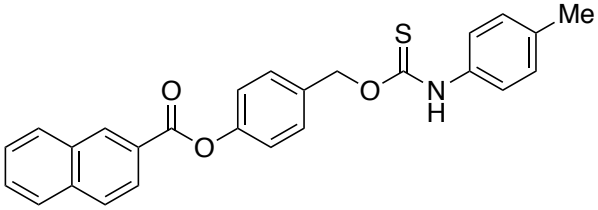

TCM9 was prepared with p-tolyl isothiocyanate and Nap-OH according to the general synthetic procedure described above. (112 mg, 76% yield). ^{1}H NMR (500 MHz, DMSO-d_6, 60 °C) δ (ppm): 11.01 (s, 1H), 8.85 (s, 1H), 8.21 (2, *J*=8.24, 1H), 8.13 (m, 2H), 8.07 (d, *J*=8.24, 1H), 7.73 (t, *J*=7.79, 1H), 7.68 (t, *J*=7.79, 1H), 7.63-7.09 (m, 8H), 5.61 (s, 2H), 2.29 (s, 3H). Broadness is observed in the ^{1}H NMR spectrum due to rotation around the C-N bond of the thiocarbamate. ^{13}C{^{1}H} NMR (125 MHz, DMSO-d_6, 25 °C) δ (ppm): 187.87, 187.23, 165.24, 151.05, 136.48, 135.84, 135.59, 134.88, 134.33, 133.94, 132.58, 132.05, 130.33, 130.02, 129.93, 129.71, 129.52, 129.36, 129.13, 128.26, 127.67, 126.56, 125.50, 123.44, 122.57, 71.94, 70.28, 55.38, 21.00, 20.91, 14.57. Splitting of peaks is observed in the ^{13}C{^{1}H} NMR spectrum due to slow rotation around the C-N bond of the thiocarbamate, yielding rotamers. IR (cm^{-1}) 3216.92, 3160.40, 3084.34, 3034.41, 2919.03, 2853.89, 1730.67, 1629.73, 1596.74, 1542.65, 1507.24, 1460.72, 1400.09, 1343.64, 1280.39, 1179.23, 1161.82, 1127.63, 1061.28. HRMS m/z [M + H]$^{+}$ calcd. For $[C_{26}H_{21}NO_3S]^{+}$ 428.1302; found 428.1290.

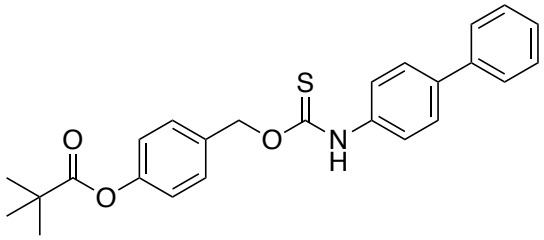

TCM10 was prepared with 4-biphenylyl isothiocyanate and *t*Bu-OH according to the general synthetic procedure described above. (90.9 mg, 45% yield). ^{1}H NMR (500 MHz, DMSO-d_6, 60 °C) δ (ppm): 11.18 (s, 1H), 7.64 (m, 5H), 7.52 (d, J=8.1 Hz, 2H), 7.45 (t, J= 7.6 Hz, 2H), 7.35 (m, 1H), 7.13 (d, J= 8.8 Hz, 2H), 5.61 (s, 2H), 1.34 (s, 9H). Broadness is observed in the ^{1}H NMR spectrum due to rotation around the C-N bond of the thiocarbamate.^{13}C{^{1}H} NMR (125 MHz, DMSO-d_6, 60 °C) δ (ppm): 187.7, 176.8, 151.3, 140.0, 137.2, 133.8, 129.9, 129.4, 127.8, 127.4, 126.9, 123.2, 122.2, 39.1, 27.2. FTIR (ATR, cm^{-1}): 3212.31, 3035.48, 2969.43, 1748.39, 1594.62, 1578.16, 1540.37, 1509.08, 1401.48, 1335.13, 1115.22, 1098.76, 1001.31, 833.74, 755.88, 685.14. HRMS m/z [M + H^{+}] calc. 420.1633; found 420.1595.

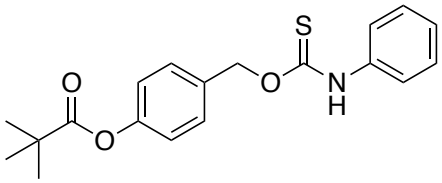

TCM11 was prepared with phenyl isothiocyanate and *t*Bu-OH according to the general synthetic procedure described above. (71.2 mg, 55% yield). ^{1}H NMR (500 MHz, DMSO-d_6, 60 °C) δ (ppm): 11.07 (s, 1H), 7.63-7.42 (m, 4H), 7.33 (m, 2H), 7.16 (m, 1H), 7.35 (m, 1H), 7.12 (d, J= 8.7 Hz, 2H), 5.58 (s, 2H), 1.32 (s, 9H). Broadness is observed in the ^{1}H NMR spectrum due to rotation around the C-N bond of the thiocarbamate.^{13}C{^{1}H} NMR (125 MHz, DMSO-d_6, 60 °C) δ (ppm): 187.9, 176.8, 151.3, 138.8, 133.8, 129.9, 129.1, 125.4, 123.1, 122.2, 39.1, 27.3. FTIR (ATR, cm^{-1}): 3218.40, 3125.23, 3061.19, 2973.40, 1746.87, 1595.52, 1545.05, 1494.26, 1406.69, 1309.81, 1202.79, 1163.67, 1117.27, 1013.63, 898.00, 782.7-, 685.16. HRMS m/z [M + H^{+}] calc. 344.1320; found 344.1309.

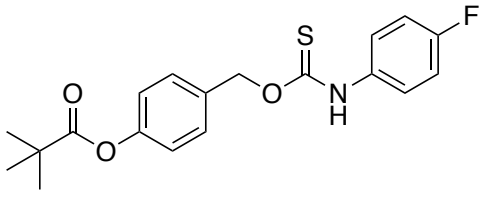

TCM12 was prepared with p-fluorophenyl isothiocyanate and *t*Bu-OH according to the general synthetic procedure described above. (100.1 mg, 58% yield). ^{1}H NMR (500 MHz, DMSO-d_6, 60 °C) δ (ppm): 11.08 (s, 1H), 7.82-7.31 (m, 4H), 7.21-7.06 (m, 4H), 5.57 (s, 2H), 1.33 (s, 9H). Broadness is observed in the ^{1}H NMR spectrum due to rotation around the C-N bond of the thiocarbamate. ^{13}C{^{1}H} NMR (125 MHz, DMSO-d_6, 60 °C)

δ (ppm): 176.8, 160.9, 158.9, 151.2, 133.6, 129.9, 125.5, 122.4, 123.1, 115.7, 39.0, 27.2. ^{19}F NMR (460.6 MHz, DMSO-d_6, 60 °C) δ (ppm): -117.17. FTIR (ATR, cm^{-1}): 3181.22, 2971.41, 1747.38, 1596.49, 1537.94, 1504.04, 1393.87, 1336.73, 1275.72, 1186.62, 1151.67, 1069.09, 1014.34, 893.61, 805.78, 684.83. HRMS m/z [M + H$^+$] calc. 362.1226; found 362.1208.

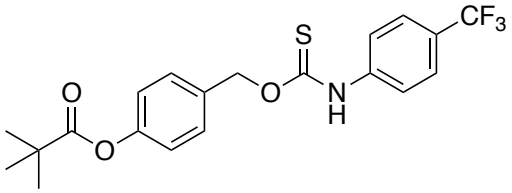

TCM13 was prepared with *p*-trifluoromethylphenyl isothiocyanate and *t*Bu-OH according to the general synthetic procedure described above. (99.9 mg, 51% yield). ^{1}H NMR (500 MHz, DMSO-d_6, 60 °C) δ (ppm): 11.40 (s, 1H), 7.80 (br s, 2H), 7.68 (d, *J*= 8.4 Hz, 2H), 7.52 (d, *J*= 8.5 Hz, 2H), 7.13 (d, *J*= 8.5 Hz, 2H), 5.61 (s, 2H), 1.32 (s, 9H). Broadness is observed in the ^{1}H NMR spectrum due to rotation around the C-N bond of the thiocarbamate. ^{13}C{^{1}H} NMR (125 MHz, DMSO-d_6, 60 °C) δ (ppm): 188.1, 176.8, 151.3, 133.5, 130.0, 126.3, 125.7, 123.4, 122.6, 39.0, 27.2. ^{19}F NMR (460.6 MHz, DMSO-d_6, 60 °C) δ (ppm): -60.6. FTIR (ATR, cm^{-1}): 3185.58, 2969.83, 1746.81, 1601.25, 1544.38, 1510.27, 1461.11, 1396.96, 1317.40, 1164.31, 1110.57, 1067.89, 1014.47, 895.83, 837.74, 730.01. HRMS m/z [M + H$^+$] calc. 412.2294; found 412.1174.

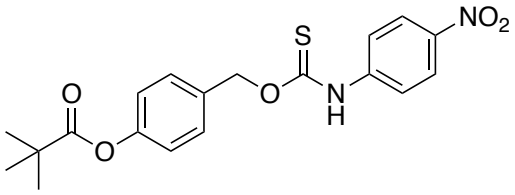

14S was prepared with *p*-nitrophenyl isothiocyanate and *t*Bu-OH according to the general synthetic procedure described above. (67.9l mg, 47% yield). ^{1}H NMR (500 MHz, DMSO-d_6, 60 °C) δ (ppm): 11.60 (s, 1H), 8.19 (d, *J*= 9.2 Hz, 2H), 7.85 (br s, 2H), 7.52 (d, *J*= 6.7 Hz, 2H), 7.13 (d, *J*= 6.7 Hz, 2H), 5.59 (s, 2H), 1.32 (s, 9H). Broadness is observed in the ^{1}H NMR spectrum due to rotation around the C-N bond of the thiocarbamate. ^{13}C{^{1}H} NMR (125 MHz, DMSO-d_6, 60 °C) δ (ppm): 176.7, 151.3, 143.6, 133.4, 130.1, 124.9, 122.2, 122.0, 39.0, 27.3. FTIR (ATR, cm^{-1}): 3213.46, 3075.42, 2969.58, 1746.40, 1595.02, 1548.26, 1507.20, 1393.72, 1333.09, 1162.50, 1102.61, 1014.04, 893.97, 831.49, 747.03, 681.70. HRMS m/z [M + H$^+$] calc. 389.1171; found 389.1154.

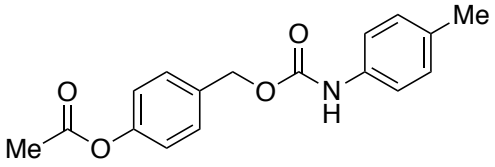

CM1 was prepared with p-tolyl isocyanate and Me-OH according to the general synthetic procedure described above. (65 mg, 36% yield). ^{1}H NMR (500 MHz, $CDCl_3$) δ (ppm) 7.42 (d, *J*=8.35, 2H), 7.28 (m, 2H), 7.12 (m, 4H), 6.75 (bs, 1H), 5.19 (s, 2H), 2.32 (m, 6H). ^{13}C NMR (125 MHz, $CDCl_3$) δ (ppm) 169.45, 153.42, 150.59, 135.15, 133.84, 133.13, 129.55, 121.76, 118.87, 66.22, 21.13, 20.77. IR (cm^{-1}) 3326.83, 2922.76, 2360.39, 2341.56, 1762.07, 1704.91, 1597.57, 1524.66, 1508.13, 1451.05, 1406.66, 1368.20, 1314.74, 1295.48, 1191.34, 1164.63, 1049.44, 1016.58. HRMS m/z $[M + H]^+$ calcd. For $[C_{17}H_{18}NO_4]^+$ 300.1236; found 300.1228.

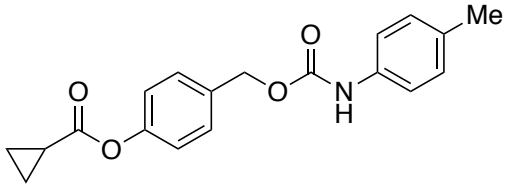

CM2 was prepared with p-tolyl isocyanate and Cp-OH according to the general synthetic procedure described above. (96 mg, 57% yield). ^{1}H NMR (500 MHz, $CDCl_3$) δ (ppm) 7.42 (d, *J*=8.11, 2H), 7.28 (m, 2H), 7.12 (m, 4H), 6.69 (bs, 1H), 5.19 (s, 2H), 2.33 (s, 3H), 1.87 (m, 1H), 1.19 (m, 2H), 1.05 (m, 2H). ^{13}C NMR (125 MHz, $CDCl_3$) δ (ppm) 173.42, 153.39, 150.74, 135.14, 133.63, 133.13, 129.55, 129.50, 121.76, 118.76, 66.26, 20.76, 13.03, 9.31. IR (cm^{-1}) 3334.74, 3015.89, 2969.69, 2360.04, 2341.58, 1727.03, 1598.07, 1526.98, 1508.92, 1448.66, 1406.77, 1381.64, 1314.94, 1295.88, 1204.23, 1165.01, 1138.93, 1049.63, 1017.09. HRMS m/z $[M + H]^+$ calcd. For $[C_{19}H_{20}NO_4]^+$ 326.1392; found 326.1392.

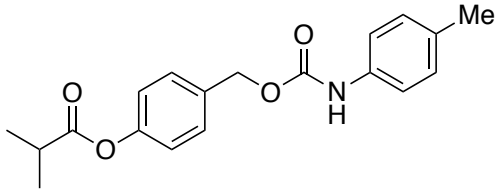

CM3 was prepared with p-tolyl isocyanate and iPr-OH according to the general synthetic procedure described above. (88 mg, 52% yield). ^{1}H NMR (500 MHz, $CDCl_3$) δ (ppm) 7.44 (d, *J*=8.20, 2H), 7.28 (m, 2H), 7.13 (d, *J*=8.17, 2H), 7.10 (d, *J*=8.20, 2H), 6.60 (bs, 1H), 5.20 (s, 2H), 2.83 (hept, *J*=7.0, 1H), 2.33 (s, 3H), 1.34 (d, *J*=7.0, 6H). ^{13}C NMR (125 MHz, $CDCl_3$) δ (ppm) 175.50, 153.32, 150.84, 135.08, 133.59, 133.19, 129.56, 129.52, 121.69, 118.86, 66.29, 34.18, 20.76, 18.92. IR (cm^{-1}) 3347.50, 2970.71, 2936.12, 1755.62, 1702.87, 1594.82, 1528.43, 1508.77, 1459.20, 1407.82, 1314.10, 1229.85,

1178.37, 1164.49, 1118.47, 1069.53, 1041.40. HRMS m/z $[M + H]^+$ calcd. For $[C_{19}H_{22}NO_4]^+$ 328.1549; found 328.1565.

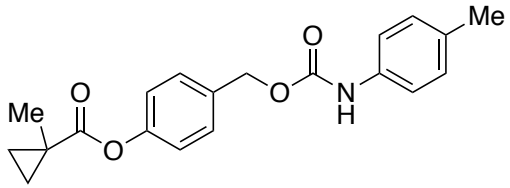

CM4 was prepared with p-tolyl isocyanate and MCp-OH according to the general synthetic procedure described above. (87 mg, 90% yield). ^{1}H NMR (500 MHz, $CDCl_3$) δ (ppm) 7.41 (d, *J*=8.03, 2H), 7.28 (d, *J*=8.11, 2H), 7.12 (d, *J*=8.03, 2H), 7.08 (d, *J*=8.11, 2H), 6.68 (bs, 1H), 5.18 (s, 2H), 2.33 (s, 3H), 1.45 (bs, 5H), 0.87 (m, 2H). ^{13}C NMR (125 MHz, $CDCl_3$) δ (ppm) 174.55, 153.40, 150.95, 135.14, 133.51, 133.12, 129.55, 129.47, 121.74, 118.87, 66.28, 20.76, 19.43, 18.82, 17.49. IR (cm^{-1}) 3336.98, 3042.16, 2969.35, 1730.15, 1696.57, 1595.43, 1525.80, 1509.41, 1454.78, 1406.03, 1325.66, 1312.51, 1226.40, 1211.00, 1198.55, 1166.74, 1139.45, 1129.51, 1073.47, 1050.49. HRMS m/z $[M + H]^+$ calcd. For $[C_{20}H_{22}NO_4]^+$ 340.1549; found 340.1528.

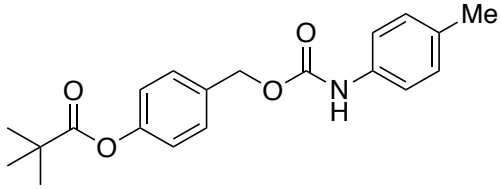

CM5 was prepared with p-tolyl isocyanate and tBu-OH according to the general synthetic procedure described above. (108 mg, 83% yield). Spectral data is in agreement with those reported in the literature.[207]

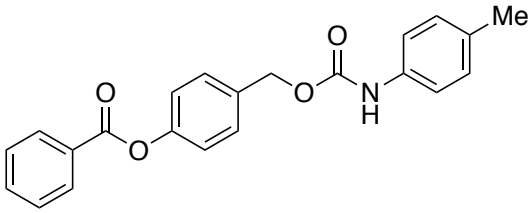

CM6 was prepared with p-tolyl isocyanate and Ph-OH according to the general synthetic procedure described above. (246 mg, 79% yield). ^{1}H NMR (500 MHz, $CDCl_3$) δ (ppm): 8.23 (m, 2H), 7.67 (m, 1H), 7.54 (t, *J*=7.84, 2H), 7.50 (d, *J*=8.49, 2H), 7.29 (m, 2H), 7.26 (d, *J*=8.49, 2H), 7.14 (d, *J*=8.16, 2H), 6.63 (bs, 1H), 5.24 (s, 2H), 2.33 (s, 3H). ^{13}C{^{1}H} NMR (125 MHz, $CDCl_3$) δ (ppm): 165.09, 150.90, 135.09, 133.86, 133.67, 133.20, 130.20, 129.62, 129.58, 129.44, 128.60, 121.91, 118.90, 66.30, 20.77. IR (cm^{-1}) 3320.43, 2916.58, 1732.04, 1694.16, 1593.59, 1525.22, 1508.19, 1406.42, 1313.55,

1269.13, 1235.09, 1193.82, 1162.28, 1062.11, 1015.89. HRMS m/z $[M + H]^+$ calcd. For $[C_{22}H_{20}NO_4]^+$ 362.1392; found 362.1391.

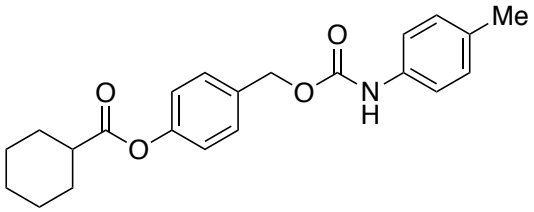

CM7 was prepared with p-tolyl isocyanate and Cy-OH according to the general synthetic procedure described above. (640 mg, 79% yield). ^{1}H NMR (500 MHz, $CDCl_3$) δ (ppm): 7.41 (d, *J*=8.36, 2H), 7.28 (m, 2H), 7.12 (d, *J*=8.10, 2H), 7.09 (d, *J*=8.10, 2H), 6.78 (bs, 1H), 5.18 (s, 2H), 2.59 (m, 1H), 2.33 (s, 3H), 2.09 (m, 2H), 1.85 (m, 2H), 1.73 (m, 1H), 1.62 (m, 2H), 1.38 (m, 3H). $^{13}C\{^1H\}$ NMR (125 MHz, $CDCl_3$) δ (ppm): 174.51, 153.45, 150.84, 135.20, 133.60, 133.08, 129.53, 129.51, 121.74, 118.88, 66.26, 43.21, 28.96, 25.74, 25.38, 20.77. IR (cm^{-1}) 3357.69, 2963.07, 2934.63, 2858.40, 1740.97, 1701.30, 1594.02, 1526.50, 1508.57, 1461.03, 1407.81, 1314.55, 1301.71, 1227.85, 1211.49, 1191.90, 1179.93, 1010.75. HRMS m/z $[M + H]^+$ calcd. For $[C_{22}H_{26}NO_4]^+$ 368.1862; found 368.1859.

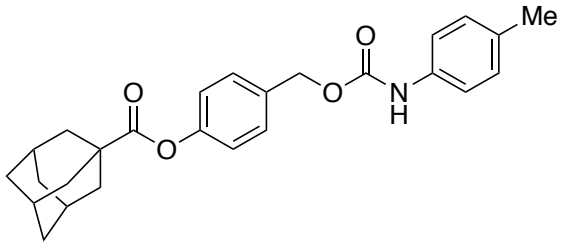

CM8 was prepared with p-tolyl isocyanate and Ad-OH according to the general synthetic procedure described above. (78 mg, 53% yield). ^{1}H NMR (500 MHz, $CDCl_3$) δ (ppm): 7.43 (d, *J*=8.10, 2H), 7.29 (m, 2H), 7.13 (d, *J*=8.10, 2H), 7.07 (d, *J*=8.46, 2H), 6.59 (bs, 1H), 5.20 (s, 2H), 2.33 (s, 3H), 2.11 (bs, 3H), 2.08 (d, *J*=2.92, 6H), 1.80 (m, 6H). $^{13}C\{^1H\}$ NMR (125 MHz, $CDCl_3$) δ (ppm): 176.09, 153.35, 151.09, 135.09, 133.41, 133.18, 129.57, 129.51, 121.76, 118.81, 66.33, 41.05, 38.75, 36.46, 27.91, 20.77. IR (cm^{-1}) 3335.00, 2905.92, 2852.06, 2360.58, 2341.57, 1728.80, 1598.69, 1528.20, 1508.60, 1452.54, 1407.35, 1315.33, 1217.92, 1195.02, 1165.11, 1051.05. HRMS m/z $[M + H]^+$ calcd. For $[C_{26}H_{30}NO_4]^+$ 420.2175; found 420.2152.

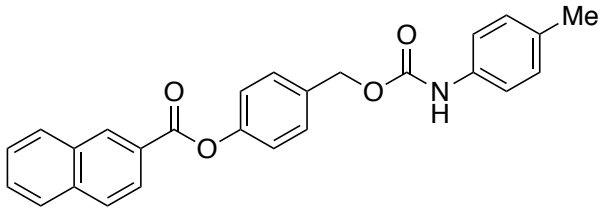

CM9 was prepared with p-tolyl isocyanate and Nap-OH according to the general synthetic procedure described above. (302 mg, 71% yield). ^{1}H NMR (500 MHz, $CDCl_3$) δ (ppm): 8.82 (s, 1H), 8.22 (dt, *J*=8.67, 1.74, 1.74), 8.03 (d, *J*=8.18, 1H), 7.98 (d, *J*=8.67,

1H), 7.95 (d, *J*=8.18, 1H), 7.66 (m, 1H), 7.61 (m, 1H), 7.52 (m, 2H), 7.30 (m, 3H), 7.14 (d, *J*=8.12, 2H), 6.63 (bs, 1H), 5.26 (s, 3H), 2.34 (s, 3H). $^{13}C\{^{1}H\}$ NMR (125 MHz, $CDCl_3$) δ (ppm): 165.27, 151.00, 135.86, 135.10, 133.89, 133.21, 132.51, 131.99, 129.65, 129.59, 129.51, 128.69, 128.43, 127.86, 126.88, 126.62, 125.44, 121.97, 118.87, 66.32, 20.77. IR (cm^{-1}) 3275.44, 2915.16, 1731.08, 1697.51, 1631.77, 1598.64, 1406.97, 1353.34, 1314.70, 1281.60, 1260.92, 1218.37, 1197.35, 1129.82, 1065.23. HRMS m/z $[M + H]^+$ calcd. For $[C_{26}H_{22}NO_4]^+$ 412.1549; found 412.1529.

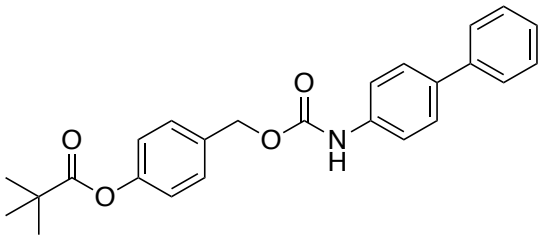

CM10 was prepared with 4-biphenylyl isocyanate and *t*Bu-OH according to the general synthetic procedure described above. (161.9 mg, 56% yield). ^{1}H NMR (500 MHz, $CDCl_3$, rt) δ (ppm): 7.57-7.54 (m, 4H), 7.46-7.40 (m, 6H), 7.34-7.30 (m, 1H), 7.09-7.05 (m, 2H), 5.21 (s, 2H), 1.36 (s, 9H). $^{13}C\{^{1}H\}$ NMR (125 MHz, $CDCl_3$, rt) δ (ppm): 176.9, 151.1, 140.5, 137.0, 136.5, 133.4, 129.6, 128.7, 127.7, 127.0, 126.8, 119.0, 66.5, 39.1, 27.1. FTIR (ATR, cm^{-1}): 3313.48, 2969.35, 1746.36, 1689.12, 1592.73, 1509.58, 1480.26, 1405.51, 1314.67, 1195.27, 1164.21, 1112.53, 1062.14, 896.62, 828.77, 784.19, 695.36. HRMS m/z $[M + H^+]$ calc. 404.1862; found 404.1845.

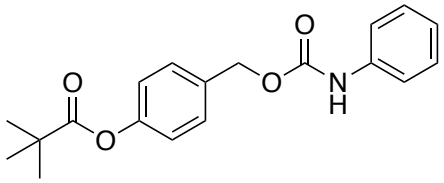

CM11 was prepared with phenyl isocyanate and *t*Bu-OH according to the general synthetic procedure described above. (122.6 mg, 78% yield). ^{1}H NMR (500 MHz, $CDCl_3$, rt) δ (ppm): 7.41-7.37 (m, 4H), 7.32-7.28 (m, 2H), 7.08-7.03 (m, 3H), 6.66 (s, 1H), 5.18 (s, 2H), 1.36 (s, 9H). $^{13}C\{^{1}H\}$ NMR (125 MHz, $CDCl_3$, rt) δ (ppm): 176.9, 151.1, 137.7, 133.4, 129.5, 129.1, 123.6, 121.7, 118.7, 66.4, 39.1, 27.1. FTIR (ATR, cm^{-1}): 3306.13, 2970.18, 1746.49, 1693.12, 1595.72, 1529.13, 1508.09, 1395.71, 1314.76, 1195.33, 1163.48, 1112.67, 1053.18, 1015.91, 896.33, 759.44, 694.14. HRMS m/z $[M + H^+]$ calc. 328.1549; found 328.1553.

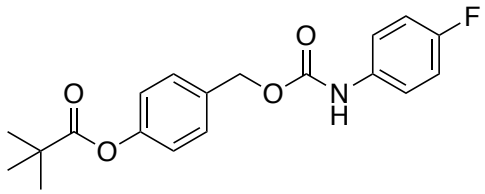

CM12 was prepared with *p*-fluorophenyl isocyanate and *t*Bu-OH according to the general synthetic procedure described above. (124.3 mg, 75% yield). ^{1}H NMR (500 MHz, $CDCl_3$, rt) δ (ppm): 7.41-7.39 (m, 2H), 7.33 (br m, 2H), 7.08-7.05 (m, 2H), 7.01-

6.98 (m, 2H), 6.63 (br s, 1H), 5.17 (s, 2H), 1.36 (s, 9H). $^{13}C\{^{1}H\}$ NMR (125 MHz, $CDCl_3$, rt) δ (ppm): 177.0, 151.1, 133.3, 129.6, 121.7, 120.5, 115.8, 115.6, 66.5, 39.1, 27.1. ^{19}F NMR (460.6 MHz, $CDCl_3$, rt) δ (ppm): -119.4. FTIR (ATR, cm^{-1}): 3323.18, 2967.74, 1744.75, 1691.02, 1589.24, 1527.64, 1508.77, 1406.82, 1314.52, 1194.09, 1164.68, 1111.68, 1062.02, 897.11, 827.95, 704.67, 695.28. HRMS m/z [M + Na^+] calc. 368.1274; found 368.1271.

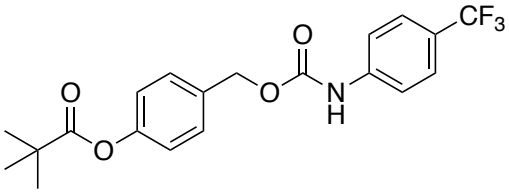

CM13 was prepared with *p*-trifluoromethylphenyl isocyanate and *t*Bu-OH according to the general synthetic procedure described above. (171.7 mg, 90% yield). ^{1}H NMR (500 MHz, $CDCl_3$, rt) δ (ppm): 7.55 (d, *J*= 9.1 Hz, 2H), 7.49 (d, *J*= 7.4 Hz, 2H), 7.41 (d, *J*= 9.1 Hz, 2H), 7.07 (d, *J*= 7.4 Hz, 2H), 6.87 (s, 1H), 5.19 (s, 2H), 1.36 (s, 9H). $^{13}C\{^{1}H\}$ NMR (125 MHz, $CDCl_3$, rt) δ (ppm): 177.0, 152.9, 151.2, 140.9, 133.0, 129.7, 126.3, 125.5, 125.2, 123.1, 121.8, 118.1, 66.7, 39.1, 27.1.^{19}F NMR (460.6 MHz, $CDCl_3$, rt) δ (ppm): -62.0. FTIR (ATR, cm^{-1}): 3328.25, 2969.45, 1745.17, 1692.87, 1589.14, 1528.07, 1508.84, 1314.86, 1256.64, 1215.86, 1194.32, 1164.25, 1110.81, 1062.66, 895.70, 831.85, 700.40, 694.55. HRMS m/z [M + H^+] calc. 396.1423; found 396.1410.

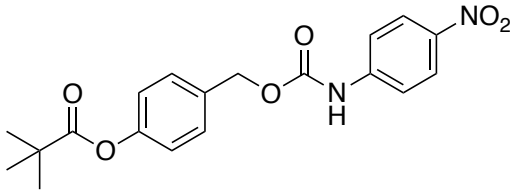

CM14 was prepared with *p*-nitrophenyl isocyanate and *t*Bu-OH according to the general synthetic procedure described above. (142.6 mg, 80% yield). ^{1}H NMR (500 MHz, $CDCl_3$, rt) δ (ppm): 8.19 (d, *J*= 7.3 Hz, 2H), 7.54 (d, *J*= 7.3 Hz, 2H), 7.41 (d, *J*= 8.5 Hz, 2H), 7.08 (d, *J*= 8.5l Hz, 2H), 5.21 (s, 2H), 1.36 (s, 9H). $^{13}C\{^{1}H\}$ NMR (125 MHz, $CDCl_3$, rt) δ (ppm): 177.1, 152.5, 151.3, 143.8, 143.1, 132.7, 129.8, 125.2, 121.9, 117.8, 66.1, 39.1, 27.1. FTIR (ATR, cm^{-1}): 3327.31, 2971.82, 1729.89, 1691.69, 1598.33, 1507.95, 1407.53, 1335.48, 1276.09, 1216.16, 1195.58, 1164.38, 1112.36, 1051.41, 1016.71, 897.17, 832.11, 750.35, 689.05. HRMS m/z [M + Na^+] calc. 395.1219; found 395.1212.

NMR Spectra

^{1}H (500 MHz, $CDCl_3$) and ^{13}C (125 MHz, $CDCl_3$) NMR spectra of **Ad-OH.**

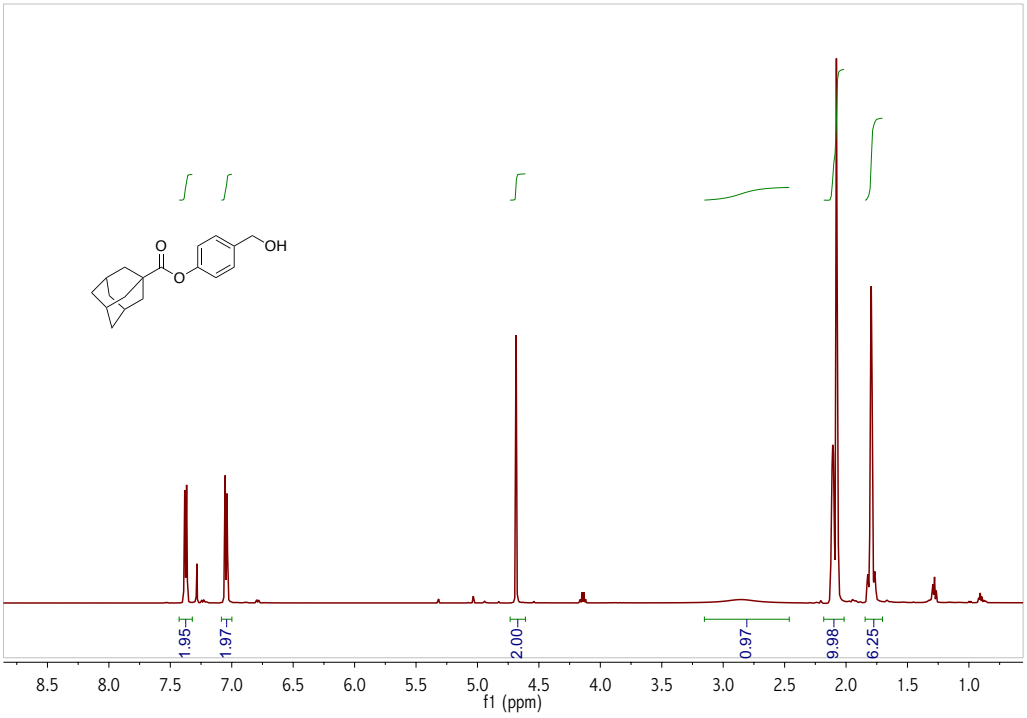

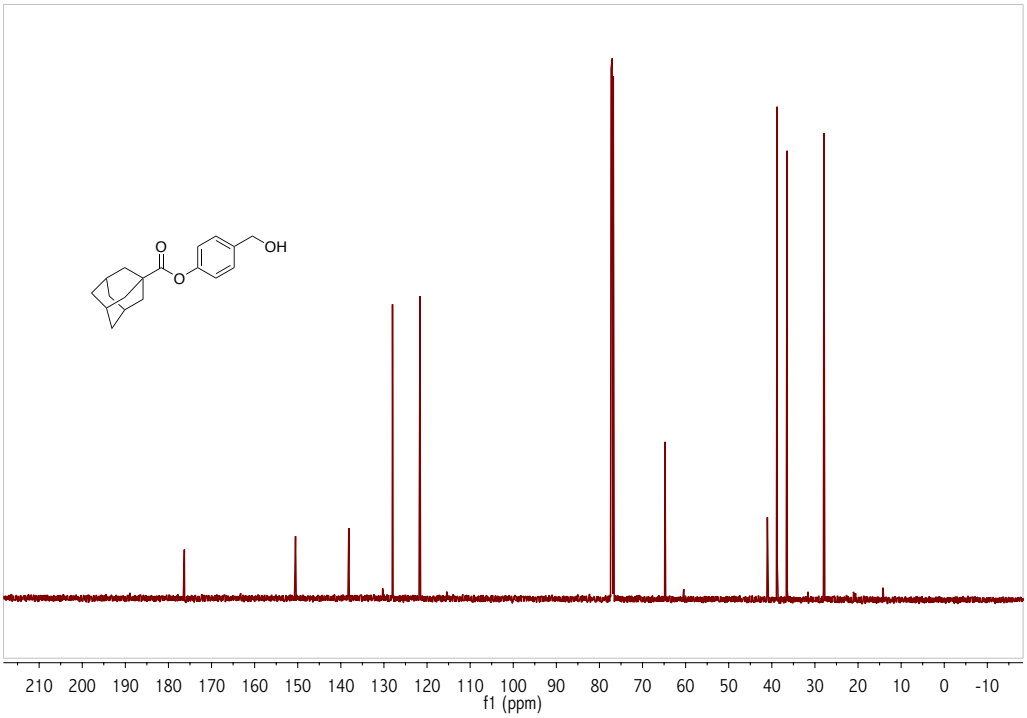

^{1}H (500 MHz, $CDCl_3$) and ^{13}C (125 MHz, $CDCl_3$) NMR spectra of **Nap-OH.**

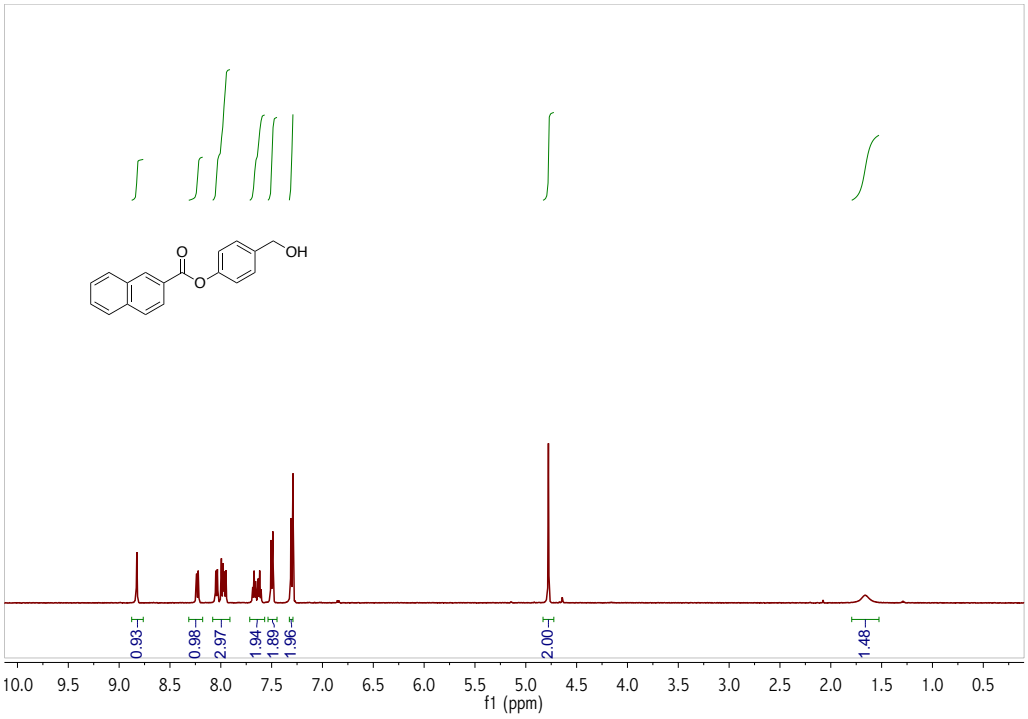

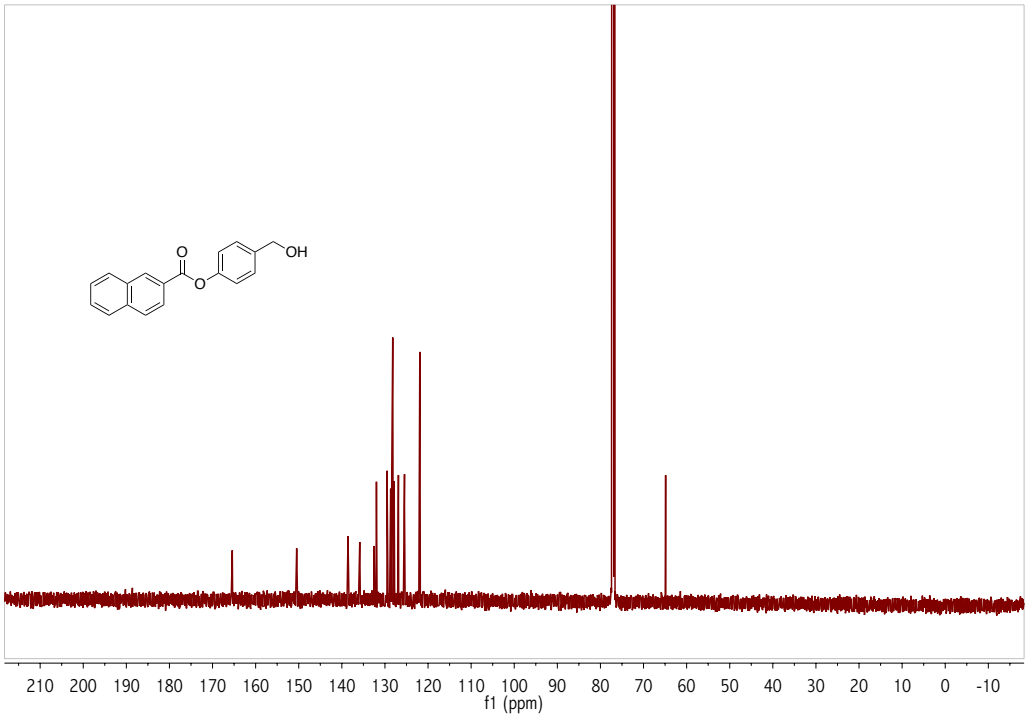

^{1}H (500 MHz, $CDCl_3$) and ^{13}C (125 MHz, $CDCl_3$) NMR spectra of **MCp-OH.**

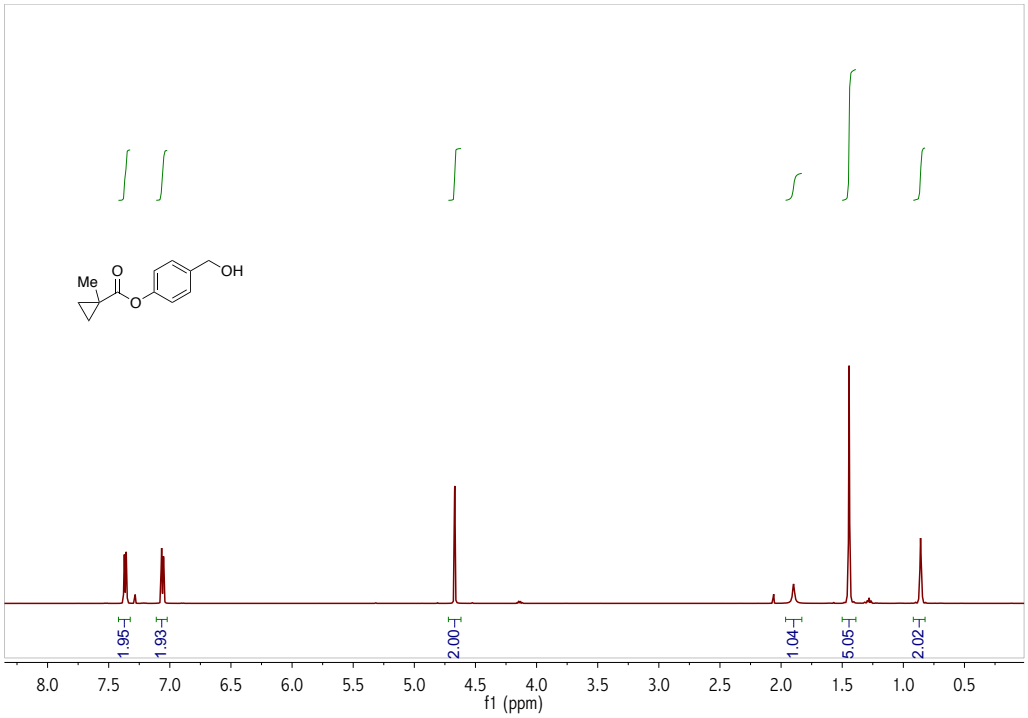

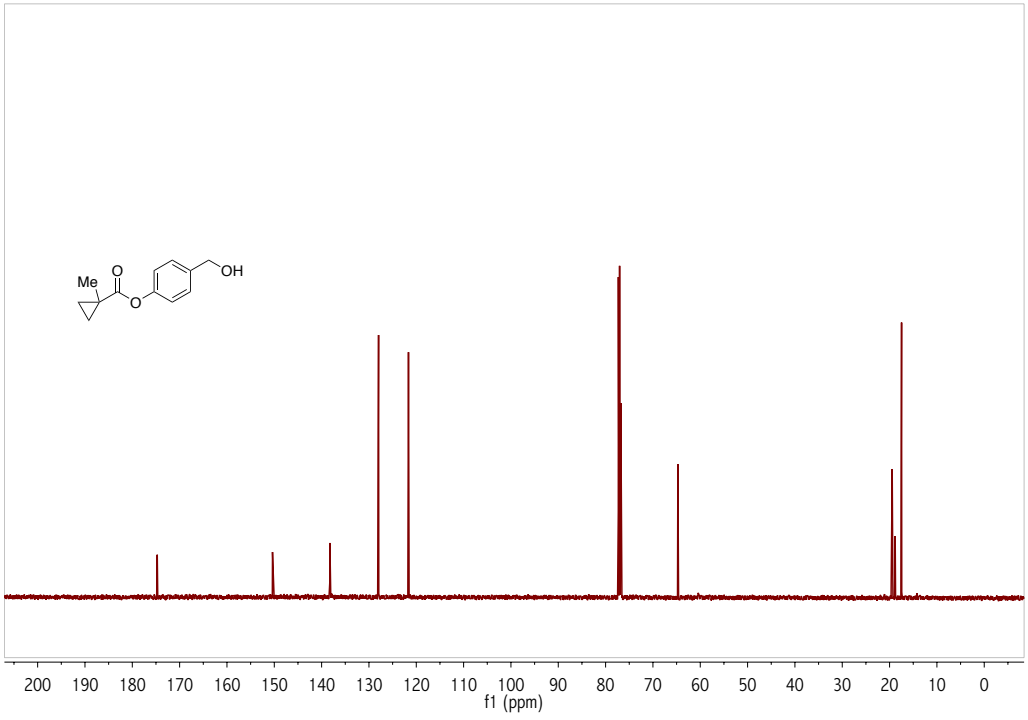

^{1}H (500 MHz, DMSO-d_6, 60 °C) and ^{13}C (125 MHz, DMSO-d_6, 25 °C) NMR spectra of **TCM1.**

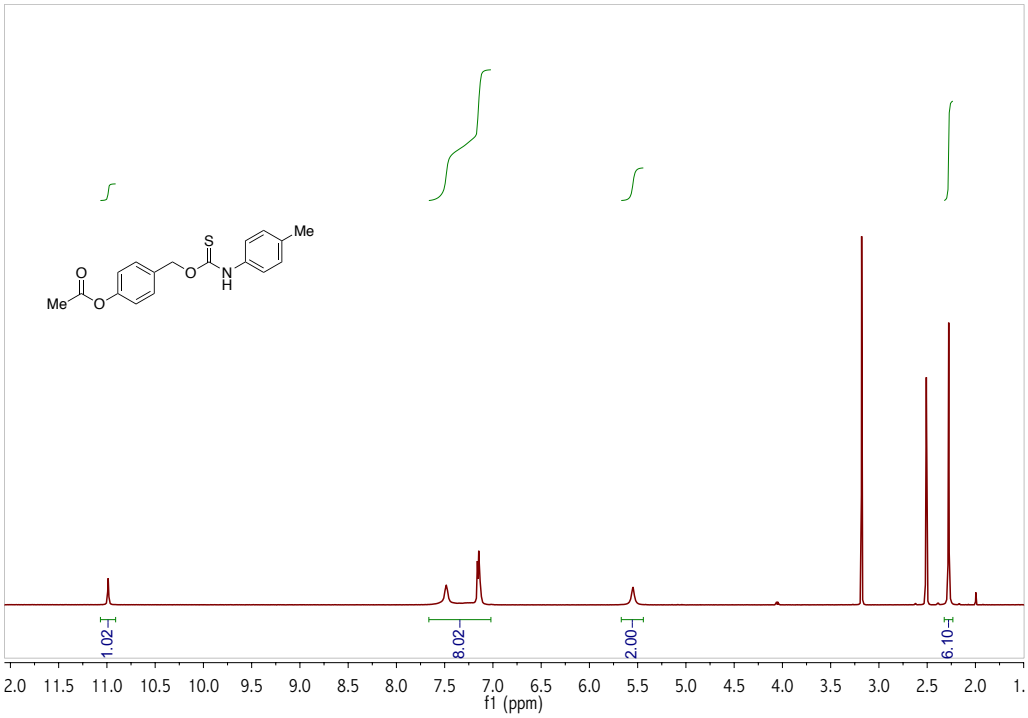

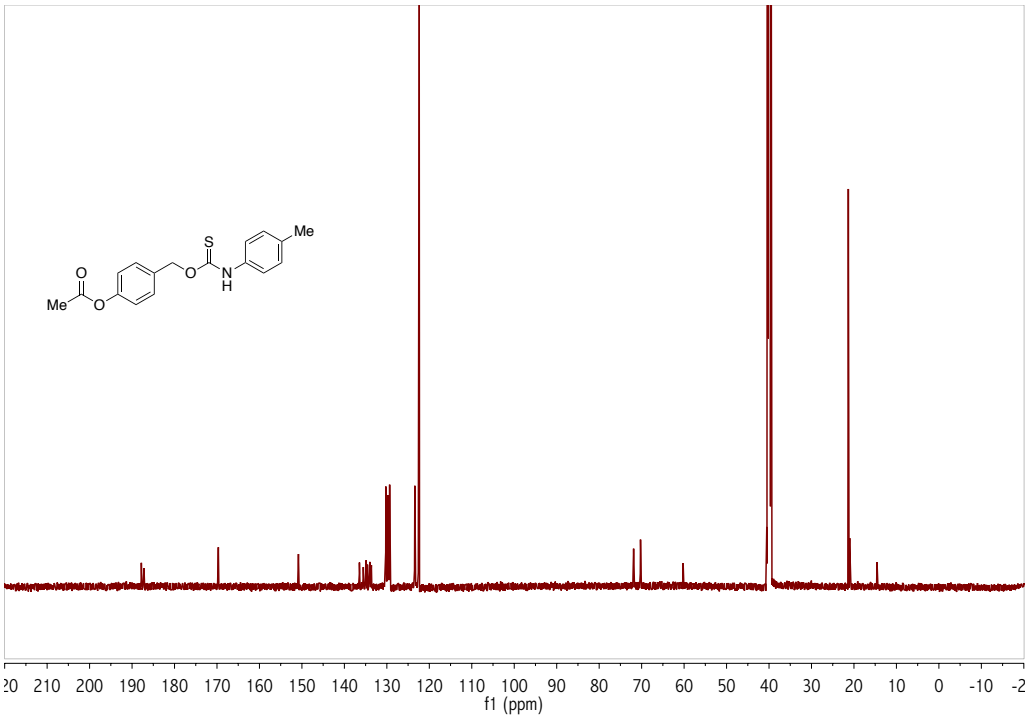

^{1}H (500 MHz, DMSO-d_6, 60 °C) and ^{13}C (125 MHz, DMSO-d_6, 25 °C) NMR spectra of **TCM2.**

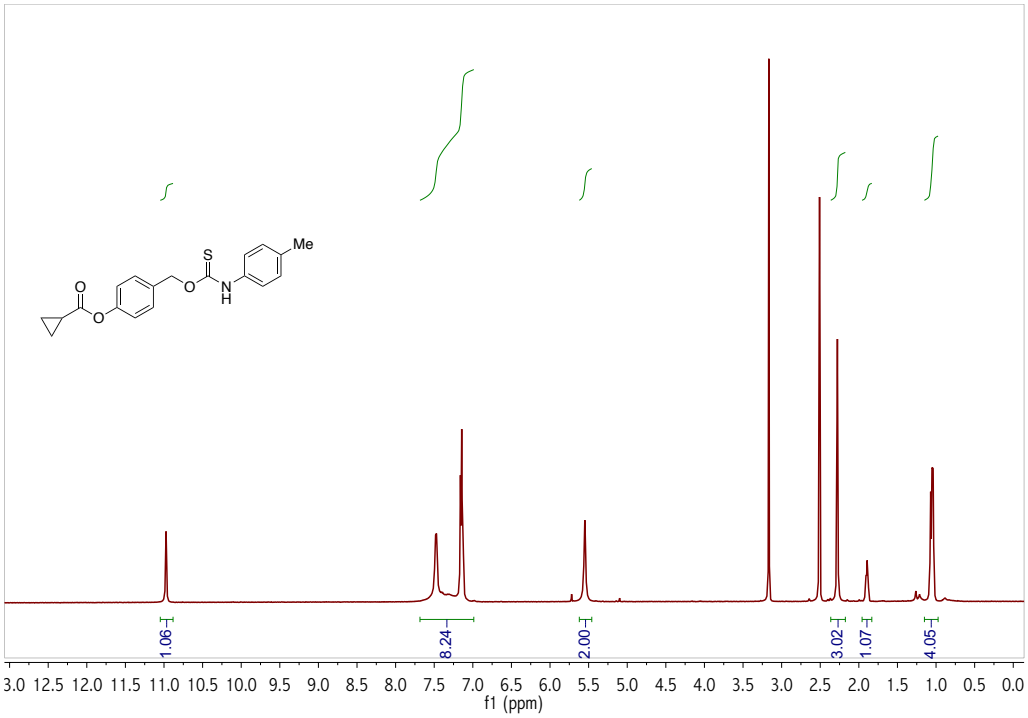

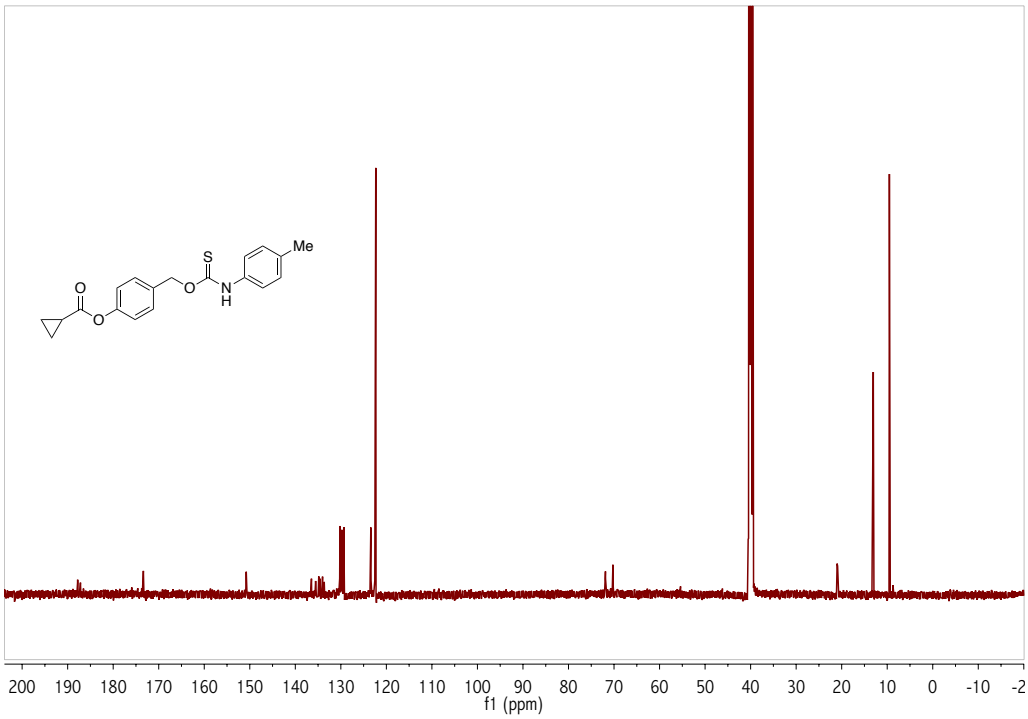

^{1}H (500 MHz, DMSO-d_6, 60 °C) and ^{13}C (125 MHz, DMSO-d_6, 25 °C) NMR spectra of **TCM3.**

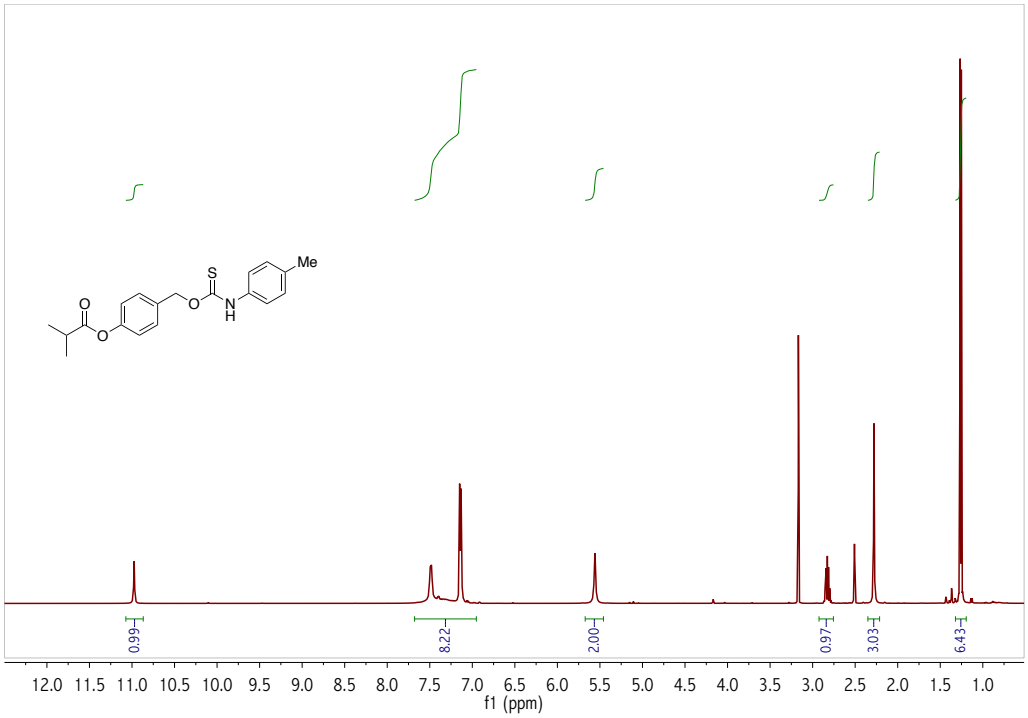

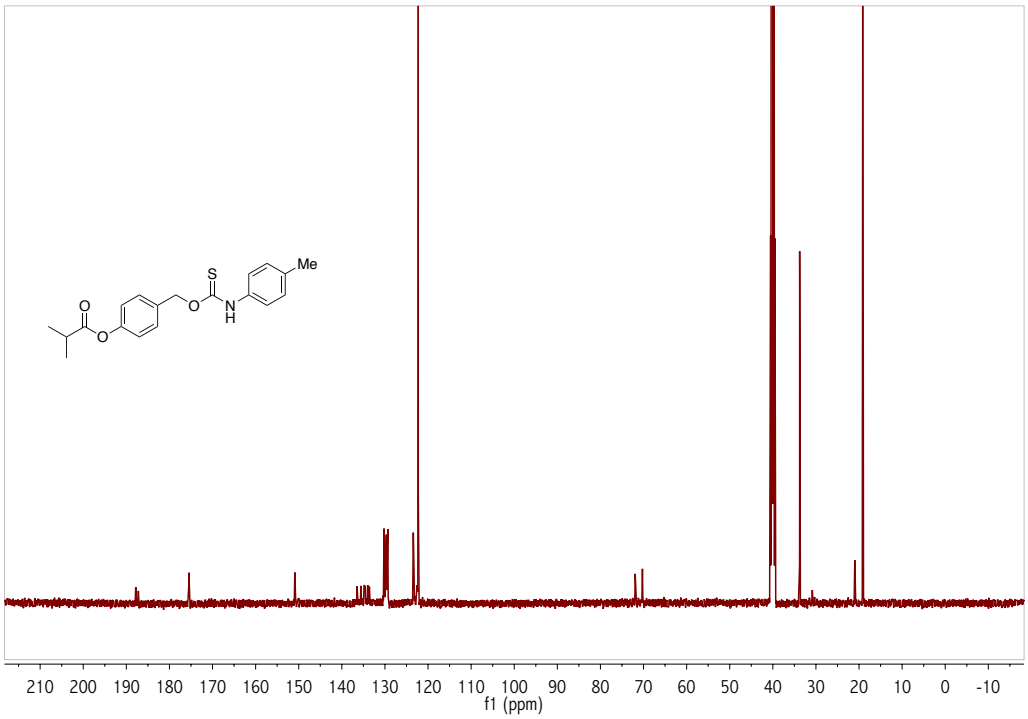

^{1}H (500 MHz, DMSO-d_6, 60 °C) and ^{13}C (125 MHz, DMSO-d_6, 25 °C) NMR spectra of **TCM4.**

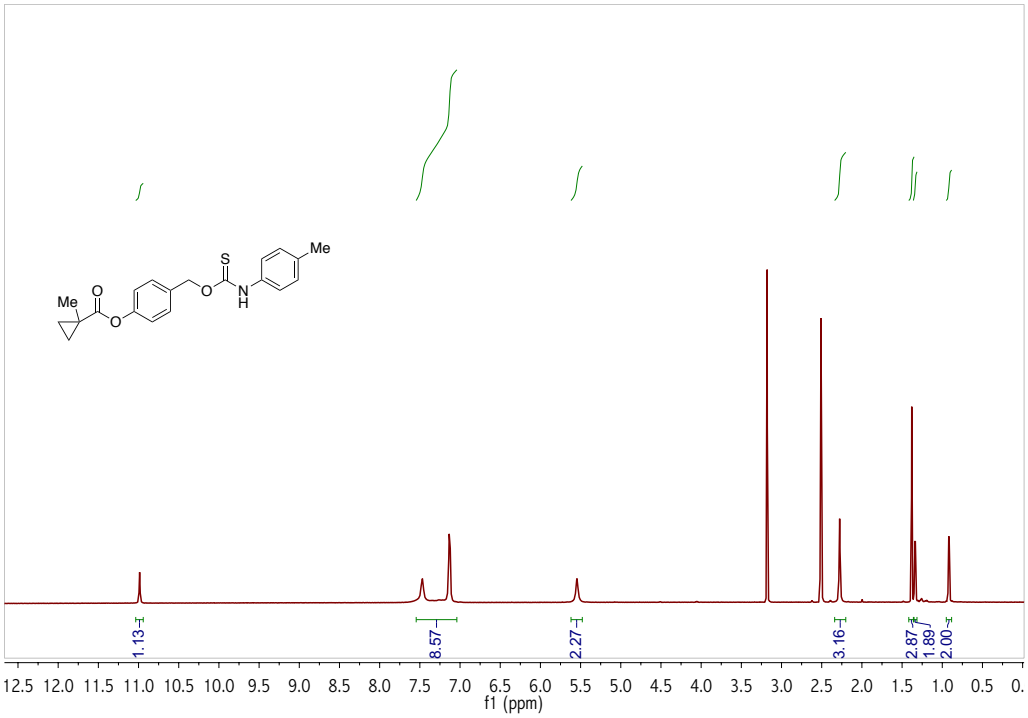

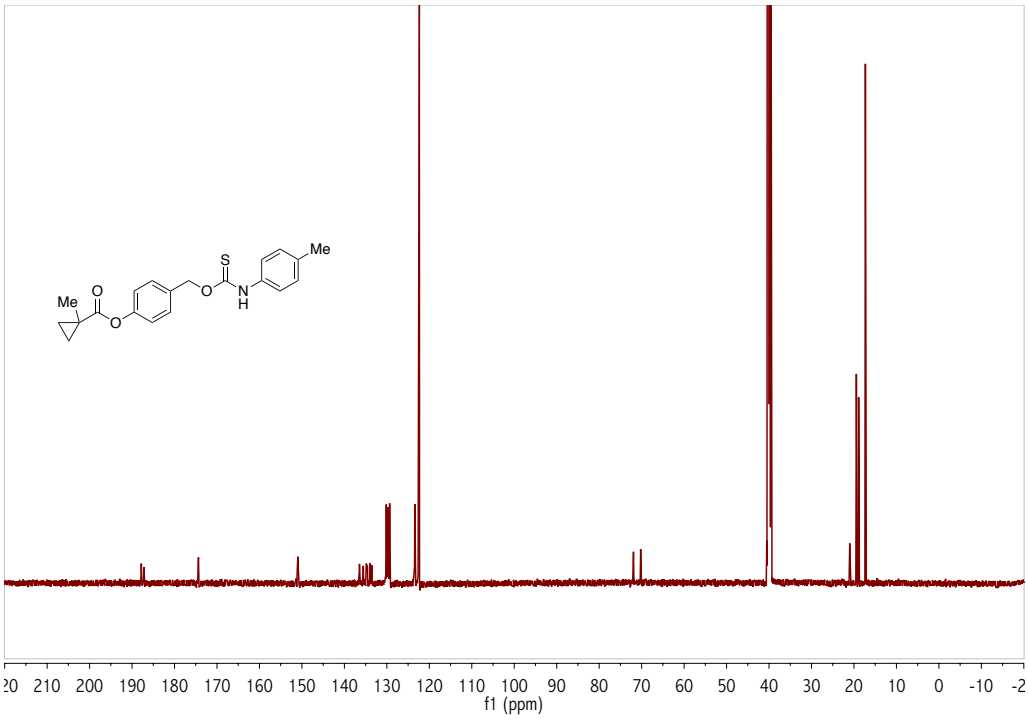

^{1}H (500 MHz, DMSO-d_6, 60 °C) and ^{13}C (125 MHz, DMSO-d_6, 25 °C) NMR spectra of **TCM6.**

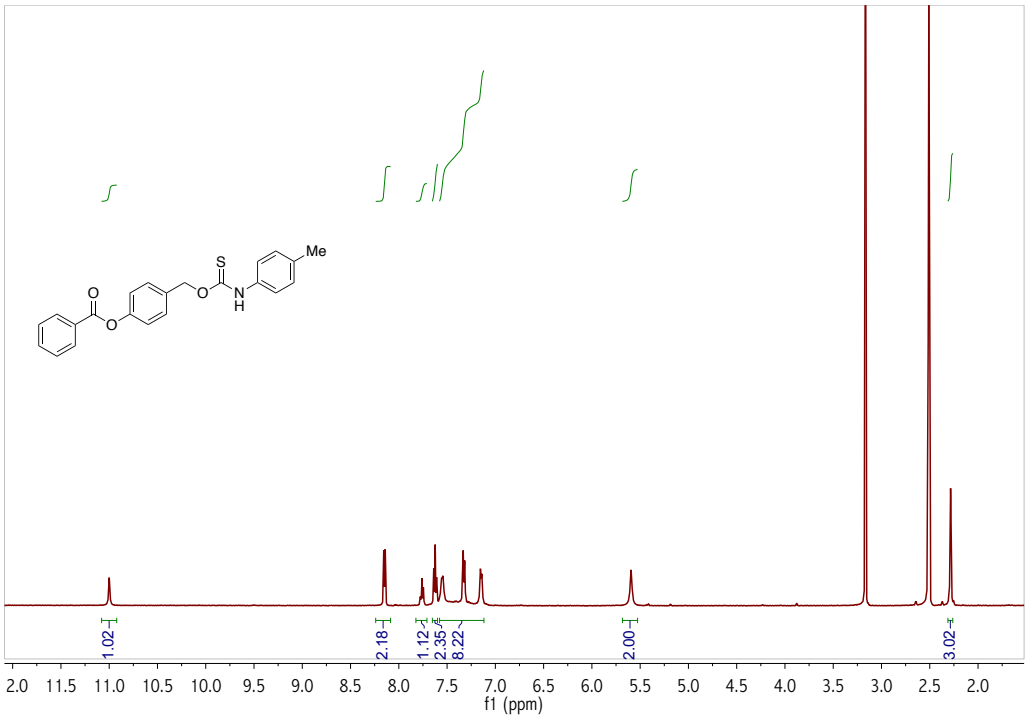

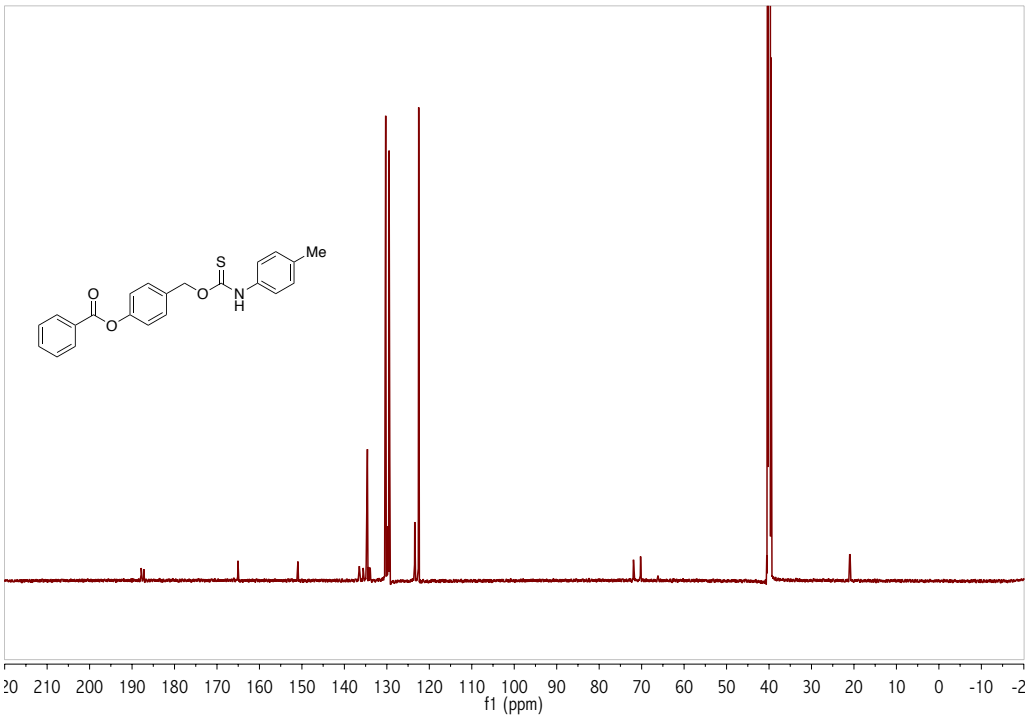

^{1}H (500 MHz, DMSO-d_6, 60 °C) and ^{13}C (125 MHz, DMSO-d_6, 25 °C) NMR spectra of **TCM7.**

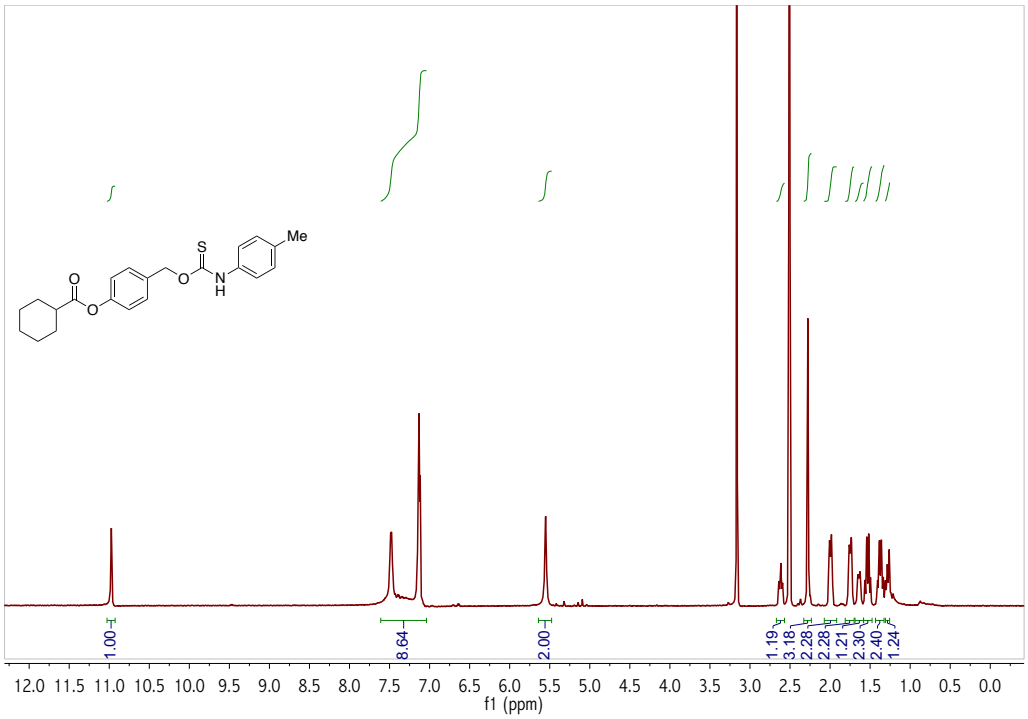

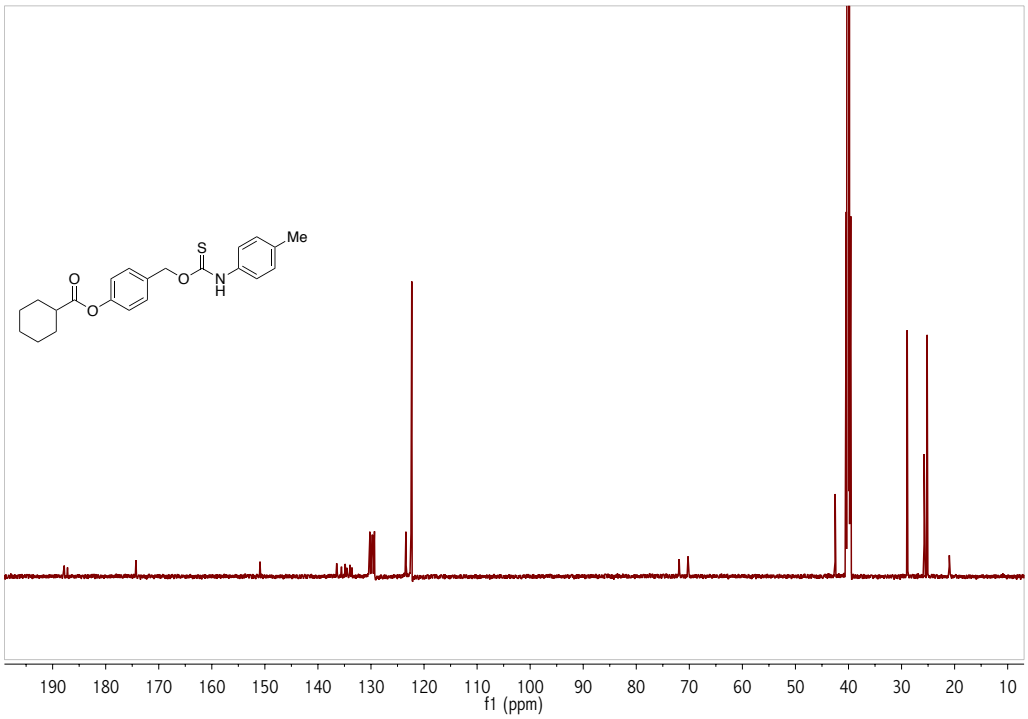

^{1}H (500 MHz, DMSO-d_6, 60 °C) and ^{13}C (125 MHz, DMSO-d_6, 25 °C) NMR spectra of **TCM8.**

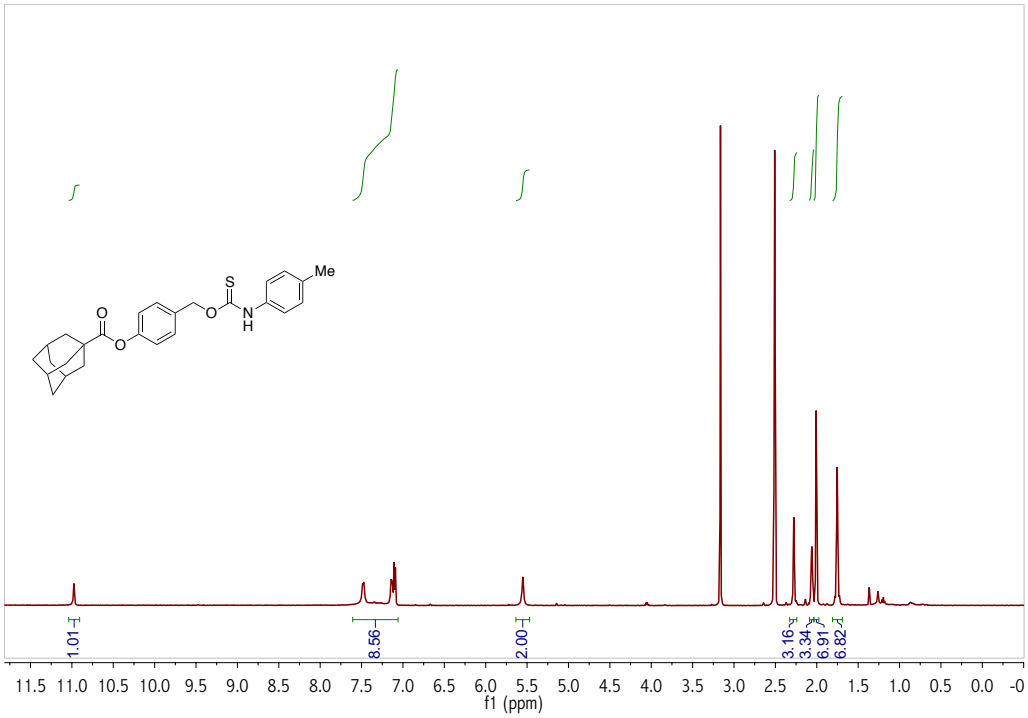

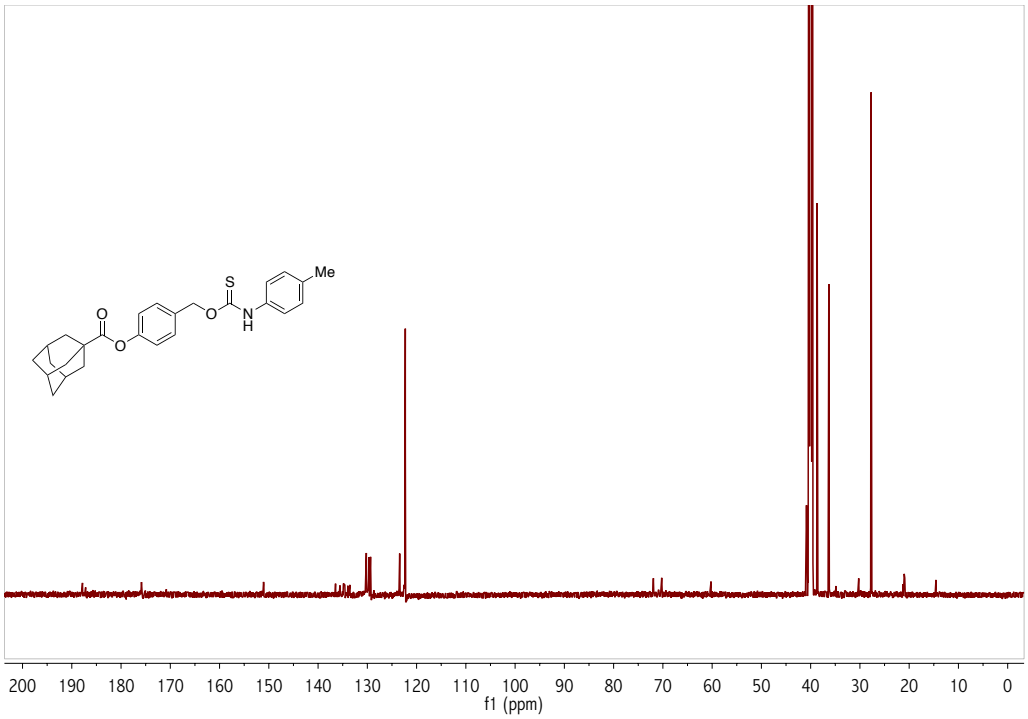

^{1}H (500 MHz, DMSO-d_6, 60 °C) and ^{13}C (125 MHz, DMSO-d_6, 25 °C) NMR spectra of **TCM9.**

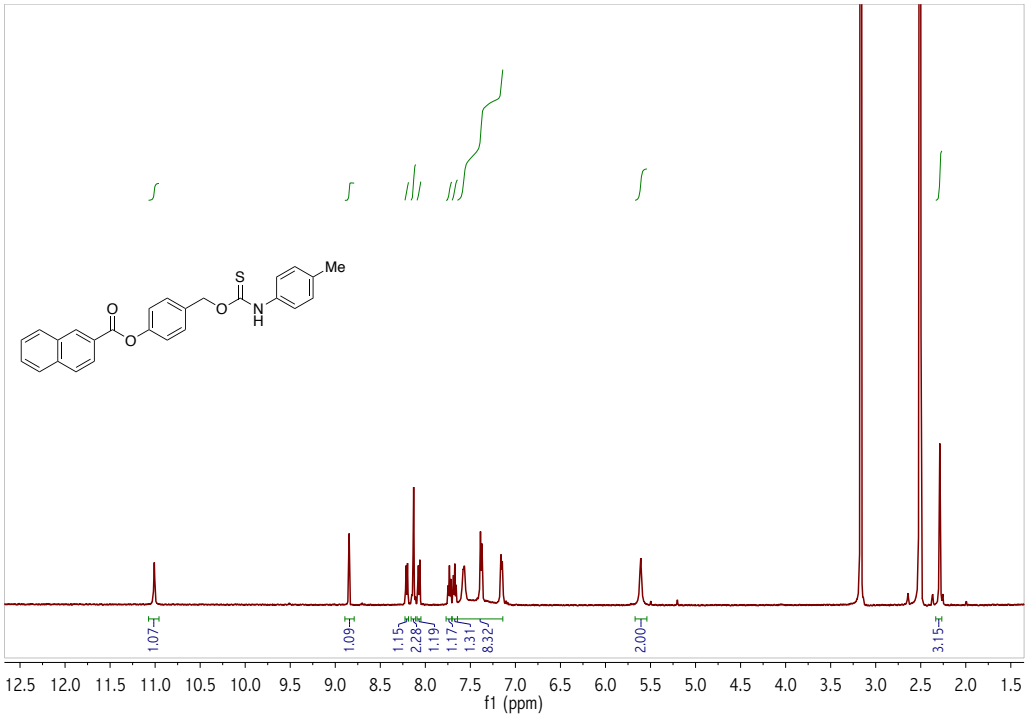

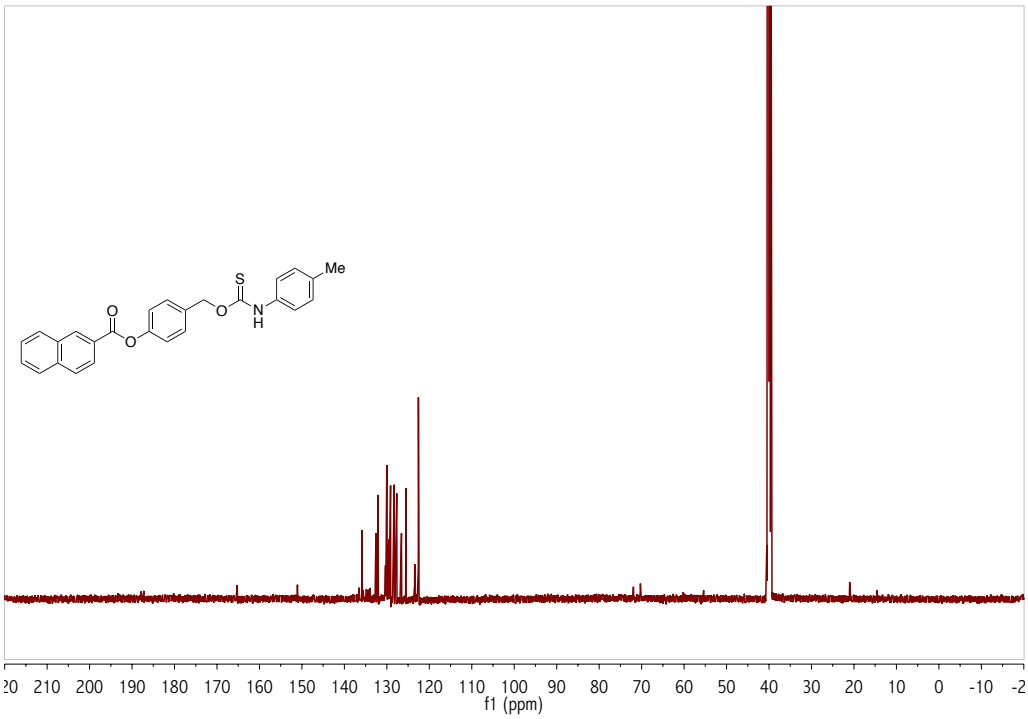

^{1}H (500 MHz, DMSO-d_6, 60 °C) and ^{13}C (125 MHz, DMSO-d_6, 60 °C) NMR spectra of **TCM10.**

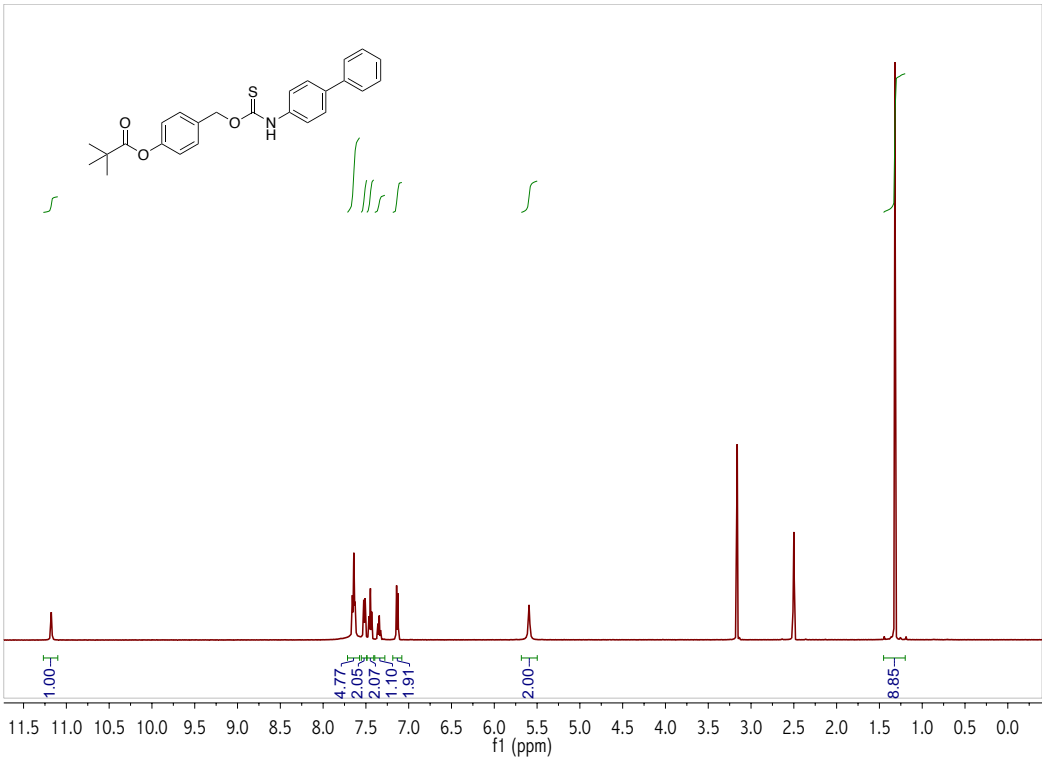

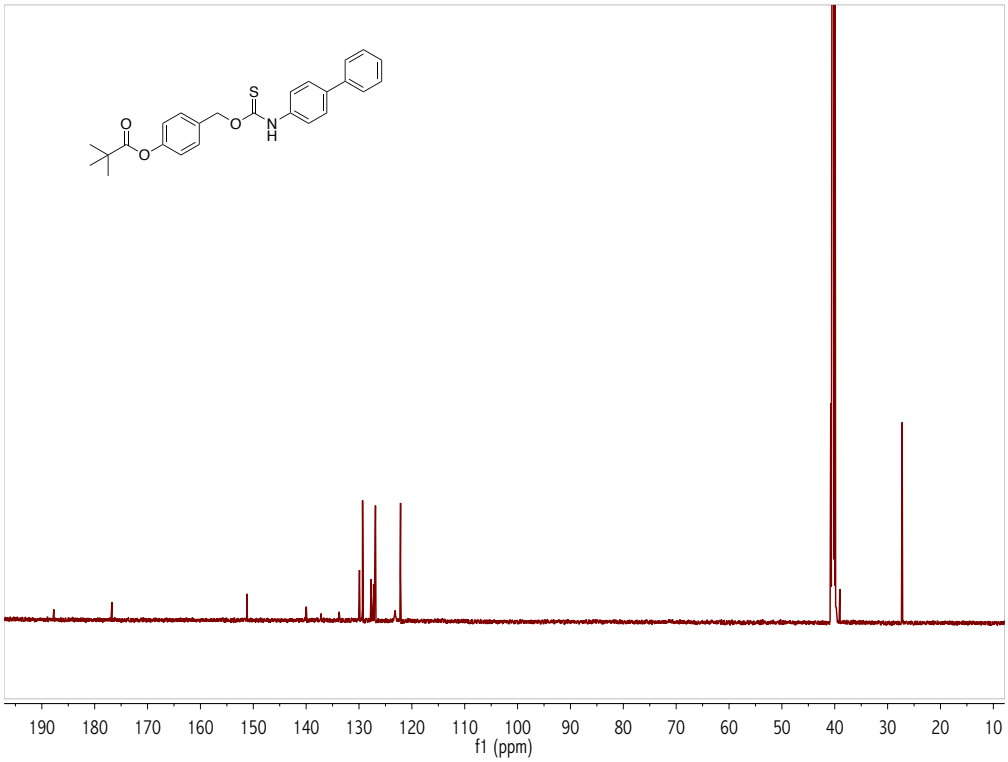

^{1}H (500 MHz, DMSO-d_6, 60 °C) and ^{13}C (125 MHz, DMSO-d_6, 60 °C) NMR spectra of **TCM11**.

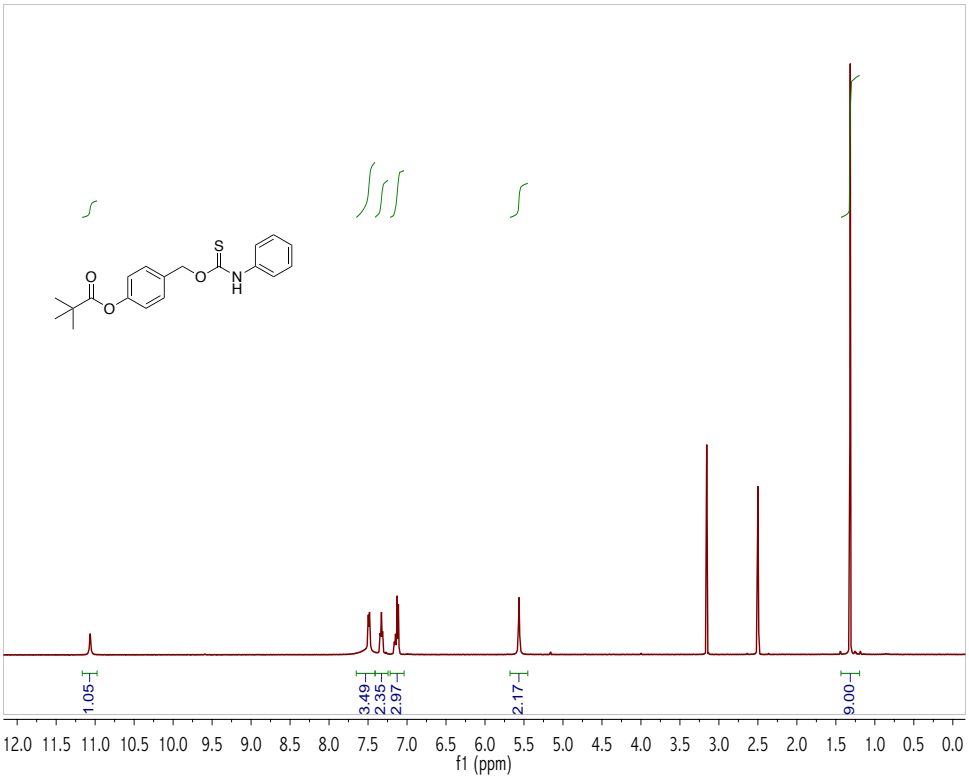

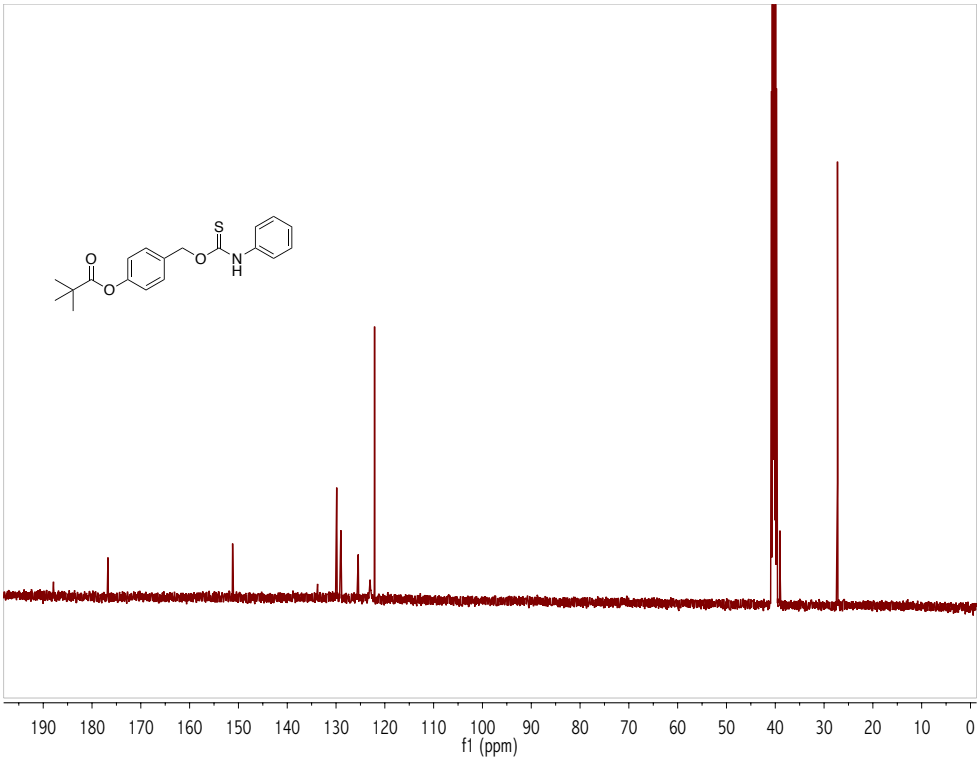

^{1}H (500 MHz, DMSO-d_6, 60 °C), ^{13}C (125 MHz, DMSO-d_6, 60 °C), and ^{19}F (470 MHz, DMSO-d_6, 60 °C) NMR spectra of **TCM12.**

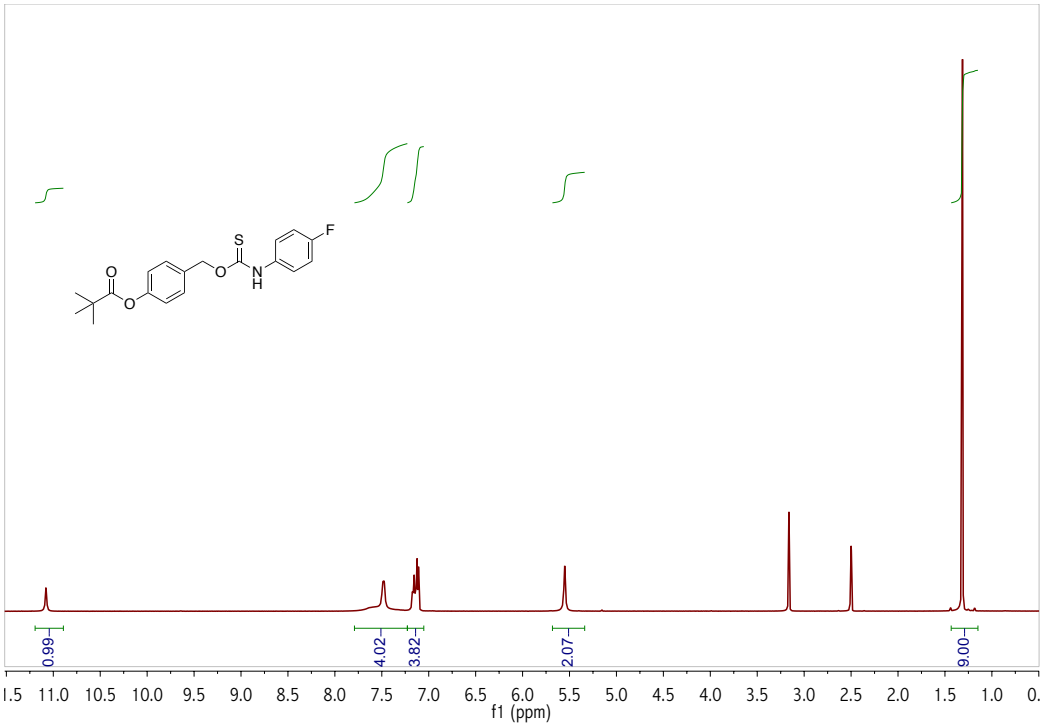

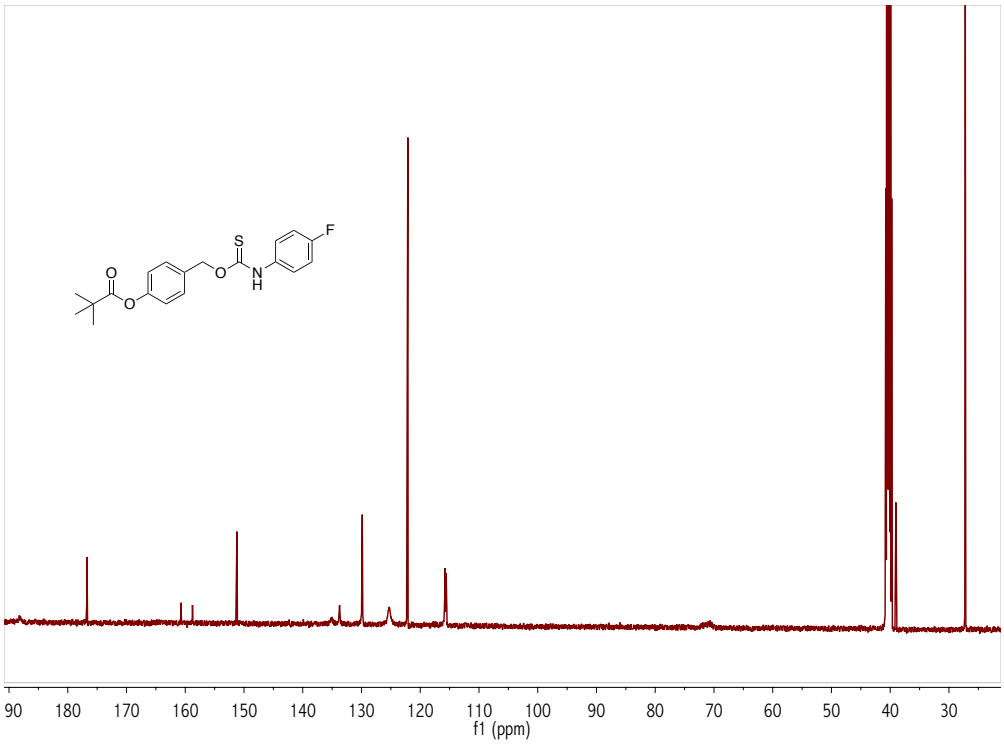

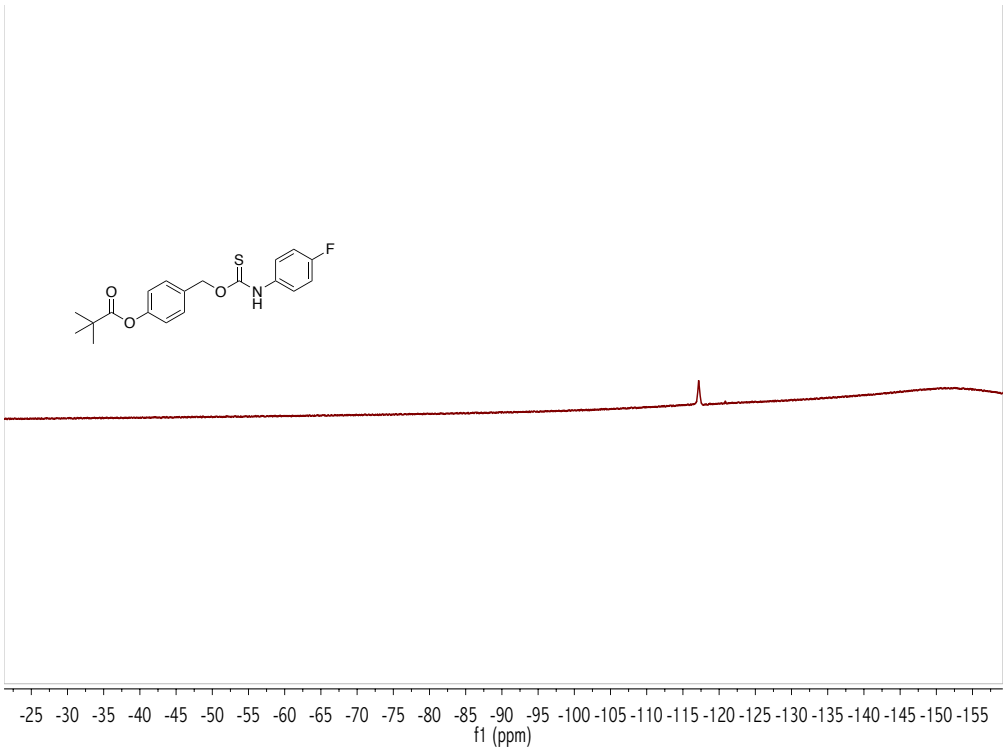

^{1}H (500 MHz, DMSO-d_6, 60 °C), ^{13}C (125 MHz, DMSO-d_6, 60 °C), and ^{19}F (470 MHz, DMSO-d_6, 60 °C) NMR spectra of **TCM13.**

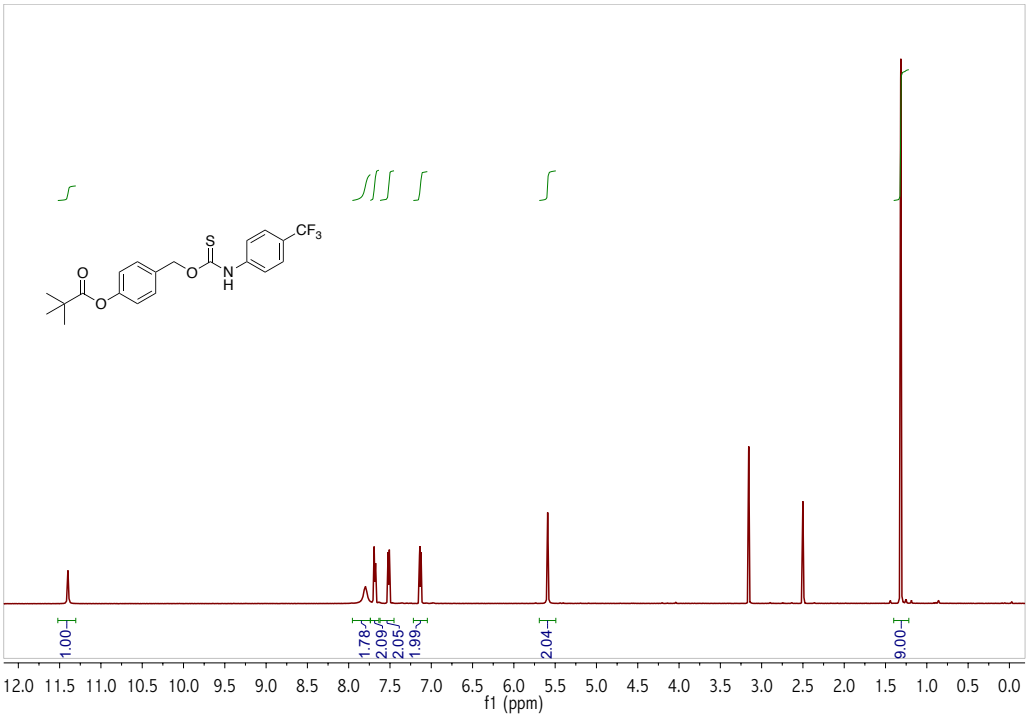

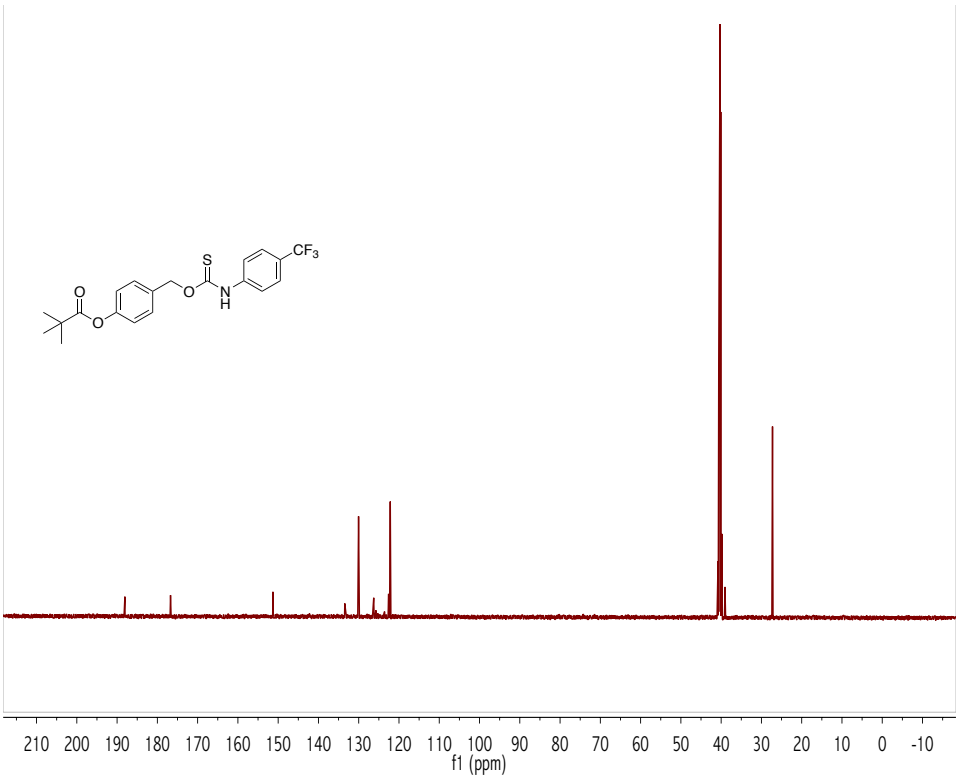
O
O
S
O
N
H
CF3
210 200 190 180 170 160 150 140 130 120 110 100 90 80 70 60 50 40 30 20 10 0 -10
f1 (ppm)

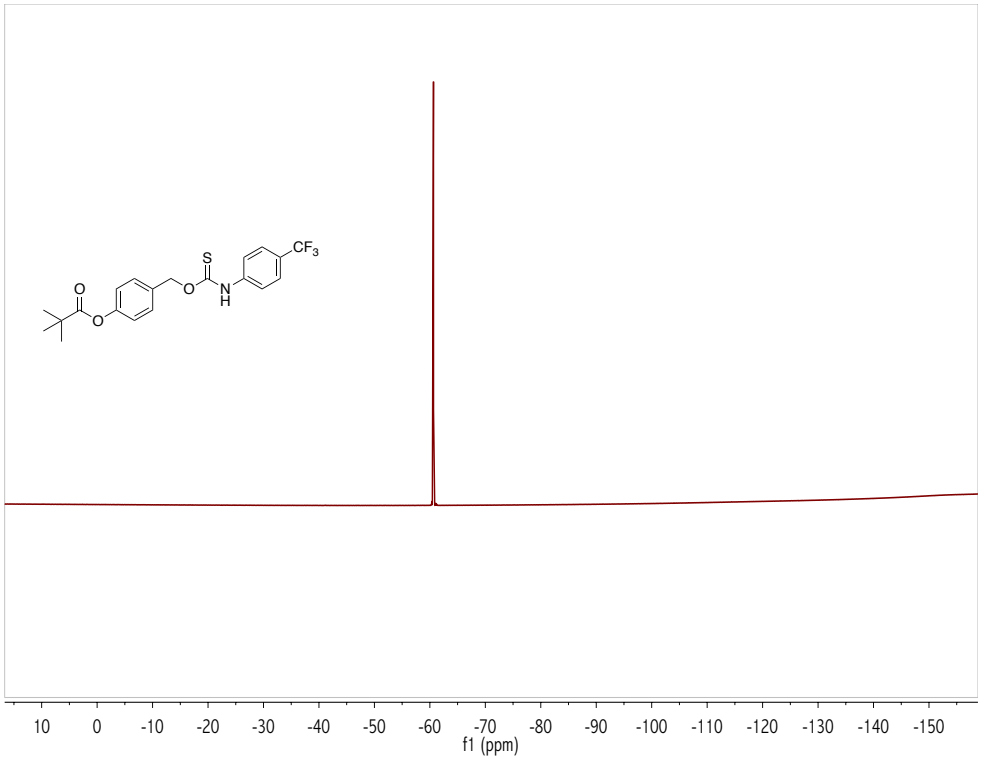
O
O
S
O
N
H
CF3
10 0 -10 -20 -30 -40 -50 -60 -70 -80 -90 -100 -110 -120 -130 -140 -150
f1 (ppm)

^{1}H (500 MHz, DMSO-d_6, 60 °C) and ^{13}C (125 MHz, DMSO-d_6, 60 °C), NMR spectra of **TCM14**

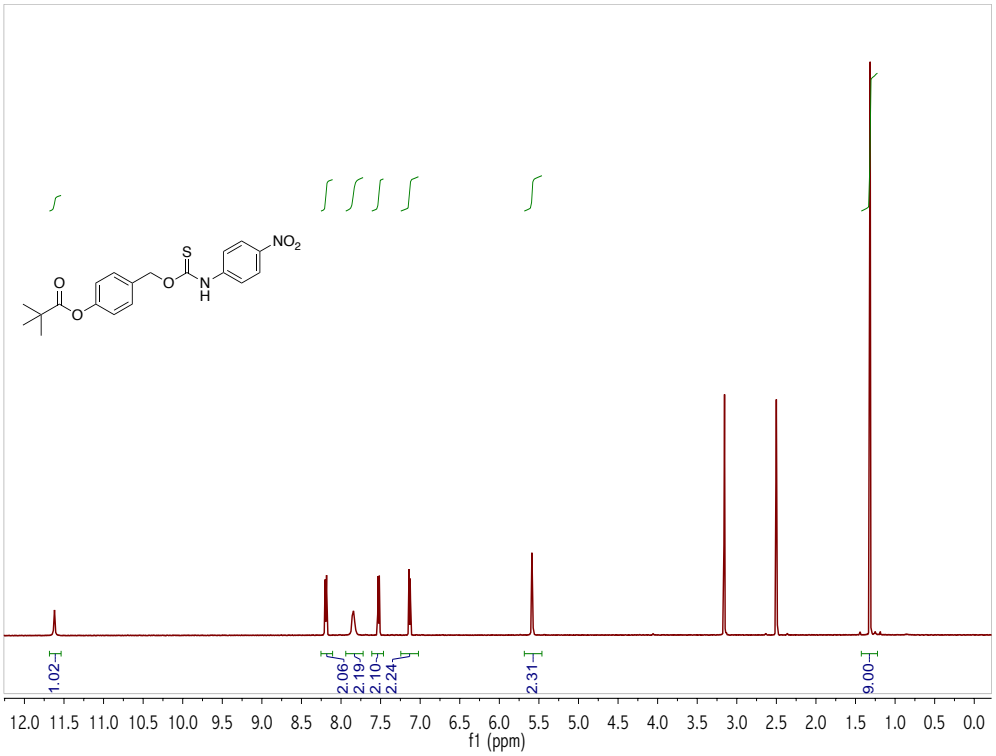

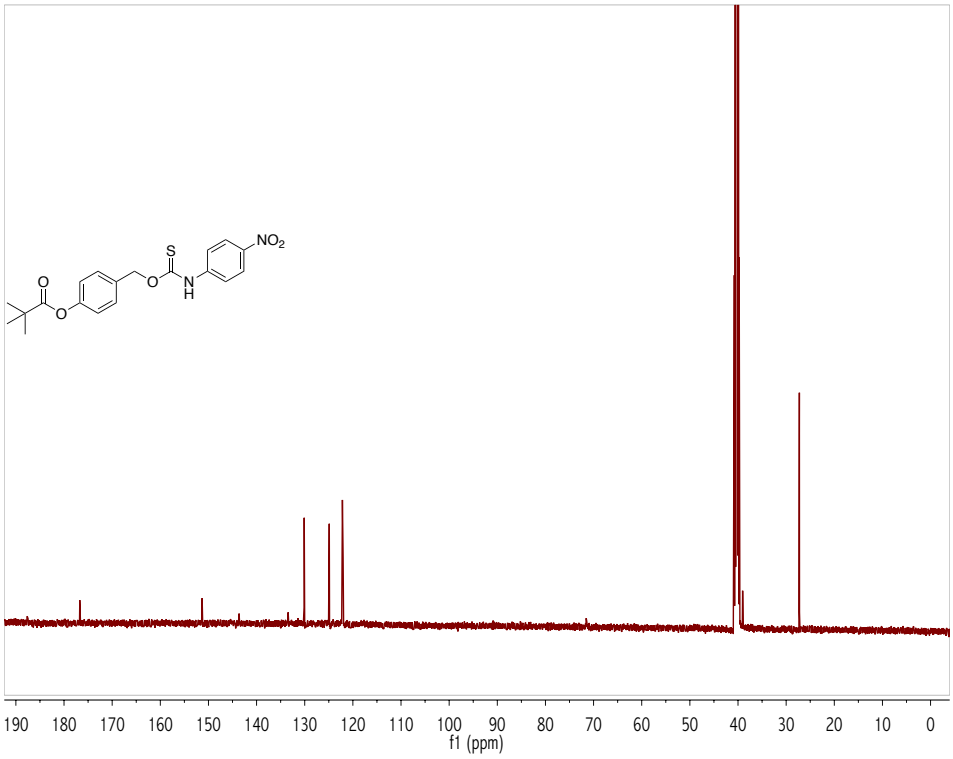

^{1}H (500 MHz, $CDCl_3$, RT) and ^{13}C (125 MHz, $CDCl_3$, RT) NMR spectra of **CM1**

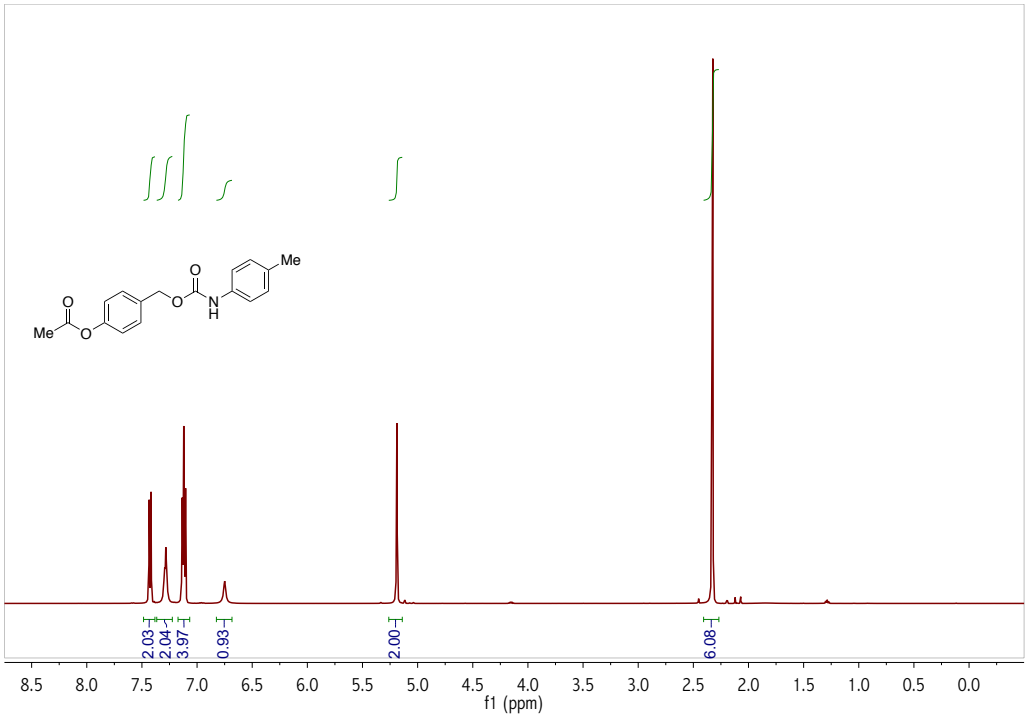

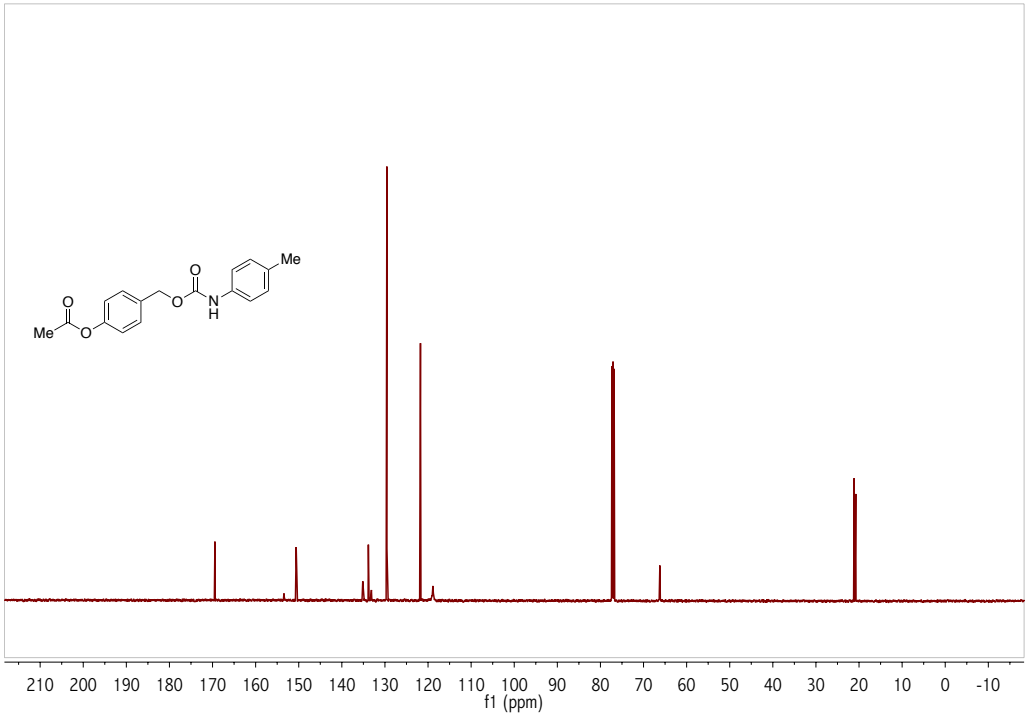

^{1}H (500 MHz, $CDCl_3$, RT) and ^{13}C (125 MHz, $CDCl_3$, RT) NMR spectra of **CM2.**

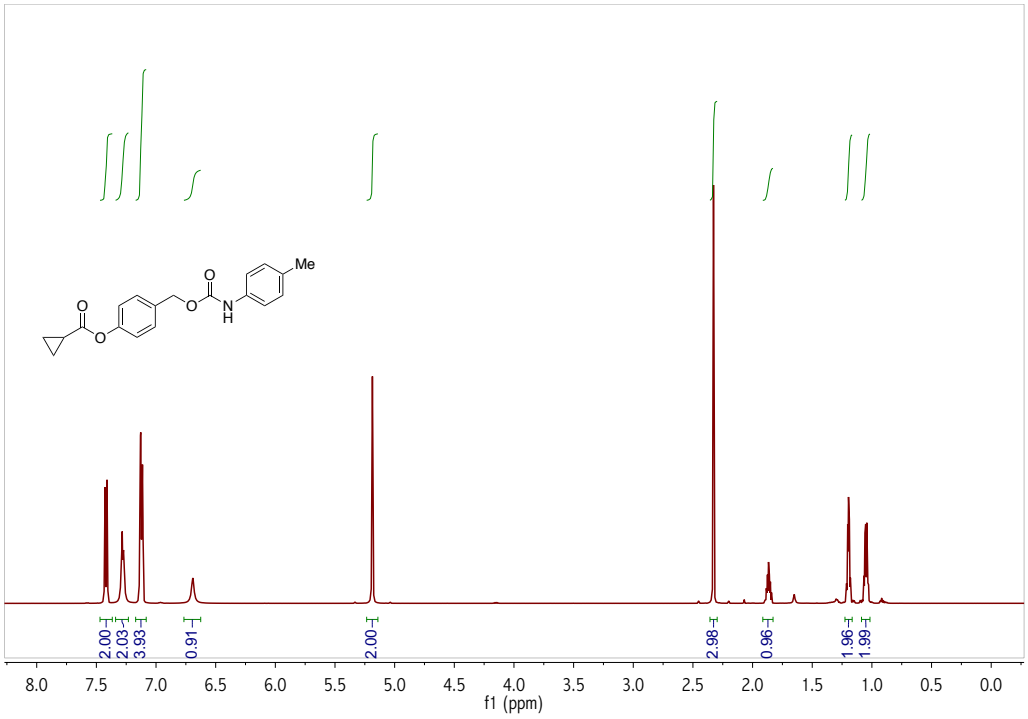

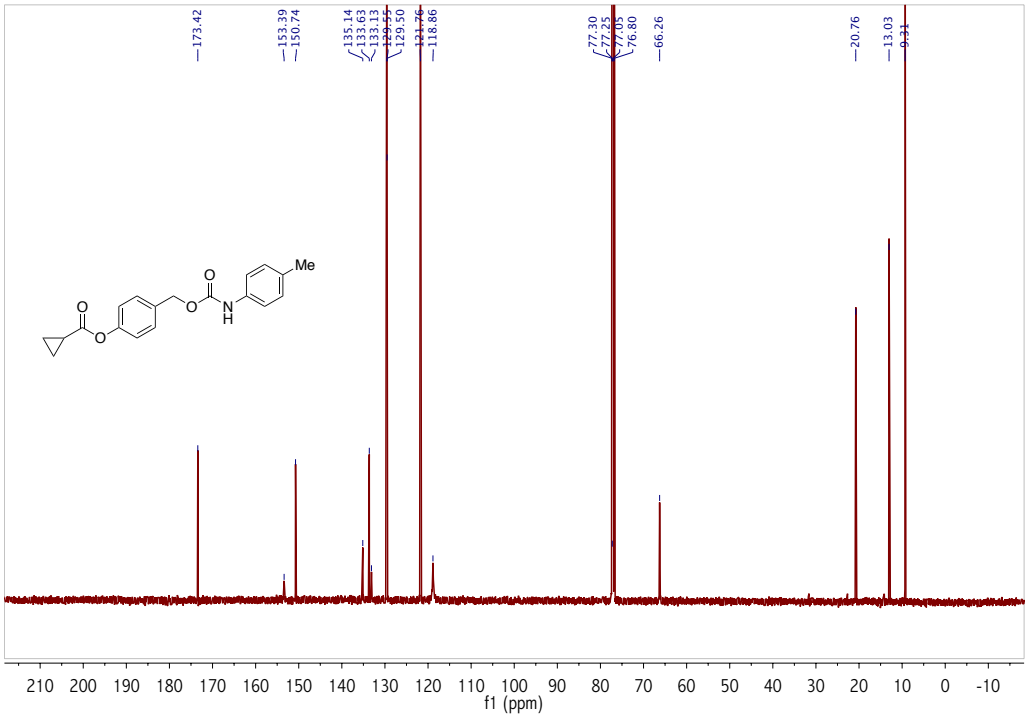

^{1}H (500 MHz, $CDCl_3$, RT) and ^{13}C (125 MHz, $CDCl_3$, RT) NMR spectra of **CM3.**

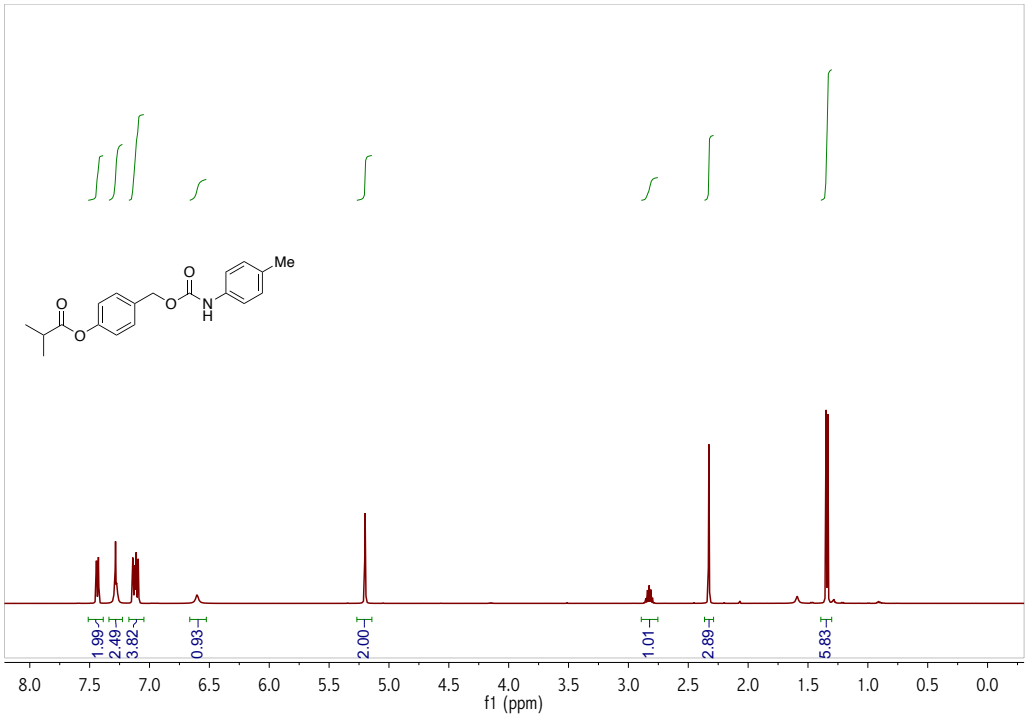

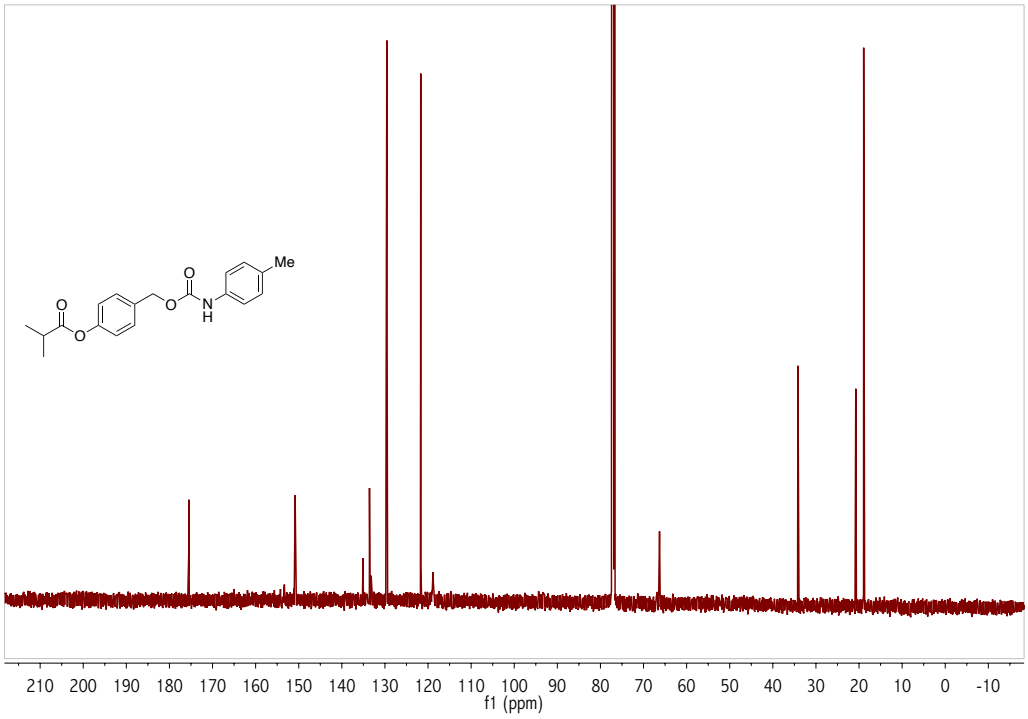

^{1}H (500 MHz, $CDCl_3$, RT) and ^{13}C (125 MHz, $CDCl_3$, RT) NMR spectra of **CM4.**

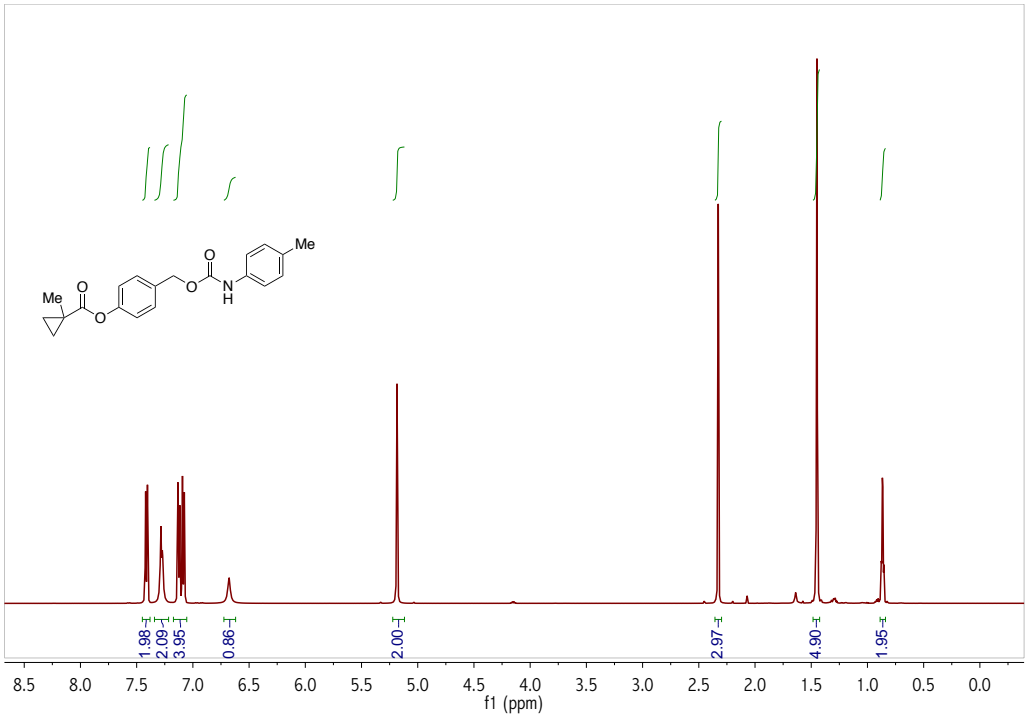

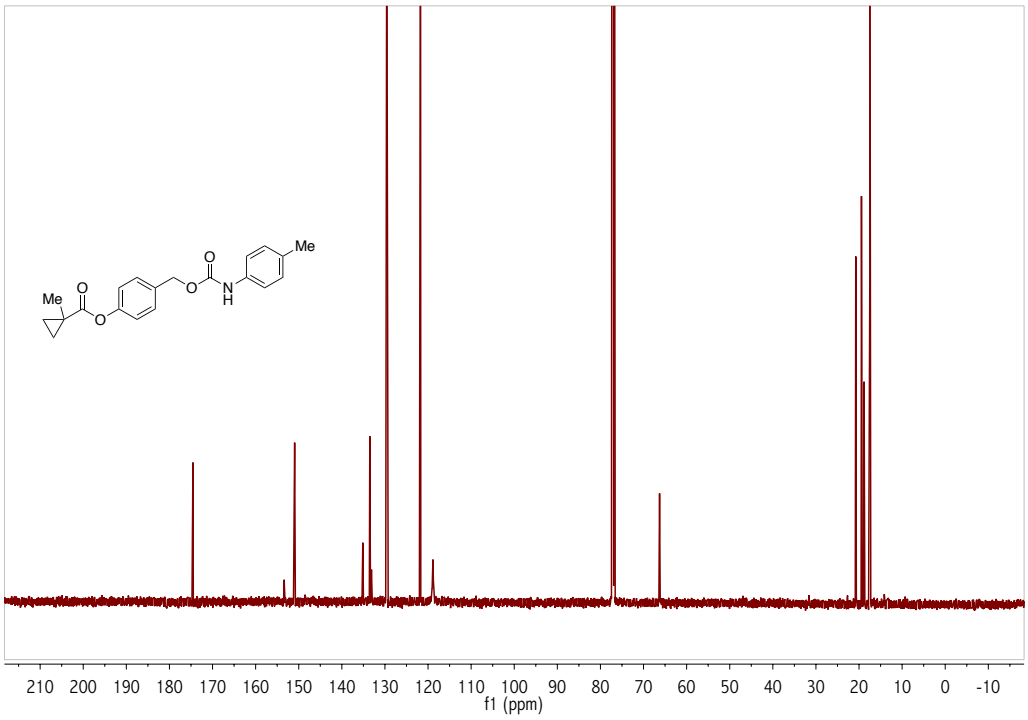

^{1}H (500 MHz, $CDCl_3$, RT) and ^{13}C (125 MHz, $CDCl_3$, RT) NMR spectra of **CM6.**

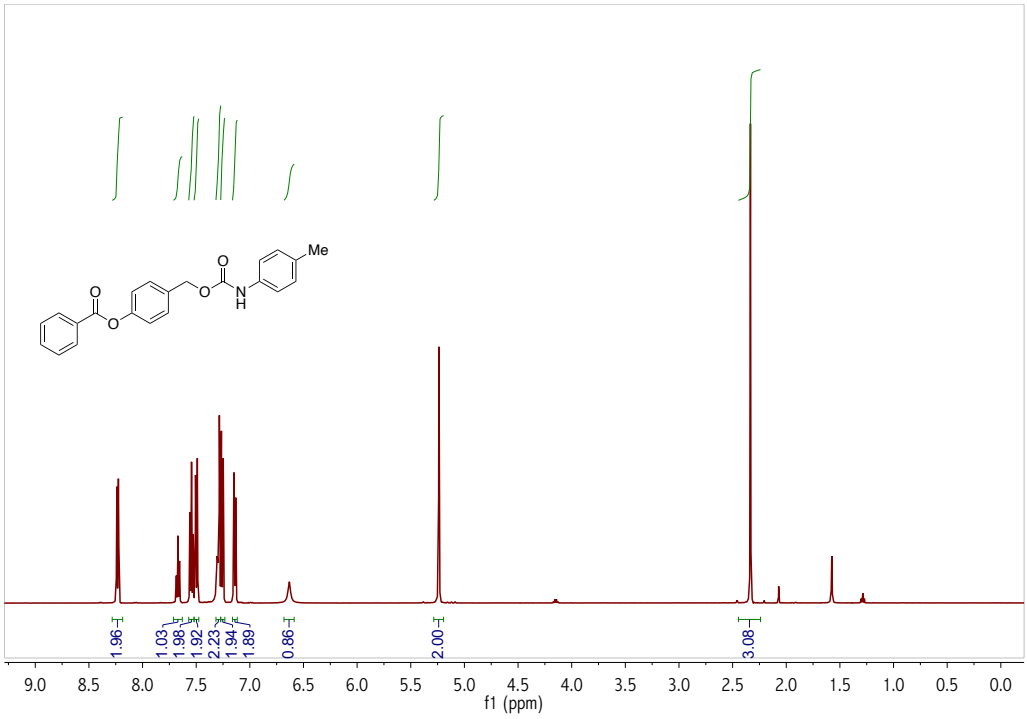

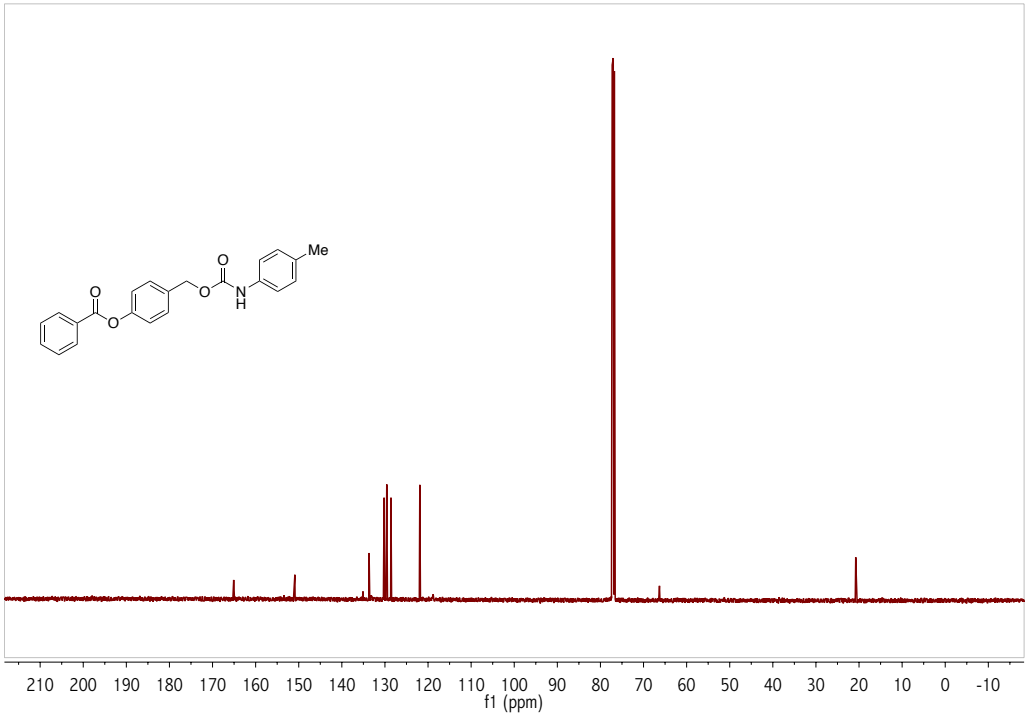

^{1}H (500 MHz, $CDCl_3$, RT) and ^{13}C (125 MHz, $CDCl_3$, RT) NMR spectra of **CM7.**

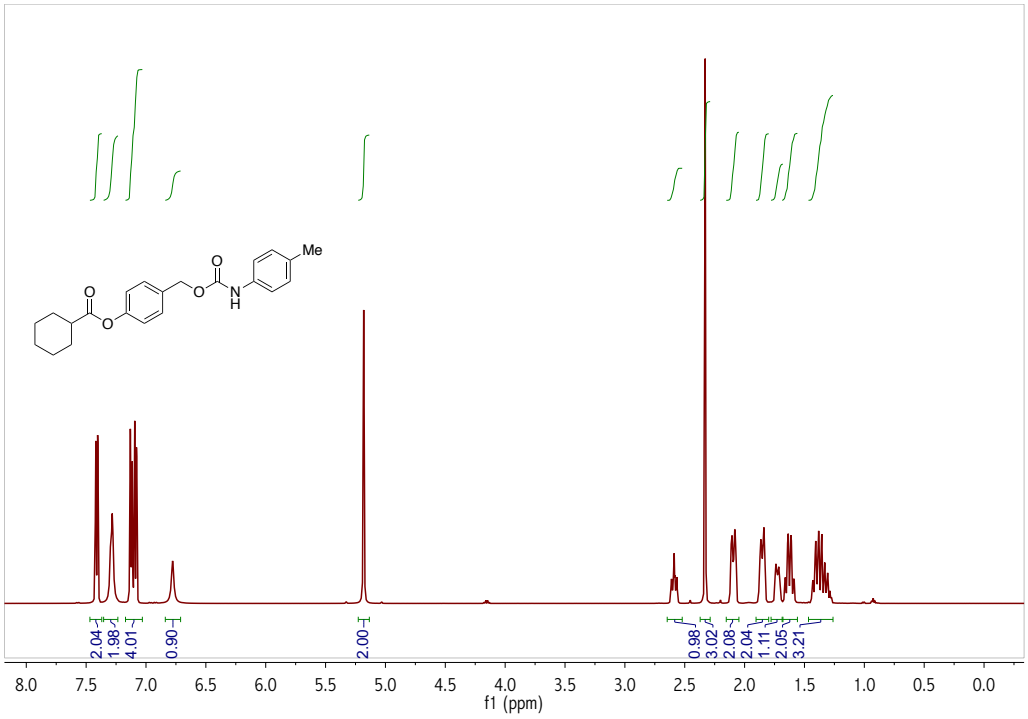

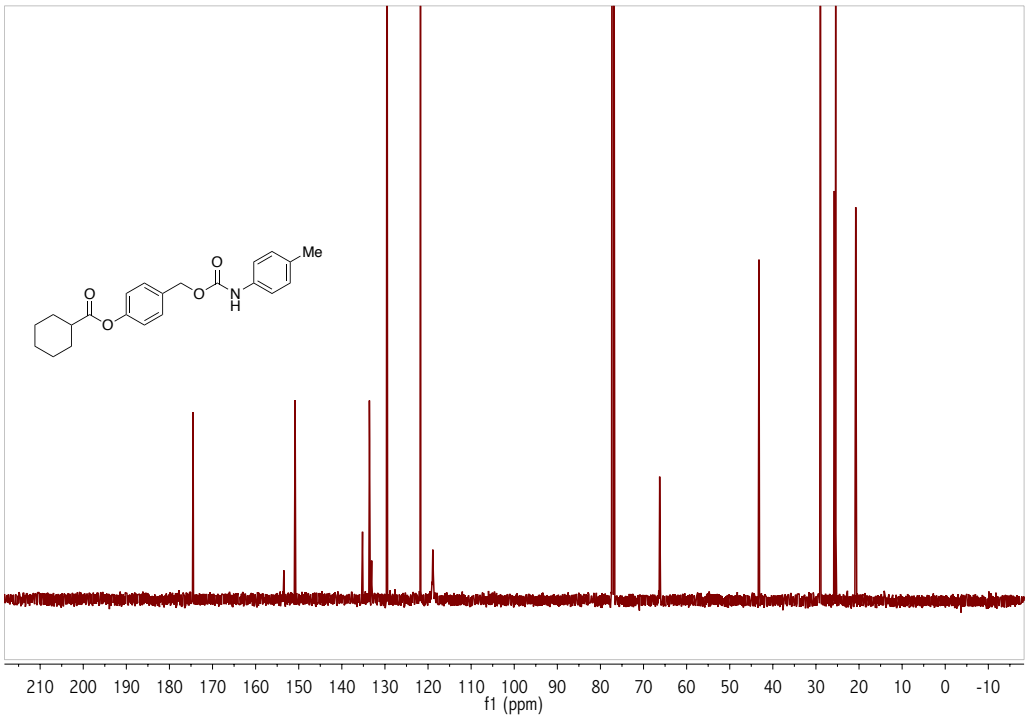

^{1}H (500 MHz, $CDCl_3$, RT) and ^{13}C (125 MHz, $CDCl_3$, RT) NMR spectra of **CM8.**

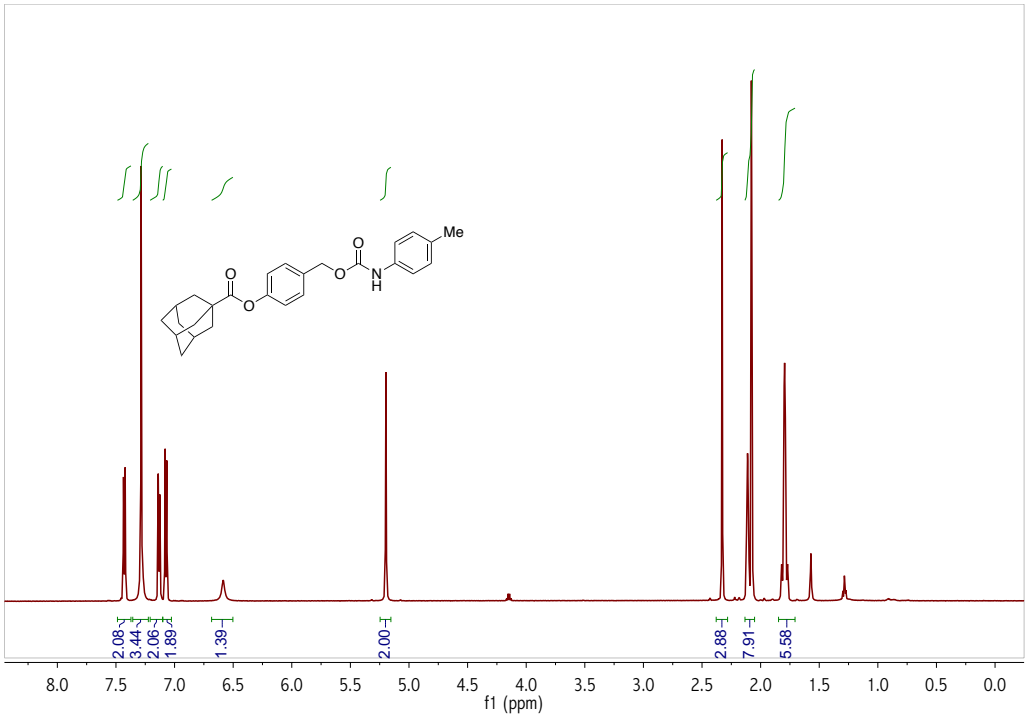

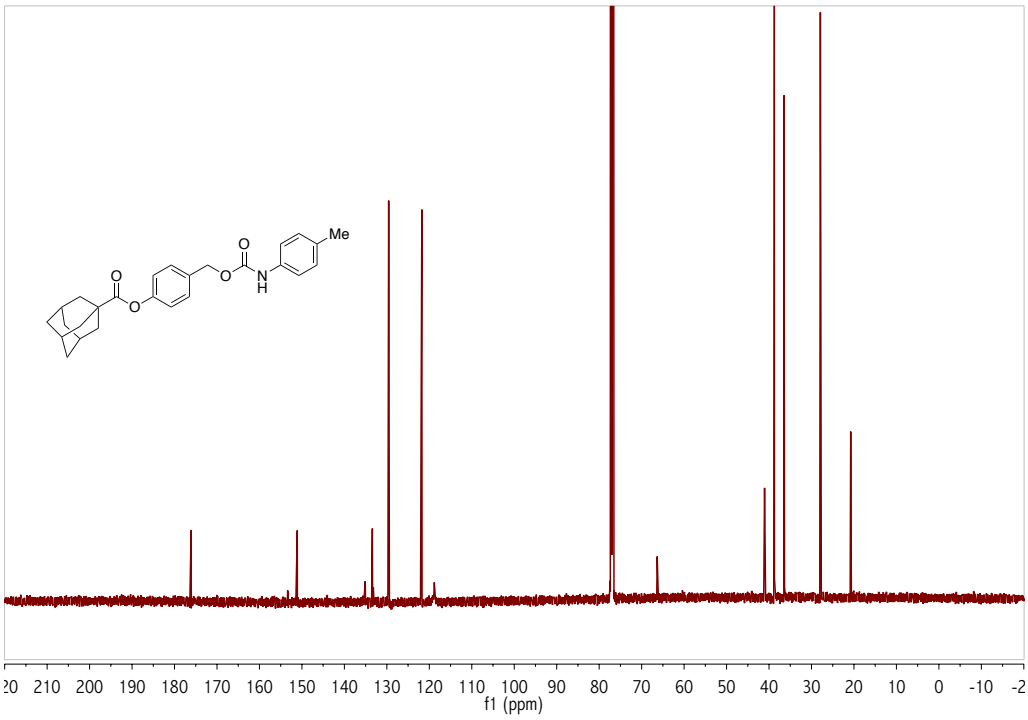

^{1}H (500 MHz, $CDCl_3$, RT) and ^{13}C (125 MHz, $CDCl_3$, RT) NMR spectra of **CM9**

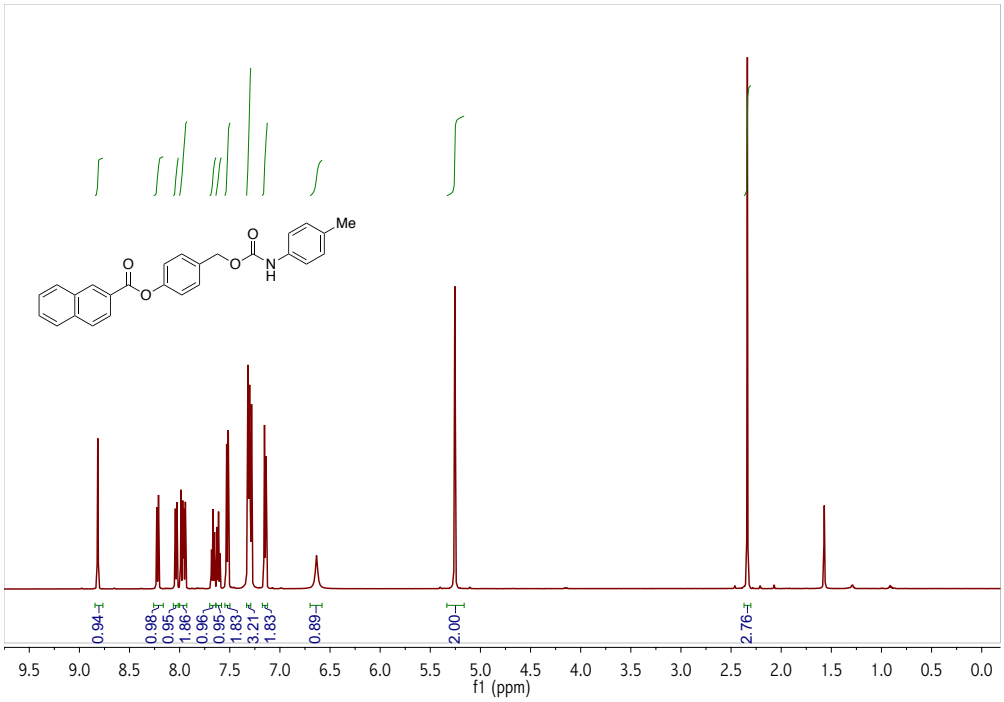

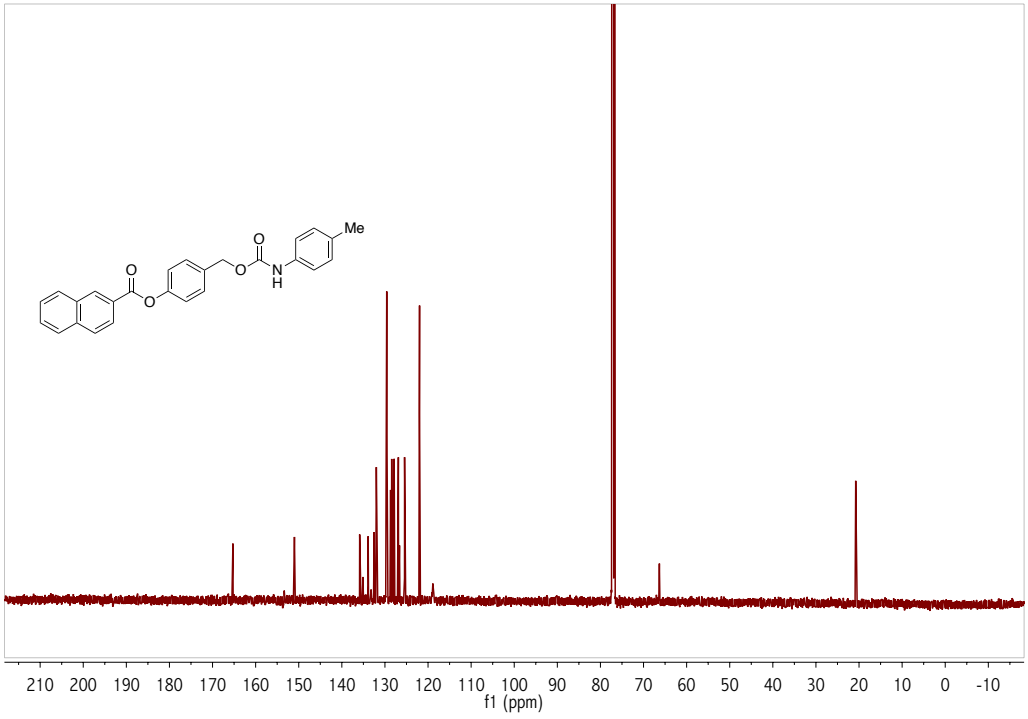

^{1}H (500 MHz, $CDCl_3$, RT) and ^{13}C (125 MHz, $CDCl_3$, RT) NMR spectra of **CM10.**

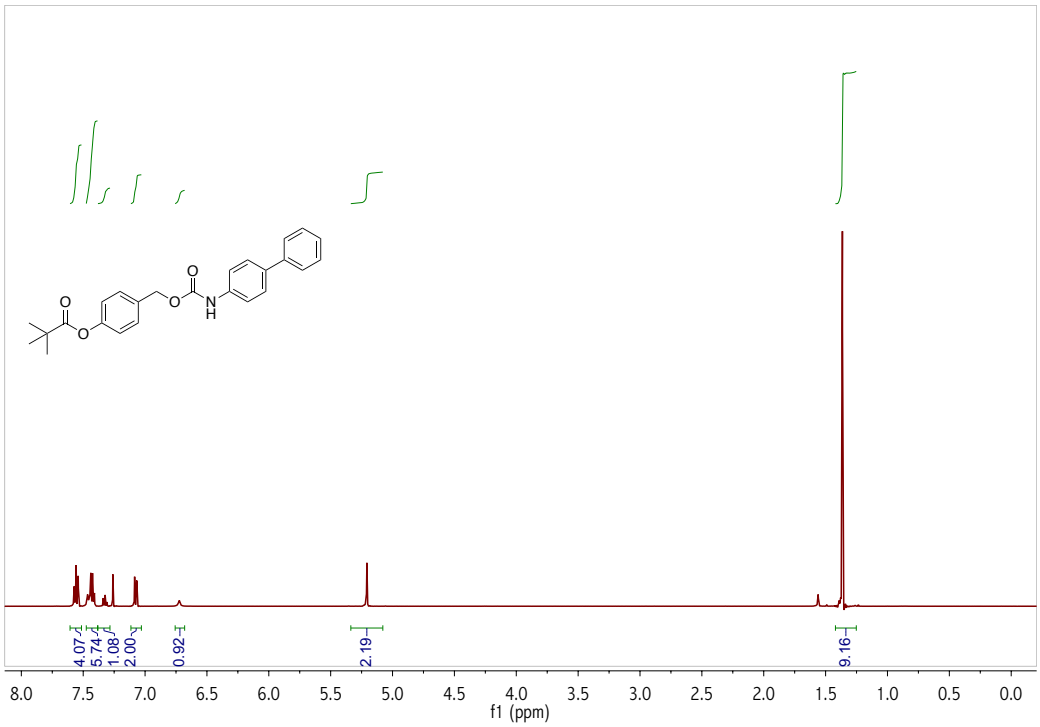

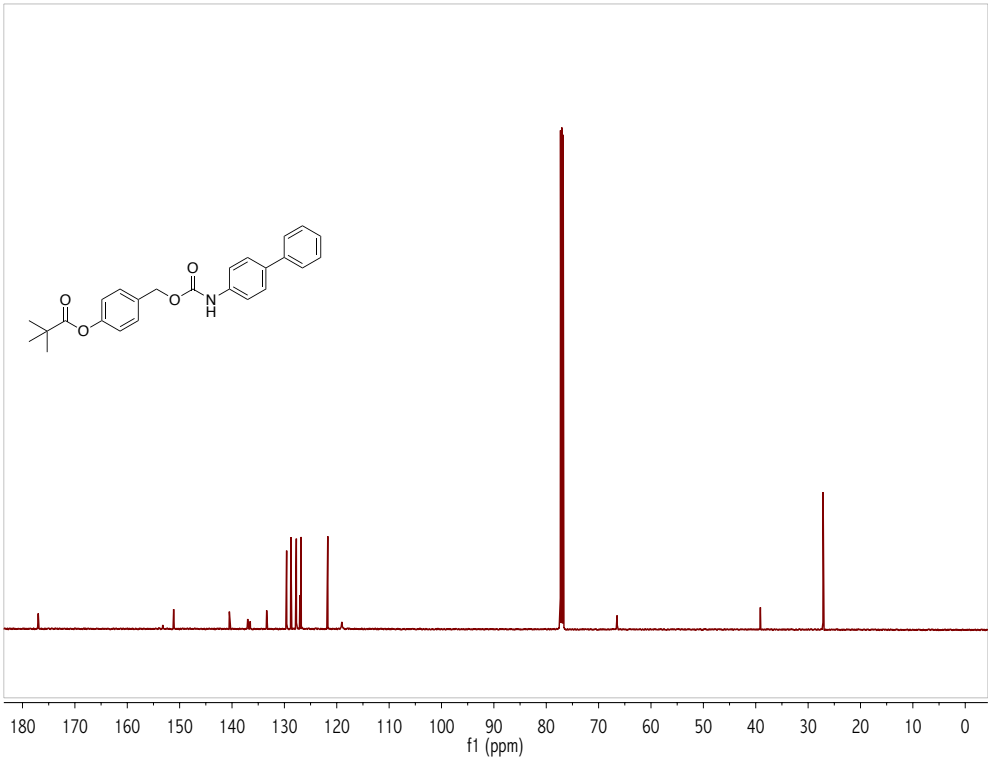

^{1}H (500 MHz, $CDCl_3$, RT) and ^{13}C (125 MHz, $CDCl_3$, RTNMR spectra of **CM11.**

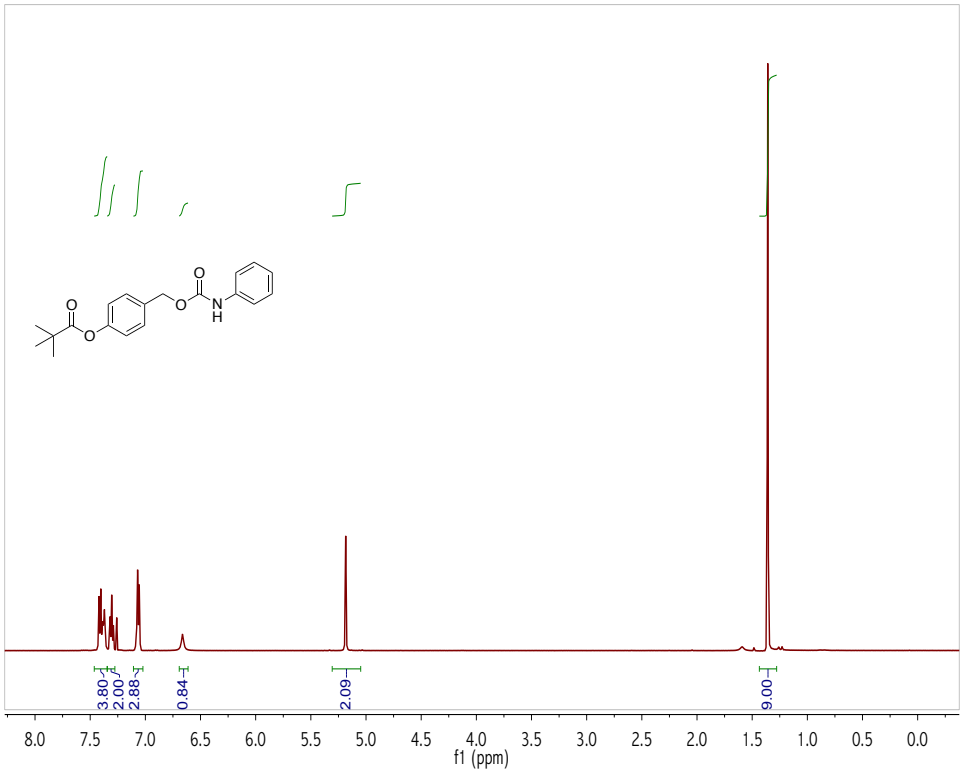

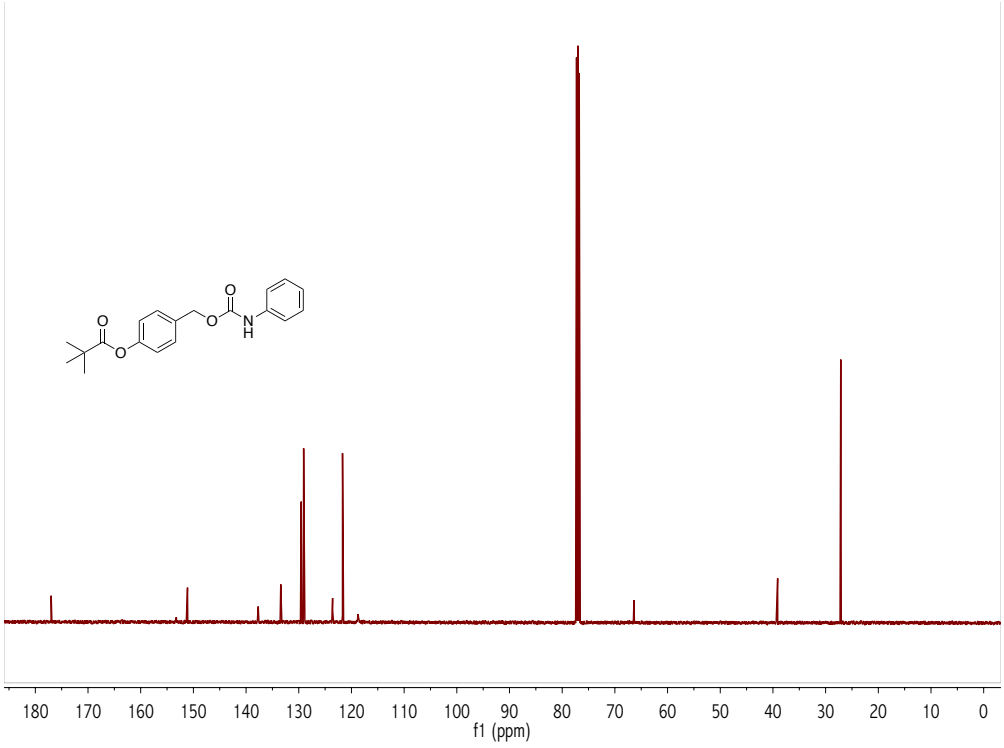

^{1}H (500 MHz, $CDCl_3$, RT), ^{13}C (125 MHz, $CDCl_3$, RT), and ^{19}F (470 MHz, $CDCl_3$, RT) NMR spectra of **CM12.**

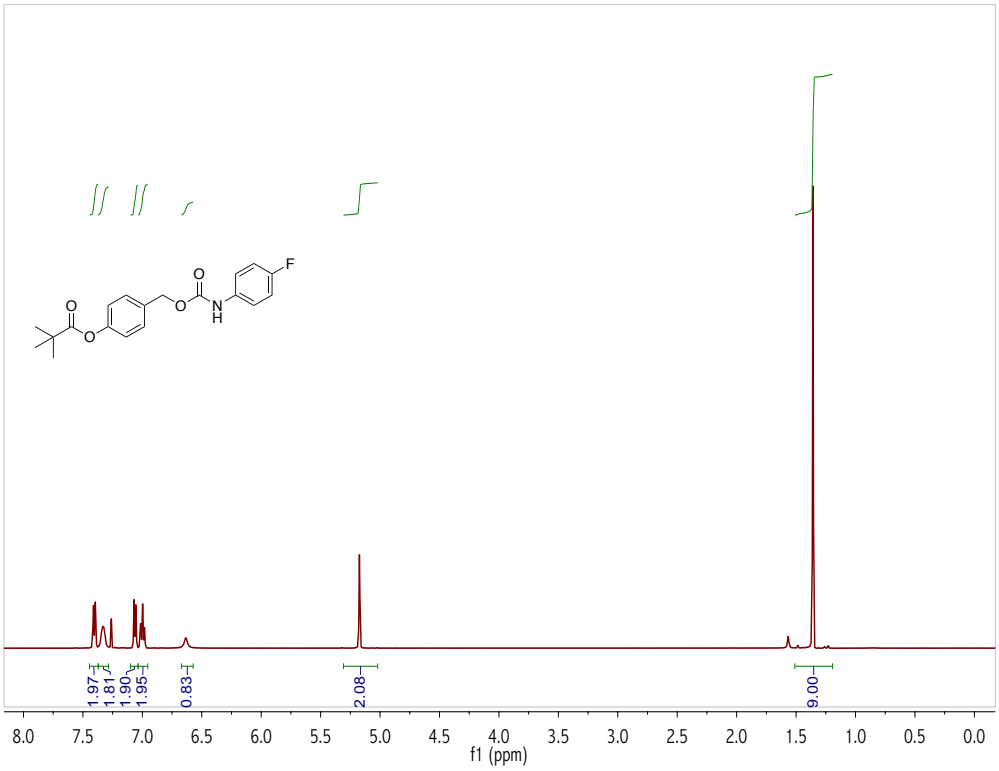

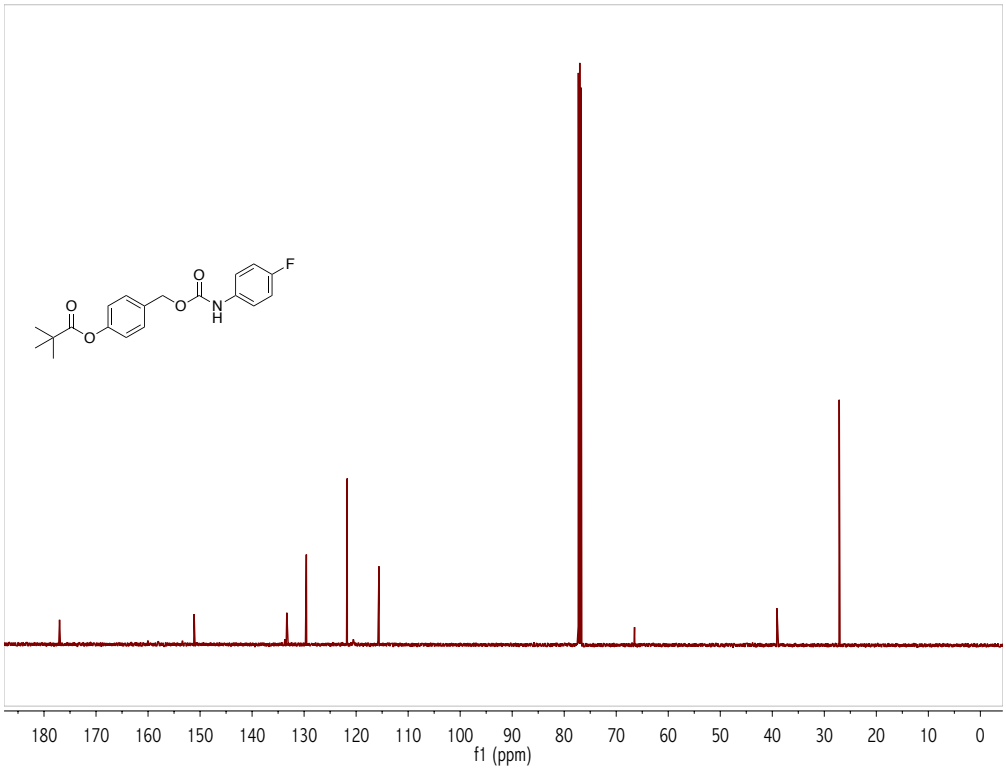

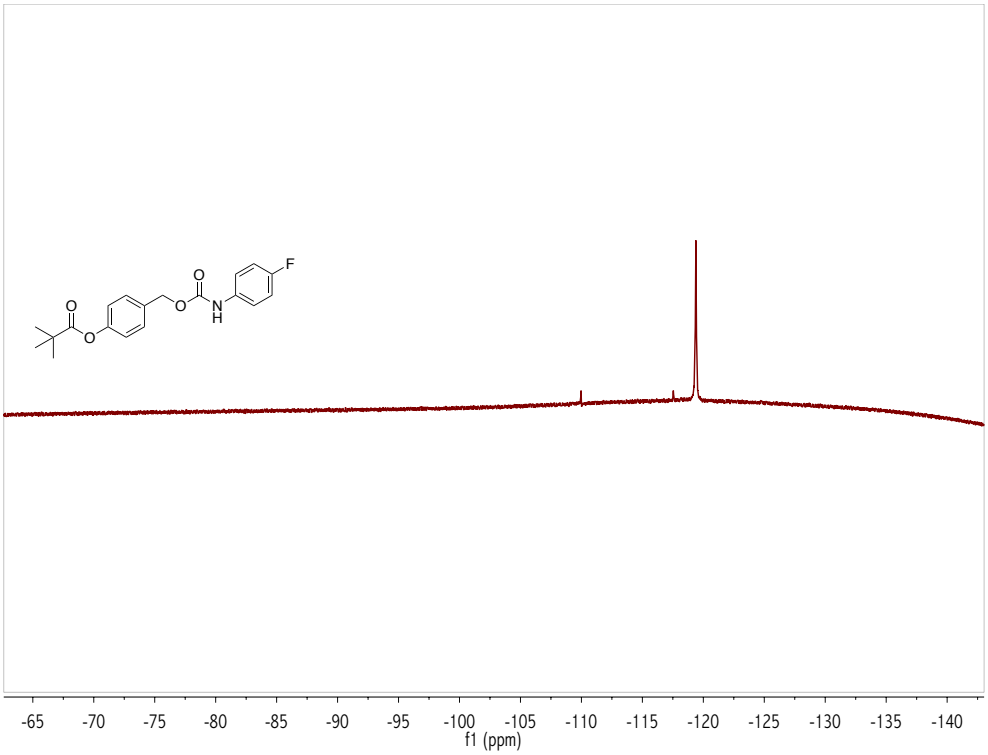

^{1}H (500 MHz, $CDCl_3$, RT), ^{13}C (125 MHz, $CDCl_3$, RT), and ^{19}F (470 MHz, $CDCl_3$, RT) NMR spectra of **CM13.**

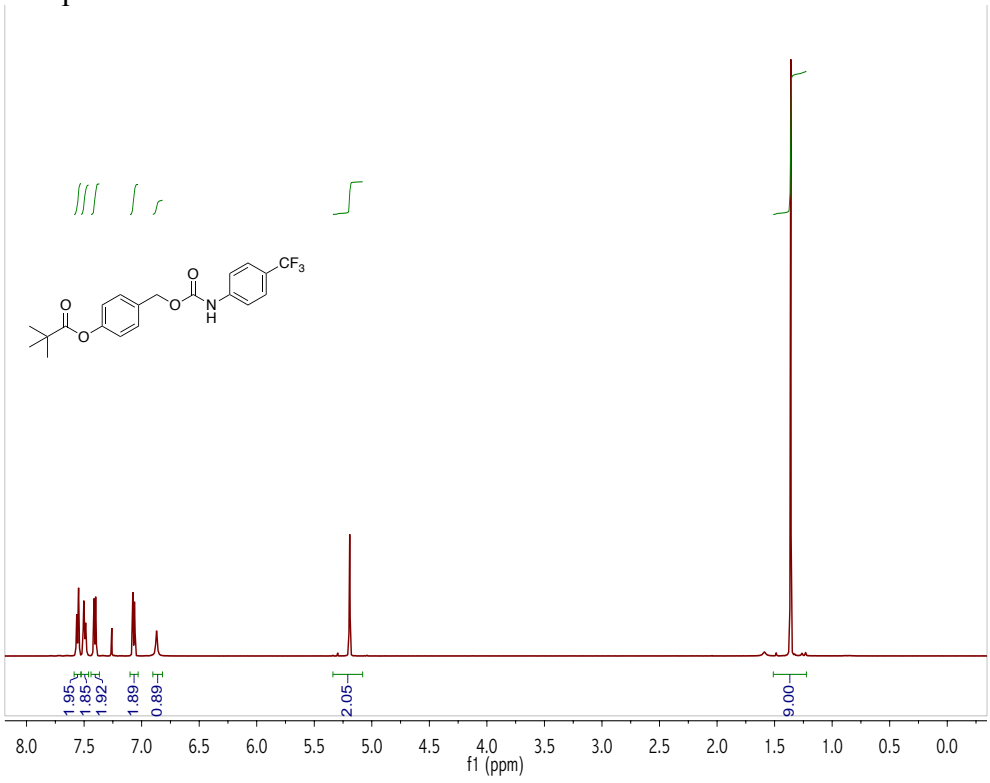

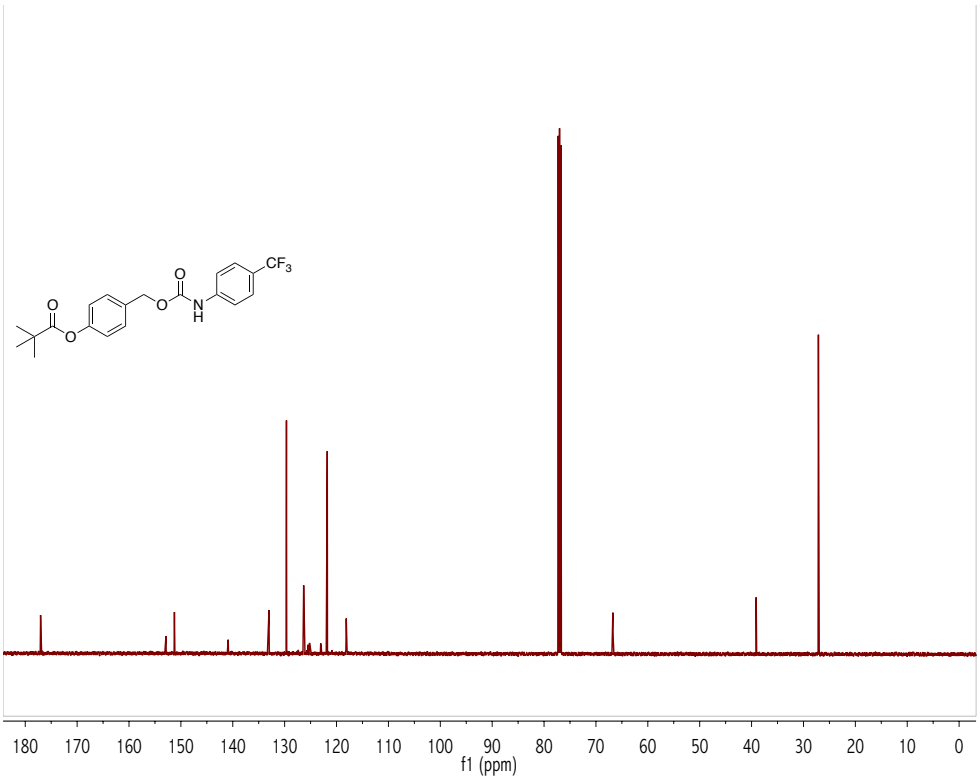
CF3
O
O
O
N
H
180 170 160 150 140 130 120 110 100 90 80 70 60 50 40 30 20 10 0
f1 (ppm)

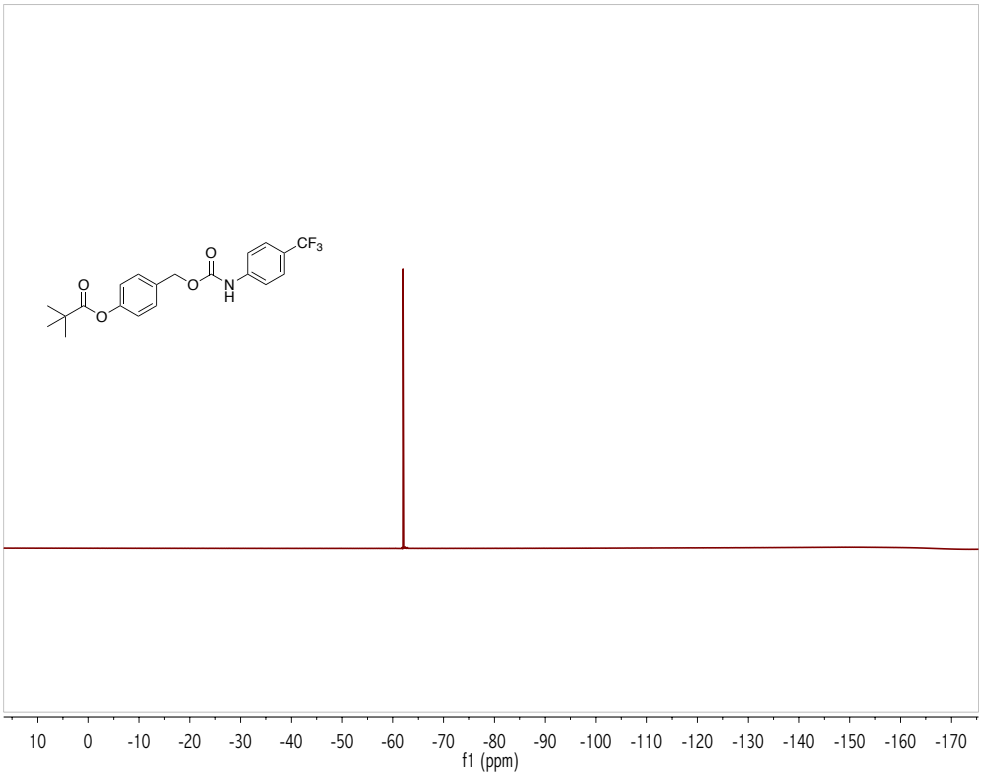
CF3
O
O
O
N
H
10 0 -10 -20 -30 -40 -50 -60 -70 -80 -90 -100 -110 -120 -130 -140 -150 -160 -170
f1 (ppm)

^{1}H (500 MHz, $CDCl_3$, RT) and ^{13}C (125 MHz, $CDCl_3$, RT) NMR spectra of **CM14.**

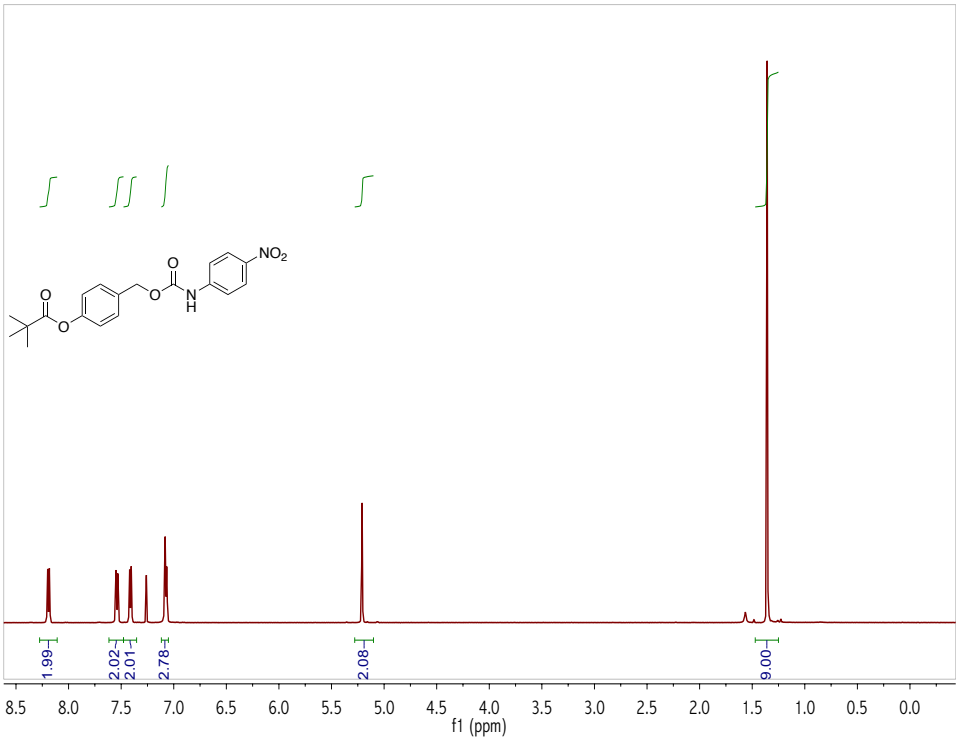

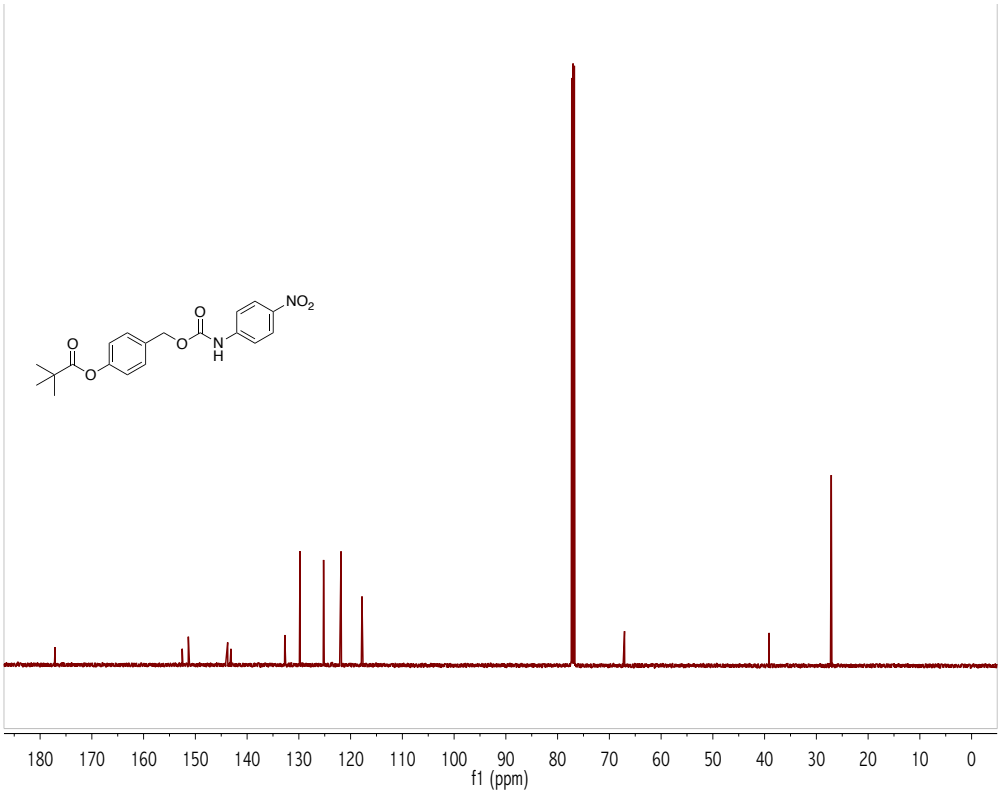

REFERENCES CITED

1. R. Wang, *Antioxidants & Redox Signaling*, 2003, **5**, 493-501.

2. R. Wang, *Physiological Reviews*, 2012, **92**, 791-896.

3. L. Y. Wu and R. Wang, *Pharmacological Reviews*, 2005, **57**, 585-630.

4. D. S. Bredt and S. H. Snyder, *Annual Review of Biochemistry*, 1994, **63**, 175-195.

5. S. Moncada, R. M. J. Palmer and E. A. Higgs, *Pharmacological Reviews*, 1991, **43**, 109-142.

6. P. Pacher, J. S. Beckman and L. Liaudet, *Physiological Reviews*, 2007, **87**, 315-424.

7. O. Kabil and R. Banerjee, *J. Biol. Chem.*, 2010, **285**, 21903-21907.

8. M. D. Maines, *Annual Review of Pharmacology and Toxicology*, 1997, **37**, 517-554.

9. K. R. Olson, *Am. J. Physiol.-Regul. Integr. Comp. Physiol.*, 2011, **301**, R297-R312.

10. M. Valko, D. Leibfritz, J. Moncol, M. T. D. Cronin, M. Mazur and J. Telser, *International Journal of Biochemistry & Cell Biology*, 2007, **39**, 44-84.

11. R. Wang, *Trends in Biochemical Sciences*, 2014, **39**, 227-232.

12. R. Wang, *FASEB Journal*, 2002, **16**, 1792-1798.

13. E. Anggard, *Lancet*, 1994, **343**, 1199-1206.

14. D. A. Wink and J. B. Mitchell, *Free Radical Biology and Medicine*, 1998, **25**, 434-456.

15. L. E. Otterbein and A. M. K. Choi, *American Journal of Physiology-Lung Cellular and Molecular Physiology*, 2000, **279**, L1029-L1037.

16. C. A. Piantadosi, *Antioxidants & Redox Signaling*, 2002, **4**, 259-270.

17. C. A. Piantadosi, *Free Radical Biology and Medicine*, 2008, **45**, 562-569.

18. W. A. Pryor, K. N. Houk, C. S. Foote, J. M. Fukuto, L. J. Ignarro, G. L. Squadrito and K. J. A. Davies, *Am. J. Physiol.-Regul. Integr. Comp. Physiol.*, 2006, **291**, R491-R511.

19. S. W. Ryter and L. E. Otterbein, *Bioessays*, 2004, **26**, 270-280.

20. C. L. Bianco and J. M. Fukuto, *Proceedings of the National Academy of Sciences of the United States of America*, 2015, **112**, 10573-10574.

21. M. Whiteman, L. Li, I. Kostetski, S. H. Chu, J. L. Siau, M. Bhatia and P. K. Moore, *Biochemical and Biophysical Research Communications*, 2006, **343**, 303-310.

22. M. M. Cortese-Krott, B. O. Fernandez, J. L. T. Santos, E. Mergia, M. Grman, P. Nagy, M. Kelm, A. Butler and M. Feelisch, *Redox Biology*, 2014, **2**, 234-244.

23. M. M. Cortese-Krott, G. G. C. Kuhnle, A. Dyson, B. O. Fernandez, M. Grman, J. F. DuMond, M. P. Barrow, G. McLeod, H. Nakagawa, K. Ondrias, P. Nagy, S. B. King, J. E. Saavedra, L. K. Keefer, M. Singer, M. Kelm, A. R. Butler and M. Feelisch, *Proceedings of the National Academy of Sciences of the United States of America*, 2015, **112**, E4651-E4660.

24. M. R. Filipovic, J. L. Miljkovic, T. Nauser, M. Royzen, K. Klos, T. Shubina, W. H. Koppenol, S. J. Lippard and I. Ivanovic-Burmazovic, *Journal of the American Chemical Society*, 2012, **134**, 12016-12027.

25. T. S. Bailey, H. A. Henthorn and M. D. Pluth, *Inorganic Chemistry*, 2016, **55**, 12618-12625.

26. E. D'Araio, N. Shaw, A. Millward, A. Demaine, M. Whiteman and A. Hodgkinson, *Acta Diabetologica*, 2014, **51**, 155-157.

27. W. Hua, Q. Chen, F. Q. Gong, C. H. Xie, S. L. Zhou and L. C. Gao, *Life Sciences*, 2013, **93**, 949-954.

28. G. A. Prathapasinghe, Y. L. Siow, Z. B. Xu and O. Karmin, *American Journal of Physiology-Renal Physiology*, 2008, **295**, F912-F922.

29. M. Puranik, C. L. Weeks, D. Lahaye, O. Kabil, S. Taoka, S. B. Nielsen, J. T. Groves, R. Banerjee and T. G. Spiro, *J. Biol. Chem.*, 2006, **281**, 13433-13438.

30. J. L. Miljkovic, I. Kenkel, I. Ivanovic-Burmazovic and M. R. Filipovic, *Angewandte Chemie-International Edition*, 2013, **52**, 12061-12064.

31. J. P. Marcolongo, U. N. Morzan, A. Zeida, D. A. Scherlis and J. A. Olabe, *Physical Chemistry Chemical Physics*, 2016, **18**, 30047-30052.

32. N. D. Mathew, D. I. Schlipalius and P. R. Ebert, *Journal of Toxicology*, 2011, **2011**, 14.

33. H. Mitsuhashi, S. Yamashita, H. Ikeuchi, T. Kuroiwa, Y. Kaneko, K. Hiromura, K. Ueki and Y. Nojima, *Shock*, 2005, **24**, 529-534.

34. Y. Huang, C. Tang, J. Du and H. Jin, *Oxidative Medicine and Cellular Longevity*, 2016, **2016**, 9.

35. T. P. Singer and E. B. Kearney, *Archives of Biochemistry and Biophysics*, 1956, **61**, 397-409.

36. M. H. Stipanuk, *Annual Review of Nutrition*, 1986, **6**, 179-209.

37. D. Haussinger, B. Gorg, R. Reinehr and F. Schliess, *Metab. Brain Dis.*, 2005, **20**, 285-294.

38. I. Suarez, G. Bodega, M. Rubio and B. Fernandez, *Metab. Brain Dis.*, 2009, **24**, 395-408.

39. M. A. Kamboures, D. R. Blake, D. M. Cooper, R. L. Newcomb, M. Barker, J. K. Larson, S. Meinardi, E. Nussbaum and F. S. Rowland, *Proceedings of the National Academy of Sciences of the United States of America*, 2005, **102**, 15762-15767.

40. S. S. Sehnert, L. Jiang, J. F. Burdick and T. H. Risby, *Biomarkers*, 2002, **7**, 174-187.

41. M. Balazy, I. A. Abu-Yousef, D. N. Harpp and J. Park, *Biochemical and Biophysical Research Communications*, 2003, **311**, 728-734.

42. C. P. Chengelis and R. A. Neal, *Toxicology and Applied Pharmacology*, 1980, **55**, 198-202.

43. J. Kesselmeier, N. Teusch and U. Kuhn, *Journal of Geophysical Research-Atmospheres*, 1999, **104**, 11577-11584.

44. S. Schenk, J. Kesselmeier and E. Anders, *Chemistry-a European Journal*, 2004, **10**, 3091-3105.

45. C. Huber and G. Wachtershauser, *Science*, 1998, **281**, 670-672.

46. L. Leman, L. Orgel and M. R. Ghadiri, *Science*, 2004, **306**, 283-286.

47. R. J. Ferm, *Chemical Reviews*, 1957, **57**, 621-640.

48. M. T. Beck and G. B. Kauffman, *Polyhedron*, 1985, **4**, 775-781.

49. L. A. Pursglove and H. W. Wainwright, *Analytical Chemistry*, 1954, **26**, 1835-1839.

50. B. Johansson, *Drug Metabolism and Disposition*, 1989, **17**, 351-353.

51. C. P. Chengelis and R. A. Neal, *Biochemical Pharmacology*, 1987, **36**, 363-368.

52. P. D. N. Svoronos and T. J. Bruno, *Industrial & Engineering Chemistry Research*, 2002, **41**, 5321-5336.

53. C. Hugod, *Atherosclerosis*, 1981, **40**, 181-190.

54. W. Rusihu, L. Xiaohui, C. Xiaobo, Z. Linfu and T. Xianchang, Chengdu, Sichuan, China, 1999.

55. P. L. Hanst, L. L. Spiller, D. M. Watts, J. W. Spence and M. F. Miller, *Journal of the Air Pollution Control Association*, 1975, **25**, 1220-1226.

56. S. F. Watts, *Atmospheric Environment*, 2000, **34**, 761-779.

57. C. L. Lee and P. Brimblecombe, *Earth-Science Reviews*, 2016, **160**, 1-18.

58. M. Aydin, M. B. Williams, C. Tatum and E. S. Saltzman, *Atmospheric Chemistry and Physics*, 2008, **8**, 7533-7542.

59. M. A. K. Khalil and R. A. Rasmussen, *Atmospheric Environment*, 1984, **18**, 1805-1813.

60. S. J. Taubman and J. F. Kasting, *Geophysical Research Letters*, 1995, **22**, 803-805.

61. K. Minami and S. Fukushi, *Soil Science and Plant Nutrition*, 1981, **27**, 339-345.

62. S. Lindskog, *Pharmacology & Therapeutics*, 1997, **74**, 1-20.

63. T. H. Maren, *Physiological Reviews*, 1967, **47**, 595-&.

64. J. C. Kernohan, *Biochimica et Biophysica Acta (BBA) - Specialized Section on Enzymological Subjects*, 1964, **81**, 346-356.

65. V. S. Haritos and G. Dojchinov, *Comparative Biochemistry and Physiology C-Toxicology & Pharmacology*, 2005, **140**, 139-147.

66. M. J. Smeulders, A. Pol, H. Venselaar, T. R. M. Barends, J. Hermans, M. S. M. Jetten and H. J. M. Op den Camp, *Journal of Bacteriology*, 2013, **195**, 4046-4056.

67. L. C. Seefeldt, M. E. Rasche and S. A. Ensign, *Biochemistry*, 1995, **34**, 5382-5389.

68. S. A. Ensign, *Biochemistry*, 1995, **34**, 5372-5381.

69. G. H. Lorimer and J. Pierce, *J. Biol. Chem.*, 1989, **264**, 2764-2772.

70. T. Ogawa, K. Noguchi, M. Saito, Y. Nagahata, H. Kato, A. Ohtaki, H. Nakayama, N. Dohmae, Y. Matsushita, M. Odaka, M. Yohda, H. Nyunoya and Y. Katayama, *Journal of the American Chemical Society*, 2013, **135**, 3818-3825.

71. P. Piazzetta, T. Marino and N. Russo, *Physical Chemistry Chemical Physics*, 2015, **17**, 14843-14848.

72. J. W. Fahey, A. T. Zalcmann and P. Talalay, *Phytochemistry*, 2001, **56**, 5-51.

73. R. Cipollone, P. Ascenzi and P. Visca, *Iubmb Life*, 2007, **59**, 51-59.

74. R. Wever, W. M. Kast, J. H. Kasinoedin and R. Boelens, *Biochimica Et Biophysica Acta*, 1982, **709**, 212-219.

75. Y. Katayama, Y. Narahara, Y. Inoue, F. Amano, T. Kanagawa and H. Kuraishi, *J. Biol. Chem.*, 1992, **267**, 9170-9175.

76. T. Arakawa, Y. Kawano, S. Kataoka, Y. Katayama, N. Kamiya, M. Yohda and M. Odaka, *Journal of Molecular Biology*, 2007, **366**, 1497-1509.

77. Y. Katayama, Y. Matsushita, M. Kaneko, M. Kondo, T. Mizuno and H. Nyunoya, *Journal of Bacteriology*, 1998, **180**, 2583-2589.

78. E. Y. Bezsudnova, D. Y. Sorokin, T. V. Tikhonova and V. O. Popov, *Biochimica Et Biophysica Acta-Proteins and Proteomics*, 2007, **1774**, 1563-1570.

79. M. J. Smeulders, T. R. M. Barends, A. Pol, A. Scherer, M. H. Zandvoort, A. Udvarhelyi, A. F. Khadem, A. Menzel, J. Hermans, R. L. Shoeman, H. Wessels, L. P. van den Heuvel, L. Russ, I. Schlichting, M. S. M. Jetten and H. den Camp, *Nature*, 2011, **478**, 412-416.

80. R. R. Dalvi, R. E. Poore and R. A. Neal, *Life Sciences*, 1974, **14**, 1785-1796.

81. R. R. Dalvi, A. L. Hunter and R. A. Neal, *Chemico-Biological Interactions*, 1975, **10**, 349-361.

82. C. P. Chengelis and R. A. Neal, *Biochemical and Biophysical Research Communications*, 1979, **90**, 993-999.

83. O. R. Flock, M. O. Andreae and M. Drager, *Marine Chemistry*, 1997, **59**, 71-85.

84. A. Kamyshny, A. Goifman, D. Rizkov and O. Lev, *Environmental Science & Technology*, 2003, **37**, 1865-1872.

85. T. Chivers and P. J. W. Elder, *Chemical Society Reviews*, 2013, **42**, 5996-6005.

86. T. Chivers, *Nature*, 1974, **252**, 32-33.

87. H. Kimura, *Antioxidants & Redox Signaling*, 2015, **22**, 362-376.

88. H. Kimura, *Neurochemistry International*, 2013, **63**, 492-497.

89. M. D. Pluth, T. S. Bailey, M. D. Hammers, M. D. Hartle, H. A. Henthorn and A. K. Steiger, *Synlett*, 2015, **26**, 2633-2643.

90. L. Ciaffoni, R. Peverall and G. A. D. Ritchie, *Journal of Breath Research*, 2011, **5**.

91. A. K. Mustafa, M. M. Gadalla and S. H. Snyder, *Science Signaling*, 2009, **2**.

92. D. Boehning and S. H. Snyder, *Annual Review of Neuroscience*, 2003, **26**, 105-131.

93. R. F. Furchgott and J. V. Zawadzki, *Nature*, 1980, **288**, 373-376.

94. L. J. Ignarro, G. M. Buga, K. S. Wood, R. E. Byrns and G. Chaudhuri, *Proceedings of the National Academy of Sciences of the United States of America*, 1987, **84**, 9265-9269.

95. S. Moncada and E. A. Higgs, *British Journal of Pharmacology*, 2006, **147**, S193-S201.

96. R. Zakhary, K. D. Poss, S. R. Jaffrey, C. D. Ferris, S. Tonegawa and S. H. Snyder, *Proceedings of the National Academy of Sciences of the United States of America*, 1997, **94**, 14848-14853.

97. C. L. Ordonez, N. R. Henig, N. Mayer-Hamblett, F. J. Accurso, J. L. Burns, J. F. Chmiel, C. L. Daines, R. L. Gibson, S. McNamara, G. Z. Retsch-Bogart, P. L. Zeitlin and M. L. Aitken, *American Journal of Respiratory and Critical Care Medicine*, 2003, **168**, 1471-1475.

98. W. E. Regelmann, G. R. Elliott, W. J. Warwick and C. C. Clawson, *American Review of Respiratory Disease*, 1990, **141**, 914-921.

99. B. W. Ramsey, H. L. Dorkin, J. D. Eisenberg, R. L. Gibson, I. R. Harwood, R. M. Kravitz, D. V. Schidlow, R. W. Wilmott, S. J. Astley, M. A. McBurnie, K. Wentz and A. L. Smith, *New England Journal of Medicine*, 1993, **328**, 1740-1746.

100. J. V. Briggman, R. E. Tashian and S. S. Spicer, *American Journal of Pathology*, 1983, **112**, 250-257.

101. M. Fanjul, C. Salvador, L. Alvarez, S. Cantet and E. Hollande, *European Journal of Cell Biology*, 2002, **81**, 437-447.

102. D. Kaiser and E. Drack, *European Journal of Clinical Investigation*, 1974, **4**, 261-265.

103. US Patent # 4749555, 1988.

104. R. S. Dewey, E. F. Schoenewaldt, H. Joshua, W. J. Paleveda, H. Schwam, H. Barkemeyer, B. H. Arison, D. F. Veber, R. G. Strachan, J. Milkowski, R. G. Denkewalter and R. Hirschmann, *Journal of Organic Chemistry*, 1971, **36**, 49-59.

105. W. S. Farrell, P. Y. Zavalij and L. R. Sita, *Angewandte Chemie-International Edition*, 2015, **54**, 4269-4273.

106. L. J. Leman, L. E. Orgel and M. R. Ghadiri, *Journal of the American Chemical Society*, 2006, **128**, 20-21.

107. C. T. Supuran and A. Scozzafava, *Expert Opinion on Therapeutic Patents*, 2000, **10**, 575-600.

108. C. T. Supuran, A. Scozzafava and A. Casini, *Med. Res. Rev.*, 2003, **23**, 146-189.

109. S. Pastorekova, S. Parkkila, J. Pastorek and C. T. Supuran, *Journal of Enzyme Inhibition and Medicinal Chemistry*, 2004, **19**, 199-229.

110. C. T. Supuran and A. Scozzafava, *Bioorg. Med. Chem.*, 2007, **15**, 4336-4350.

111. C. T. Supuran, *Bioorganic & Medicinal Chemistry Letters*, 2010, **20**, 3467-3474.

112. C. T. Supuran, *Journal of Enzyme Inhibition and Medicinal Chemistry*, 2012, **27**, 759-772.

113. M. Feelisch, *Naunyn-Schmiedebergs Archives of Pharmacology*, 1998, **358**, 113-122.

114. L. J. Ignarro, C. Napoli and J. Loscalzo, *Circulation Research*, 2002, **90**, 21-28.

115. P. G. Wang, M. Xian, X. P. Tang, X. J. Wu, Z. Wen, T. W. Cai and A. J. Janczuk, *Chemical Reviews*, 2002, **102**, 1091-1134.

116. H. Kojima, N. Nakatsubo, K. Kikuchi, S. Kawahara, Y. Kirino, H. Nagoshi, Y. Hirata and T. Nagano, *Analytical Chemistry*, 1998, **70**, 2446-2453.

117. X. Q. Chen, X. Z. Tian, I. Shin and J. Yoon, *Chemical Society Reviews*, 2011, **40**, 4783-4804.

118. L. E. McQuade and S. J. Lippard, *Current Opinion in Chemical Biology*, 2010, **14**, 43-49.

119. M. D. Pluth, E. Tomat and S. J. Lippard, *Annual Review of Biochemistry*, 2011, **80**, 333-355.

120. C. Szabo, *Nature Reviews Drug Discovery*, 2007, **6**, 917-935.

121. K. Kashfi and K. R. Olson, *Biochemical Pharmacology*, 2013, **85**, 689-703.

122. Z. J. Song, M. Y. Ng, Z. W. Lee, W. Dai, T. Hagen, P. K. Moore, D. Huang, L. W. Deng and C. H. Tan, *Medchemcomm*, 2014, **5**, 557-570.

123. J. L. Wallace and R. Wang, *Nature Reviews Drug Discovery*, 2015, **14**, 329-345.

124. Y. Zhao, J. Kang, C. M. Park, P. E. Bagdon, B. Peng and M. Xian, *Org Lett*, 2014, **16**, 4536-4539.

125. V. S. Lin and C. J. Chang, *Current Opinion in Chemical Biology*, 2012, **16**, 595-601.

126. N. Kumar, V. Bhalla and M. Kumar, *Coordination Chemistry Reviews*, 2013, **257**, 2335-2347.

127. A. R. Lippert, *Journal of Inorganic Biochemistry*, 2014, **133**, 136-142.

128. B. Peng and M. Xian, *Asian Journal of Organic Chemistry*, 2014, **3**, 914-924.

129. M. D. Hartle and M. D. Pluth, *Chemical Society Reviews*, 2016, **45**, 6108-6117.

130. I. Chakraborty, S. J. Carrington and P. K. Mascharak, *Accounts of Chemical Research*, 2014, **47**, 2603-2611.

131. A. K. Steiger, S. Pardue, C. G. Kevil and M. D. Pluth, *Journal of the American Chemical Society*, 2016, **138**, 7256-7259.

132. P. L. Carl, P. K. Chakravarty and J. A. Katzenellenbogen, *Journal of Medicinal Chemistry*, 1981, **24**, 479-480.

133. R. Labruere, A. Alouane, T. Le Saux, I. Aujard, P. Pelupessy, A. Gautier, S. Dubruille, F. Schmidt and L. Jullien, *Angewandte Chemie-International Edition*, 2012, **51**, 9344-9347.

134. R. J. Amir, N. Pessah, M. Shamis and D. Shabat, *Angewandte Chemie-International Edition*, 2003, **42**, 4494-4499.

135. C. A. Blencowe, A. T. Russell, F. Greco, W. Hayes and D. W. Thornthwaite, *Polymer Chemistry*, 2011, **2**, 773-790.

136. M. E. Roth, O. Green, S. Gnaim and D. Shabat, *Chemical Reviews*, 2016, **116**, 1309-1352.

137. D. Shabat, *Journal of Polymer Science Part a-Polymer Chemistry*, 2006, **44**, 1569-1578.

138. B. C. Dickinson, C. Huynh and C. J. Chang, *Journal of the American Chemical Society*, 2010, **132**, 5906-5915.

139. E. W. Miller, A. E. Albers, A. Pralle, E. Y. Isacoff and C. J. Chang, *Journal of the American Chemical Society*, 2005, **127**, 16652-16659.

140. Y. Zhao and M. D. Pluth, *Angewandte Chemie-International Edition*, 2016, **55**, 14638-14642.

141. L. A. Montoya and M. D. Pluth, *Chemical Communications*, 2012, **48**, 4767-4769.

142. R. M. Versteegen, R. Rossin, W. ten Hoeve, H. M. Janssen and M. S. Robillard, *Angewandte Chemie-International Edition*, 2013, **52**, 14112-14116.

143. M. Gregoritza and F. P. Brandl, *European Journal of Pharmaceutics and Biopharmaceutics*, 2015, **97**, 438-453.

144. M. L. Blackman, M. Royzen and J. M. Fox, *Journal of the American Chemical Society*, 2008, **130**, 13518-13519.

145. N. K. Devaraj, G. M. Thurber, E. J. Keliher, B. Marinelli and R. Weissleder, *Proceedings of the National Academy of Sciences of the United States of America*, 2012, **109**, 4762-4767.

146. R. Rossin, P. R. Verkerk, S. M. van den Bosch, R. C. M. Vulders, I. Verel, J. Lub and M. S. Robillard, *Angewandte Chemie-International Edition*, 2010, **49**, 3375-3378.

147. A. K. Steiger, Y. Yang, M. Royzen and M. D. Pluth, *Chemical Communications*, 2017, **53**, 1378-1380.

148. B. E. Alexander, S. J. Coles, B. C. Fox, T. F. Khan, J. Maliszewski, A. Perry, M. B. Pitak, M. Whiteman and M. E. Wood, *Medchemcomm*, 2015, **6**, 1649-1655.

149. L. K. Keefer, R. W. Nims, K. M. Davies and D. A. Wink, *Nitric Oxide, Pt a - Sources and Detection of NO; NO Synthase*, 1996, **268**, 281-293.

150. C. R. Powell, J. C. Foster, B. Okyere, M. H. Theus and J. B. Matson, *Journal of the American Chemical Society*, 2016, **138**, 13477-13480.

151. D. Vullo, M. Durante, F. S. Di Leva, S. Cosconati, E. Masini, A. Scozzafava, E. Novellino, C. T. Supuran and F. Carta, *Journal of Medicinal Chemistry*, 2016, **59**, 5857-5867.

152. P. Chauhan, P. Bora, G. Ravikumar, S. Jos and H. Chakrapani, *Organic Letters*, 2017, **19**, 62-65.

153. R. Y. Tsien, *Nature*, 1981, **290**, 527-528.

154. C. Wei, Q. Zhu, W. W. Liu, W. B. Chen, Z. Xi and L. Yi, *Organic & Biomolecular Chemistry*, 2014, **12**, 479-485.

155. K. R. Olson, *Journal of Comparative Physiology B-Biochemical Systemic and Environmental Physiology*, 2012, **182**, 881-897.

156. A. V. Mishanina, M. Libiad and R. Banerjee, *Nature Chemical Biology*, 2015, **11**, 457-464.

157. B. N. G. Giepmans, S. R. Adams, M. H. Ellisman and R. Y. Tsien, *Science*, 2006, **312**, 217-224.

158. L. D. Lavis and R. T. Raines, *ACS Chem. Biol.*, 2008, **3**, 142-155.

159. M. Schaferling, *Angewandte Chemie-International Edition*, 2012, **51**, 3532-3554.

160. R. N. Day and M. W. Davidson, *Chemical Society Reviews*, 2009, **38**, 2887-2921.

161. D. M. Chudakov, M. V. Matz, S. Lukyanov and K. A. Lukyanov, *Physiological Reviews*, 2010, **90**, 1103-1163.

162. E. M. Sletten and C. R. Bertozzi, *Angewandte Chemie-International Edition*, 2009, **48**, 6974-6998.

163. X. H. Li, X. H. Gao, W. Shi and H. M. Ma, *Chemical Reviews*, 2014, **114**, 590-659.

164. E. L. Que, D. W. Domaille and C. J. Chang, *Chemical Reviews*, 2008, **108**, 1517-1549.

165. D. W. Domaille, E. L. Que and C. J. Chang, *Nature Chemical Biology*, 2008, **4**, 168-175.

166. L. M. Hyman and K. J. Franz, *Coordination Chemistry Reviews*, 2012, **256**, 2333-2356.

167. H. Cheng, W. J. Lederer and M. B. Cannell, *Science*, 1993, **262**, 740-744.

168. E. L. Que, R. Bleher, F. E. Duncan, B. Y. Kong, S. C. Gleber, S. Vogt, S. Chen, S. A. Garwin, A. R. Bayer, V. P. Dravid, T. K. Woodruff and T. V. O'Halloran, *Nature Chemistry*, 2015, **7**, 130-139.

169. Y. Zhao, S. Bhushan, C. Yang, H. Otsuka, J. D. Stein, A. Pacheco, B. Peng, N. O. Devarie-Baez, H. C. Aguilar, D. J. Lefer and M. Xian, *ACS Chem Biol*, 2013, **8**, 1283-1290.

170. Y. Zhao, H. Wang and M. Xian, *J Am Chem Soc*, 2011, **133**, 15-17.

171. Y. Zheng, B. Yu, K. Ji, Z. Pan, V. Chittavong and B. Wang, *Angewandte Chemie*, 2016, **55**, 4514-4518.

172. K. M. Holmstrom and T. Finkel, *Nat. Rev. Mol. Cell Biol.*, 2014, **15**, 411-421.

173. M. N. Hughes, *Biochimica Et Biophysica Acta-Bioenergetics*, 1999, **1411**, 263-272.

174. B. D'Autreaux and M. B. Toledano, *Nat. Rev. Mol. Cell Biol.*, 2007, **8**, 813-824.

175. J. Chan, S. C. Dodani and C. J. Chang, *Nature Chemistry*, 2012, **4**, 973-984.

176. V. S. Lin, W. Chen, M. Xian and C. J. Chang, *Chemical Society Reviews*, 2015, **44**, 4596-4618.

177. R. Erez and D. Shabat, *Org Biomol Chem*, 2008, **6**, 2669-2672.

178. R. B. Greenwald, A. Pendri, C. D. Conover, H. Zhao, Y. H. Choe, A. Martinez, K. Shum and S. Y. Guan, *Journal of Medicinal Chemistry*, 1999, **42**, 3657-3667.

179. J. L. Bolton, S. B. Turnipseed and J. A. Thompson, *Chemico-Biological Interactions*, 1997, **107**, 185-200.

180. S. Elliott, E. Lu and F. S. Rowland, *Environmental Science & Technology*, 1989, **23**, 458-461.

181. J. Gieldanowski and W. Prastowski, *Arch Immunol Ther Exp*, 1964, **12**, 113-117.

182. X. G. Shen, E. A. Peter, S. Bir, R. Wang and C. G. Kevil, *Free Radical Biology and Medicine*, 2012, **52**, 2276-2283.

183. V. Vitvitsky, P. K. Yadav, A. Kurthen and R. Banerjee, *J. Biol. Chem.*, 2015, **290**, 8310-8320.

184. M. D. Hammers, M. J. Taormina, M. M. Cerda, L. A. Montoya, D. T. Seidenkranz, R. Parthasarathy and M. D. Pluth, *Journal of the American Chemical Society*, 2015, **137**, 10216-10223.

185. H. A. Henthorn and M. D. Pluth, *Journal of the American Chemical Society*, 2015, **137**, 15330-15336.

186. B. Chen, P. Wang, Q. Jin and X. Tang, *Organic & Biomolecular Chemistry*, 2014, **12**, 5629-5633.

187. M. Alajarin, M. Marin-Luna, M.-M. Ortin, P. Sanchez-Andrada and A. Vidal, *Tetrahedron*, 2009, **65**, 2579-2590.

188. S. Lindskog and P. O. Nyman, *Biochimica Et Biophysica Acta*, 1964, **85**, 462-474.

189. X. Shen, S. Chakraborty, T. R. Dugas and C. G. Kevil, *Nitric Oxide-Biology and Chemistry*, 2014, **41**, 97-104.

190. X. Shen, C. B. Pattillo, S. Pardue, S. C. Bir, R. Wang and C. G. Kevil, *Free Radical Biology and Medicine*, 2011, **50**, 1021-1031.

191. J. M. Mejia Oneto, I. Khan, L. Seebald and M. Royzen, *ACS central science*, 2016, **2**, 476-482.

192. R. Rossin, S. M. J. van Duijnhoven, W. ten Hoeve, H. M. Janssen, L. H. J. Kleijn, F. J. M. Hoeben, R. M. Versteegen and M. S. Robillard, *Bioconjugate Chemistry*, 2016, **27**, 1697-1706.

193. M. T. Taylor, M. L. Blackman, O. Dmitrenko and J. M. Fox, *Journal of the American Chemical Society*, 2011, **133**, 9646-9649.

194. X. Ji, C. Zhou, K. Ji, R. E. Aghoghovbia, Z. Pan, V. Chittavong, B. Ke and B. Wang, *Angewandte Chemie International Edition*, 2016, DOI: 10.1002/anie.201608732, 10.1002/anie.201608732.

195. B. Peng, W. Chen, C. R. Liu, E. W. Rosser, A. Pacheco, Y. Zhao, H. C. Aguilar and M. Xian, *Chemistry-a European Journal*, 2014, **20**, 1010-1016.

196. V. S. Lin, A. R. Lippert and C. J. Chang, *Proc Natl Acad Sci U S A*, 2013, **110**, 7131-7135.

197. Z. Zhao, L. Cao, T. Zhang, R. Hu, S. Wang, S. Li, Y. Li and G. Yang, *ChemistrySelect*, 2016, **1**, 2581-2585.

198. X. Fan, Y. Ge, F. Lin, Y. Yang, G. Zhang, W. S. C. Ngai, Z. Lin, S. Zheng, J. Wang, J. Zhao, J. Li and P. R. Chen, *Angewandte Chemie International Edition*, 2016, **55**, 14046-14050.

199. K. Abe and H. Kimura, *The Journal of Neuroscience*, 1996, **16**, 1066-1071.

200. C. Szabo, *Antioxid. Redox. Signal.*, 2012, **17**, 68-80.

201. M. R. Filipovic, J. Zivanovic, B. Alvarez and R. Banerjee, *Chem. Rev.*, 2018, **118**, 1253-1337.

202. C. Szabo and A. Papapetropoulos, *Pharmacol. Rev.*, 2017, **69**, 497.

203. Y. Zhao, A. Pacheco and M. Xian, *Handb. Exp. Pharmacol.*, 2015, **230**, 365-388.

204. Y. Zheng, B. Yu, L. K. De La Cruz, M. Roy Choudhury, A. Anifowose and B. Wang, *Med. Res. Rev.*, 2018, **38**, 57-100.

205. A. K. Steiger, Y. Zhao and M. D. Pluth, *Antioxid Redox Signal*, 2018, **28**, 1516-1532.

206. Y. Zhao, H. A. Henthorn and M. D. Pluth, *Journal of the American Chemical Society*, 2017, **139**, 16365-16376.

207. A. K. Steiger, M. Marcatti, C. Szabo, B. Szczesny and M. D. Pluth, *ACS Chem Biol*, 2017, **12**, 2117-2123.

208. Y. Zhao, S. G. Bolton and M. D. Pluth, *Organic Letters*, 2017, **19**, 2278-2281.

209. A. K. Sharma, M. Nair, P. Chauhan, K. Gupta, D. K. Saini and H. Chakrapani, *Org. Lett.*, 2017, **19**, 4822-4825.

210. S. R. Malwal, D. Sriram, P. Yogeeswari, V. B. Konkimalla and H. Chakrapani, *J Med Chem*, 2012, **55**, 553-557.

211. K. A. Pardeshi, S. R. Malwal, A. Banerjee, S. Lahiri, R. Rangarajan and H. Chakrapani, *Bioorg. Med. Chem. Lett.*, 2015, **25**, 2694-2697.

212. E. H. Silva Sousa, L. A. Ridnour, F. S. Gouveia, Jr., C. D. Silva da Silva, D. A. Wink, L. G. de Franca Lopes and P. J. Sadler, *ACS Chem. Biol.*, 2016, **11**, 2057-2065.

213. D. Dalzoppo, V. Di Paolo, L. Calderan, G. Pasut, A. Rosato, A. M. Caccuri and L. Quintieri, *Anticancer Agents Med Chem*, 2017, **17**, 4-20.

214. P. Blondeau, R. Gauthier, C. Berse and D. Gravel, *Can J Chemistry*, 1971, **49**, 3866-3876.

215. N. J. Leonard and R. Y. Ning, *J. Org. Chem.*, 1966, **31**, 3928-3935.

216. X. Yang, Y. Guo and R. M. Strongin, *Angew. Chem. Int. Ed.*, 2011, **50**, 10690-10693.

217. R. R. Nawimanage, B. Prasai, S. U. Hettiarachchi and R. L. McCarley, *Anal. Chem.*, 2017, **89**, 6886-6892.

218. Y. Qi, Y. Huang, B. Li, F. Zeng and S. Wu, *Anal. Chem.*, 2018, **90**, 1014-1020.

219. J. F. Wang, B. Li, W. Y. Zhao, X. F. Zhang, X. Luo, M. E. Corkins, S. L. Cole, C. Wang, Y. Xiao, X. M. Bi, Y. Pang, C. A. McElroy, A. J. Bird and Y. Z. Dong, *Acs Sensors*, 2016, **1**, 882-887.

220. Q. Wu, K. Wang, Z. Wang, Y. Sun, D. Cao, Z. Liu, R. Guan, S. Zhao and X. Yu, *Talanta*, 2018, **181**, 118-124.

221. T. Soboleva, H. J. Esquer, A. D. Benninghoff and L. M. Berreau, *J. Am. Chem. Soc.*, 2017, **139**, 9435-9438.

222. A. K. Steiger, Y. Zhao, W. J. Choi, A. Crammond, M. R. Tillotson and M. D. Pluth, *Biochem. Pharmacol.*, 2018, **149**, 124-130.

223. A. R. Sarkar, C. H. Heo, E. Kim, H. W. Lee, H. Singh, J. J. Kim, H. Kang, C. Kang and H. M. Kim, *Chem. Commun.*, 2015, **51**, 2407-2410.

224. J. W. Elrod, J. W. Calvert, J. Morrison, J. E. Doeller, D. W. Kraus, L. Tao, X. Jiao, R. Scalia, L. Kiss, C. Szabo, H. Kimura, C. W. Chow and D. J. Lefer, *Proc Natl Acad Sci U S A*, 2007, **104**, 15560-15565.

225. M. Whiteman and P. G. Winyard, *Expert review of clinical pharmacology*, 2011, **4**, 13-32.

226. G. Yang, L. Wu, B. Jiang, W. Yang, J. Qi, K. Cao, Q. Meng, A. K. Mustafa, W. Mu, S. Zhang, S. H. Snyder and R. Wang, *Science*, 2008, **322**, 587-590.

227. K. R. Olson, *Antioxid Redox Signal*, 2012, **17**, 32-44.

228. G. A. Benavides, G. L. Squadrito, R. W. Mills, H. D. Patel, T. S. Isbell, R. P. Patel, V. M. Darley-Usmar, J. E. Doeller and D. W. Kraus, *Proc Natl Acad Sci U S A*, 2007, **104**, 17977-17982.

229. L. Li, M. Whiteman, Y. Y. Guan, K. L. Neo, Y. Cheng, S. W. Lee, Y. Zhao, R. Baskar, C. H. Tan and P. K. Moore, *Circulation*, 2008, **117**, 2351-2360.

230. S. Fiorucci, S. Orlandi, A. Mencarelli, G. Caliendo, V. Santagada, E. Distrutti, L. Santucci, G. Cirino and J. L. Wallace, *Br J Pharmacol*, 2007, **150**, 996-1002.

231. A. Alouane, R. Labruere, T. Le Saux, F. Schmidt and L. Jullien, *Angewandte Chemie-International Edition*, 2015, **54**, 7492-7509.

232. S. Gnaim and D. Shabat, *Acc. Chem. Res.*, 2014, **47**, 2970-2984.

233. S. M. Studer, J. B. Orens, I. Rosas, J. A. Krishnan, K. A. Cope, S. Yang, J. V. Conte, P. B. Becker and T. H. Risby, *J. Heart Lung Transplant.*, 2001, **20**, 1158-1166.

234. S. Izumi, Y. Urano, K. Hanaoka, T. Terai and T. Nagano, *J Am Chem Soc*, 2009, **131**, 10189-10200.

235. B. M. Liederer and R. T. Borchardt, *Journal of pharmaceutical sciences*, 2006, **95**, 1177-1195.

236. K. M. Huttunen, H. Raunio and J. Rautio, *Pharmacol Rev*, 2011, **63**, 750-771.

237. H. J. Jessen, T. Schulz, J. Balzarini and C. Meier, *Angewandte Chemie*, 2008, **47**, 8719-8722.

238. Q. B. Zhou and S. E. Rokita, *Proc Natl Acad Sci U S A*, 2003, **100**, 15452-15457.

239. D. Lee, S. Park, S. Bae, D. Jeong, M. Park, C. Kang, W. Yoo, M. A. Samad, Q. Ke, G. Khang and P. M. Kang, *Sci Rep*, 2015, **5**.

240. B. Szczesny, M. Marcatti, J. R. Zatarain, N. Druzhyna, J. E. Wiktorowicz, P. Nagy, M. R. Hellmich and C. Szabo, *Sci Rep*, 2016, **6**, 36125.

241. S. Le Trionnaire, A. Perry, B. Szczesny, C. Szabo, P. G. Winyard, J. L. Whatmore, M. E. Wood and M. Whiteman, *MedChemComm*, 2014, **5**, 728.

242. T. J. Monks and D. C. Jones., *Current Drug Metabolism*, 2002, **3**, 425-438.

243. C. Szabo, C. Ransy, K. Modis, M. Andriamihaja, B. Murghes, C. Coletta, G. Olah, K. Yanagi and F. Bouillaud, *Br J Pharmacol*, 2014, **171**, 2099-2122.

244. L. C. Petersen, *Biochimica et Biophysica Acta (BBA) - Bioenergetics*, 1977, **460**, 299-307.

245. A. W. Nutt, J. M. Benson, E. B. Barr, D. G. Burt, F. F. Hahn, J. L. Lewis and A. R. Dahl, *Soc. Toxicol. Proc.*, 1996, **18**, 151-152.

246. D. L. Morgan, P. B. Little, D. W. Herr, V. C. Moser, B. Collins, R. Herbert, G. A. Johnson, R. R. Maronpot, G. J. Harry and R. C. Sills, *Toxicology and Applied Pharmacology*, 2004, **200**, 131-145.

247. D. J. Polhemus, J. W. Calvert, J. Butler and D. J. Lefer, *Scientifica*, 2014, **2014**, 768607.

248. C. R. Powell, K. M. Dillon and J. B. Matson, *Biochem Pharmacol*, 2018, **149**, 110-123.

249. Y. Y. Zheng, X. Y. Ji, K. L. Ji and B. H. Wang, *Acta Pharmaceutica Sinica B*, 2015, **5**, 367-377.

250. Y. Zhao, T. D. Biggs and M. Xian, *Chemical Communications*, 2014, **50**, 11788-11805.

251. Y. Zhao, A. K. Steiger and M. D. Pluth, *Chem Commun (Camb)*, 2018, **54**, 4951-4954.

252. P. Stacko, L. Muchova, L. Vitek and P. Klan, *Organic Letters*, 2018, **20**, 4907-4911.

253. L. Tian, Y. L. Yang, L. M. Wysocki, A. C. Arnold, A. Hu, B. Ravichandran, S. M. Sternson, L. L. Looger and L. D. Lavis, *Proceedings of the National Academy of Sciences of the United States of America*, 2012, **109**, 4756-4761.

254. P. Barton, A. P. Laws and M. I. Page, *J Chem Soc Perk T 2*, 1994, DOI: Doi 10.1039/P29940002021, 2021-2029.

255. G. B. Kistiakowsky and P. C. Mangelsdorf, *Journal of the American Chemical Society*, 1956, **78**, 2964-2969.

256. H. Kimura, N. Shibuya and Y. Kimura, *Antioxid Redox Signal*, 2012, **17**, 45-57.

257. B. Szczesny, K. Modis, K. Yanagi, C. Coletta, S. Le Trionnaire, A. Perry, M. E. Wood, M. Whiteman and C. Szabo, *Nitric oxide : biology and chemistry*, 2014, **41**, 120-130.

258. C. P. Chengelis and R. A. Neal, *Toxicology and Applied Pharmacology*, 1980, **55**, 198-202.

259. T. H. Maren, *Physiol Rev*, 1967, **47**, 595-781.

260. F. Carta, M. Aggarwal, A. Maresca, A. Scozzafava, R. McKenna, E. Masini and C. T. Supuran, *J Med Chem*, 2012, **55**, 1721-1730.

261. F. Carta, A. Akdemir, A. Scozzafava, E. Masini and C. T. Supuran, *J Med Chem*, 2013, **56**, 4691-4700.

262. A. W. DeMartino, M. L. Souza and P. C. Ford, *Chem. Sci.*, 2017, **8**, 7186-7196.

263. Y. Pocker and J. T. Stone, *Biochemistry*, 1967, **6**, 668-678.

264. S. Lu and X. Zhang, *Synlett*, 2005, **2005**, 1535-1538.

265. M. Hatano, S. Kamiya, K. Moriyama and K. Ishihara, *Org Lett*, 2011, **13**, 430-433.

266. N. Chen, X. Zhong, P. Li and J. Xu, *European Journal of Organic Chemistry*, 2015, **2015**, 802-809.

267. S. Bräse, S. Dahmen and M. Pfefferkorn, *Journal of Combinatorial Chemistry*, 2000, **2**, 710-715.

268. K. Inamoto, C. Hasegawa, K. Hiroya and T. Doi, *Org Lett*, 2008, **10**, 5147-5150.

269. B. Movassagh and M. Tavoosi, *Monatshefte für Chemie - Chemical Monthly*, 2008, **139**, 251-253.

270. J. B. Christensen, M. Pittelkow and R. Lewinsky, *Synthesis*, 2002, DOI: 10.1055/s-2002-34859, 2195-2202.

271. R. T. A. M. John Chiefari, Catherine L. Moad, Graeme Moad, Ezio Rizzardo, Almar Postma, Melissa A. Skidmore, San H. Thang, *Macromolecules*, 2003, **36**, 2273-2283.

272. M. D. Stephens, N. Yodsanit and C. Melander, *Org Biomol Chem*, 2016, **14**, 6853-6856.

273. J. Lee, T. Ryu, S. Park and P. H. Lee, *Journal of Organic Chemistry*, 2012, **77**, 4821-4825.

274. K. A. Pardeshi, G. Ravikumar and H. Chakrapani, *Organic Letters*, 2018, **20**, 4-7.

275. H. Seki, S. Xue, S. Pellet, P. Silhar, E. A. Johnson and K. D. Janda, *Journal of the American Chemical Society*, 2016, **138**, 5568-5575.

276. H. X. Liu, Y. Q. Dang, Y. F. Yuan, Z. F. Xu, S. X. Qiu and H. B. Tan, *Organic Letters*, 2016, **18**, 5584-5587.